Chlorophyll Breakdown: Modifications of Colorless Chlorophyll Catabolites

Dissertation

zur Erlangung der naturwissenschaftlichen Doktorwürde
(Dr. sc. nat.)
vorgelegt
der
Mathematisch-naturwissenschaftlichen Fakultät
der Universität Zürich
von

Bastien Christ

von
Gänsbrunnen SO

Promotionskomitee

Prof. Dr. Stefan Hörtensteiner
Prof. Dr. Enrico Martinoia
Prof. Dr. Ivo Feussner

Zürich, 2013

ABSTRACT

Chlorophyll (Chl) plays central roles in most ecosystems. Heterotrophic organisms use energy directly or indirectly derived from Chl-containing autotrophic organisms. Mitochondria consume oxygen, a by-product of photosynthesis, and Chl-derived energy to create ATP, the cell's main source of energy. Chl biosynthesis and breakdown occur in all green organs, e.g. in leaves, fruits or seeds, and are regulated by developmental and environmental factors. The context of my PhD research is the degradation of Chl, which represents one of the most obvious signs of foliar senescence. Chl degradation is part of the organized transdifferentiation of chloroplasts to so called gerontoplasts and is a direct prerequisite for the remobilization of a significant amount of the nitrogen contained in chloroplast proteins, which represent 75% of the nitrogen content in photosynthetic tissues. Indeed, Chl can convert light into chemical energy only when integrated within photosystems. Accumulation of free Chl or photoactive Chl catabolites during leaf senescence would lead to the production of toxic reactive oxygen species and disable the plant to efficiently remobilize leaf nutrients to other organs.

Chl degradation during leaf senescence is biochemically well-characterized. It follows a multi-steps pathway, termed the "PAO pathway", that allows organized and controlled degradation of the catabolites. The "PAO pathway" can be divided into two main parts. The first one, occurring in the chloroplast, involves the following enzymes: STAY-GREEN (SGR), which is thought to destabilize Chl protein complexes; NON-YELLOW COLORING1 (NYC1), NYC1-like (NOL) and 7-HYDROXYMETHYL Chl *a* REDUCTASE (HCAR), which reduce Chl *b* to Chl *a*; PHEOPHYTINASE (PPH), responsible for the removal of the phytol chain; PHEOPHORBIDE *a* OXYGENASE (PAO) and RED Chl CATABOLITE (RCC) REDUCTASE (RCCR), which, respectively, open and reduce the catabolite macrocycle. SGR, NYC/NOL/HCAR, PPH, PAO and RCCR interact at the thylakoid membrane to allow metabolic chanelling of the phototoxic catabolites until the release of the primary fluorescent Chl catabolite (*p*FCC) into the stroma. The second part of the "PAO pathway" involves species-specific modifications of *p*FCC, such as demethylation, hydroxylation or glucosylation, leading to the formation of different FCCs. In parallel to these modifications, FCCs are translocated from the chloroplast to the vacuole where they are non-enzymatically isomerized to respective nonfluorescent chlorophyll catabolites (NCCs).

The aim of my work was to determine the nature of the enzymes responsible for FCC modifications in Arabidopsis. I could identify and characterise MES16, a methyl esterase responsible for FCC demethylation in Arabidopsis. This study revealed that demethylation of FCCs facilitates their isomerization to NCCs inside the vacuole. Thus, senescent leaves of *mes16*

mutants accumulate methylated FCCs and therefore are fluorescing under UV light.

This thesis also reports on the identification of novel Chl catabolites in Arabidopsis, termed nonfluorescent dioxobilin-type chlorophyll catabolites (NDCCs), that surprisingly account for more than 90% of the Chl present in green leaves. I identified cytochrome P450 monooxygenase CYP89A9 as being responsible for NDCC formation. The reaction catalyzed by CYP89A9, an oxidative deformylation, is unprecedented in the cytochrome P450 family.

A third aspect of my thesis was to localize the site of FCC hydroxylation, the only FCC modification that seems to be common to all higher plants. I could show that this reaction occurs in gerontoplasts. I also developed a method to characterize FCC export from isolated gerontoplasts that makes use of recombinant MES16 to allow distinction of exported FCCs from nonexported ones.

The results of my work considerably improve our knowledge on FCC modifications occuring during leaf senescence. However, several questions arise from these new findings and require further investigations: What is the nature of the enzyme(s) responsible for *p*FCC hydroxylation in the chloroplast? What are the physiological and/or ecological role(s) of FCCs modifications? What happens to the by-products of MES16 and CYP89A9? How are FCCs translocated from the chloroplast to the vacuole?

In the frame of my PhD, I also collaborated with other research groups on three different projects that were related to leaf senescence. A study of Chl breakdown during desiccation of the resurrection plant *Xerophyta viscosa* revealed that Chl degradation via the "PAO pathway" occurs also in tissues that are not considered as senescent. Re-examination of the function(s) of RCCR indicates that this enzyme, localized in both chloroplasts and mitochondria, is responsible for the protection against pro-death molecules (such as RCC) that are mobile within the cell. Finally, I participated in the functional identification and biochemical characterization of the α-galactosidase *At*DIN10 during leaf senescence and cold acclimation.

ZUSAMMENFASSUNG

Chlorophyll (Chl) spielt in den meisten Ökosystemen eine zentrale Rolle. Heterotrophe Organismen nutzen direkt oder indirekt die Energie Chl haltiger autotopher Organismen. Mitochondriale Atmung verbraucht Sauerstoff, ein Nebenprodukt der Photosynthese, und, mit Hilfe von Chl gewonnene, Energie, um ATP, den wichtigsten zellulären Energieträger, herzustellen. Chl Biosynthese und Abbau findet in allen grünen Pflanzenorganen statt, z.B. in Blättern, Früchten oder Samen, und wird durch Entwicklungs- und Umweltfaktoren reguliert. Meine Doktorarbeit beinhaltete Untersuchungen zum Chl Abbau, der eines der auffälligsten Merkmale der Blattseneszenz darstellt. Der Chl Abbau ist Teil der Transdifferenzierung von Chloroplasten zu sogenannten Gerontoplasten und ist eine unmittelbare Voraussetzung für die Wiederverwertung eines Teils des Stickstoffs, der sich in chloroplastidären Proteinen befindet. Diese Proteine repräsentieren mehr als 75% des gesamten zellulären Stickstoffs photosynthetisch aktiver Gewebe. In der Tat ist die Lokalisierung on Chl innerhalb der Photosysteme eine Voraussetzung für ihre Funktion, Sonnenenergie in chemische Energie umzuwandeln. Die Änhäufung von freiem Chl oder photoreaktiven Chl Kataboliten während der Seneszenz würde zur Bildung reaktiven Sauerstoffs führen und es der Pflanze verunmöglichen, Nährstoffe aus den Blättern effizient in andere Organe zu transferieren.

Biochemisch ist der Chl Abbau während der Blattseneszenz recht gut untersucht. Er erfolgt in einem mehrstufigen Abbauweg, der als „PAO-Weg" bezeichnet wird und den organisierten und kontrollierten Abbau von Chl und seinen Abbauprodukten erlaubt. Der „PAO Weg" kann in zwei Teile eingeteilt werden. Der erste Teil erfolgt im Chloroplasten und beinhaltet die folgenden Enzyme: STAY-GREEN (SGR), ein Protein, von dem man annimmt, dass es an der Destabilisierung von Chl-Proteinkomplexen beteiligt ist; NON-YELLOW COLORING1 (NYC1), NYC1-like (NOL) und 7-HYDROXYMETHYL Chl *a* REDUCTASE (HCAR), die zusammen Chl *b* zu Chl *a* reduzieren; PHEOPHYTINASE (PPH), die für die Entfernung der Phytolkette des Chls verantwortlich ist; und PHEOPHORBIDE *a* OXYGENASE (PAO) und RED Chl CATABOLITE (RCC) REDUCTASE (RCCR), zwei Enzyme, die den Makroring der Kataboliten öffnen bzw. reduzieren. SGR, NYC/NOL/HCAR, PPH, PAO und RCCR interagieren an der Thylakoidmembran und erlauben damit die metabolische Kanalsierung phototoxischer Kataboliten, bis hin zur Freisetzung eines primären fluoreszierenden Chl Kataboliten (*p*FCC) ins Stroma. Der zweite Teil des „PAO Wegs" beinhaltet artspezifische Modifikationen des *p*FCC, wie Demethylierung, Hydroxylierung und Glykosylierung, und führt zur Bildung unterschiedlicher FCCs. Zusammen mit den Modifikationen erfolgt ein Transfer der FCCs vom Chloroplasten zur Vakuole, wo die FCCs durch nichtenzymatische Isomerisierung zu entsprechenden nichtfluoreszierenden Chl Kataboliten (NCCs) umgewandelt werden.

Das Ziel meiner Arbeit war die Identifizierung von Enzymen, die für FCC Modifikationen in Arabidopsis verantwortlich sind. Es gelang mir MES16, eine Methylesterase, die in Arabidopsis FCCs demethyliert, zu identifizieren und zu charakterisieren. Diese Untersuchungen zeigten, dass FCC Demethylierung die Isomerisierung zu NCCs innerhalb der Vakuole erleichtert. So akkumulierten seneszente Blätter von *mes16* Mutanten methylierte FCCs und fluoreszierten deshalb im UV Licht.

Die vorliegende Arbeit berichtet ausserdem über die Identifikation neuer Chl Kataboliten in Arabidopsis, die als nichtfluoreszierende dioxobilan-ähnliche Chl Kataboliten (NDCCs) bezeichnet werden. Überraschenderweise stellen diese NDCCs die Mehrheit der Kataboliten dar, da sie mehr als 90% des Chls grüner Blätter entsprechen. Es gelang mir eine Cytochrom P450 Monooxygenase, CYP89A9, zu identifizieren, die für die NDCC Bildung verantwortlich ist. CYP89A9 katalysiert eine oxidative Deformylierung, ein Reaktionstyp, der für P450 Enzyme bisher unbekannt war.

Ein dritter Teil meiner Arbeit beschäftigte sich mit der FCC Hydroxylierung, die die einzige FCC Modifikation darstellt, die ubiquitär in allen Pflanzen vorkommt. Ich konnte zeigen, dass diese Reaktion in Gerontoplasten abläuft. Darüberhinaus entwickelte ich eine Methode, mit deren Hilfe sich der Export von FCCs aus isolierten Gerontoplasten untersuchen lässt und die auf dem Einsatz der MES16 beruht, um exportierte FCCs von nicht-exportierten unterscheiden zu können.

Die Ergebnisse meiner Arbeit tragen erheblich zum Verständnis der FCC Modifikationen bei, die während der Blattseneszenz auftreten. Gleichzeitig stellen sich neue Fragen, die weitere Untersuchungen erfordern: Was ist die Identität der FCC hydroxylierenden Aktivität in den Chloroplasten? Haben FCC Modifikationen physiologische und/oder ökologische Funktionen? Was passiert mit den Nebenprodukten, die bei der MES16 und CYP89A9 Reaktion anfallen? Wie werden FCCs aus den Chloroplasten und in die Vakuole transportiert?

Im Rahmen meiner Dissertation war ich ausserdem an Untersuchungen zu drei unterschiedlichen Projekten anderer Arbeitsgruppen beteiligt, die alle einen Bezug zur Seneszenz aufweisen. Die Untersuchung des Chl Abbaus während des Austrocknens der Wiederauferstehungspflanze *Xerophyta viscosa* zeigte, dass der Abbau über den „PAO Weg“ auch in Geweben erfolgt, die als nicht seneszierend bezeichnet werden. Die vertiefte Untersuchung der Funktion(en) der RCCR, eines Enzyms das sowohl in Chloroplasten als auch Michochondrien zu finden ist, zeigte, dass die RCCR verantwortlich ist für den Schutz vor toxischen Molekülen (wie dem RCC), die innerhalb der Zelle beweglich sind. Schlussendlich, war ich an der funktionellen

Analyse und biochemischen Charakterisierung von *At*DIN10, einer α-Galaktosidase, während der Seneszenz und Kälteadaption in Arabidopsis beteiligt.

TABLE OF CONTENT

INTRODUCTION

Contextualization and review of chlorophyll breakdown during leaf senescence

The context of my PhD research is the degradation of Chl, which represents one of the most obvious signs of foliar senescence. Chl degradation is part of the organized transdifferentiation of chloroplasts to so-called gerontoplasts and is a direct prerequisite for the remobilization of a significant amount of the nitrogen contained in chloroplast proteins, which represent 75% of the nitrogen content in photosynthetic tissues. This chapter integrates a review of Chl degradation with more general aspects about regulation and biochemical processes of leaf senescence.

LEAF SENESCENCE: ONSET AND REGULATION

Plant physiology is governed by highly organized processes and regulated responses. The developmental age of a plant cell, tissue, or organ is defined by the status of numerous parameters that are controlled by internal and external factors (Lim et al., 2007). Senescence, a physiological process illustrated by an increase of catabolism and a decrease of anabolism, leads to the end of viability at a cellular, tissue, organ, or organismal level. For annual or biennal plants, this age-dependent deterioration process leads to death of individuals when they reach the end of their temporal niche and is closely linked with flowering and seed maturation. In the case of perennial plants, major senescence events are restricted to leaf senescence, one of the only biochemical processes that can be observed from outer space (Gierloff-Emden and Buchroithner, 1989; Herring, 2000). This section describes external and internal information influencing the complex molecular network of leaf senescence. Figure I.1 tries to integrate and summarize key concepts of the highly complex network regulating leaf senescence.

Environmental factors

A wide range of exogenous factors affect leaf senescence. These environmental signals can be divided into abiotic (such as drought, nutrient limitation, extreme temperature, oxidative stress by UV-B irradiation and ozone) and biotic stresses (such as pathogen infection) (Lim et al., 2007). Unsurprisingly, plant responses to environmental stresses share common features with senescence processes, as suggested by an expression profile study in Arabidopsis (Chen et al., 2002). Among 43 transcriptions factor genes that are up-regulated during senescence, 28 are also induced by stress treatments, indicating that stress responses and senescence may share overlapping signaling pathways. This crosstalk between stress and senescence is highlighted by studies on phytohormones, key players in plant signaling pathways (see section “Phytohormones”).

Sugar levels

The exact nature and threshold value of the parameters triggering the onset of senescence are not known (Lim et al., 2007). Sugar levels, i. e. the cell energy status, seem to influence the pathway that induces leaf senescence. However, it is still debated whether leaf senescence can be induced by low or high sugar levels (reviewed in Doorn, 2008). Dark incubation of detached leaves in high sugar media seems to prevent senescence whereas genetic modifications increasing sugar levels in the leaf may trigger senescence (for references, see Doorn, 2008). Indeed, loss of Arabidopsis hexokinase *At*HXK1, the enzyme catalyzing the essential step of glucose and fructose phosphorylation, results in glucose insensitivity and delayed leaf senescence (Moore et al., 2003). In contrast, glucose-hypersensitivity induced by overexpression of SUCROSE NONFERMENTING-1-RELATED PROTEIN KINASE-1 (SnRK1) retards flowering time and senescence (Baena-Gonzalez et al., 2007; Jossier et al., 2009). Experiments performed by Swartzberg et al. (2011) suggest that apoplastic hexoses, in contrast to intracellular sugars, inhibit senescence (see also “Cytokinins” and “ABA” sections). Collectively considered, these studies suggest that, with some exceptions, internal high sugar levels have a positive role during the onset of senescence. Whether high sugar content is a cause or a consequence of leaf senescence still needs to be elucidated. It is important to consider that catabolic activities occurring during senescence remobilize sugars that may themselves influence the progress of senescence. This raises the more general question of “When does senescence start exactly?”. Photosynthesis, i.e. production of sugars, has been shown to decline before symptoms of senescence become apparent, but it is not clear if this decrease occurs before or after initiation of the senescence program (Buchanan-Wollaston, 1997; Lim et al., 2007; Thomas, 2013a).

Phytohormones

Plant hormones such as auxin, cytokinins, ethylene, abscisic acid (ABA), salicylic acid (SA) and jasmonates (JA) are signal substances that govern all steps of plant development and interplay in complex regulatory networks (Vanstraelen and Benková, 2012). This section emphasises the central roles played by phytohormones during the regulation of senescence, from the onset to the terminal phase.

Auxin

Auxin is suggested to be involved in senescence processes but its exact way of action remains unknown. Downregulation of SENESCENCE ASSOCIATED GENE 12 (SAG12) and delayed leaf abscission in bean has been observed following exogenous application of auxin (Noh and Amasino, 1999; Sacher, 1957; Shoji et al., 1951). Artificial increase of indole-3-acetic acid biosynthesis, the major naturally occurring auxin, appears to also delay plant senescence in Arabidopsis (Kim et al., 2011). Furthermore, the transcription factor AUXIN RESPONSE FACTOR2 (ARF2) seems to positively regulate senescence and floral organ abscission, and is proposed to be a major player in controlling auxin-mediated leaf longevity (Ellis et al., 2005; Okushima et al., 2005). However, these studies do not explain whether auxin pathways influence leaf senescence directly, or indirectly by pleiotropic effects on plant growth (Lim et al., 2007).

Cytokinins

Cytokinins are a group of phytohormones that induce cell division and regulate various biological processes associated with active growth. Delay of senescence by cytokinins has long been recognized (Noodén et al., 1979). Overexpression of ISOPENTENYL TRANSFERASE (IPT), the rate-limiting enzyme of the cytokinin biosynthesis pathway, results in the suppression of leaf senescence (Gan and Amasino, 1995). Parts of the cytokinin signaling cascade have been characterized using Arabidopsis mutants (Kim et al., 2006; Riefler et al., 2006). The plasma membrane-localized receptor ARABIDOPSIS HISTIDINE KINASE 3 (AHK3) was shown to phosphorylate ARABIDOPSIS RESPONSE REGULATOR 2 (ARR2) in response to extracellular cytokinin. ARR2 then regulates cytokinin-responsive genes and, directly or indirectly, induces a set of target genes responsible for delaying the leaf senescence program (Kim et al., 2006; Riefler et al., 2006). Furthermore, studies revealed that sugar levels and cytokinins interplay in the regulation of leaf senescence. For instance, extracellular invertase, which is involved in source-sink regulation and supply of carbohydrates to sink tissues, has been shown to be required for the delay of senescence by cytokinins (Lara et al., 2004). Interestingly, acceleration of senescence induced by intracellular sugar sensing via *At*HXK1 is dominant over cytokinin-mediated response induced by extracellular sugar via the extracellular invertase (see also section "Sugar levels"; Swartzberg et al., 2011).

Ethylene

The idea that ethylene positively regulates leaf, flower and fruit senescence is not new. In 1968, Burg already reviewed evidences supporting this hypothesis (Burg, 1968). Our current knowledge on the role of ethylene in plant senescence is mainly derived from analysis of mutants. *ein2*, an Arabidopsis ethylene-insensitive mutant, was shown to exhibit a delayed-senescence phenotype (Oh et al., 1997). Furthermore, ethylene-induced senescence in Arabidopsis appears to be regulated, at least in part, by the F-box protein ORESARA9 (ORE9), because *ore9* mutants display a delayed ethylene-induced senescence phenotype (Woo et al., 2001). Ethylene-induced senescence via EIN2 and ORE9 was shown to be negatively regulated by ENHANCED DISEASE RESISTANCE 1 (EDR1), a protein kinase also involved in disease resistance (Frye et al., 2001; Tang et al., 2005). The implication of ethylene during senescence was also highlighted by altering the ethylene biosynthetic pathway in tomato through silencing of 1-aminocyclopropane-1-carboxylic acid (ACC) oxidase (John et al., 1995). In this study, tomato plants with reduced expression of ACC oxidase exhibit delayed leaf senescence. Despite its positive effect, ethylene is not essential for the onset and progression of senescence (Grbić and Bleecker, 1995). Studies on *onset of leaf death (old)* Arabidopsis mutants revealed that the effect of ethylene on leaf senescence depends on age-related changes linked to these OLD genes (Jing et al., 2002, 2005). Indeed, the effect of ethylene on leaf senescence increases with aging and finally, beyond a certain age, senescence is triggered even without ethylene (Buchanan-Wollaston et al., 2005; Grbić and Bleecker, 1995; Park et al., 1998). These findings suggest the existence of a "senescence window", corresponding to an ethylene-dependent phase of leaf development (Fischer, 2012; Jing et al., 2002, 2005, 2003). Therefore it seems that a plant, organ, tissue or cell must acquire the competence to senescence (also referred to as "ripeness to senesce") before additional factors, such as ethylene, can initiate senescence

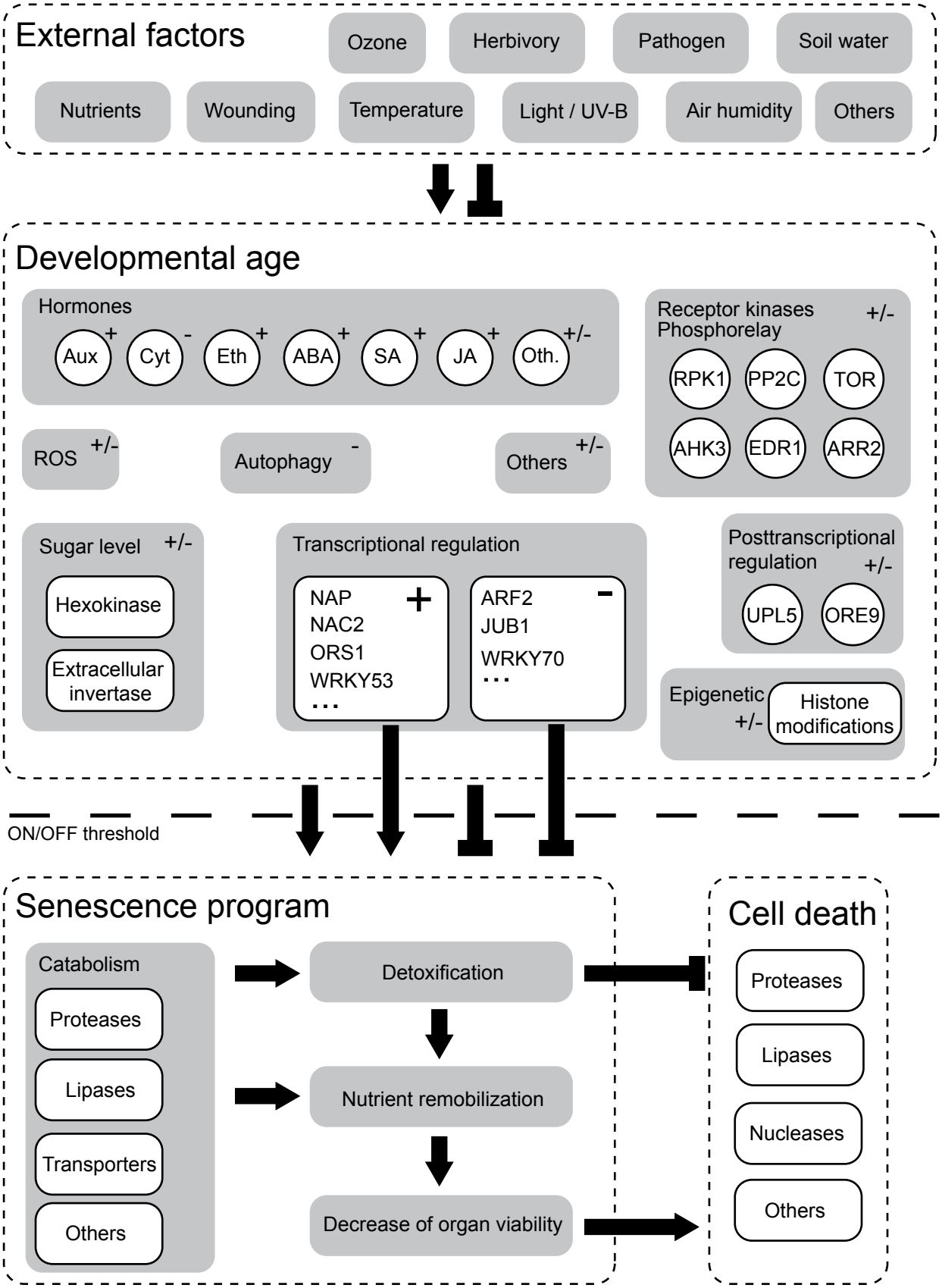

Figure I.1. Regulation of leaf senescence. This model tries to schematize regulatory pathways between external and internal factors that define the developmental age of a leaf and influence the onset and the progress of senescence. When the senescence program is transcriptionally initiated, catabolic activities allow nutrient remobilization to other organs but also lead to decreased viability and, thus, ultimately to death.

processes (Bopp, 1996; Fischer, 2012; Jansson and Thomas, 2008).

Abscisic acid

The phytohormone ABA is now known to be involved in environnemental stress responses such as stomatal closure (Finkelstein and Rock, 2002; Oka et al., 2012). ABA levels were shown to increase in leaves during senescence of many different plant species but the exact mechanism of ABA action on senescence processes is difficult to approach due to its pleotropic effects on plant physiology (Even-Chen and Itai, 1975; Gepstein and Thimann, 1980; He et al., 2005; Philosoph-Hadas et al., 1993; Zhao et al., 2010). Exogenous application of ABA was reported to promote leaf senescence (Gepstein and Thimann, 1980; Lee et al., 2011; Quiles et al., 1995; Raab et al., 2009). Furthermore, gene expression profiles in senescent leaves suggest a connection between ABA signaling and age-dependent leaf senescence (Buchanan-Wollaston et al., 2005; Tan et al., 2003). An additional genetic insight into the relation between ABA and senescence was provided by the finding that RECEPTOR PROTEIN KINASE 1 (RPK1) at the plasma membrane regulates ABA-mediated leaf senescence responses (Lee et al., 2011). A *rpk1* mutant displays delayed senescence caused by exogenous application of ABA. Recently, Zhang and Gan (2012) proposed an elegant model that links ABA signaling, stomatal movement and leaf senescence in Arabidopsis (Zhang and Gan, 2012). In this hypothesis, ABA indirectly induces, via the *At*NAP transcription factor, expression of a protein phosphatase 2C (PP2C) which in turn is thought to inhibit stomatal closure. Water loss through open stomata could then stress the plant and promote senescence. ABA signaling and senescence have been discovered to be connected via primary metabolism (Jin et al., 2009). ABA inhibits extracellular invertase activity in tomato by induction of INHIBITOR OF CELL WALL INVERTASE (INVINH1). Jin et al. (2009) showed that silencing of *INVINH1* expression increases apoplasmic invertase activity and delays ABA-mediated and age-dependent leaf senescence (Jin et al., 2009). Primary metabolism can therefore regulate leaf senescence by both cytokinins (see section "Cytokinins") and abscisic acid. Finally, ABA-mediated senescence appears to be also regulated by ubiquitin-dependent proteolysis (Raab et al., 2009). The Arabidopsis *senescence-associated E3 ubiquitin ligase 1* (*saul1*) mutant shows premature senescence that can be explained by the accumulation in the mutant of the ABA-biosynthetic enzyme ARABIDOPSIS ALDEHYDE OXIDASE 3 (AAO3), a SAUL1 target, and its positive effect on ABA biosynthesis (Raab et al., 2009).

Salicylic acid

Despite its central role in plant-pathogen interactions, SA has also been reported to be involved during senescence. Using Arabidopsis plants defective in SA-signaling, it has been demonstrated that higher levels of SA in mature leaves are responsible for the up-regulation of several SAG genes during senescence (Morris et al., 2000). Cell-death associated with senescence processes seems to be dependent on the SA signaling pathway as revealed by analysis of the *phytoalexin deficient 4* (*pad4*) mutant. Altered SA-signaling in *pad4* dramatically reduced necrosis occurring in the last stage of leaf senescence. Furthermore, transcriptomic analysis of transgenic plants with reduced SA level revealed that the expression of many genes involved during senescence is dependent on SA (Buchanan-Wollaston et al., 2005). It has recently been described that the early senescence and excessive immunity-related cell-death phenotypes of autophagy mutants are related to the SA pathway (see section "Autophagy and senescence-associated vesicles (SAV)"; Yoshimoto et al., 2009). The results of this study also show that autophagy-defective plants accumulate high levels of SA and suggest that autophagy counteracts SA signaling. Thus, autophagy seems to limit senescence and immunity-related programmed cell death (PCD) in plants.

Jasmonates

JAs are known to promote leaf senescence since the 1980s (Ueda and Kato, 1979). Exogenous application of JA was shown to promote senescence in attached and detached leaves of wild-type Arabidopsis but not of the JA-insensitive *coronatine-insensitive 1* (*coi1*) mutant (He et al., 2002). Furthermore, JA levels increase in senescent leaves and genes involved in JA biosynthesis show increased transcript levels during senescence (Buchanan-Wollaston et al.,

2005; He et al., 2002). In rice, a nuclear-localized CCCH-type zinc finger protein (OsDOS) was shown to be a negative regulator of senescence, at least in part by modulating the JA pathway (Kong et al., 2006). Histone acetylation was also reported to influence JA-mediated senescence (see also section "Epigenetic control"; Wu et al., 2008). Arabidopsis plants defective in HISTONE DEACETYLASE 6 (HDA6) show down-regulation of JA responsive gene expression and delayed leaf senescence. Recently, a mechanism of JA action during senescence was proposed in a study on Rubisco activase (Shan et al., 2011). During JA-induced senescence, Rubisco activase transcript and protein levels are down-regulated in a COI1-dependent manner, leading to typical senescence-associated features.

Brassinosteroids, gibberellins and nitric oxide

Plant brassinosteroids (BRs) are polyhydroxylated steroid hormones that are involved in regulating numerous developmental processes (Vert et al., 2005; Wang et al., 2012). External application of BRs has been shown to induce premature leaf senescence (for reviews, see Clouse and Sasse, 1998; Schippers et al., 2007). In addition, the receptor kinases BRASSINOSTEROID INSENSITIVE 1 (BRI1) and BRI1-ASSOCIATED RECEPTOR KINASE (BAK1) were shown to be implicated in senescence regulation (He et al., 2007). Loss of BRI1 results in delayed senescence as well as in reduced male fertility, and altered light responses. However, a transcriptomic study of 99 BR-related genes suggests that the BR signaling pathway is not specifically regulated during senescence. By contrast, mutants impaired in BR biosynthesis and signaling suggest a role of BRs during senescence (Chory et al., 1991; Yin et al., 2002). In summary, more research is required to better understand the role of BR during senescence.

Gibberellins (GAs) are diterpene-type phytohormones that are known to promote stem and leaf development (Richards et al., 2001; Sun and Gubler, 2004). The effect of GAs on senescence is poorly understood. Studies from the 1960s using *Rumex* leaf discs and detached *Taraxacum* leaves indicate that GAs could delay leaf senescence (Fletcher and Osborne, 1966; Goldthwaite and Laetsch, 1968). Although not extensively characterized, several more recent reports suggest a retarding effect of GA on leaf senescence (reviewed in Schippers et al., 2007).

Nitric oxide (NO), a member of the reactive oxygen species (ROS) family also considered as a phytohormone, is a signaling molecule implicated in numerous physiological processes (Besson-Bard et al., 2008). Published evidence suggests that NO negatively regulates senescence (Guo and Crawford, 2005; Mishina et al., 2007). Moreover, in pea, NO levels decrease during senescence (Corpas et al., 2004). Recently, Ma et al. (2010) provided genetic evidence that Ca^{2+} uptake and NO production are linked and play central roles in leaf senescence (Ma et al., 2010).

Reactive oxygen species

ROS, continuously formed in mitochondria, chloroplasts and peroxisomes, are by-products of aerobic metabolism (Apel and Hirt, 2004). The ROS family includes oxygen-containing molecules with unpaired electrons, i.e. singlet oxygen, superoxide, nitric oxide (see above) and hydroxyl radicals. ROS production affects plant cells either through damage by reacting with macromolecules or by acting as signaling molecules (Møller et al., 2007). Moreover, some oxidation products generated by ROS damage act as secondary signaling molecules. Plants possess enzymes (catalase, superoxide dismutase, ascorbate peroxidase) and antioxidant molecules (ascorbate, glutathione, tocopherol and others) involved in scavenging ROS (Apel and Hirt, 2004; Procházková and Wilhelmová, 2007).

Leaf senescence involves the breakdown of proteins, lipids, DNA and tetrapyrroles that often results in ROS production (Fischer, 2012; Thompson et al., 1998). As a result, antioxidant enzymes such as alternative oxidases, glutaredoxins and enzymes involved in the synthesis of tocopherol seem to be upregulated during senescence in Arabidopsis (Buchanan-Wollaston et al., 2005). However, the finding that CATALASE2 is down-regulated during senescence highlights the fact that ROS homeostasis during senescence is more complex than expected (Zimmermann et al., 2006). ROS are not only toxic by-products but also signaling molecules. Indeed, a systematic review of studies assessing activities of plant antioxidant

Study of leaf senescence *in vivo*: experimental considerations

Two main different approaches are used to study leaf senescence *in vivo*. The first one, with sampling of naturally senescent leaves on the plant, is recommended to investigate age-dependent leaf senescence. The limitation of this procedure is the possible heterogeneity and amount of material that can be sampled, especially in the case of small annual plants such as Arabidopsis. The other approach uses the fact that prolonged darkness triggers leaf senescence. The plant is either entirely incubated in the dark (whole darkened plants; DP) or only partially, a treatment known as individual darkened leaves (IDL). Another way to induce leaf senescence with darkness is to detach leaves from the plant and incubate them in the dark, a method often used to study Chl breakdown. In addition to these two approaches, phytohormones such as ethylene, JA or ABA are often used to promote and/or accelerate leaf senescence (see section "Phytohormones"). While interpreting the result(s) of studies on leaf senescence, it is very important to consider which of these methods has been used. Indeed, genome-wide transcriptional and physiological comparisons revealed similarities but also some differences between these different treatments used to induce leaf senescence (Buchanan-Wollaston et al., 2005; Keech et al., 2007; Van der Graaff et al., 2006).

enzymes revealed that ROS homeostasis during senescence is not completely understood due to the involvement of ROS in both signaling and cellular damage (Procházková and Wilhelmová, 2007).

Up-regulation of SAGs and senescence-associated transcription factors during oxidative stress revealed an overlap between senescence mechanisms and oxidative stress responses (Balazadeh et al., 2011, 2010; Navabpour et al., 2003). Recently, the NAC transcription factor JUNGBRUNNEN1 (JUB1) (see section "NAC transcription factors") was identified as a positive regulator of leaf longevity because of its negative effect on H_2O_2 levels (Wu et al., 2012). Leaf longevity and oxidative stress tolerance have also been linked in studies of Arabidopsis *ore1*, *ore3*, and *ore9* (Woo et al., 2004). These mutants exhibit delayed senescence as well as oxidative stress tolerance. This effect does not seem to be due to enhanced ROS-scavenging enzyme activity, indicating that other mechanism(s) are responsible for the extended leaf longevity.

ROS homeostasis is also connected to redox balance (Foyer and Noctor, 2005). Arabidopsis CONSTITUTIVE EXPRESSION OF PATHOGENESIS-RELATED GENES 5 (CPR5) has been proposed to regulate cell-death and senescence by controlling redox balance (Jing et al., 2007, 2008). Early senescence induced by mutations in *CPR5* has been linked with the up-regulation of many genes in the ROS gene network and increase of glutathione S-transferase protein levels. Moreover, defects in biosynthesis of the redox carrier NAD described in the *old5* mutant also results in early age-induced leaf senescence (Schippers et al., 2008). Taken together, these results clearly show that ROS production is a consequence but also a cause of leaf senescence and suggest the existence of cross-talk between onset of senescence, ROS signaling and redox homeostasis. These studies illustrate that ROS homeostasis is a metabolic interface for signals derived from metabolism and the environment (Foyer and Noctor, 2005).

Transcription factors

Up to 185 transcription factors, belonging to 20 different families, have been shown to be positively or negatively regulated during senescence (Balazadeh et al., 2008; Buchanan-Wollaston et al., 2005; Chen et al., 2002; Guo et al., 2004; Lin and Wu, 2004). Most studies on transcriptional regulation of leaf senescence involved transcription factors of the NAC and WRKY families. NAC is an acronym derived from the names of the three genes first described as containing the conserved domain of this family, namely NO APICAL MERISTEM (NAM), ARABIDOPSIS TRANSCRIPTION ACTIVATION FACTOR 1 and 2 (ATAF1 and 2), and CUP-SHAPED COTYLEDON 2 (CUC2) (Aida et al., 1997; Souer et al., 1996). WRKY comes from the highly conserved amino acid sequences occurring within this family of DNA-binding proteins (Rushton et al., 1996).

NAC transcription factors

The Arabidopsis NAC family contains around 100 transcription factors that are involved in embryo and shoot meristem development, lateral root formation, auxin signaling, and defense response (Guo and Gan, 2006). Twenty NAC transcription factors (one fifth of the family) showed enhanced expression during natural and dark-induced senescence. *At*NAP, one of the senescence-enhanced NAC transcription factors, has been shown to positively regulate senescence (Guo and Gan, 2006). Inducible overexpression of AtNAP causes precocious senescence and its mutation results in increased leaf longevity. Recently, AtNAP, ABA signaling and a protein phosphatase 2C were shown to be implicated in a regulatory mechanism that controls stomatal movement and water loss during leaf senescence (see also section "Abscisic acid"; Zhang and Gan, 2012). Another Arabidopsis NAC transcripton factor, AtNAC2 (also called ANAC092 or ORE1), was first identified by the delayed leaf senescence phenotype resulting from its mutation (Oh et al., 1997). A role for small RNAs during senescence was discovered while characterizing how AtNAC2 negatively regulates leaf longevity (Kim et al., 2009b). Small RNAs are 19–27 nucleotide long RNAs that post-transcriptionally silence genes involved in many developmental processes (Chen, 2010; Chuck and O'Connor, 2010). Kim et al. (2009b) provide evidences that miR164 down-regulates AtNAC2 during growth and development of young leaves. JUB1, an Arabidopsis H_2O_2-induced NAC transcription factor, was shown to increase leaf longevity by regulating the cellular H_2O_2 homeostasis network (see also section "Reactive oxygen species"; Wu et al., 2012). Notably, JUB1 overexpression down-regulates the expression of SAG genes, whereas these SAGs are up-regulated in *jub1*. It is not clear yet whether JUB1 controls SAG expression by its impact on H_2O_2 levels or via other target genes (Wu et al., 2012). In contrast to JUB1, ORE1 SISTER1 (ORS1), another H_2O_2-induced NAC transcription factor, was described as a positive regulator of senescence in Arabidopsis that adds to the functions of *At*NAP and *At*NAC2 (Balazadeh et al., 2011).

WRKY transcription factors

Besides disease resistance, roles for WRKY transcription factors during senescence have been described (Balazadeh et al., 2008; Eulgem and Somssich, 2007). WRKY53 is involved in the first events of senescence and acts as a positive regulator (Hinderhofer and Zentgraf, 2001; Miao et al., 2004). Putative targets of WRKY53 include SAGs, stress-related genes and six other members of the WRKY gene family (Miao et al., 2004). Recently, a study demonstrated that degradation of WRKY53 was mediated by E3 UBIQUITIN LIGASE PROTEIN 5 (UPL5), showing that selective ubiquitination can negatively regulate leaf senescence (Miao and Zentgraf, 2010). The JA-inducible protein EPITHIOSPECIFYING SENESCENCE REGULATOR (ESR) was identified to interact with WRKY53. Leaf senescence is accelerated in *esr* mutants indicating a cross-talk between ESR, WRKY53 and JA during senescence processes (Miao and Zentgraf, 2007). Loss of WRKY70, another WRKY transcription factor, promotes dark-induced senescence and is thought to negatively regulate leaf senescence (Ülker et al., 2007). Finally, other WRKY transcription factors, WRKY4, 6, 7, 11, were shown to be strongly expressed in senescent leaves but their roles remain unknown (Robatzek and Somssich, 2001). WRKY6 is highly up-regulated during senescence and regulates expression of genes associated with senescence and pathogen response but its loss does not seem to affect leaf senescence (Robatzek and Somssich, 2002).

Kinases

During plant senescence, kinases play roles as receptors and enzymes (reviewed in Fischer, 2012). Several studies on leaf senescence, already mentioned in other sections, involve kinases. RPK1 and AHK3 kinases have been shown to be involved in cytokinin signaling (see section "Cytokinins"). *At*HXK1 and SUCROSE NONFERMENTING-1-RELATED PROTEIN KINASE-1 (SnRK1) are known to link primary metabolism and leaf senescence (see section "Sugar levels"). Finally, a study of BRI1 and BAK1 connect senescence and brassinosteroid signaling (see section "Brassinosteriods, Gibberellins and Nitric oxide"). In addition, other studies highlight functions of protein kinases during senescence. For instances, a mitogen-activated protein kinase (MAPK) signaling pathway seems to positively regulate senescence via a MITOGEN-ACTIVATED PROTEIN KINASE 6 (MPK6) - MAPK KINASE 9 (MKK9) cascade and

a soybean leucine-rich repeat receptor kinase seems to regulate chloroplast development and chlorophyll (Chl) accumulation (Li et al., 2006; Zhou et al., 2009). Finally, silencing of Arabidopsis TARGET OF RAPAMYCIN (TOR) kinase is known to induce early leaf yellowing as well as to arrest growth (Deprost et al., 2007). However, since TOR has broad functions in plant development, it is not clear if TOR directly or indirectly regulates senescence.

Selective protein degradation

Components of the ubiquitin-dependent protein degradation appear to be involved in senescence regulation. The F-box protein ORE9 (see also section "Ethylene") was shown to interact with components of the ubiquitin E3 ligase complex (Woo et al., 2001). Woo et al. (2001) suggested that Arabidopsis *ORE9* limits leaf longevity through proteasome-mediated ubiquitin-dependent proteolysis of proteins that delay leaf senescence. This idea is corroborated by the finding that mutation of a rice ORE9 orthologous gene leads to increased leaf longevity (Yan et al., 2007). Other evidence for the involvement of ubiquitin-dependent protein degradation in senescence regulation comes from studies that show degradation of the transcription factor WRKY53 by the proteasome (see also section "WRKY transcription factors") and the involvement of SAUL1 in ABA regulation (see section "Abscisic acid").

Epigenetic control

Evidence suggests that chromatin architecture remodelling is involved in senescence regulation. The protein ORE7, containing an AT-hook DNA-binding motif, was shown to negatively regulate leaf senescence via changes in chromatin structure (Lim et al., 2007). Furthermore, histone deacetylation by HDA6, a histone deacetylase of Arabidopsis (see section "Jasmonates"), can alter the expression of FLOWERING LOCUS C (FLC), a transcription factor that controls the transition from vegetative to reproductive development (Wu et al., 2008). Histone methylation, another histone modification, is also implicated in the control of leaf senescence. Indeed, overexpression of SU(VAR)3-9 HOMOLOG 2 (SUVH2) histone methyltransferase gene inhibits the transcriptional initiation of WRKY53 and several SAGs, resulting in delayed leaf senescence (Ay et al., 2009). Finally, a recent genome-wide study of histone methylation classified activating and silencing marks in mature and naturally senescent Arabidopsis leaves, providing an initial epigenetic framework for the onset of senescence (Brusslan et al., 2012). Correlation between differences in histone methylation patterns and changes in gene expression revealed that H3K4me3 and H3K27me3 marks modulate the expression of senescence-regulated genes.

LEAF SENESCENCE: STRUCTURAL AND BIOCHEMICAL CHANGES

After the onset of senescence, leaves undergo processes that should be seen as "transdifferentiation" rather than as "deterioration" (Thomas et al., 2003). Recycling and detoxification of (macro-) molecules are indeed the consequences of structural and biochemical changes occurring during leaf senescence. Disintegration of cellular components is mediated through fine-tuned catabolic as well as anabolic steps that reduce deleterious effects of degradation intermediates and maximize nutrient remobilization (e.g. nitrogen, phosphorus, sulphur, minerals, metals ions and carbon skeletons; see Fig. I.1). This section has a clear focus on chloroplast-to-gerontoplast transition, one of the early cellular events of senescence which involves the degradation of Chl.

Changes at the whole leaf level

Age-dependent leaf senescence usually occurs from the tip or the margins towards the base (Lim et al., 2007; Thomas and Stoddart, 1980). Yellowing of the leaf can also be observed locally, for instance at the site of pathogen infection. In Arabidopsis, it has been demonstrated that local leaf chlorosis triggered by *Pseudomonas syringae* infection is mediated by a senescence-associated Chl degradation program (Mecey et al., 2011; Mur et al., 2010). At the tissue level, development of leaf senescence seems to share similar features with senescence of rice coleoptiles (Inada et al., 1998). Senescence starts from the inner mesophyll cells towards the outer epidermis, excluding tissues along vascular bundles. Little is known about the senescence pattern of epidermis cell. Interestingly, guard cells have been shown to keep intact chloroplasts until the latest steps of senescence, in order to maintain their function in gas exchange (Zeiger and Schwartz, 1982). In most genetic and biochemical studies, leaf senescence is mostly referred to as mesophyll senescence, despite the fact that whole leaf samples were collected. However, each of the other tissues of the leaf has its own pattern and timing of senescence, not necessarily synchronized with that of the mesophyll (Thomas and Stoddart, 1980). Therefore, single-cell "–omics" studies could provide more accurate measurements by excluding the "noise" from vascular and epidermal tissues (Fischer, 2012).

Disintegration of intracellular organelles and cytoskeleton

Dismantling of the different organelles during leaf senescence is not synchronized. The first structural changes appear in the chloroplast (see section "Focus on chloroplast-to-gerontoplast transition" for details) whereas the mitochondria and nucleus remain (at least partially) intact until the latest steps of leaf senescence (Del Rio et al., 2003; Inada et al., 1998; Keech et al., 2007). Interestingly, mitochondria numbers of Arabidopsis mesophyll cells have been reported to dramatically decrease (up to 75%) whereas chloroplast numbers were shown to be only partially reduced (up to 30%) in IDL treated leaves (Keech et al., 2007; Wada et al., 2009). However, chloroplast size decreases considerably during leaf. The energy produced by the remaining mitochondria is thought to be essential for the degradation and recycling of other cellular components (e.g. chloroplasts) and to contribute to an efficient remobilization of nutrients from senescing leaves towards the rest of the plant (Keech et al., 2007).

During leaf senescence, changes also occur in the cytoskeleton network. Natural and dark-induced leaf senescence was shown to be accompanied by a partial degradation of cortical microtubules and actin microfilaments (Keech et al., 2010). It is still unclear if the remaining fraction of the cytoskeleton in senescent cells is sufficient to sustain intracellular trafficking such as vesicles shuttling or if other mechanisms are involved. This partial loss of the cytoskeleton could explain that chloroplasts and mitochondria tend to aggregate in senescent cells (Keech et al., 2007; Simeonova et al., 2000). However, mitochondria are still moving in the cytosol during senescence (Keech, 2011). Analysis of transcript abundance of genes encoding cytoskeleton-related proteins suggests that actin filaments could be responsible for their remaining mobility (Keech, 2011).

Disruption of the nucleus (DNA laddering), disintegration of the mitochondria and peroxisomes, and vacuolar collapse are the very late steps or the inevitable fate of leaf senescence, depending on the

Regreening after yellowing: study of poikilochlorophyllous resurrection plants

Leaf senescence is considered to be reversible until a point of no return (Thomas et al., 2003). Indeed, chloroplast-to-gerontoplast transition has been shown to be reversible in *Nicotiana rustica* (Zavaleta-Mancera et al., 1999a, 1999b). Shoot decapitation of senescing *Nicotiana rustica* plants leads to leaf regreening, an effect that is enhanced by cytokinin treatment. Leaf regreening was shown to involve resynthesis of functional thylakoid membranes within gerontoplasts and not to be due to a *de novo* formation of chloroplasts. In Chapter "4", we provide evidence that de- and re-greening of leaves observed during dehydration of the resurrection plant *Xerophyta viscosa* share similar features with the mechanism described above for *Nicotiana rustica*. *Xerophyta viscosa* is a poikilochlorophyllous plants, meaning that it loses most of the Chl and dismantles the photosynthetic apparatus during dehydration (Sherwin and Farrant, 1996; Tuba et al., 1998, 1994). Upon rehydration, leaves of poikilochlorophyllous plants regreen and recover their photochemical activity rapidly (Farrant, 2000). In the study presented in Chapter "4", we demonstrate that Chl breakdown during transition of chloroplasts to xeroplasts (chloroplasts of dehydrated *X. viscosa* leaves) follows the "PAO pathway". This finding indicates that chloroplast dismantling during dehydration of resurrection plants and leaf senescence involves similar mechanisms sharing the same goal: maintenance of cell viability. In this comparison, processes such as ordered degradation of Chl maximize cell viability to ensure efficient nutrient remobilization (leaf senescence) or survival under drought stress (dehydration of resurrection plants).

point of view (see section "Leaf senescence and programmed cell-death: a semantic debate"; Cao et al., 2003; Jiménez et al., 1998; Simeonova et al., 2000; Yen and Yang, 1998; Zimmermann and Zentgraf, 2005). The disruption of the plasma membrane is the final event leading to cell death.

Leaf senescence and programmed cell-death: a semantic debate

The concept of plant "senescence" and "programmed cell-death" are often used together. However, definition of "ageing", "death" and "senescence" is still debated and confusions arise from the different definitions given to these terms (reviewed in Thomas, 2013b; van Doorn and Woltering, 2004). Leaf senescence implies PCD or leads to PCD, depending on the definition of senescence employed. Some authors propose that PCD and senescence are overlapping processes, suggesting the idea of a "leaf senescence-associated cell death" (Lim et al., 2007). Others claim that there is no overlap at all between senescence and PCD. This second opinion argues that senescence corresponds to leaf yellowing before a point of no return and PCD to the process after it (Thomas et al., 2003). Even if a few cases of "regreening after yellowing" have been described (See separated panel "Regreening after yellowing: study of poikilochlorophyllous resurrection plants"), there is no doubt that leaf senescence processes lead directly or indirectly to death (Thomas, 2013b; Thomas et al., 2003; van Doorn and Woltering, 2004). However, defining the chronology of events occurring between the onset of senescence and cell death remains one of the main challenges for scientists working on plant senescence.

On one hand, molecular comparisons between senescence and PCD processes involved in others plant responses revealed that proteins involved in pathogen-induced hypersensitive response (HR) (such as pathogenesis-related proteins and HAIRPIN-INDUCED 1 (HIN1), an HR cell death marker) are also up-regulated in the late stages of senescence (Quirino et al., 2000, 1999; Takahashi et al., 2004). Moreover, members of the vacuolar processing enzymes (VPE) family, which are involved in vacuole-mediated cell death in response to a variety of stress inducers such as TMV infection, were shown to be up-regulated during senescence (Hatsugai et al., 2004; Yamada et al., 2005). Donnison et al. (2007) demonstrated that the VPE protease See2β of tobacco plays a major role in nitrogen use efficiency and resource allocation (Donnison et al., 2007). See2β was also shown to have a minor but significant function during senescence. On the other hand, some genes are specific either for HR or for senescence (e.g. SAG12) and a global transcriptome

comparison between natural leaf senescence and starvation-induced death of suspension culture cells revealed some similarities but also many differences between these two treatments (Buchanan-Wollaston et al., 2005; Pontier et al., 1999). Cytochrome C release by the mitochondria has been described to be a trigger for some plant PCD processes but there is no evidence for that during senescence processes (reviewed in Vianello et al., 2007).

Collectively considered, these observations indicate that some proteins involved in PCD processes such as the HR play also a role during leaf senescence. However, it is important to consider that the main function of most PCD is to kill the cell (HR, xylem formation,...) whereas the goal of leaf senescence processes is to remobilize cell nutrients to other plant organs. This remobilization, which involves partial breakdown of many plant components, is absolutely dependent on cell viability (Fig. I.1; Thomas, 2013b; Thomas et al., 2003). This is in line with the finding that genes suppressing PCD, such as Bax inhibitor-1 and DEFECTIVE IN ANTHER DEHISCENCE 1 (DAD1), are up-regulated during senescence and their expression is repressed only when recycling has been completed (see Reape and McCabe (2008) for more details). In cucumber, PCD markers were not found until 12 h before the death of the organ, suggesting that PCD starts only when nutrient remobilization, the senescence phase, is completed (Delorme et al., 2000; Reape and McCabe, 2008). To conclude, there are strong arguments in favour of a clear distinction between senescence (transdifferentiation phase) and PCD that is triggered when nutrient remobilization has occurred. The fact that some proteins involved in PCD such as the HR play also a role during nutrient remobilization can partially explain this confusion.

FOCUS ON CHLOROPLAST-TO-GERONTOPLAST TRANSITION

Dismantling of complex photosynthetically active chloroplasts should be seen as breaking down a nuclear power plant: each step must be organized and regulated in order to avoid potential damage by a release of free components. Chloroplasts contain up to 75% of the nitrogen present in mesophyll cells (Peoples and Dalling, 1988). Most of this nitrogen is contained within proteins involved in photosynthesis, the most abundant one being Rubisco. This section describes the transition of chloroplasts to gerontoplasts that occurs during leaf senescence. Chloroplast to gerontoplast transition involves many biochemical reactions that are reflected by a decrease of chloroplast size, loss of stromal and thylakoid components, and formation of vesicular bodies called pastoglobules (PGs). The envelope of developing gerontoplasts remains intact during all sub-organellar modifications, indicating that we should consider this process more as a developmental rather than disintegration event (Matile et al., 1999; Parthier, 1988). This section highlights that lipid and protein remobilization from the chloroplast during leaf senescence is intimately connected to Chl degradation, the focus of my thesis.

Chloroplast lipid degradation during leaf senescence

Thylakoid membranes comprise about 70% of the membrane lipids in mesophyll cells (Smallwood et al., 1996). The most abundant lipids are the glyceroglycolipids monogalactosyldiacylglycerol (MGDG) and digalactosyldiacylglycerol (DGDG), which represent around 50 and 25 mol%, respectively, of total thylakoid lipids (Block et al., 1983). MGDG and DGDG are also abundant in the inner and outer envelope membranes of plastids. The galactose head of MGDG is linked to the glycerol backbone through a β-glycosidic bound. DGDG contains an additional galactose moiety bound in an α-glycosidic linkage to the galactose of MGDG (Dörmann and Benning, 2002). Phosphatidylcholine, phosphatidylinositol, phosphatidylglycerol and sulfolipids are minor constituents of plastid membranes (Smallwood et al., 1996).

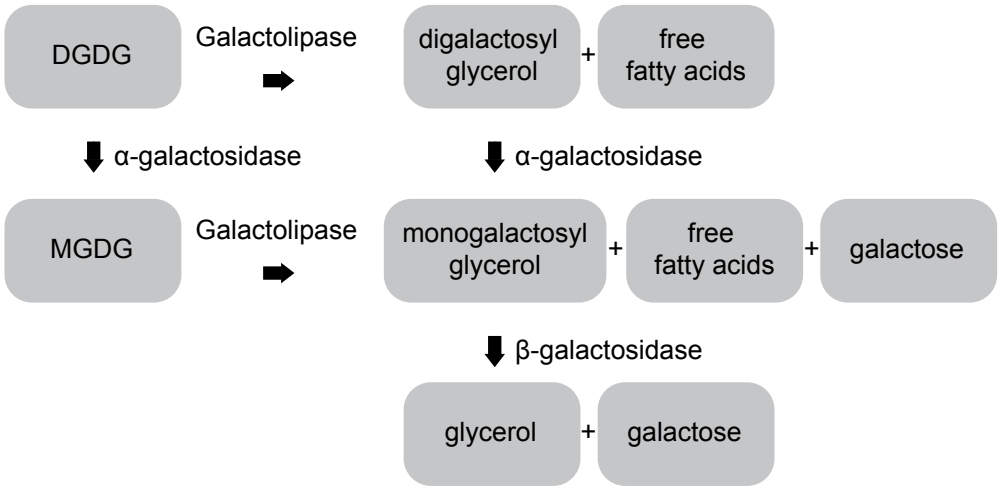

Figure I.2. Galactolipid degradation. MGDG and DGDG can theoretically be degraded by galactolipases and galactosidases, leading to the formation of free fatty acids, glycerol and galactose. See text for more information. Adapted from Bhalla and Dalling (1984).

Thylakoid galactolipid degradation is considered to be one of the first steps of the chloroplast to gerontoplast transition (Lee et al., 2009). α-galactosidase, β-galactosidase and galactolipase, rather than non-enzymatic peroxidation induced by ROS, are thought to mediate MGDG and DGDG degradation during senescence (Fig. I.2; Thompson et al., 1998). In rice, the α-galactosidase OsAkαGal was shown to be localized to the chloroplast, and to degrade α-1,6-galactosyl oligosaccharides and DGDG *in vitro* (Lee et al., 2009). Furthermore, OsAkαGal expression is induced by phytohormones (JA and SA), extended darkness and other stresses, and an OsAkαGal null mutant displays delayed leaf senescence. Lee et al. (2009) proposed that OsAkαGal converts DGDG to MGDG and plays a critical role during thylakoid membrane disassembly. However, their study does not provide any lipid measurement, and thus, cannot confirm if DGDG is retained during senescence of OsAkαGal null mutant. Indeed, the first steps of galactolipid degradation may also be the deesterification of the fatty acid moieties by galactolipases, enzymes that are induced by drought stress, chilling, and senescence (Fig. I.2; Kaniuga and Gemel, 1984; Kaniuga et al., 1999; Matos et al., 2001). Galactolipase activity produces free fatty acids and either mono- or digalactosylglycerol as by-products, depending on whether the substrate is MGDG or DGDG, respectively (Anderson et al., 1974; Bhalla and Dalling, 1984). It can therefore be suggested that α-galactosidases such as OsAkαGala act on digalactosylglycerols rather than DGDG. Interestingly, characterization of the closest homologue of OsAkαGala in Arabidopsis (*At*DIN10) presented in Chapter "6", reveals that *At*DIN10 is most probably not involved in galactolipid degradation during senescence but rather in chloroplastic raffinose degradation during cold deacclimation.

Phospholipase D , phosphatidic acid phosphatase, acyl hydrolase and lipoxygenase are up-regulated during senescence and may also participate to thylakoid degradation (Thompson et al., 1998). Despite the low abundance of phospholipids, compared to glyceroglycolipids, in chloroplast, their degradation has been proposed to be a trigger of chloroplast dismantling (He and Gan, 2002; Thompson et al., 1998). Silencing of SAG101, an acylhydrolase, was shown to delay the onset of leaf senescence in Arabidopsis (He and Gan, 2002). SAG101 is thought to initiate the hydrolysis of phospholipids, perturb the thylakoid membrane and thus to facilitate hydrolysis of membrane lipids by other lipid-degrading enzymes. Finally, suppression of phospholipase D α in Arabidopsis has been shown to delay senescence of detached leaves treated with ABA and ethylene but does not affect age-dependent senescence (Fan et al., 1997).

Free fatty acids produced by thylakoid lipid degradation during senescence are either oxidized to provide energy for the senescence processes or metabolized to α-ketoglutarate via the glyoxylate cycle (Hörtensteiner and Feller, 2002; Thompson et al., 1998). The energy contained in α-ketoglutarate can be remobilized by its conversion into phloem-

mobile sugars through gluconeogenesis or used for mobilization of amino acids produced by senescence-associated protein degradation. Recently, a study of two acyltransferases localized in PGs suggested that a part of the fatty acid pool produced during leaf senescence is converted into fatty acid phytyl esters and triacylglycerol (see below).

PG are low-density lipoprotein particles of a size of 45 to 60 nm and are considered as distinct subcompartments of the thylakoid membrane (Austin et al., 2006; Bréhélin and Kessler, 2008; Piller et al., 2012). These plastid lipid droplets are surrounded by a polar lipid monolayer contiguous with the thylakoid outer lipid layer and in their center contain neutral lipids such as prenylquinones, triacylglycerols and carotenoids (Austin et al., 2006; Vidi et al., 2006). Size and number of PGs increase during chloroplast to gerontoplast transition. This observation led to the idea that PGs may be involved in lipid storage when stress or plant development affects thylakoid components. In fact, proteomic studies revealed PG function to go beyond passive lipid storage, because they contain more than 30 proteins classified in plastoglobulins, chloroplast metabolic enzymes, and proteins with unknown function (Vidi et al., 2006; Ytterberg et al., 2006). Plastoglobulins (also called plastid lipid-associated protein or fibrillins) surround PGs and play a structural role (Deruère et al., 1994). PG-localized tocopherol cyclase VITAMIN E 1 (VTE1) and NAD(P)H dehydrogenase C1 (NDC1) have been shown to be involved in prenylquinone (tocopherol or vitamin E), phylloquinone (vitamin K1) and plastoquinone biosynthesis (Besagni and Kessler, 2013; Piller et al., 2012; Vidi et al., 2006). Furthermore, two acyltransferases identified in the plastoglobule proteome, called PHYTYL ESTER SYNTHASE (PES) 1 and 2, catalyze the synthesis of phytyl ester and participate in the regulation of free phytol and fatty acid content during stress and senescence (Lippold et al., 2012). Chl breakdown generates significant amounts of free phytol which was thought to be remobilized via phytol-diphosphate through the action of two kinases (Ischebeck et al., 2006; Valentin et al., 2006). Characterization of PES 1 and 2 provides evidences for an alternative route for the fate of free phytol, through fatty acid phytyl esters (FAPEs) synthesis in PG. Finally, Lippold et al. (2012) suggested that PES1 and 2 may also be implicated in triacylglycerol (TAG) accumulation in PGs because their accumulation is decreased by 30% in leaves of *pes1pes2* during nitrogen deprivation (Lippold et al., 2012).

Chloroplast protein degradation during leaf senescence

Chloroplasts have been shown to contain up to 75% of the nitrogen content in phytosynthetic tissues (Makino and Osmond, 1991; Peoples and Dalling, 1988). Rubisco, the most abundant protein of the chloroplast, accounts for 20–30% of total leaf nitrogen (Feller et al., 2008 and references therein). Protein complexes of the thylakoids such as photosystems (PS) constitute the second largest pool of chloroplast nitrogen (Hörtensteiner and Feller, 2002). During leaf senescence, stromal and thylakoid proteins are degraded and nitrogen contained within the amino acids is directly or indirectly remobilized to growing organs (Hörtensteiner and Feller, 2002). Chloroplast protein degradation starts and takes place, at least in part, in the chloroplasts. It has been shown that intact isolated chloroplasts or chloroplast lysates can degrade Rubisco (Feller et al., 2008 and references therein). Exo- and endopeptidases are thought to cleave stromal and thylakoid proteins into oligopeptides and amino acids that are then exported into the cytosol (Hörtensteiner and Feller, 2002). To my knowledge, no chloroplast oligopeptide or amino acid transporters have been shown to be specifically involved in amino acid transport across the envelope during senescence. It can be speculated that members of the PLANT PREPROTEIN AND AMINO ACID TRANSPORTER (PRAT) superfamily localized at the inner and outer envelopes may export protein degradation products during chloroplast senescence (Pudelski et al., 2010). An alternative pathway for chloroplast protein degradation, described separately in section “Autophagy and senescence-associated vesicles (SAV)”, assumes that a fraction of chloroplast proteins is transported and extraplastidially degraded by senescence-associated vesicles (SAVs) and autophagy mechanisms.

Despite the identification of numerous plant proteases and the senescence-specific expression of some of them, there are only few evidences that clearly demonstrate their specific involvement in chloroplast

One visual stay-green phenotype, several different genetic disorders

Visual stay-green phenotypes (retention of Chl) during leaf senescence of mutants from natural populations, mutagenesis screens or genetically-modified lines can be due to different genetic lesions leading to diverse physiological changes (Thomas and Howarth, 2000). Five ways of "staying green" have been defined by looking at the evolution of Chl content and photosynthetic capacity during leaf senescence of different stay-green mutants (Fig. I.3). These five groups (Type A to E) differ by the initial value of these two parameters prior to senescence as well as by the time of initiation and rate of their decrease during leaf senescence. As a general rule, modifications of expression of genes involved in the regulation of leaf senescence, e. g. transcription factors, lead to functional stay-green phenotypes (Type A and B), whereas deletions of genes involved in chloroplast dismantling processes, such as Chl breakdown, result in Type C (cosmetic stay-green) or Type D (cell-death phenotype) due to the retention of Chl or soluble toxic Chl catabolites, respectively.

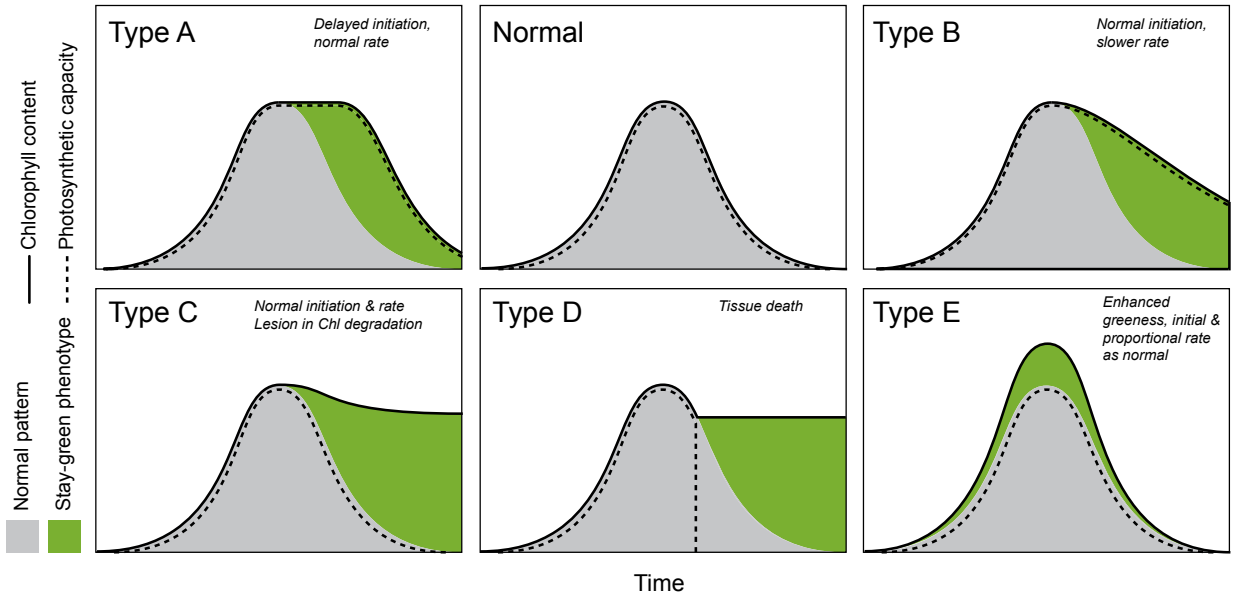

Figure I.3. Five ways to stay-green. Curves show Chl content and photosynthetic capacity (arbitrary scale). After a delay of initiation of senescence, type A stay-greens lose Chl and function at the normal rate. In Type B, senescence is initiated on time, but subsequently proceeds slower. Type C stay-greens undergo senescence on a normal time scale, but have a lesion in Chl breakdown. Type D represents stay-greens that retain color because of a sudden death. In type E behaviour, the photosynthetic capacity of an intensely green genotype may follow the normal ontogenetic pattern but comparison of absolute pigment contents identifies it as a stay-green. Copied and redrawn from Thomas and Howarth, (2000).

protein degradation during leaf senescence (Bhalerao et al., 2003; Buchanan-Wollaston et al., 2003; Guo et al., 2004; Roberts et al., 2012). The following paragraphs describe a selection of senescence-related studies on members of the four plant protease families: serine proteases, aspartic proteases, cysteine proteases and metalloproteases (for a detailed review, see Roberts et al., 2012).

Serine proteases (SPs) are the largest class of proteases in plants (Van der Hoorn, 2008). SPs seem to play a role during leaf senescence in wheat and barley (Roberts et al., 2012 and references therein). Up-regulation of SP members, called subtilisin-like proteases, has been correlated with Rubisco and light harvesting complex (LHC) II degradation, and nitrogen remobilization. However, there is no *in vivo* evidence demonstrating the direct involvement of subtilisin-like proteases in chloroplast protein degradation during senescence. Subunits of the proteolytic core of the Clp protease (caseinolytic protease) complex of plastids, which is highly homologous to prokaryotic proteases, are also classified as SPs (Olinares et al., 2011; Roberts et al., 2012). The Clp protease system consists of two multi-subunit components, a catalytic core and a chaperone with ATPase activity involved in the recognition, unfolding and translocation of protein substrates into the proteolytic compartment (Roberts et al., 2012). In

Arabidopsis, most Clp subunits are localized to the stroma of plastids and are thought to be implicated in degradation of abnormal, damaged or short-lived proteins (Kato and Sakamoto, 2010). Several chloroplast Clp protease subunits are specifically regulated during dark-induced senescence (Lin and Wu, 2004). For instance, mRNA levels of Arabidopsis EARLY RESPONSE TO DEHYDRATION 1 (ERD1, also called ClpD, ClpC-like or SAG15), a component of the chaperone multi-subunit, was shown to increase during senescence whereas its protein level decreases (Weaver et al., 1999). The inconsistency between mRNA and protein levels of ERD1 in senescent leaves could either be due to post-translational regulation or to degradation of ERD1 together with its substrate(s) in the proteolytic core of the Clp protease system. To date, no senescence-related phenotype has been found in ERD1 mutants and direct evidences for an involvement of the Clp protease system during senescence are still lacking (Olinares et al., 2011; Bastien Christ and Stefan Hörtensteiner, unpublished data). Finally, members of Deg proteases, another subfamily of SPs, are associated with the stromal side of the thylakoid membrane (Kato and Sakamoto, 2010; Roberts et al., 2012). Recent studiesy of Arabidopsis Deg1 and Deg2 revealed that these proteases are involved in LHCII protein degradation (Lucinski et al., 2011; Zienkiewicz et al., 2012). Moreover, repression of Deg2 seems to delay senescence, clearly indicating the involvement of Deg2 in the chloroplast senescence program (Lucinski et al., 2011).

Members of the class of aspartic proteases (APs), the second largest class of plant proteases, have been suggested to be involved in chloroplast-to-gerontoplast transition (see Roberts et al., 2012; van der Hoorn, 2008 for more information). The strongest evidence comes from the studies on the *CHLOROPLAST NUCLEOID DNA-BINDING PROTEIN 41* (CND41) protease from tobacco leaves (Kato et al., 2005, 2004). Suppression of CND41 results in delayed leaf senescence as well as in retention of Rubsico in older leaves whereas overexpression of CND41 has the opposite effects.

One of the most known and studied member of the class of cysteine proteases (CPs) is SAG12, often used as senescence marker because of its senescence-specific expression (Guo et al., 2004). SAG12 was shown to accumulate in SAVs (see section " Autophagy and senescence-associated vesicles (SAV)"; Otegui et al., 2005). Presence of SAG12, Rubisco and glutamine in SAVs suggests them to be involved in the degradation of chloroplast stromal proteins during senescence (Martínez et al., 2008). The expression of two papain-like CP genes has been reported during senescence in barley, sweet potatoes and soybean, and it was suggested that this family of CPs may be involved in bulk protein degradation during senescence (Roberts et al., 2012 and references therein). VPEs are CPs involved in vacuole-mediated cell death during stresses and developmental processes such as senescence (Hara-Nishimura et al., 2005). Rojo et al. (2003) suggested a role for γVPE in the activation of downstream proteases involved in amino acid recycling during senescence (Rojo et al., 2003). Finally, metacaspases and cathepsins belonging to the class of plant CPs were proposed to be involved in cell death mechanisms, but direct evidence for their involvement during senescence are lacking (see Roberts et al., 2012 for more detail).

The membrane-bound FtsH proteases are the best characterized subfamily of metalloproteases (MPs) (Kato and Sakamoto, 2010). FtsHs are ATP-dependent proteases that contain a zinc-binding domain. Nine out of twelve Arabidopsis FtsHs are predicted to be targeted to the chloroplast and four of them have experimentally been demonstrated to localize to thylakoid membranes (Kato and Sakamoto, 2010). Despite the up-regulation during senescence of some members of the Arabidopsis FtsH family, there is no *in vivo* study demonstrating a role for FtsHs during this process (Guo et al., 2004; Roberts et al., 2012). Zelisko et al. (2005) suggested a possible involvement of FtsH6 in LHCb3 degradation during dark-induced senescence, but this hypothesis was later rejected (Zelisko et al., 2005). Wagner et al. (2011) did not find any differences in LHCb3 degradation between wild-type plant and three mutant lines for FtsH6 during natural growth, high light acclimation or senescence (Wagner et al., 2011). Lastly, loss of MPs belonging to the leucine aminopeptidase and matrix metalloproteinase families has been associated with accelerated leaf senescence in Arabidopsis but their exact role remains unknown (Golldack et al., 2002; Waditee-Sirisattha et al., 2011).

Autophagy and senescence-associated vesicles (SAVs)

Autophagy (meaning "self-eating") is defined as a degradation pathway for recycling cytoplasmic components during stress and development (Liu and Bassham, 2012). The core of the autophagy pathway seems to be conserved among between yeast, animals and plants, and is composed of about 20 autophagy-related genes (ATG; Liu and Bassham, 2012 and references therein; Nakatogawa et al., 2009). Compared with wild-type plants, several ATG mutants display an early senescence phenotype and are more affected by stress conditions. In Arabidopsis, autophagy mechanisms have been reported to be responsible for the slight decrease of chloroplast numbers observed during senescence of mesophyll cells (Wada et al., 2009). Wada et al. (2009) demonstrated that whole chloroplast autophagy in the vacuole is responsible for a 30% decrease in chloroplast number of IDL treated leaves (Wada et al., 2009). Several reports indicate that autophagy is also involved in chloroplast degradation during senescence via Rubisco-containing bodies (RCBs) (Chiba et al., 2003; Ishida et al., 2008; Izumi et al., 2010; Wada et al., 2009). RCBs are thought to emerge from the chloroplast envelope into the cytosol and then to be engulfed by the vacuole (Ishida and Wada, 2009). Absence of RCBs in IDLs of autophagy-defective plants indicates that RCB formation is autophagy-dependent. Moreover, chloroplast shrinkage during senescence (gerontoplasts are much smaller that chloroplasts) is suppressed in IDLs of autophagy mutants (Wada et al., 2009). Thus, chloroplast size decrease seems to be connected with autophagy and presumably with RCB formation (Ono et al., 1995; Wada et al., 2009).

Although Rubsico has been shown to be translocated to the vacuole in an autophagy-dependent manner, Rubisco is degraded at the same rate in IDLs of ATG mutants and wild-type plants (Wada et al., 2009). This raises the question: What is the contribution of RCBs to Rubisco degradation during senescence? It has recently been shown that, with up to 40 percent during the first days of IDL treatment, autophagy substantially contributes to Rubisco degradation (Ono et al., 2013). Loss autophagy contribution to Rubisco degradation in ATG mutants is proposed to be compensated by other mechanisms.

Another type of chloroplast-derived vesicles called SAVs has been described in senescent leaves of soybean, Arabidopsis and tobacco (Martínez et al., 2008; Otegui et al., 2005). SAVs, like RCBs, contain Rubisco, but their formation is autophagy-independent (Otegui et al., 2005). The presence of SAG12 and other cysteine proteases was reported in SAVs, suggesting that SAVs could participate in Rubisco degradation. The mechanisms involved in the formation of SAVs remain unknown (Martínez et al., 2008; Otegui et al., 2005).

CHLOROPHYLLS: STRUCTURES AND BIOSYNTHESIS

Chlorophylls: structures, chemical properties and integration in photosystems

Two mechanisms exist in living organisms for capturing and converting light into chemical energy (Bryant and Frigaard, 2006): rhodopsins in some Archea and bacteria and Chl in chlorophototrophic organisms (Chew and Bryant, 2007). Rhodopsins are retinal-binding proteins that act as light-driven proton or chloride pumps. Chlorophototrophs synthesize bacteriochlorophylls (BChls) and/or (Chls), which function in both light harvesting and photochemistry (Bryant and Frigaard, 2006). In addition, red algae and cyanobacteriae synthesize phycobilisomes for light harvesting (Gantt, 1981). Phycobilisomes are composed of open tetrapyrroles, called phycobilins, covalently bound to phycobiliproteins. Finally, chlorophototrophs also synthesize carotenoids, accessory pigments having functions in photoprotection and light harvesting (DellaPenna and Pogson, 2006).

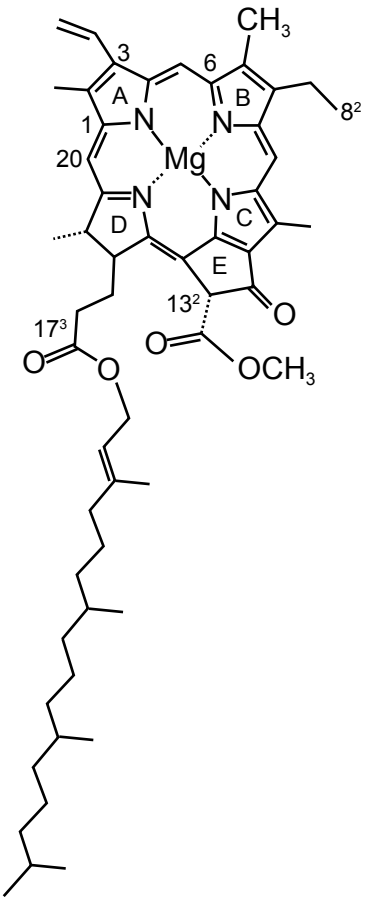

Fig. I.4. Chemical structure of Chl *a*. Relevant carbon atoms and ring letters are labeled.

(B)Chls are defined as aromatic tetrapyrroles carrying an additional isocyclic ring E (see Fig. I.4 for Chl *a* structure as example; Scheer, 2006). (B) Chl are liganded with Mg^{2+} and have a long-chain alcohol (e.g. phytol) attached with an ester bound at $C17^3$. Bchl diversity and structures are not discussed here in detail (for more information, see Bryant and Frigaard, 2006; Scheer, 2006). To date, five chemically distinct Chls have been identified and termed Chl *a*, *b*, *c* ,*d* and *f* (Chen et al., 2010; Scheer, 2006). Chl *a*, the most abundant Chl, is present in PS reaction centers of all oxygenic organisms, except for the cyanobacterium *Acaryochloris marina* and other related taxa (Miyashita et al., 1996; Schliep et al., 2013). In *Acaryochloris marina*, Chl *d* can replace Chl *a* as primary pigment, thereby extending the light absorption capacity of its PSs to longer wavelengths. Chl *d* differs from Chl *a* in that a formyl group replaces the C3 vinyl group of Chl *a*. Chl *a* has two intense but narrow absorption maxima (at 430 and 680 nm; (Scheer, 2006)). In order to increase light-harvesting capacity of PSs, Chl *a* is almost always accompanied by accessory pigments present in the light-harvesting antennae. Chl *b*, the supplementary pigment of type-II cyanobacteria, green algae and plants, structurally differs from Chl *a* only at the C-7 head group: Chl *a* has a methyl moiety and Chl *b* a formyl group (Scheer, 2006). The absorption maxima of Chl *b* (at 460 nm and 650 nm) extend the light absorption range of PSs towards green wavelengths. Members of the Chl *c* family are light-harvesting pigments of golden-brown algae termed chromophytes (Zapata et al., 2006). A major characteristic of Chls *c* is the presence of a *trans* acrylic (propenoic) acid on ring D at C17 instead of the propionic acid of Chl *a* and *b*. Furthermore, this acrylic acid is not esterified to phytol or other aliphatic long chain alcohols (for instance, some Chls *c* are esterified to MGDG (Zapata et al., 2006 and references therein)). Recently, Chl *f*, a new type of Chl, has been identified in a cyanobacteriae community from stromatolites and was shown to absorb even further to the red region of the spectrum than Chl *d* (Chen et al., 2010).

Chls are bound to proteins in multi-subunit membrane-protein complexes (Nelson and Yocum, 2006; Scheer,

2006). In higher plants and green algae, Chls are integrated into PSI and PSII, which are composed of core subunits (PSa and PSb, respectively) and light-harvesting protein antennae (LHCII and LHCII, respectively; Nelson and Yocum, 2006). High resolution structure analysis revealed that about 170-175 Chl molecules are integrated into each plant PS (Nelson and Yocum, 2006 and references therein). In addition to Chl, several carotenoids participate in the absorption of light energy and its transfer to the reaction center. PSs, cytochrome b_6f complex and F-ATPase interact at the thylakoid membrane in supercomplexes which are the core of the light reactions of photosynthesis (For more information on "Structure and Function of Photosystems I and II", see Nelson and Yocum, 2006).

Tetrapyrrole biosynthesis

The enzymatic steps involved in plant tetrapyrrole biosynthesis have been extensively investigated and almost entirely elucidated (for detailed reviews see, Tanaka and Tanaka, 2007; Tanaka et al., 2011). Higher plants synthesize four classes of tetrapyrroles: Chl, phytochromobilin, heme, and siroheme (Fig. I.5). Heme and siroheme are macrocycles containing iron. Heme plays a crucial role in various biological processes such as respiration and photosynthesis and siroheme is the cofactor of enzymes involved in nitrogen and sulfur assimilation (Tanaka and Tanaka, 2007; Tripathy et al., 2010). Phytochromobilin, an open tetrapyrrole, is the chromophore of the red/far-red light receptor phytochrome (Nagatani, 2010; Rockwell et al., 2006). Chl structure and function is described in the section "Chlorophylls: structures, chemical properties and integration in photosystems". All four classes of tetrapyrroles are synthesised from glutamate in the plastids (Fig. I.5; Tanaka and Tanaka, 2007 and references therein). Only a few steps of heme biosynthesis could also occur in the mitochondria. The first part of the pathway, from glutamate to uroporphyrinogen III, is common to all classes of tetrapyrroles and involves nine enzymatic steps. The next steps, from uroporphyrinogen III to protoporphyrin IX are common to Chl (see below for more details), heme, and phytochromobilin.

Some of the intermediates of the tetrapyrrole biosynthesis pathway are highly toxic for the cell. In addition, the need of tetrapyrroles is not constant during plant development and stress. As a result, steps of the different branches of the pathway have to be regulated in response to the demand of a particular tetrapyrrole (Mochizuki et al., 2010). Several regulation mechanisms of tetrapyrrole biosynthesis have been described, in particular for the formation of 5-aminolevulinic acid (ALA, an intermediate of the common branch of the pathway) as well as at the branch point of the pathway towards Chl and heme (Czarnecki and Grimm, 2012; Tanaka and Tanaka, 2007). Regulation of tetrapyrrole synthesis has been shown to occur at the transcriptional and post-transcriptional level (Czarnecki and Grimm, 2012; Mochizuki et al., 2010). For example, heme regulates ALA formation through a negative feedback loop inhibiting GLUTAMYL-tRNA REDUCTASE (GluTR), the first committed enzyme of tetrapyrrole biosynthesis (Czarnecki and Grimm, 2012 and references therein). Furthermore, the Chl branch of the pathway has been shown to regulate ALA formation *via* the FLUORESCENT IN BLUE LIGHT (FLU) protein (Meskauskiene et al., 2001). Suppression of *FLU* in Arabidopsis leads to the accumulation of protochlorophyllide in the dark due to an enhanced ALA synthesis. FLU is thought to interact with GluTR at the thylakoid membrane to inhibit ALA synthesis in response to a feedback mechanism derived from the Mg branch of tetrapyrrole biosynthesis. Moreover, MAGNESIUM CHELATASE (MgCh; see also below), the first enzyme of the Chl-specific branch, seems to be regulated by thioredoxin, Mg^{2+} concentration, ATP/ADP ratios and GENOME UNCOUPLED 4 (GUN4) (Tanaka and Tanaka, 2007 and references therein). The GUN4 protein, originally identified in a screen for defective plastid-to-nucleus retrograde signaling, has been shown to bind the different subunits of MgCh and improve their substrate-binding capacity. Furthermore, GUN4 seems to participate in a complex post-translational feedback regulation mechanism acting on ALA synthesis (for more information, see Czarnecki and Grimm, 2012). Finally, the description of several pairwise protein-protein interactions between enzymes of tetrapyrrole biosynthesis suggests the occurrence of metabolic channelling within the pathway (for compilations of references, see Czarnecki and Grimm, 2012; Tanaka and Tanaka, 2007). However, the existence

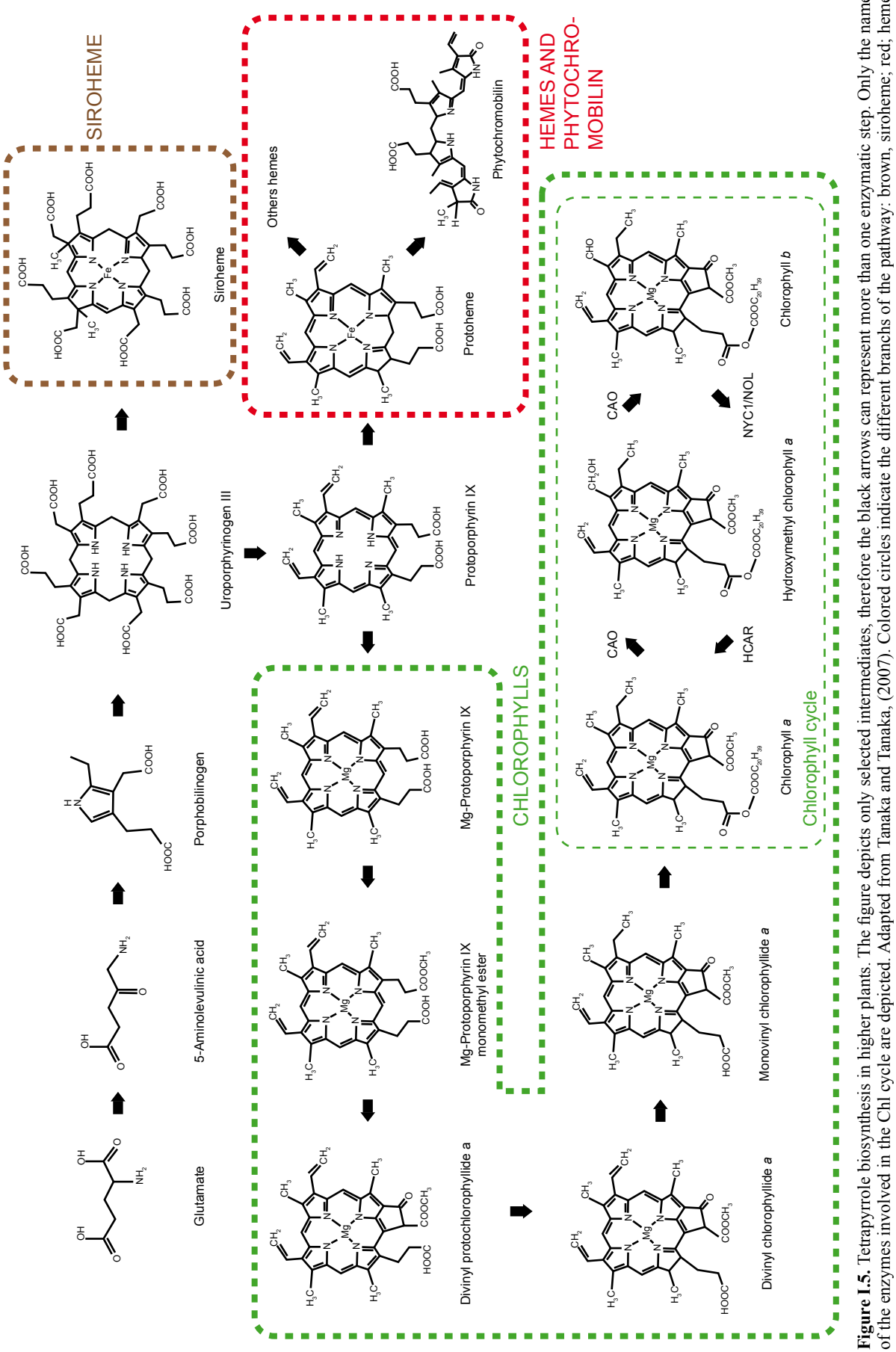

Figure I.5. Tetrapyrrole biosynthesis in higher plants. The figure depicts only selected intermediates, therefore the black arrows can represent more than one enzymatic step. Only the names of the enzymes involved in the Chl cycle are depicted. Adapted from Tanaka and Tanaka, (2007). Colored circles indicate the different branches of the pathway: brown, siroheme; red; hemes and phytochromobilin; green, Chls.

of supercomplexes involving several enzymes of the tetrapyrrole biosynthesis pathway remains to be proven.

Chlorophyll *a* biosynthesis

MgCh catalyzes the first step of the Chl branch in the tetrapyrrole biosynthetic pathway (Fig. I.5; Eckhardt et al., 2004; Tanaka and Tanaka, 2007; Tanaka et al., 2011). This reaction catalyzes the ATP-dependent insertion of Mg^{2+} into the macrocycle of protoporphyrin IX, producing Mg-protoporphyrin IX. Then, four subsequent steps convert Mg-protoporphyrin IX into monovinyl chlorophyllide *a*. The reaction catalyzed by PROTOCHLOROPHYLLIDE OXIDOREDUCTASE (POR; conversion of divinyl protochlorophyllide *a* into divinyl chlorophyllide *a*) is strictly light-dependent in angiosperms (Masuda and Takamiya, 2004). The light-dependent activity of POR is illustrated in etiolated seedlings of the *flu* mutant (see above), which shows enhanced ALA synthesis and consequently accumulates protochlorophyllide in the dark. Lastly, the addition of a phytol moiety to monovinyl chlorophyllide *a* is mediated by Chl synthase (CS) and produces Chl *a* (Tanaka and Tanaka, 2007; Tanaka et al., 2011).

The chlorophyll cycle

Chl biosynthesis first leads to the formation of Chl *a* (Tanaka and Tanaka, 2007; Tanaka et al., 2011). The section "Chl *b* synthesis" describes Chl *a* to Chl *b* conversion, mediated by Chl *a* OXYGENASE (CAO). Conversely, Chl *b* can be reconverted to Chl *a* by the activity of two enzymes, Chl *b* reductase and 7-HYDROXYMETHYL Chl *a* REDUCTASE (HCAR) (Tanaka and Tanaka, 2011). This reconversion, considered to be the first step of Chl breakdown, is described in the section "Reconversion of chlorophyll *b* to *a*". The interconversion between Chl *a* and Chl *b* is known as the "chlorophyll cycle", which is depicted in Figure I.5. For simplicity, the cycle is described as involving Chls only. However, it is unclear if Chl and/or chlorophyllide (Chlide) species together with CS and CHLOROPHYLLASE (CLH, see section "Cleavage of the phytol chain") are involved in the Chl cycle. As already mentioned, higher plants possess Chl *a* and Chl *b* in their PSs. Chl *a* is a component of both core and antenna complexes whereas Chl *b* is found only in the antenna. The Chl *a*/*b* ratio, regulated by the Chl cycle, has been shown to be influenced by developmental and environmental factors and to reflect the ratio between core and antenna complexes in PSs (Tanaka and Tanaka, 2011).

Chlorophyll *b* synthesis

Chl *b* synthesis is mediated by CAO, a Rieske-type monooxygenase (Tanaka et al., 1998). The conversion of the 7-methyl group of Chl *a* into a formyl group is a three-step oxygenation reaction with hydroxymethyl-Chl(ide) *a* (HMChl *a*) and an instable dihydroxymethyl-Chl(ide) *a* as intermediates. *In vitro* activity assays suggested that CAO acts on Chlide *a* rather than at the Chl *a* level (Oster et al., 2000). However, it is possible that CAO cannot act on Chl *a* *in vitro* due to its low solubility, and therefore it cannot be excluded that Chl *a* is a substrate of CAO *in vivo* (Tanaka and Tanaka, 2011). Suppression of CAO in *Chlamydomonas reinhardtii* and Arabidopsis (*chlorina* mutants) completely abolishes Chl *a* to *b* conversion (Espineda et al., 1999; Oster et al., 2000; Tanaka et al., 1998). Arabidopsis *chlorina* mutants are viable but smaller and yellowish when compared to wild-type plants (Kim et al., 2009a). Moreover, Chl *b* depletion in Arabidopsis results in a decrease of major LHC proteins under normal growth conditions, an effect enhanced under high light conditions (Kim et al., 2009a; Tanaka and Tanaka, 2011, 2005). These observations clearly demonstrate that Chl *b* is necessary for LHC stabilization. Interestingly, overexpression of Arabidopsis CAO leads to only a slight decrease of the chl *a*/*b* ratio, despite high levels of CAO mRNA (Tanaka et al., 2001; Yamasato et al., 2005). This inconsistency between CAO expression and Chl *b* levels in CAO-overexpressing plants was shown to be due to post-transcriptional regulation of CAO (Sakuraba et al., 2009; Yamasato et al., 2005). The A-domain of CAO contains a specific sequence of 10 amino acids, called degron, responsible for CAO-specific degradation by the chloroplast Clp protease complex (Nakagawara et al., 2007; Sakuraba et al., 2009). The exact mechanism of CAO regulation by high Chl *b* levels is still unknown. It has been suggested that Chl *b* binding to CAO changes the conformation of the A-domain and exposes the degron to the exterior of the protein. Then, a Clp

protease subunit binds to the exposed degron and drags the entire CAO into the proteolytic core of the Clp system (Sakuraba et al., 2009).

CHLOROPHYLL BREAKDOWN VIA THE "PAO PATHWAY"

Breakdown of colored and phototoxic chlorophyll catabolites

Reconversion of chlorophyll b to a

Chl *b* is reconverted to Chl *a* by the action of two enzymes, Chl *b* REDUCTASE (CBR) and HCAR (Fig. I.5-6; Tanaka and Tanaka, 2011). Plants possess two isoforms of CBR called NON-YELLOW COLORING1 (NYC1) and NYC1-like (NOL) (Kusaba et al., 2007; Sato et al., 2009). *In silico* hydrophobicity analysis of NYC1 and NOL protein sequences predicted NYC1 to be a membrane protein and NOL to be a soluble protein (Kusaba et al., 2007). Furthermore, *in vitro* immunoprecipitation and localization experiments in rice suggested that the two proteins could form heterodimers at the thylakoid membrane (Kusaba et al., 2007; Sato et al., 2009). Although only NOL activity has been demonstrated *in vitro*, the two enzymes are thought to catalyze the same reaction, i. e. the reduction of Chl *b* to HMChl *a*. Interestingly, an Arabidopsis *nyc1nol* double mutant does not show an altered Chl *a*/*b* ratio during the unstressed vegetative phase, but displays a stay-green phenotype during leaf senescence and seed maturation due to the retention of Chl *b* (Horie et al., 2009). Taken together, these data suggest that NYC and NOL do not participate actively to Chl *a*/*b* ratio regulation during the vegetative growth, but are required for developmental processes such as leaf senescence (Tanaka and Tanaka, 2011). Finally, Chl *b* to *a* reduction appears to be crucial for LHC degradation during senescence since *nyc1nol* mutants retain LHC proteins, at least mainly LHCII (Horie et al., 2009; Kusaba et al., 2007).

Recently, the enzyme catalyzing the second step of Chl *b* to Chl *a* reduction, conversion of HMChl *a* into Chl *a*, was characterized in Arabidopsis (Fig; I.5; Meguro et al., 2011). HCAR contains a flavin adenine dinucleotide and an iron-sulfur center as cofactors, and phylogenetic analysis revealed that HCAR evolved from divinyl chlorophyllide vinyl reductase of the Chl biosynthesis pathway (Meguro et al., 2011). HCAR is able to catalyze the conversion of HMChl *a* to Chl *a* *in vitro* and T-DNA insertion

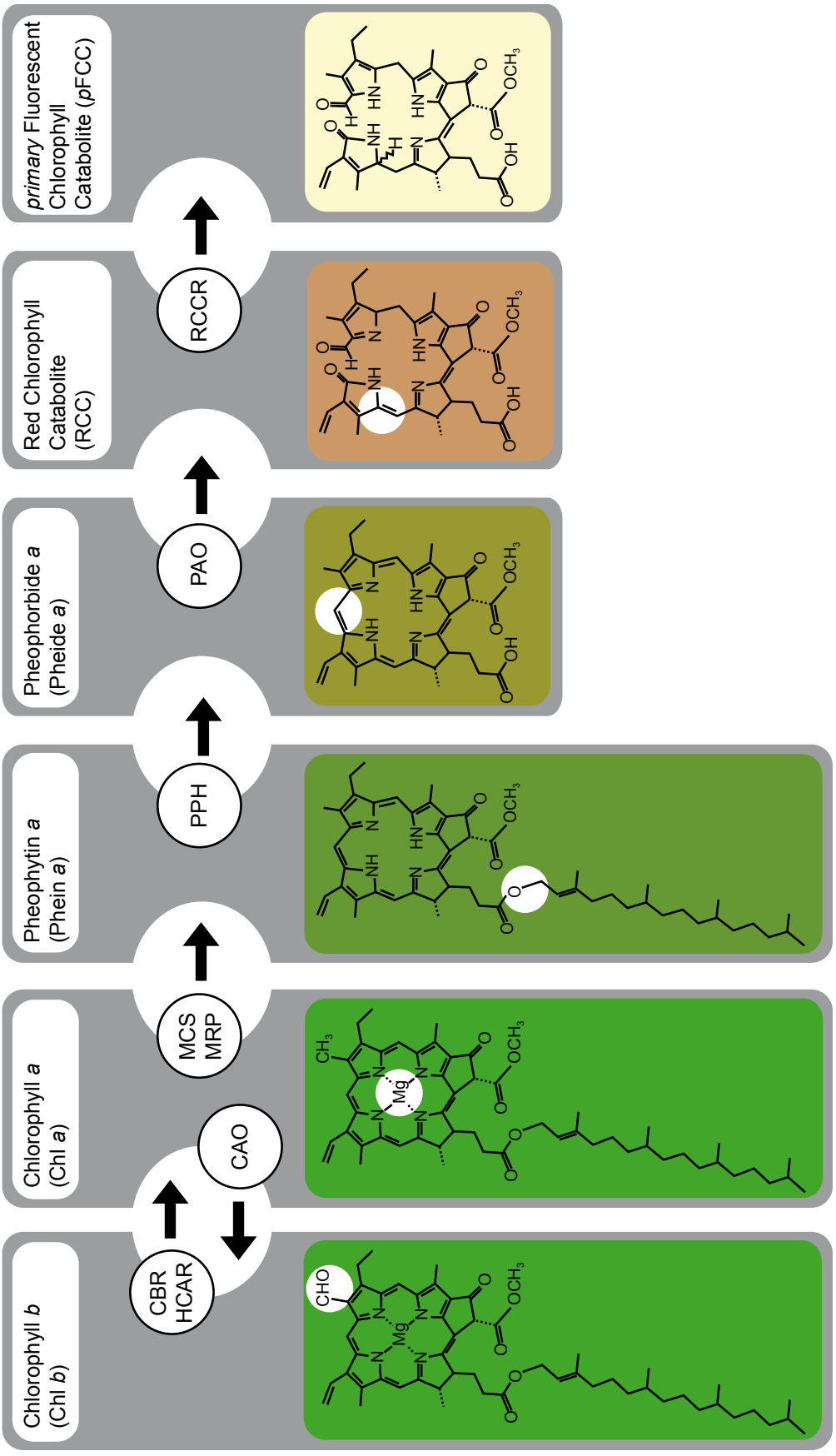

Figure I.6. Colored Chl catabolite degradation by the "PAO Pathway". The name of the enzymes involved in each steps are shown. For each steps, the part of the catabolites that is modified by the enzyme is depicted in white. See text for more information.

mutants for HCAR accumulate low levels of HMChl *a* during leaf senescence. Surprisingly, *hcar* mutants retain significant amounts of pheophorbide (Pheide) *a*, a downstream intermediate of the Chl degradation pathway. Pheide *a* OXYGENASE (PAO, the enzyme catalyzing the further degradation of Pheide into red Chl catabolite (RCC)) protein levels were unchanged in *hcar* as compared with wild-type plants. These observations, together with the fact that Pheide *a* is not accumulating in a *hcarnyc1nol* triple mutant, suggest that HMChl or some degradation products of HMChl could inhibit PAO activity by an unknown mechanism and results in the accumulation of Pheide *a* (Meguro et al., 2011).

There are strong evidences that the first step of Chl *b* degradation is its conversion to Chl *a*. The main argument is that PAO is specific for the "*a*" form of Pheide (see section " Opening and reducing of the macrocycle"; Hörtensteiner et al., 1995; Pružinská et al., 2003). In addition, *nyc1nol* mutants are unable to degrade Chl *b* during leaf senescence (see above). As mentioned above *nyc1nol* mutants retain large amounts of LHC protein indicating that Chl *b* to *a* conversion is a prerequisite for both LHC and Chl *b* degradation. Finally, it has been shown that Chl *b* to *a* conversion must precede demetalation and dephytylation because HCAR is able to reduce HMChl *a* but not 7-hydroxymethyl pheophytin *a* or 7-hydroxymethyl Pheide *a* *in vitro* (Shimoda et al., 2012). All together, these data indicate that Chl *b* to *a* conversion is necessary for Chl *b* and Chl *b*-containing complex (LHC) degradation, and that Chl *b* to *a* conversion (but not demetalation or dephytylation) is the first step of Chl *b* degradation. Thus, Chl *a* degradation seems to be independent of Chl *b* to *a* reduction. In line with this, Arabidopsis *nyc1nol* degrades Chl *a* and PS core complexes as wild-type (Horie et al., 2009). Furthermore, *nyc1cao* double mutants of rice, in which the Chl cycle is totally abolished, produce only Chl *a* during vegetative growth and are able to degrade it during leaf senescence (Kusaba et al., 2007).

Interestingly, it has been demonstrated that overproduction of Chl *b* in Arabidopsis leads to the incorporation of Chl *b* into PS core complexes, which seems to partially inhibit their degradation during senescence (Hirashima et al., 2006; Sakuraba et al., 2012a, 2010; Shimoda et al., 2012). These findings indicate that Chl *b* to *a* conversion has evolved specifically to act on LHC complexes. It is interesting to note that Chl *b* overproduction in Arabidopsis appears also to retard age-dependent senescence via transcriptional down-regulation of SAG genes (Sakuraba et al., 2012a). Incorporation of Chl *b* in PS core complexes, and their consequent increased stability, is thought to maintain active PS during the senescence phase. The increased photosynthetic capacity resulting from Chl *b* overproduction could modulate SAG gene expression through an unknown signaling pathway (Sakuraba et al., 2012a).

Destabilization of Chl-apoprotein complexes by Stay-Green

Deletion of the chloroplast-localized protein STAY-GREEN (SGR), as its name says, triggers a stay-green phenotype (see separated panel " One visual stay-green phenotype, several different genetic disorders"; Hörtensteiner, 2009). Conversely, many but not all mutations triggering a stay-green phenotype affect the *SRG* gene. Among more than 14 stay-green mutants identified in natural populations, mutagenesis screens or breeding programs of different plant species, eight are deficient of SGR (Hörtensteiner, 2009 and references therein; Schelbert et al., 2009). Notably, presence or absence of a functional *SGR* gene in pea determines the color of the cotyledons (green or yellow), originally described by Mendel (Armstead et al., 2007; Mendel, 1866). Furthermore, the commercialized tomato variety called "*green-flesh"* is also deficient in SGR (Barry et al., 2008). The brown coloration of ripe *green-flesh* fruits is due to Chl retention and simultaneous carotenoid accumulation.

The exact role of the SGR protein, which does not contain any known domain, is still unclear (Hörtensteiner, 2009). Suppression of *SGR* leads to a cosmetic stay-green phenotype (Type C, see separated panel " One visual stay-green phenotype, several different genetic disorders" and Fig. I.3; Jiang et al., 2007; Park et al., 2007; Ren et al., 2007). Photosynthesis capacity of *sgr* decreases as in wild-type during leaf senescence but several LHC and core subunits of PSI and II are partially retained (Aubry et al., 2008; Jiang et al., 2007; Park et al., 2007). Taken

together with the finding that SGR can interact with LHCb proteins, these observations suggest that SGR participates in the destabilization of Chl-apoprotein complexes of PSs during senescence. Recently, this hypothesis has been corroborated by the finding that SGR plays a central role in recruiting Chl catabolitic enzymes at the thylakoid membrane (Sakuraba et al., 2013, 2012b). Notably, overexpression of SGR in Arabidopsis has been shown to cause spontaneous necrotic flecking during vegetative growth due to the absence of PAO and consequent accumulation of Pheide (Mur et al., 2010). Pheide accumulation in SGR-overexpressing plant is thought to generate toxic singlet oxygen ($^1O_2$) which, in turn, triggers a hypersensitive response. Moreover, SGR appears to be necessary for the development of chlorosis upon infection of Arabidopsis with *Pseudomonas syringae* pv *tomato* (Mecey et al., 2011).

Interestingly, SGR seems to have also other functions, not directly related to Chl degradation. SGR appear to be implicated in root nodule senescence (Zhou et al., 2011). Root nodules of legume species such as alfalfa and *Medicago truncatula* are specialized organs hosting soil bacteria capable of reducing atmospheric nitrogen (N_2) to ammonium. Nodule senescence stops nitrogen fixation and results in the loss of the symbiotic interaction. Silencing of *SGR* in *M. truncatula* was shown to affect nodule senescence, and thus indicates that SGR could also have a function in non-photosynthetic tissues (Zhou et al., 2011). Recently, SGR has been shown to regulate lycopene and β-carotene biosynthesis in tomato fruits (Luo et al., 2013). SGR directly interacts with PHYTOENE SYNTHASE 1 (PSY1), a carotenoid synthetic enzyme and can inhibit its activity. These two studies clearly demonstrate that SGR, despite its involvement in Chl breakdown, is also involved in other biochemical processes.

Cleavage of the phytol chain

One century ago, Willstätter and Stoll already described an enzyme, called CHLOROPHYLLASE (CLH), that was able to cleave the phytol tail of Chl (Willstaetter and Stoll, 1911). Later, Mayer et al. (1930) found CLH activity in several plant species and Holden (1961) partially purified CLHs from sugar beet and pea and further characterized their activity (Holden, 1961; Mayer, 1930). To date, more than 250 studies have been performed on plant CLHs according to the Web of Knowledge database (search performed with "chlorophyllase(s)" in titles). The majority of these studies describe the (partial) purification of CLHs from different plant species and the characterization of their *in vitro* activity. Cloning of CLH genes from plants such as *Chenopodium album*, Arabidopsis and Citrus revealed that CLHs contain a lipase motif. In addition, transcription of most CLHs is highly induced by ethylene and JA treatments, which are known to promote senescence (Jakob-Wilk et al., 1999; Tsuchiya et al., 1999). However, two CLHs (Arabidopsis *At*CLH2 and *Chenopodium album Ca*CLH) are not induced by phytohormones and show constitutively low levels of expression (Jakob-Wilk et al., 1999; Tsuchiya et al., 1999). Using biochemical and immunolocalization approaches, several studies could localize CLH in the chloroplast (Azoulay-Shemer et al., 2011; Brandis et al., 1996; Harpaz-Saad et al., 2007; Matile et al., 1997). In Citrus, CLH appears to be post-translationally regulated by N- and C-terminal proteolysis within chloroplast membranes and mature CLH was shown to be more active than the CLH precursor (Azoulay-Shemer et al., 2011; Harpaz-Saad et al., 2007). Collectively considered, all these data suggested a major role for CLH in hydrolyzing the phytol chain of Chl. However, reverse genetic approaches of CLH-deficient plants did not corroborate this hypothesis (Benedetti and Arruda, 2002; Schenk et al., 2007). Although silencing of Arabidopsis *At*CLH1 (Arabidopsis has two CLH homologues) was believed to the decrease Chlide/Chl ratio in green leaves, analysis of T-DNA insertion mutant lines for *At*CLH1 (*clh1*) and *At*CLH2 (*clh2*) did not reveal any delay of Chl degradation during senescence in single as well as double mutants (Benedetti and Arruda, 2002; Schenk et al., 2007). Decrease and increase of Chlide/Chl ratios caused by, respective, silencing and overexpressing of CLH in Arabidopsis reported by Bendetti et al. (2002) could be an experimental artefact. Indeed, in this study, extraction of green pigments from plant tissue was performed in acetone at 4°C during 12 h. However, CLH has been reported to be active *in vitro* under such conditions. Thus, Chlide/Chl ratio values given for silencing and overexpressing lines may reflect the *in vitro* activity of the CLH protein extracted together with the

pigments, rather than the *in vivo* Chlide/Chl ratio. Lastly, the hypothesis that Arabidopsis CLHs are not involved in Chl degradation during age-dependent and dark-induced leaf senescence is corroborated by the finding that *At*CLHs are located in the cytosol of senescent cells (Schenk et al., 2007).

Nevertheless, indirect evidence suggests that CLH could be involved in Chl breakdown, at least under certain conditions. Heterologous expression of mature Citrus CLH in squash (*Cucurbita pepo*) and tobacco induced Chl breakdown and leaf chlorosis, suggesting that CLH may be the rate limiting enzyme of Chl degradation in these species (Harpaz-Saad et al., 2007). Furthermore, *At*CLH1 was proposed to be involved in pathogen response (Kariola et al., 2005). Silencing of *At*CLH1 was shown to alter resistance or susceptibility of plants towards two different types of necrotrophic pathogens, *Erwinia carotovora* and *Alternaria brassicicola*. Kariola et al. (2005) connected ROS production during necrotrophic pathogen attack with the absence of CLH1, which is thought to degrade Chl in damaged tissue (Kariola et al., 2005). ROS production due to the suppression of *At*CLH1 could then activate and inactivate SA-dependent and JA-dependent responses, respectively. However, this model for CLH function during pathogen attack is based on indirect observations and has to be considered with caution. To conclude, our current knowledge suggests that CLHs are not involved in Chl degradation during leaf senescence but rather play a role during biotic and abiotic stress responses.

The key question "How is the phytol group of Chl hydrolyzed during age-dependent leaf senescence?" remained unanswered until recently. Using an elegant *in silico* approach in Arabidopsis, Schelbert et al. (2009) could identify a chloroplast-targeted serine-type hydrolase the mutation of which leads to a stay-green phenotype during leaf senescence (Schelbert et al., 2009). Surprisingly, this senescence-induced hydrolase is not active on Chl *in vitro* but was found to hydrolyze the phytol chain of pheophytin (Phein) and to produce Pheide. The protein, termed Phein Pheide HYDROLASE (PPH), was shown to be indispensable for Chl degradation during leaf senescence in Arabidopsis and rice (Morita et al., 2009; Ren et al., 2010; Schelbert et al., 2009). Arabidopsis *pph* mutants are also affected in LHC and PS core subunit degradation, indicating that phytol cleavage (as well as Chl *b* to *a* reduction, see section "Reconversion of chlorophyll *b* to *a*") is crucial for degradation of PS proteins during leaf senescence (Schelbert et al., 2009).

Demetalation

With regard to the recent knowledge acquired about dephytylation of Chl during leaf senescence (see section "Cleavage of the phytol chain"), it is likely that demetalation precedes dephytylation and thus occurs on Chl *a* (Morita et al., 2009; Ren et al., 2010; Schelbert et al., 2009; Shimoda et al., 2012). To date, the mechanism involved in Chl demetalation is unknown (Hörtensteiner, 2012). Several biochemical approaches described the involvement of either a heat-stable metal-chelating substance (MCS) or a metal-releasing protein (MRP) (Büchert et al., 2011; Shioi et al., 1996a; Suzuki and Shioi, 2002; Vicentini et al., 1995). All these studies used chlorophyllin (an artificial and soluble Chl derivative) as substrate and not Chl (Hörtensteiner, 2012). A recent proteomic study of plastoglobules annotated a protein as possible MRP (At5g17450; Lundquist et al., 2012). However, analysis of T-DNA insertion lines in this gene did not show any delay in Chl degradation during dark-induced senescence (Luzia Guyer and Stefan Hörtensteiner, unpublished data). Release of Mg^{2+} from Chl is known to occur at acidic pH (for a review on chemical aspects of Chl demetalation, Saga and Tamiaki, 2012). Thus, it can be speculated that the decrease of photosynthesis during senescence lowers the stromal pH sufficiently to remove Mg^{2+} from the Chl macrocycle (Stefan Hörtensteiner, personal communication). Thereby SGR (see section "Destabilization of Chl-apoprotein complexes by Stay-Green") could have a decisive role; during vegetative growth, the stromal pH also decreases during the night, but absence of senescence-regulated SGR could avoid massive demetalation of Chls before the onset of senescence.

Opening and reducing of the macrocycle

The light absorption capacity of tetrapyrroles and thus the potential phototoxicity of some Chl catabolites is mostly due to electron conjugation of the porphyrin ring (Hörtensteiner and Kräutler,

2011; Hörtensteiner, 2006; Scheer, 2006). Opening of Pheide *a* by PAO and reduction of the conjugated C20/C1 double bond of red Chl catabolite produce (RCC) by RCC REDUCTASE (RCCR) are the two steps of the Chl degradation pathway that lead to the loss of Chl catabolite phototoxicity (Hörtensteiner and Kräutler, 2011; Hörtensteiner, 2006). Thus, *primary* fluorescent Chl catabolite (*p*FCC), the product of the consecutive PAO and RCCR activities, is considered as non-phototoxic (Hörtensteiner and Kräutler, 2011; Hörtensteiner, 2012, 2006).

Enzymatic activities responsible for opening of the Pheide macrocycle and production of *p*FCC were originally detected in isolated gerontoplasts and were shown to be promoted by glucose-6-phosphate (G6P) and ATP (Matile et al., 1992; Schellenberg et al., 1990). Later, *p*FCC production from Pheide was shown to be possible *in vitro* by using isolated thylakoid membranes and reduced ferredoxin (Ginsburg et al., 1994; Schellenberg et al., 1993). Partial purification of this activity from *Brassica napus* revealed its dependency on a stromal fraction, senescence inductibility and specificity towards Pheide *a*, i. e. Pheide *b* not being a substrate (Hörtensteiner et al., 1995). Dependency of the activity on a stromal fraction was confirmed by the finding that the conversion of Pheide to *p*FCC was a two-step reaction performed by two enzymes, one localized in chloroplast membranes (PAO) and the other in the stroma (RCCR) (Rodoni et al., 1997). For a long time, PAO was considered to be localized in the chloroplast envelope but recent reconsideration of Chl catabolic enzyme localization revealed that PAO is rather inserted into the thylakoid membrane (see also section "Topology of chlorophyll breakdown in the chloroplast"; Kleffmann et al., 2004; Matile et al., 1996; Pružinská et al., 2003; Sakuraba et al., 2012b). Further characterization of PAO has shown that the enzyme is a Fe-dependent monooxygenase belonging to the Rieske-type iron-sulfur oxygenase family (Gray et al., 2002; Hörtensteiner et al., 1998; Pružinská et al., 2003). Interestingly, an additional factor, called RCC FORMING FACTOR (RFF), indispensable for PAO/RCCR activity *in vitro* has also been described (Pružinská et al., 2005). RFF could be a ROS-scavenging protein such as a peroxidase possibly required to remove ROS likely produced as by-products of PAO activity (Stefan Hörtensteiner and Silvain Aubry, unpublished data).

Suppression of PAO in Arabidopsis, maize, rice and tomato has been shown to induce premature cell death (Pružinská et al., 2005, 2003; Spassieva and Hille, 2002; Tanaka et al., 2003; Tang et al., 2011). Cell death in Arabidopsis *pao1* mutants (originally identified as *accelerated cell death 1* (*acd1*) (Greenberg and Ausubel, 1993)) is due to the accumulation of Pheide, thus displaying a type D stay-green phenotype (see section " One visual stay-green phenotype, several different genetic disorders"; Pružinská et al., 2003; Tanaka et al., 2003). Surprisingly, the cell death phenotype of *acd1* is not strictly connected to light, but also occurs in the dark (Hirashima et al., 2009; Pružinská et al., 2005, 2003). Thus, rather than being solely phototoxic, Pheide has been speculated to act as signaling molecule that would be exported from the chloroplast, like suggested for Mg-protoporphyrin IX, the first intermediate of the Chl branch of tetrapyrrole biosynthesis pathway (Hirashima et al., 2009; Mochizuki et al., 2001). However, characterization of METYHL ESTERASE (MES) 16, the enzyme demethylating fluorescent Chl catabolites (FCCs) in the cytosol of Arabidopsis, revealed that an export of Pheide from the chloroplasts of *pao1* is unlikely (see Chapter "1"; Christ et al., 2012). *In vitro*, MES16 can demethylate Pheide and convert it to pyroPheide but pyroPheide was not detected in *pao1*. However, when MES16 was mistargeted to the chloroplast using the PPH transit peptide, 75% of the Pheide accumulating in *pao1* was converted to PyroPheide (Christ et al., 2012; Schelbert et al., 2009). This finding indicates that Pheide is most probably not a chloroplast-to-nucleus retrograde signal itself but rather seems to trigger a signaling cascade involving other factors.

RCCR has originally been cloned from barley and Arabidopsis, and was localized in the chloroplast (Wüthrich et al., 2000). Reduction of RCC by RCCR occurs in a stereospecific fashion, which can be different between RCCR orthologues (Mühlecker et al., 2000, 1997). For instance, Arabidopsis RCCR produces *p*FCC whereas *Capsicum annuum* RCCR converts RCC into *epi-p*FCC, the other *p*FCC isomer (see Table ""; Hörtensteiner et al., 2000). Interestingly, this stereospecificity can be manipulated by a Phe-to-Val exchange at the residue 218 of the Arabidopsis RCCR (Pružinská et al., 2007). RCCR crystallisation

and site-directed mutagenesis confirmed that residue 218 together with Glu154 and Asp291 are located within the substrate-binding pocket of RCCR and are required for its activity (Pattanayak et al., 2012; Sugishima et al., 2010, 2009). In contrast to PAO expression, Northern blot analysis of RCCR revealed a constitutive expression in leaves and roots (Wüthrich et al., 2000). Furthermore, RCCR was shown to be also targeted to the mitochondria, suggesting that RCCR could have other roles besides converting RCC to *p*FCC (Mach et al., 2001). Loss of RCCR in Arabidopsis caused the *acd2* phenotype, which is characterized by the spontaneous spreading of light-dependent cell death lesions during plant growth and development, and by constitutive activation of defenses in the absence of environmental stress (Mach et al., 2001; Pružinská et al., 2007; Yao and Greenberg, 2006). *acd2* accumulates RCC and RCC-like pigments in the vacuole, meaning that these tetrapyrroles can move within the cell (Pružinská et al., 2007). RCC and RCC-like pigments are thought to act as signaling molecules and trigger cell death observed in *acd2* (Type D stay-green phenotype, see section " One visual stay-green phenotype, several different genetic disorders"; Mach et al., 2001; Pattanayak et al., 2012; Yao and Greenberg, 2006). Part of the cascade leading to cell death in *acd2* is the loss of mitochondrial membrane potential and mitochondrial H_2O_2 production (Yao and Greenberg, 2006).

The Chapter "5" of my thesis describes further investigations of the role of RCCR in the protection against cell death (published in Pattanayak et al., 2012). Specific targeting of RCCR to the mitochondria of *acd2* dramatically reduces RCC accumulation, cell death and mitochondrial ROS production. This rescue effect is dependent on the activity of RCCR since a mitochondria-targeted Glu154Ala variant of RCCR did not complement the cell death phenotype of *acd2*. Collectively, these *in vivo* data on RCCR function(s) provide evidence that this enzyme is involved in protection against pro-death molecules (such as RCC) in both chloroplast and mitochondria. These pro-death molecules, substrates of RCCR, are mobile within cells and have a major effect on mitochondria (Pattanayak et al., 2012).

Topology of chlorophyll breakdown in the chloroplast

Recently, advances have been made in understanding the topology of the first steps of Chl breakdown during leaf senescence (Fig. I.7; Sakuraba et al., 2012b). Using co-immunoprecipitation and bimolecular fluorescence complementation approaches, it has been demonstrated that SGR, NYC1, NOL, PPH, PAO and RCCR interact at the thylakoid membrane. These interactions are proposed to create an enzyme complex, which mediates channelling of phototoxic catabolites. The observation that these interactions do not occur in a *sgr* mutant suggests the possibility that SGR recruits the other Chl catabolic enzymes at the thylakoid membrane and acts as a hub. In the model proposed by Sakuraba et al. (2012b), all these steps of Chl degradation of PSII occur at the thylakoid membrane and ultimately lead to the release of *p*FCC, the first non-phototoxic catabolite into the stroma. SGR has been shown to interact specifically with LHCII but not with LHCI subunits, and to participate in the destabilization of the Chl-apoprotein complexes (Park et al., 2007). Existence of the same or a similar complex for Chl degradation of PSI is highly probable but has not yet been demonstrated.

Enzymatic modifications of colorless chlorophyll catabolites

Diversity of colorless chlorophyll catabolites

After its release into the chloroplast stroma, non-phototoxic and colorless *p*FCC is modified by different enzymes, leading to the production of modified FCCs (*m*FCCs). Our current knowledge of FCCs modifications, including new findings provided in this thesis, is summarized in this chapter. All colorless Chl catabolites are thought to derive from *p*FCC, to be modified in the chloroplast and the cytosol and to be finally non-enzymatically isomerized and stored in the vacuole as nonfluorescent Chl catabolites (NCCs) or nonfluorescent dioxobilin-type Chl catabolite (NDCCs), also termed urobilinogenoidic Chl catabolites (UCCs; see section "Non-enzymatic isomerization of chlorophyll catabolites in the vacuole" for more detail on the isomerization and storage in the vacuole). To date, numerous colorless catabolites have been structurally characterized (see

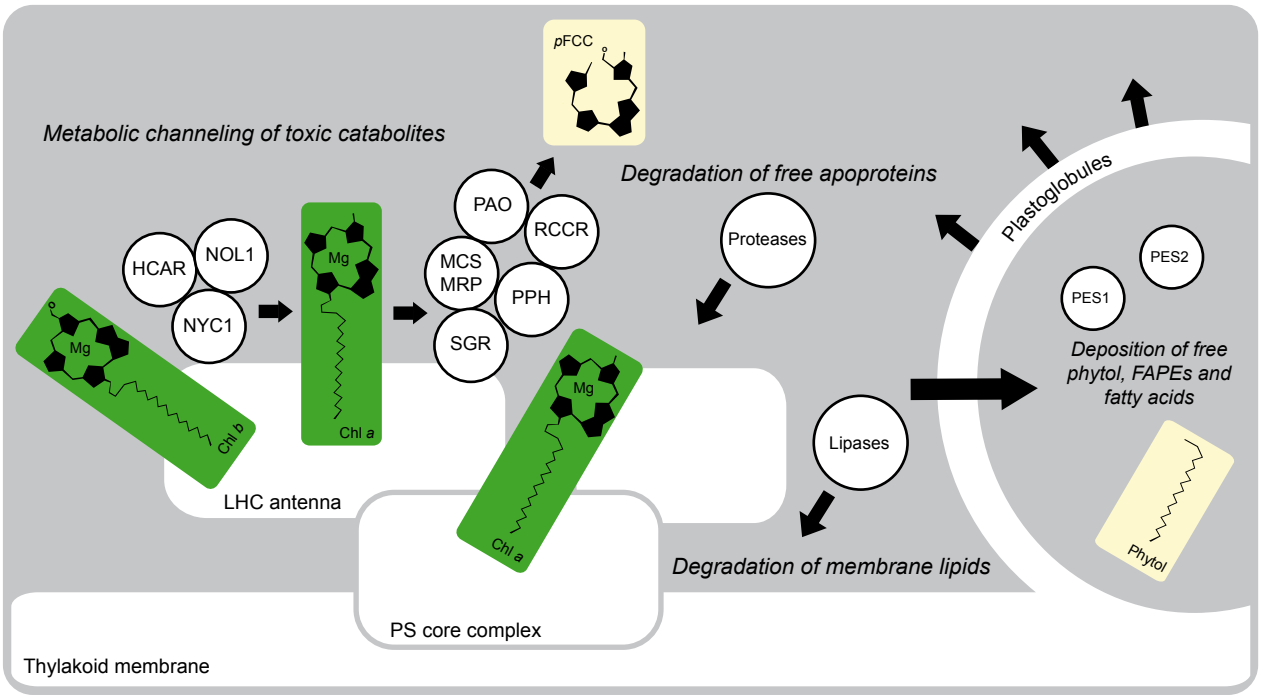

Figure I.7. Degradation of colored Chl catabolites at the thylakoid membrane. Chl catabolic enzymes interact to allow metabolic channelling of phototoxic intermediates. In parallel of Chl degradation, PS subunits and thylakoid lipids are degraded. The size of plastoglobules increases due to the accumulation of thylakoid degradation products. See text for more information.

Table C.1). Except for *Hv*-UCC-1, *Cj*-NCC-1, *Lo*-NCC-1 and *Ls*-NCC-1, identification and structure determination of all other colorless catabolites compiled in Table C.1 have been performed by the group of Prof. B. Kräutler, Innsbruck. Since the identification of the first NCC in 1991, up to 40 different colorless catabolites have been structurally characterized (Hörtensteiner, 2012; Kräutler et al., 1991). These catabolites are divided into four classes (FCCs, NCCs, UCCs/NDCCs and YCCs) depending on specific modifications, which determines a distinct UV/Vis spectrum for each class of catabolites (Fig. I.8). The recently identified yellow Chl catabolites (YCCs) have been speculated to originate from the oxidation of NCCs in the vacuole (Moser et al., 2008b; Scherl et al., 2012).

Hydroxylation, Glucosylation and Malonylation of FCCs (see Chapter "3")

C8^2 hydroxylation of *p*FCC is the only side chain modification found in all species from which NCCs have been structurally characterized (see Table C.1). The nature of the enzyme(s) responsible for this hydroxylation is not known. However, isolation of gerontoplasts from barley revealed that not only *p*FCC is produced in isolated plastids but also another, more polar, FCC (Matile et al., 1992). The structure of this polar FCC could not be determined, but has been speculated to be C8^2 hydroxy-*p*FCC (Matile et al., 1999). The Chapter "3" of this thesis provides experimental evidences that *p*FCC hydroxylation at the C8^2 position occurs in gerontoplasts of Arabidopsis. Furthermore, *p*FCC hydroxylation activity seems to be also present in isolated chromoplasts from *Capsicum annuum*. Preliminary results suggest that FCC hydroxylation depends on electron derived from G6P or NADPH and is lost after washing of chromoplast membranes. Cytochromes P450 monooxygenase have been speculated to be possible candidates for hydroxylation of *p*FCC (Stefan Hörtensteiner, personal communication; Matile et al., 1999). Although the majority of the 244 full-length P450 genes present in Arabidopsis genome are predicted to localize in the ER, some P450 have been shown experimentally to be targeted to the chloroplast (Schuler et al., 2006). However, dark-incubation of detached Arabidopsis leaves in carbon monoxide (CO), known to be an inhibitor of cytochrome P450s, does not seem to prevent FCC hydroxylation (see Chapter "2"). If we assume that CO can diffuse into the chloroplast, FCC hydroxylation appears to be

mediated by a nonheme cytochrome P450 or other enzymes, which cannot be inhibited by CO.

The C8^2 hydroxyl group of FCCs appears to be subsequently malonylated and/or glucosylated and in some species such as Arabidopsis, tobacco and oilseed rape (see Table C.1; Berghold et al., 2004; Hörtensteiner, 1998; Pružinská et al., 2005). The molecular nature of these activities remains unknown, although a malonyltransferase activity has been purified from oilseed rape (Hörtensteiner, 1998). Arabidopsis UDP-DEPENDENT GLYCOSYLTRANSFERASES (UGTs) are known to catalyze the addition of a sugar group to hydroxyl groups of target molecules by formation of a glycosidic bond (Osmani et al., 2009; Paquette et al., 2003). Therefore, it can be imagined that one or several of the 120 cytosol-localized UGTs (Paquette et al., 2003) are responsible for the addition of glucose on C8^2-OH-FCCs in Arabidopsis.

Demethylation (see Chapter "1"; Christ et al., 2012)

Demethylation of Chl catabolites at C13^2 is species-specific: demethylated Chl catabolites have only been found in Arabidopsis, oilseed rape and *Spinacia oleracea* (Berghold et al., 2002; Hörtensteiner and Kräutler, 2011; Mühlecker and Kräutler, 1996; Pružinská et al., 2005). An enzyme being able to demethylate Pheide to pyroPheide, called pheophorbidase, has been characterized in *Chenopodium album* and radish (Shioi et al., 1996b; Suzuki et al., 2006, 2002). The Chapter "1" of this thesis describes the identification of Arabidopsis MES16 as the enzyme involved in demethylation of Chl catabolites. MES16 localizes to the cytosol and *in vivo* acts within the Chl degradation pathway on the level on FCCs but not on Pheide, as suggested by the previous studies mentioned above. Notably, our results revealed that demethylation of FCCs accelerates their isomerization in the vacuole (see also section "Non-enzymatic isomerization of colorless chlorophyll catabolites"). As a consequence, senescent leaves of *mes16* mutants are fluorescent under UV light due the accumulation of methylated FCCs in the vacuole.

Oxidative deformylation of FCCs (see Chapter "2")

The Chapter "2" of my thesis is dedicated to the discovery of a new type of Chl catabolites in Arabidopsis. These catabolites have already been described in barley and Norway maple and are known as UCCs or NDCCs (Losey and Engel, 2001; Müller et al., 2011). NCCs and NDCCs differ on pyrrole ring A, where the side groups at C6 is a formyl group in NCCs and an oxo group in NDCCs (Fig. I.8; Müller et al., 2011). We demonstrate that NDCCs are the major Chl catabolites in Arabidopsis, accounting for more than 80% of all final Chl catabolites. We further identified cytochrome P450 CYP89A9 of Arabidopsis as being responsible for the oxidative deformylation of FCCs to FDCCs in the cytosol.

Hypermodification of FCCs

Hypermodified FCCs (*h*FCCs) are *m*FCCs in which the C17 propionic chain is substituted with different groups such as digalactosylglyceryl or daucic acid (Banala et al., 2010; Kräutler et al., 2010; Moser et al., 2009a, 2008a). *h*FCCs were shown to be persistant and to accumulate in senescent leaves, most probably because the C17 modifications as well as the intact C13^2 methyl group retained in them inhibits their isomerization in the vacuole (see Chapter "1"; Moser et al., 2009a). Although it remains to be proven, *h*FCCs most probably are as well imported into the vacuole. As a consequence of the accumulation of *h*FCCs, ripe fruits and senescent leaves of some species such as *Musa acuminata*, *Musa cavendish* and *Spathiphyllum wallisii* are fluorescing under UV light. Interestingly, more intense fluorescence than other parts of the peel is observed around necrotic spots in a yellow banana fruit (Moser et al., 2009a). Formation of these highly fluorescent rings was shown to be due to the conversion of *m*FCCs to specific *h*FCCs just prior to cell death. The mechanism increasing the fluorescence in the surrounding of necrotic spots remains unknown. *De novo h*FCCs synthesis from Chl precursors is unlikely. However, it could be due to the degradation of remaining Chl in the yellow peel of banana, although most of Chl has already been broken down. Another reasonable hypothesis to explain the occurrence of these highly fluorescent rings is a higher fluorescence capacity of *h*FCCs compared to *m*FCCs.

Table I.1 List of FCCs, NCCs, UCCs and YCCs identified from higher plants (modified from Hörtensteiner, 2012)

Name	R[1c]	R[2c]	R[3c]	R[4c]	C1-epimer[d]	Source[e]	Reference
			***p*FCCs**				
*p*FCC	H	CH_3	Vinyl	H	1	E	Mühlecker et al., (1997)
epi-*p*FCC	H	CH_3	Vinyl	H	*epi*	E	Mühlecker et al., (2000)
			***m*FCCs**				
At-FCC-1[a]	OH	H	Vinyl	H	1	L	Pružinská et al., (2005)
At-FCC-2[a]	H	H	Vinyl	H	1	L	Pružinská et al., (2005)
C8[2]-OH-FCC	OH	CH_3	Vinyl	H	1	C	This thesis, Chapter 3
			***h*FCCs**				
Mc-FCC-49[b]	*O*-glucosyl	CH_3	Vinyl	Daucic acid	*epi*	F	Moser et al., (2009)
Mc-FCC-56[b]	OH	CH_3	Vinyl	Daucic acid	*epi*	F	Moser et al., (2008a)
Ma-FCC-61[b]	OH	CH_3	Vinyl	Digalactosylglyceryl	*epi*	L	Banala et al., (2010)
Sw-FCC-62[b]	OH	CH_3	Vinyl	Dihydroxyphenyl-ethylglucosyl	1	L	Kräutler et al., (2010)
			NCCs				
At-NCC-1[a]	*O*-glucosyl	H	Vinyl	H	1	L	Pružinská et al., (2005)
At-NCC-2[a]	OH	H	Vinyl	H	1	L	Pružinská et al., (2005)
At-NCC-3[a]	OH[f]	H	Vinyl	H	1	L	Pružinská et al., (2005)
At-NCC-4[a]	*O*-glucosyl	CH_3	Vinyl	H	1	L	Pružinská et al., (2005)
At-NCC-5[a]	H	H	Vinyl	H	1	L	Pružinská et al., (2005)
Bn-NCC-1[a]	*O*-malonyl	H	Vinyl	H	1	L	Mühlecker and Kräutler, (1996)
Bn-NCC-2[a]	*O*-glucosyl	H	Vinyl	H	1	L	Mühlecker and Kräutler, (1996)
Bn-NCC-3[a]	OH	H	Vinyl	H	1	L	Mühlecker and Kräutler, (1996)
Bn-NCC-4[a]	H	H	Vinyl	H	1	L	Pružinská et al., (2005)
Cj-NCC-1[a]	OH	CH_3	Vinyl	H	*epi*	L	Curty and Engel, (1996)
Cj-NCC-2[a]	H	CH_3	Vinyl	H	*epi*	L	Oberhuber et al., (2003)
Hv-NCC-1[a]	OH	CH_3	Dihydroxyethyl	H	1	L	Kräutler et al., (1991)
Lo-NCC-1[a]	OH	CH_3	Vinyl	H	nd	L	Iturraspe et al., (1995)
Ls-NCC-1[a]	OH	CH_3	Vinyl	H	nd	L	Iturraspe et al., (1995)
Ms-NCC-2[a]	OH	CH_3	Vinyl	H	*epi*	F	Müller et al., (2007)
Nr-NCC-1[a]	*O*-glucosylmalonyl	CH_3	Vinyl	H	*epi*	L	Berghold et al., (2004)
Nr-NCC-2[a]	*O*-glucosyl	CH_3	Vinyl	H	*epi*	L	Berghold et al., (2004)
Pc-NCC-1[a]	*O*-glucosyl	CH_3	Vinyl	H	*epi*	F	Müller et al., (2007)
Pc-NCC-2[a]	OH	CH_3	Vinyl	H	*epi*	F	Müller et al., (2007)
So-NCC-1[a]	OH	H	Dihydroxyethyl	H	*epi*	L	Berghold et al., (2002)
So-NCC-2[a]	OH	CH_3	Dihydroxyethyl	H	*epi*	L	Oberhuber et al., (2001)
So-NCC-3[a]	OH	H	Vinyl	H	*epi*	L	Berghold et al., (2002)
So-NCC-4[a]	OH	CH_3	Vinyl	H	*epi*	L	Berghold et al., (2002)
So-NCC-5[a]	H	CH_3	Vinyl	H	*epi*	L	Berghold et al., (2002)
Sw-NCC-58[b]	OH	CH_3	Vinyl	H	1	L	Kräutler et al., (2010)
Tc-NCC-1 [a]	*O*-glucosyl	CH_3	Dihydroxyethyl	H	*epi*	L	Scherl et al., (2012)
Tc-NCC-2 [a]	*O*-glucosyl	CH_3	Vinyl	H	*epi*	L	Scherl et al., (2012)
Xv-NCC-1 [a]	*O*-glucosyl	CH_3	Vinyl	H	*epi*	L	This thesis, Chapter « 4 »
Zm-NCC-1[a]	*O*-glucosyl	CH_3	Dihydroxyethyl	H	*epi*	L	Berghold et al., (2006)
Zm-NCC-2[a]	*O*-glucosyl	CH_3	Vinyl	H	*epi*	L	Berghold et al., (2006)
			UCCs/NDCCs				
Hv-UCC-1[a,g]	OH	CH_3	Dihydroxyethyl	H	1	L	Losey and Engel, (2001)
Ap-UCC-1[a,g]	OH	CH_3	Dihydroxyethyl	H	*epi*	L	Müller et al., (2011)
At-NDCC-1[a]	OH	H	Vinyl	H	*epi*	L	This thesis, Chapter « 2 »

Table I.1 *Continued*

YCCs							
Cj-YCC-1	OH	CH_3	Vinyl	H	*N/A*	L	Moser et al., (2008b)
Tc-YCC-1	*O*-glucosyl	CH_3	Dihydroxyethyl	H	*N/A*	L	Scherl et al., (2012)

[a] A nomenclature for NCCs (and FCCs) has been defined Ginsburg and Matile, (1993) in which a prefix indicates the plant species and a suffix number indicates decreasing polarity in reversed-phase HPLC

[b] These catabolites are indexed according to their retention time in HPLC analysis. *Ap Acer platanoides*, *At Arabidopsis thaliana*, *Bn Brassica napus*, *Cj Cercidiphyllum japonicum*, *Hv Hordeum vulgare*, *Lo Liquidambar orientalis*, *Ls Liquidambar styraciflua*, *Ma Muca acuminate*, *Mc Musa cavendish*, *Ms Malus sylvestris*, *Nr Nicotiana rustica*, *So Spinacia oleracea*, *Sw Spathiphyllum wallisii*, *Tc Tilia cordata*, *Xv Xeropyhta viscosa*, *Zm Zea mays*

[c] R^1–R^4 indicate residues at C3, $C8^2$, $C13^2$ and $C17^3$ side positions, respectively, of FCCs, NCCs, UCCs and YCCs as shown in Fig. I.7

[d] C1 stereochemistry refers to the type of pFCC, i.e. *p*FCC (1) or *epi*-pFCC (*epi*), formed in the respective species or genus; nd, not determined; N/A, Not Applicable

[e] Source of material used for catabolite isolation: E, in vitro enzymatic PAO/RCCR assays; F, fruits; L, leaves; C, isolated chloroplasts

[f] In *At*-NCC-3, the site of hydroxylation is indicated to be C7 (rather than $C8^2$) (Müller et al. 2006)

[g] *Hv*-UCC-1 and *Ap*-UCC-1 are indicated to be pseudo-enantiomers (Müller et al. 2011)

Storage and transport of coloress chlorophyll catabolites

Transport of chlorophyll catabolites within the cell (see Chapter "3")

Chl degradation starts in the chloroplast and ends in the vacuole. Therefore, two translocations systems have to transport Chl catabolites across the chloroplast envelope and the tonoplast. Only one study has been published on Chl catabolite transport across the plastid envelope, which shows that the release of FCCs from isolated barley gerontoplasts is enhanced by external supply of ATP (Matile et al., 1992). This observation has led to the hypothesis that transport of FCCs across the chloroplast envelope could be mediated by ATP BINDING CASSETTE (ABC) transporter(s) (Hörtensteiner, 2006). Interestingly, suppression of BREAST CANCER RESISTANCE PROTEIN 1 (BCRP1), a mammalian ABC-type transporter, in mice triggers a porphyria-like phenotype (phototoxic ear lesions), which is due to the incapacity of the animals to detoxify food-derived Pheide and protoporphyrin IX circulating in the blood (Jonker et al., 2002). The Arabidopsis genome encodes 130 ABC transporters, which are localized in membranes of most sub-cellular compartments (Kang et al., 2011a). To date, screening and crossing of several T-DNA insertion lines for BCRP1 homologues and other ABC-transporters predicted to be localized in the chloroplast envelope did not provide any evidence for their involvement in FCCs export from the chloroplast (Sylvain Aubry, Silvia Schelbert, Maja Schellenberg, Kathrin Salinger and Stefan Hörtensteiner, unpublished data). Most probably, transport across the envelope of FCCs and potentially of other tetrapyrroles molecules such as phytochromobillin is performed by several transporters. This potential redundancy increases the difficulty of identifying these transporters *in vivo*. The Chapter "3" describes a novel method that can be used to further characterise the release of FCCs from isolated Arabidopsis chloroplasts. Usually, transport experiments performed with isolated

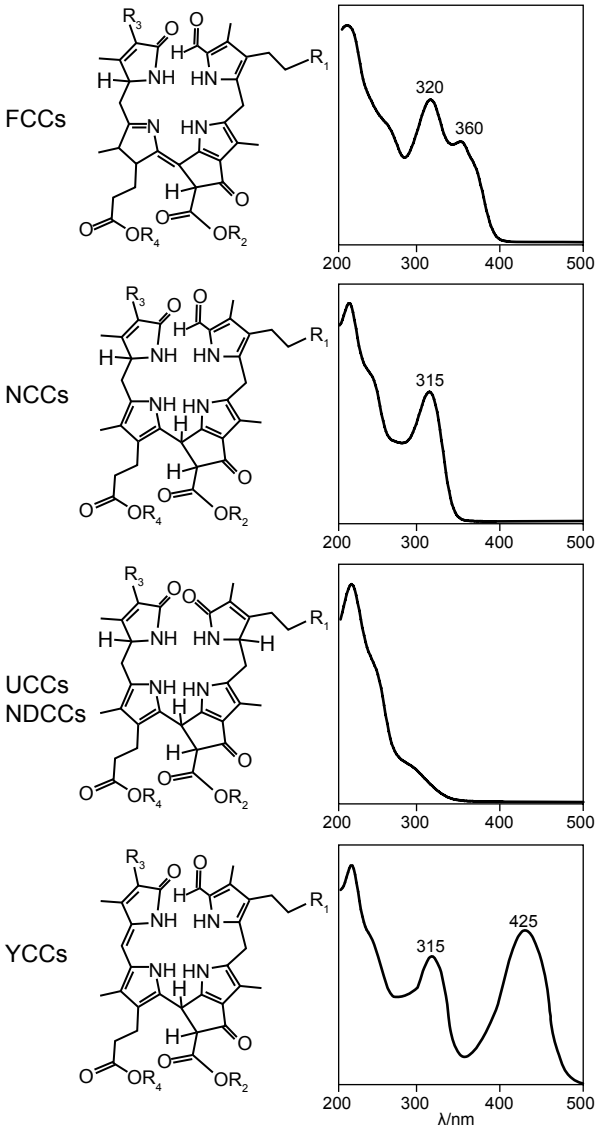

Figure I.8. Constitutional formulae and UV/Vis spectra of FCCs, NCCs, UCCs/NDCCs and YCCs. Substituents at R^1, R^2, R^3, and R^4 of colorless catabolites described from wild-type plants are presented in Table I.1.

organelles involves their repurification after the assay, in order to allow quantification of the export or import of the tested substrate. Here, we make use of the recently identified MES16, an enzyme which is able to demethylate FCCs (see Chapter "1"; Christ et al., 2012), to change the polarity of FCCs that are exported from the chloroplast during the assay. Thus, HPLC analysis of crude assays allows discriminating between exported FCCs (demethylated) and FCCs remaining in the chloroplast (methylated) (See Chapter "3" for more information).

Import of FCCs from the cytosol into the vacuole is better understood than their transport across the chloroplast envelope. Heterologous expression in yeast of Arabidopsis *At*MRP2 and *At*MRP3, two members of the MULTIDRUG RESISTANCE–ASSOCIATED PROTEIN (MRP) subfamily of ABC transporters, revealed that they are capable of importing NCCs *in vitro* (Lu et al., 1998; Tommasini et al., 1998). Although this results has been obtained using NCCs as substrate rather than FCCs, such type of transporters are most probably involved in transport of Chl catabolites across the tonoplast. However, like for the export of FCCs from the chloroplast, redundancy could render their reverse genetic identification difficult.

Non-enzymatic isomerization of colorless chlorophyll catabolites

*m*FCCs have been described to be converted into their respective NCCs in the vacuole by a nonenzymatic isomerization (Oberhuber et al., 2003). This reaction occurs significantly only under acidic conditions such as the ones found in the vacuole (pH 5-6) (Oberhuber et al., 2003). The rate of FCC-to-NCC isomerization increases with decreasing pH and seems to be also influenced by certain modifications of FCC side-chains (Christ et al., 2012; Moser et al., 2009a). Thus, *m*FCCs harbouring an intact methyl group at $C13^2$ showed slower isomerization *in vitro* when compared to demethylated FCCs (see Chapter "1"; Christ et al., 2012). Moreover, $C17^3$ modification of *h*FCCs is thought to inhibit their conversion to *h*NCCs (Moser et al., 2009a). Finally FDCCs, produced by CYP89A9 in Arabidopsis through an oxidative deformylation of FCCs, were also shown to be converted to NDCCs at pH 5 *in vitro* (see Chapter "2").

Storage of NDCC/NCCs versus further degradation?

Monopyrrolic catabolites of Chl have been shown to accumulate during leaf senescence in barley and radish (Suzuki and Shioi, 1999; Suzuki et al., 1999). This finding is consistent with the observation that NDCCs and NCCs accumulating in senescent leaves of barley represent only a minor fraction of the total amount of Chl that has been degraded (Aditi Das, Stefan Hörtensteiner and Bernhard Kräulter, unpublished data). However, in Arabidopsis, quantification of NDCCs and NCCs accumulating in yellow leaves reveals that their amount reflects the Chl content of green leaves, indicating that NDCCs and NCCs are not further fragmented (see Chapter "2"). The same observation was made in *Cercidiphyllum japonicum* (Curty and Engel, 1996). Together, these studies tend to conclude that the fate of NCCs/NDCCs in the vacuole (storage or further fragmentation) differ between plant species. However, it cannot be excluded that the inconsistency between amounts of colorless catabolites and degraded Chl in some species is due to a second and entirely different pathway for Chl breakdown that would be independent of PAO activity.

AIM OF THE THESIS

The main goal of my PhD was to advance the knowledge on modifications of colorless Chl catabolites occurring during leaf senescence of Arabidopsis. In this thesis, I report on:

(1) The identification and characterization of MES16, the enzyme responsible for FCC demethylation in Arabidopsis.
(2) The identification of novel Chl catabolites in Arabidopsis, termed NDCCs, and the characterization of the cytochrome P450 monooxygenase CYP89A9 responsible for their formation.
(3) The subcellular localization and attempt to characterize FCC hydroxylation, and the elaboration of a novel method to characterize the transport of FCCs across the gerontoplast envelope in Arabidopsis.

In the frame of my PhD, I also collaborated with other research groups on:

(4) The study of Chl breakdown during desiccation of the resurrection plant *Xerophyta viscosa.*
(5) The re-examination of the function(s) of the dual localization of RCCR in both chloroplasts and mitochondria.
(6) The investigation on the role of the α-galactosidase *At*DIN10 during leaf senescence and cold acclimation in Arabidopsis.

1 - FCC DEMETHYLATION

MES16, a member of the methylesterase protein family, specifically demethylates fluorescent chlorophyll catabolites during chlorophyll breakdown

Published in Plant Physiology (2012) 158: 628–641

This chapter describes the identification of Arabidopsis MES16 as the enzyme involved in demethylation of Chl catabolites. MES16 localizes to the cytosol and *in vivo* acts within the Chl degradation pathway on the level on FCCs but not on Pheide, as suggested by the previous studies. Notably, our results revealed that demethylation of FCCs accelerates their isomerization in the vacuole. As a consequence, senescent leaves of *mes16* mutants are fluorescent under UV light due the accumulation of methylated FCCs in the vacuole. Together, these data demonstrate that MES16 is an integral component of Chl breakdown in Arabidopsis and specifically demethylates Chl catabolites at the level of FCCs in the cytosol.

Bastien Christ, Silvia Schelbert, Sylvain Aubry, Iris Süssenbacher, Thomas Müller, Bernhard Kräutler, and Stefan Hörtensteiner

REPRINT of Christ B et al. (2012) Plant Physiol 158: 628–641

MES16, a Member of the Methylesterase Protein Family, Specifically Demethylates Fluorescent Chlorophyll Catabolites during Chlorophyll Breakdown in Arabidopsis[1,2][W][OA]

Bastien Christ, Silvia Schelbert, Sylvain Aubry[3], Iris Süssenbacher, Thomas Müller, Bernhard Kräutler, and Stefan Hörtensteiner*

Institute of Plant Biology, University of Zurich, CH–8008 Zurich, Switzerland (B.C., S.S., S.A., S.H.); and Institute of Organic Chemistry and Center of Molecular Biosciences, University of Innsbruck, A–6020 Innsbruck, Austria (I.S., T.M., B.K.)

During leaf senescence, chlorophyll (Chl) is broken down to nonfluorescent chlorophyll catabolites (NCCs). These arise from intermediary fluorescent chlorophyll catabolites (FCCs) by an acid-catalyzed isomerization inside the vacuole. The chemical structures of NCCs from Arabidopsis (*Arabidopsis thaliana*) indicate the presence of an enzyme activity that demethylates the C13[2]-carboxymethyl group present at the isocyclic ring of Chl. Here, we identified this activity as methylesterase family member 16 (MES16; At4g16690). During senescence, *mes16* leaves exhibited a strong ultraviolet-excitable fluorescence, which resulted from large amounts of different FCCs accumulating in the mutants. As confirmed by mass spectrometry, these FCCs had an intact carboxymethyl group, which slowed down their isomerization to respective NCCs. Like a homologous protein cloned from radish (*Raphanus sativus*) and named pheophorbidase, MES16 catalyzed the demethylation of pheophorbide, an early intermediate of Chl breakdown, in vitro, but MES16 also demethylated an FCC. To determine the in vivo substrate of MES16, we analyzed *pheophorbide a oxygenase1* (*pao1*), which is deficient in pheophorbide catabolism and accumulates pheophorbide in the chloroplast, and a *mes16pao1* double mutant. In the *pao1* background, we additionally mistargeted MES16 to the chloroplast. Normally, MES16 localizes to the cytosol, as shown by analysis of a MES16-green fluorescent protein fusion. Analysis of the accumulating pigments in these lines revealed that pheophorbide is only accessible for demethylation when MES16 is targeted to the chloroplast. Together, these data demonstrate that MES16 is an integral component of Chl breakdown in Arabidopsis and specifically demethylates Chl catabolites at the level of FCCs in the cytosol.

The degradation of chlorophyll (Chl) is a catabolic process that massively occurs during leaf senescence and fruit ripening (Hörtensteiner and Kräutler, 2011). It aims at the detoxification of this potentially phototoxic pigment; therefore, Chl breakdown is seen as a prerequisite for the degradation of Chl-binding proteins, which are an important nitrogen source for recycling from leaves to storage organs or seeds. This view is supported by the analysis of *stay-green* (*sgr*) mutants that are affected in certain steps of Chl breakdown; during senescence, leaves of these mutants retain large quantities of Chl-apoprotein complexes (Hilditch et al., 1989; Kusaba et al., 2007; Park et al., 2007; Morita et al., 2009; Schelbert et al., 2009). The fate of Chl was enigmatic for a long time, but since the identification of a first nonfluorescent chlorophyll catabolite (NCC) as an (end) product of Chl breakdown from barley (*Hordeum vulgare*; Kräutler et al., 1991), the breakdown pathway has largely been resolved (Kräutler and Hörtensteiner, 2006; Hörtensteiner and Kräutler, 2011).

The first part of the pathway is localized in senescing chloroplasts. It is composed of a series of reactions that are common in higher plants and that lead to the formation of a primary fluorescent chlorophyll catabolite (*p*FCC; Mühlecker et al., 1997). Thereby, first the central magnesium (Mg) atom is removed from Chl by a heat-stable, low-M_r compound, termed metal-chelating substance (Suzuki et al., 2005), whose molecular nature is so far unknown. The product of Mg dechelation,

[1] This work was supported by the Swiss National Science Foundation (grant nos. 3100A0–117940 and 31003A–132603) and the National Centre of Competence in Research Plant Survival, a research program of the Swiss National Science Foundation (to S.H.) and by the Austrian National Science Foundation (Fonds zur Förderung der wissenschaftlichen Forschung project no. P 19596 to B.K.).

[2] This article is dedicated to the memory of Prof. Philippe Matile, a pioneer in chlorophyll breakdown research, who passed away on October 29, 2011.

[3] Present address: Department of Plant Science, University of Cambridge, Cambridge CB2 3EA, United Kingdom.

* Corresponding author; e-mail shorten@botinst.uzh.ch.

The author responsible for distribution of materials integral to the findings presented in this article in accordance with the policy described in the Instructions for Authors (www.plantphysiol.org) is: Stefan Hörtensteiner (shorten@botinst.uzh.ch).

[W] The online version of this article contains Web-only data.

[OA] Open Access articles can be viewed online without a subscription.

www.plantphysiol.org/cgi/doi/10.1104/pp.111.188870

pheophytin, is then hydrolyzed to pheophorbide (Pheide) and phytol by pheophytinase (PPH; Schelbert et al., 2009). For a long time, phytol removal was thought to be catalyzed by chlorophyllase (Takamiya et al., 2000), but recent analysis of single and double knockout mutants in Arabidopsis (*Arabidopsis thaliana*) demonstrated chlorophyllase to be dispensable for Chl breakdown during leaf senescence (Schenk et al., 2007). Instead, PPH specifically dephytylates pheophytin, but not Chl, and *pph* mutants are blocked in Chl breakdown and as a consequence exhibit a stay-green phenotype (Schelbert et al., 2009). After the formation of Pheide, the porphyrin macrocycle is opened by the action of Pheophorbide *a* Oxygenase (PAO), a Rieske-type monooxygenase (Hörtensteiner et al., 1998), which has an intriguing specificity for Pheide *a* (Hörtensteiner et al., 1995; Pruzinská et al., 2003; Tanaka et al., 2003). PAO is a key enzyme, because it determines the basic structure of all downstream catabolites. Therefore, this pathway of Chl breakdown is nowadays often called the "PAO pathway." The substrate specificity of PAO is believed to force Chl *b*-to-Chl *a* conversion to occur upstream of PAO to enable Chl *b* degradation. Recently, *nonyellow coloring1* (*NYC1*), *NYC1-like*, and *7-hydroxymethyl chlorophyll a reductase* were cloned and shown to encode enzymes required to catalyze the two consecutive steps of Chl *b*-to-Chl *a* reduction (Kusaba et al., 2007; Horie et al., 2009; Sato et al., 2009; Meguro et al., 2011). Mutants deficient in NYC1 exhibit a stay-green phenotype, indicating that Chl *b* reduction could initiate the degradation of both Chl and Chl-binding proteins by destabilizing respective pigment-protein complexes (Hörtensteiner, 2006). The final step in *p*FCC formation is the site-specific and stereoselective reduction of red Chl catabolite (the product of PAO activity) catalyzed by red chlorophyll catabolite reductase (RCCR; Wüthrich et al., 2000; Pruzinská et al., 2007).

*p*FCC was shown to be exported from senescing chloroplasts in an ATP-dependent manner (Matile et al., 1992). This indicates that the later steps of the PAO pathway (i.e. modifications of different side positions of *p*FCC) likely occur in the cytosol. While hydroxylation of the $C8^2$-ethyl moiety (for atom numbering in FCCs, see Fig. 2D below) seems to be a common reaction in all species from which NCCs have been structurally characterized so far, other modifications occur in a species-specific manner. For example, catabolites with a demethylated $C13^2$-carboxymethylester have so far only been found in Arabidopsis, oilseed rape/canola (*Brassica napus*), and spinach (*Spinacia oleracea*; Mühlecker and Kräutler, 1996; Berghold et al., 2002; Pruzinská et al., 2005; Hörtensteiner and Kräutler, 2011). Finally, modified FCCs are imported into the vacuole, where they are nonenzymically isomerized to their respective NCCs, because of the acidic pH of the vacuolar sap (Oberhuber et al., 2003). Interestingly, persistent so-called "hypermodified" FCCs have recently been identified in banana (*Musa* sp.) and peace lily (*Spathiphyllum wallisii*; Moser et al., 2009; Banala et al., 2010; Kräutler et al., 2010). In these FCCs, the C17 side chain is modified with different ester moieties; thus, FCC-to-NCC isomerization, which requires a free C17-propionyl acid function, is disabled (Oberhuber et al., 2003; Hörtensteiner and Kräutler, 2011).

Besides these main steps of the PAO pathway, additional/alternative reactions of Chl breakdown have been described in the past. These were (mostly) inferred from the identification of different types of Chl degradation products, such as Chl-derived monopyrroles (Suzuki and Shioi, 1999), urobilinogenoidic catabolites (Losey and Engel, 2001), and different pigments with an intact porphyrin ring. Among the latter are pyro (=$C13^2$-decarboxymethylated) forms of Pheide and pheophytin, which have been discussed as breakdown products of Chl in algae and higher plants (Schoch and Vielwerth, 1983; Ziegler et al., 1988; Shioi et al., 1991). In support of this finding was the demonstration of Pheide-to-pyro-Pheide conversion in enzyme extracts of different higher plants species, such as satsuma (*Citrus unshiu*) fruit peel and leaves of goosefoot (*Chenopodium album*) and different Brassicaceae species (Shimokawa et al., 1990; Suzuki et al., 2002). The enzyme, named pheophorbidase (PPD), was shown to only catalyze demethylation at the $C13^2$-carboxymethyl group of Pheide to yield $O13^4$-desmethyl Pheide, while the subsequent decarboxylation to form pyro-Pheide occurred spontaneously without the contribution of PPD (Shioi et al., 1996). In contrast, an activity that directly converts Pheide to pyro-Pheide without the occurrence of the $O13^4$-desmethyl intermediate was described in *Chlamydomonas reinhardtii* (Suzuki et al., 2002). PPD was recently purified and cloned from radish (*Raphanus sativus* [RsPPD]; Suzuki et al., 2006, 2008). RsPPD specifically acts on Pheide and bacterio-Pheide, but not on phytol- and/or Mg-containing- or proto-Chl species. Homologs of RsPPD were identified in other Brassicaceae species (Suzuki et al., 2006). In Arabidopsis, RsPPD is most closely related to MES16 (At4g16690), one of the 20 members of the Arabidopsis methylesterase (MES) protein family (Yang et al., 2008). Structurally, PPD and MES proteins belong to the α/β-hydrolase protein "superfamily" and possess a catalytic Ser-His-Asp triad (Dodson and Wlodawer, 1998). MES16 was shown to hydrolyze two different methylated plant hormones, methyl-indole acetic acid (MeIAA) and methyl-jasmonic acid (MeJA), in vitro (Yang et al., 2008).

Here, we demonstrate that MES16 is involved in Chl breakdown during Arabidopsis leaf senescence. MES16-deficient mutants (*mes16*) were still able to degrade Chl, but they accumulated FCCs and NCCs with an intact $C13^2$-carboxymethyl group. As a consequence, FCC-to-NCC isomerization was compromised and the mutants accumulated large quantities of FCCs, which caused senescent leaves to fluoresce under UV light. Recombinant MES16 protein was able to demethylate both Pheide and *p*FCC, but in vivo, MES16 specifically acts on FCCs. To prove this, we show the cytosolic localization of MES16 using GFP fusions. In addition, targeting

of MES16 to the chloroplast led to an accumulation of pyro-Pheide in a PAO mutant (*pao1*) background, while *pao1* and a *mes16pao1* double mutant accumulated Pheide. In summary, we demonstrate that MES16 specifically catalyzes methylester hydrolysis at $O13^4$ ($O13^4$-demethylation) of FCCs and, thus, that this enzyme is located within the PAO pathway of the breakdown of Chl to NCCs in Arabidopsis.

RESULTS

Arabidopsis MES16 Catalyzes the $O13^4$-Demethylation of Pheide and *p*FCC in Vitro

The distribution of PPD activity was shown to correlate with the occurrence of NCCs harboring a free $C13^2$-carboxyl group. For example, all investigated Brassicaceae species have PPD activity (Suzuki et al., 2002), and $O13^4$-demethylated FCCs and NCCs have been found in canola and Arabidopsis (Mühlecker and Kräutler, 1996; Pruzinská et al., 2005), indicating that PPD could be responsible for this site-specific modification. A protein BLAST search of RsPPD against the Arabidopsis proteome uncovered high homology to members of the MES family of Arabidopsis (Vlot et al., 2008; Yang et al., 2008). Thereby, RsPPD clustered with the members of subfamily 2, as determined by Yang et al. (2008), with highest homology to MES16 (Fig. 1A). The phylogenetic tree of Figure 1A includes further MES-like EST-derived sequences from plant species for which NCC structures have been determined. The tree indicates that subfamily 2 members of the MES protein family are indeed present in other Brassicaceae species, but also in barley and maize (*Zea mays*), where evidence for hydrolysis of the methylester group at $C13^2$ has not been provided (Kräutler et al., 1991; Berghold et al., 2006).

Analysis of gene expression patterns has proven successful in the past to identify potential Chl catabolic enzymes (Schelbert et al., 2009; Ren et al., 2010). When analyzing microarray expression data of the Arabidopsis *MES* genes using the Genevestigator tool (Zimmermann et al., 2004), *MES5*, *MES9*, and *MES16* exhibited increased expression levels in senescent leaves compared with green leaves (Fig. 1B). In addition, using the ATTED tool (Obayashi et al., 2009), *MES16* was found in a network of coexpression with other Chl catabolic genes (Supplemental Fig. S1). Using semiquantitative reverse transcription (RT)-PCR, we confirmed the senescence-regulated expression of *MES16* in the wild type upon dark-induced senescence (Fig. 1C). Thereby, the expression pattern was very similar to the expression of *PAO* and *SGR*. SGR is required for the initiation of Chl breakdown and has been proposed to play a regulatory role in Chl-apoprotein complex destabilization (Hörtensteiner, 2009). From this analysis, MES16 appeared to be the most likely candidate for $O13^4$-demethylation in Arabidopsis.

To investigate its enzymatic activity, recombinant MES16 was produced in *Escherichia coli* in fusion with an N-terminal His tag. MES16 (Fig. 2A) was able to convert Pheide *a* to pyro-Pheide *a* in a time-dependent manner. As described for RsPPD (Suzuki et al., 2006), MES16 most likely only catalyzed methylester hydrolysis of Pheide *a* to $O13^4$-desmethyl Pheide *a*, while the subsequent decarboxylation to pyro-Pheide *a* occurred spontaneously without the involvement of MES16; however, this was not analyzed in more detail. When *p*FCC was used as the substrate for recombinant MES16, a new, more polar FCC peak appeared in reverse-phase HPLC (Fig. 2B), which by mass spectrometry (MS) analysis (for MS data, see "Materials and Methods") was identified as the $O13^4$-demethylated form of *p*FCC ($O13^4$-desmethyl *p*FCC). In contrast, recombinant His-tagged versions of MES17 and MES18, the two other subfamily 2 members (Fig. 1A), and MES5 and MES9, the other senescence-regulated MES proteins (Fig. 1B), were unable to demethylate *p*FCC (Supplemental Fig. S2, A–C).

As described for RsPPD (Suzuki et al., 2006), MES16 was unable to demethylate CjNCC-1, an NCC isolated from senescent leaves of *Cercidiphyllum japonicum* (Curty and Engel, 1996; Supplemental Fig. S2D). MES16 has been shown to hydrolyze MeJA and MeIAA (Yang et al., 2008). To obtain insight into the substrate specificity of recombinant MES16, we tested its *p*FCC esterase activity in the presence of 100-fold molar excesses of MeJA, MeIAA, and methyl salicylic acid (MeSA) or a 10-fold molar excess of Pheide *a*. As shown in Figure 2E, under these conditions, *p*FCC demethylation was only impaired to some extent by MeIAA, indicating that in vitro, MES16 has a high preference for an FCC as substrate.

mes16 Mutants Are Compromised in Chl Degradation

To investigate the in vivo role of MES16 in relation to Chl breakdown, two independent T-DNA insertion lines, named *mes16-1* and *mes16-2* (Fig. 3A), were obtained from the SALK resource (Alonso et al., 2003). *MES16* expression analysis of these mutants indicated both alleles to represent true knockout mutants (Fig. 3B). The absence of full-length *MES16* transcripts in these mutants did not affect the senescence-regulated expression of *PAO* and *SGR* (Fig. 3B). The mutants did not show any phenotype during normal growth under either short-day or long-day conditions. When senescence was induced in the dark with detached leaves, *mes16* mutants did not exhibit a dramatic stay-green phenotype, although, compared with the wild type, Chl was significantly retained at a low level (Fig. 3C).

When extracts of senescent leaves of *mes16-1* and *mes16-2* were analyzed for the presence of FCCs and NCCs using reverse-phase HPLC, major differences were observed in comparison with wild-type leaves (Fig. 4A). Thus, except for two peaks comigrating with *p*FCC and At-NCC-4 (Pruzinská et al., 2005), all FCCs

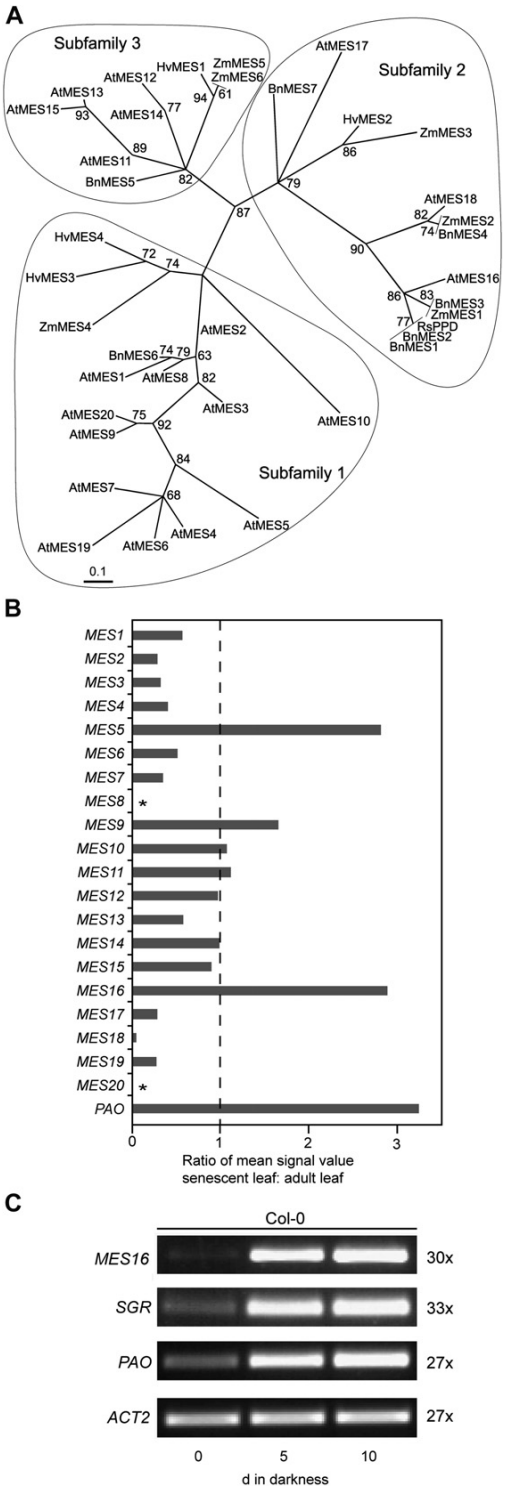

Figure 1. Identification of MES16. A, Maximum likelihood phylogenetic tree of radish PPD (RsPPD) and MES proteins from Arabidopsis (At), canola (Bn), barley (Hv), and maize (Zm). Branch support values are based on 100 bootstrap replicates and are indicated when higher than 50%. Three subfamilies as determined by Yang et al. (2008) are circled. For sequence accession numbers, see "Materials and Methods." B, Analysis of senescence-related expression of the Arabidopsis MES family using the Genevestigator Meta-Analyzer tool (Zimmermann et al., 2004). The ratio of mean fluorescence values from senescent leaves (organ no. 44; number of chips, three) and adult leaves (organ no. 42; number of chips, 274) is shown. The value for *PAO* is shown as a reference. Asterisks indicate that *MES8* and *MES20* are not represented on the ATH1 chip used for analysis. C, Analysis of gene expression during dark-induced senescence in Col-0. *ACT2* was used as a control. Expression was analyzed with nonsaturating numbers of PCR cycles as shown at the right. PCR products were separated on agarose gels and visualized with ethidium bromide.

and NCCs of the *mes16* mutants, as detected by their typical fluorescence and/or absorption properties, were likely novel Chl catabolites not found before in Arabidopsis. The three major FCC fractions, tentatively named *mes16*-FCC-1, *mes16*-FCC-2, and *mes16*-FCC-3, and the major NCC fraction (*mes16*-NCC-1) were isolated from *mes16-1* and analyzed by MS (for MS data, see "Materials and Methods"). As seen in Table I, all analyzed catabolites possessed an intact $C13^2$-carboxymethyl group. In addition, the respective identities of *mes16*-FCC-3 and *mes16*-NCC-1 with *p*FCC and At-NCC-4, the only $O13^4$-methylated catabolites detected in the wild type (Pruzinská et al., 2005), could be confirmed by MS and HPLC. To our surprise, quantification of these catabolites revealed that both *mes16* lines accumulated significantly higher overall amounts of FCC and NCC (Fig. 4B). The reason for this higher quantity of Chl catabolites in the mutants is unclear at present. Moreover, while the wild type almost exclusively accumulated NCCs, senescent *mes16* leaves contained high proportions of FCCs. As a consequence, senescent *mes16* leaves, but not wild-type leaves, exhibited blue fluorescence when excited with UV light (Fig. 4C). Intense fluorescence could also be observed in naturally senesced *mes16-1* leaves (Supplemental Fig. S3B). To investigate whether the other MES subfamily 2 members (i.e. MES17 and MES18; Fig. 1A) or other senescence-regulated MES proteins (i.e. MES5 and MES9; Fig. 1B) are involved in Chl breakdown, T-DNA insertion lines of respective genes were isolated and FCCs and NCCs were analyzed after dark-induced senescence (Supplemental Fig. S3C). None of these mutants exhibited a catabolite pattern that was different from the wild type. Together with the above-described absence of Chl catabolite esterase activity of the respective recombinant proteins (Supplemental Fig. S2), this result indicates that MES16 acts nonredundantly toward the formation of Chl catabolites that carry a free carboxylic acid function at $C13^2$.

FCC-to-NCC Isomerization Is Affected in *mes16* Mutants

To analyze why *mes16* mutants accumulated rather high amounts of FCCs, we first investigated the subcellular localization of these Chl catabolites. To this end, Chl catabolites extracted from isolated vacuoles of

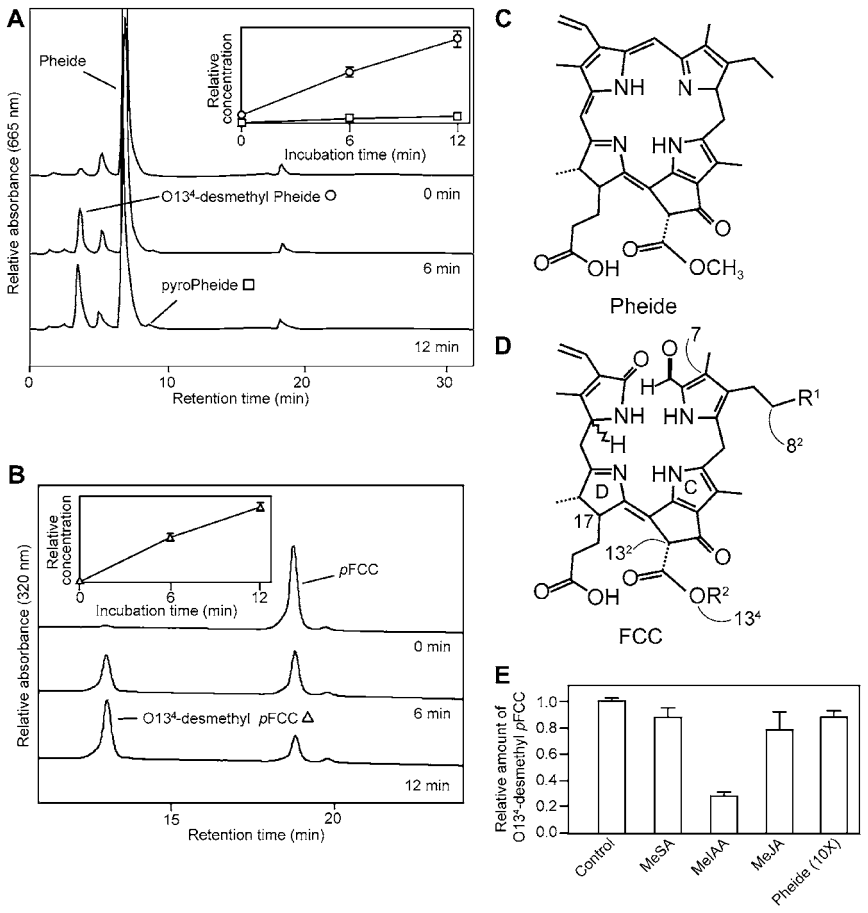

Figure 2. Analysis of recombinant MES16. A and B, HPLC analysis of assays employing *E. coli* lysate expressing 6xHis-MES16 with Pheide (A) and *p*FCC (B) as substrate. HPLC traces at A_{665} (A) or A_{320} (B) before (0 min) and after 6 and 12 min of incubation at 25°C are shown. For clarity, only a part of the HPLC traces at A_{320} (B) is shown. The insets show the relative concentrations of formed products (O13^4-desmethyl Pheide, white circles; pyro-Pheide, white squares; O13^4-desmethyl *p*FCC, white triangles). Values are means of three replicates. Error bars indicate SD. C and D, Chemical structures of Pheide *a* and FCCs, respectively. Relevant carbon atoms and pyrrole rings are indicated in the FCC structure in D. E, Competition assays were performed for 6 min using MeIAA, MeSA, or MeJA at a final concentration of 1.5 mM (100× molar excess to *p*FCC) and Pheide at a concentration of 150 μM (10×). A relative value of 1 corresponds to 0.05 nmol of O13^4-desmethyl *p*FCC being produced during the incubation under the standard conditions as described in "Materials and Methods." Values are means of three replicates. Error bars indicate SD.

senescent *mes16-1* leaf material were analyzed by reverse-phase HPLC and compared with the catabolites of protoplasts (Fig. 5A). The pattern of FCCs and NCCs was identical in the two fractions and, given a rather low contamination of the vacuolar fraction with extravacuolar compartments, also the relative amounts of different catabolites were comparable between vacuoles and protoplasts. The major difference between these two fractions was *p*FCC (=*mes16*-FCC-3), which was absent from vacuoles. This indicated that most of the FCCs and NCCs found in *mes16-1* accumulated in the vacuolar sap, as is known for wild-type Arabidopsis and other plant species (Matile et al., 1988; Hinder et al., 1996; Pruzinská et al., 2007). Using confocal microscopy, vacuolar localization of *mes16*-FCCs was confirmed in senescent *mes16-1* leaves; when excited with a 355-nm laser, mutant cells of the palisade mesophyll exhibited a strong blue fluorescence that covered the entire cellular space, indicating vacuolar origin (Fig. 5B). In contrast, wild-type mesophyll tissue only weakly fluoresced under these conditions.

These data let us assume that the isomerization of FCCs to NCCs was compromised in *mes16* mutants. We speculated that this phenomenon could result from the possibility that the presence of an intact C13^2-carboxymethyl group in the *mes16*-FCCs could affect the efficiency of their isomerization to the respective NCCs. To test this, we compared the rates of FCC-to-NCC isomerization at different pH values using either *p*FCC (with an intact C13^2-carboxymethyl group) or the product of its hydrolysis with recombinant MES16, O13^4-desmethyl *p*FCC (Fig. 5C). Both FCCs were converted to the respective NCCs, but the rates of isomerization differed considerably, as judged from the half-lives of the FCC substrates under the given pH conditions. Thus, both at pH 5 and 6, the conversion of O13^4-desmethyl *p*FCC was about three times faster than that of *p*FCC (Table II). This delay of isomerization is likely, at least in part, responsible for the observed retention of FCCs in the *mes16* mutants. A second (additional) possibility (i.e. that the vacuolar pH could be higher in *mes16* and, therefore, the acid-catalyzed FCC-to-NCC isomerization could be slower as compared with the wild type) was not experimentally tested here.

Pheide *a* Is Not an in Vivo Substrate for MES16

As shown above, the absence of MES16 in *mes16* mutants abolished the O13^4-demethylation of Chl ca-

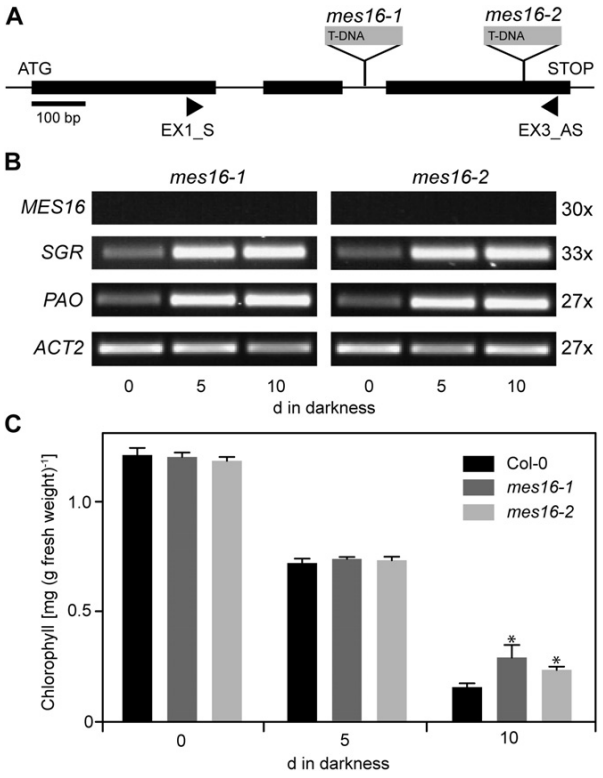

Figure 3. Deficiency of MES16 does not affect the first steps of Chl degradation. A, Gene structure of *MES16* showing the T-DNA insertion sites of two different *mes16* mutants studied here. The sites of insertion were verified by sequencing. The positions of primers used for RT-PCR are shown. B, Analysis of gene expression during dark-induced senescence in *mes16-1* and *-2*. *ACT2* was used as a control. Expression was analyzed with nonsaturating numbers of PCR cycles as shown at the right. After 30 PCR cycles, which produced clearly visible bands in Col-0 (Fig. 1C), *MES16* expression was not obvious in *mes16* mutants. PCR products were separated on agarose gels and visualized with ethidium bromide. C, Chl degradation of *mes16* mutants during dark-induced senescence. Data are mean values of a representative experiment with three replicates. Error bars indicate SD. The asterisks indicate the significance of differences between the wild type and *mes16* mutants at $P < 0.03$ as determined using a two-tailed *t* test.

tabolites, as seen in the FCCs and NCCs, the (final) products of degradation. At the same time, recombinant MES16 was able to demethylate both Pheide and *p*FCC. Therefore, the question arose, what is the in vivo substrate of MES16? To answer this, we first investigated the subcellular localization of MES16 by transiently expressing a MES16-GFP fusion protein in wild-type protoplasts and analyzing GFP fluorescence with confocal microscopy (Fig. 6A). Similar to a free GFP control, MES16-GFP localized to the cytosol. The integrity of the fusion protein was analyzed on immunoblots of transformed protoplasts using an anti-GFP antiserum (Fig. 6B). This localization excluded Pheide *a* as a likely substrate for MES16, because PAO, the exclusive Pheide *a*-catabolizing enzyme of higher plants, has been localized to the chloroplast (Matile and Schellenberg, 1996; Joyard et al., 2009) and export of Pheide from senescent chloroplasts followed by reimport of O13^4-desmethyl Pheide is unlikely to occur (Hörtensteiner, 2006). To confirm that the in vivo activity of MES16 is restricted to the cytosol, we mistargeted C-terminally hemagglutinin (HA)-tagged MES16 to the chloroplast in transgenic ecotype Columbia (Col-0) and *pao1*. To direct MES16-HA to the chloroplast, we

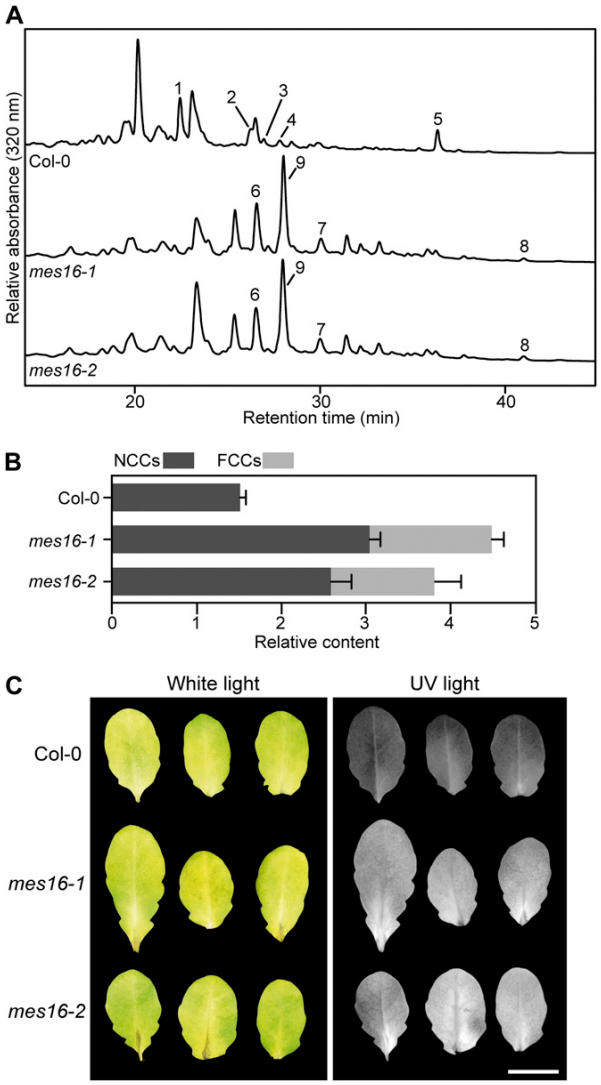

Figure 4. Colorless catabolites of *mes16* mutants. A, Colorless catabolites of dark-incubated (10 d) leaves of Col-0 and *mes16* mutants were separated by HPLC as described in "Materials and Methods." A_{320} is shown. For clarity, only a part of the HPLC traces is shown. For identification and peak numbering of FCCs and NCCs, see Table I. B, Relative contents of NCCs and FCCs. Values are means of three replicates. Error bars indicate SD. C, Photographs of dark-incubated (10 d) Col-0 and *mes16* leaves under white light and UV light (366 nm). Bar = 1 cm.

Table I. *FCCs and NCCs occurring in Col-0 and mes16 mutants during chlorophyll breakdown as identified in this work*

Name	ID[a]	R^{1b}	R^{2b}	Identification[c]	Identity with
At-NCC-1	1	*O*-Glucosyl	H	s	–
At-NCC-2	2	OH	H	s	–
At-NCC-3[d]	3	H	H	s	–
At-NCC-4	4	*O*-Glucosyl	CH_3	s	*mes16*-NCC-1
At-NCC-5	5	H	H	s	–
mes16-FCC-1	6	*O*-Glucosyl	CH_3	s, m	–
mes16-FCC-2	7	OH	CH_3	s, m	–
mes16-FCC-3	8	H	CH_3	s, m	*p*FCC
mes16-NCC-1	9	*O*-Glucosyl	CH_3	s, m	At-NCC-4

[a]ID indicates peak numbers used in Figures 5 and 6. [b]R^1 and R^2 indicate residues at $C8^2$ and $O13^4$ side positions, respectively, of FCCs or NCCs (for atom labeling, see Fig. 2D). [c]Peak identification by UV/visible spectra (s) or MS (m). [d]At-NCC-3 carries a hydroxymethyl group instead of a methyl group at C7.

N-terminally fused it to the 48 N-terminal amino acids of Arabidopsis PPH, which represent the predicted chloroplast transit peptide of PPH (Schelbert et al., 2009; Fig. 6C). Stroma localization of the chimeric construct (PPH_{TP}-MES16-HA) in Col-0 (Col-0/PPH_{TP}-MES16-HA) lines could be confirmed on immunoblots of protein extracts of protoplasts, chloroplasts, and subchloroplast fractions using anti-HA antibodies (Fig. 6D). We then compared the patterns of accumulating Pheide pigments in senescent leaves of the wild type, *pao1*/PPH_{TP}-MES16-HA, *mes16-1*, and a *mes16-1pao1* double mutant (Fig. 6E). While the wild type, as expected, was devoid of Pheide *a*, this Chl breakdown intermediate accumulated to a similar extent in *pao1* and *mes16-1pao1*. In contrast, when targeting MES16 to the chloroplast in the *pao1* background, a large proportion of the accumulating Pheide *a* had been converted to pyro-Pheide *a*. This result indicated that under natural conditions, MES16 does not have access to Pheide *a*, implying that the likely in vivo substrate of MES16 (in the cytosol) is an FCC.

DISCUSSION

Leaf senescence in higher plants is associated with the disappearance of green color and the unmasking of yellow-colored carotenoids. Thereby, Chl is degraded in the so-called PAO pathway to colorless linear tetrapyrroles (i.e. breakdown proceeds beyond the level of colored species with an intact porphyrin macrocycle; Hörtensteiner and Kräutler, 2011). Thus, green porphyrinic pigments identified as Chl breakdown products in the past (Brown et al., 1991) most likely merely represent experimental artifacts or intermediates of the PAO pathway. This pathway is considered to be active in all higher plant species (Hörtensteiner and Kräutler, 2011), and *PAO* genes are widely distributed in angiosperms, are present in mosses, and probably even appear in algae and cyanobacteria (Gray et al., 2004).

Among the NCCs, which are modified at side groups of the tetrapyrrolic backbone, are $O13^4$-demethylated catabolites. PPD from radish has been demonstrated to catalyze $O13^4$-demethylation of Pheide in vitro; however, this demethylation is followed by a spontaneous decarboxylation resulting in pyro-Pheide (Suzuki et al., 2006). Likewise, we could show here that MES16, the Arabidopsis protein most closely related to RsPPD (Fig. 1A), catalyzes the same reaction (Fig. 2A). It had been assumed that PPD is involved in Chl breakdown during leaf senescence, and pyro-Pheide was suggested to feed into the main (PAO) pathway leading to the formation of FCCs and NCCs (Suzuki et al., 2006). However, none of the known linear tetrapyrrolic breakdown products of Chl exhibit a pyro-type structure at $C13^2$ (Kräutler, 2008; Hörtensteiner and Kräutler, 2011). When targeting MES16 to the chloroplast in the *pao1* background, pyro-Pheide accumulated (Fig. 6E), indicating that also in vivo demethylation of Pheide is followed by decarboxylation. In contrast, in vitro MES16 assays with *p*FCC as substrate exclusively produced $O13^4$-desmethyl *p*FCC and not pyro-*p*FCC (Fig. 2B). Furthermore, $O13^4$-demethylated FCCs and NCCs, but no pyro-pigments, accumulate in senescent wild-type Arabidopsis leaves (Pruzinská et al., 2005), while in *mes16* mutants, all catabolites have an intact $C13^2$-carboxymethylester (Table I). Finally, like RsPPD (Suzuki et al., 2006), MES16 did not accept an NCC as substrate for demethylation. This substrate selectivity can be rationalized by comparison of the chemical constitution around the isocyclic ring and pyrrole rings C and D, which is identical in Pheide and *p*FCC but different in NCCs. This causes a significant difference in the three-dimensional shape around the $C13^2$ position, which results in the selectivity. Furthermore, the rapid spontaneous decarboxylation that specifically occurs in the $O13^4$-demethylation product of Pheide but not in *p*FCC results from an additional stabilization by the delocalized π system spanning the entire porphyrin macrocycle of Pheide, which is absent in *p*FCC.

In summary, the observations regarding the in vitro and in vivo methylesterase activity of MES16 strongly indicate that FCCs, but not Pheide or NCCs, are the in vivo substrate for demethylation. Further support for this was obtained from the subcellular localization of

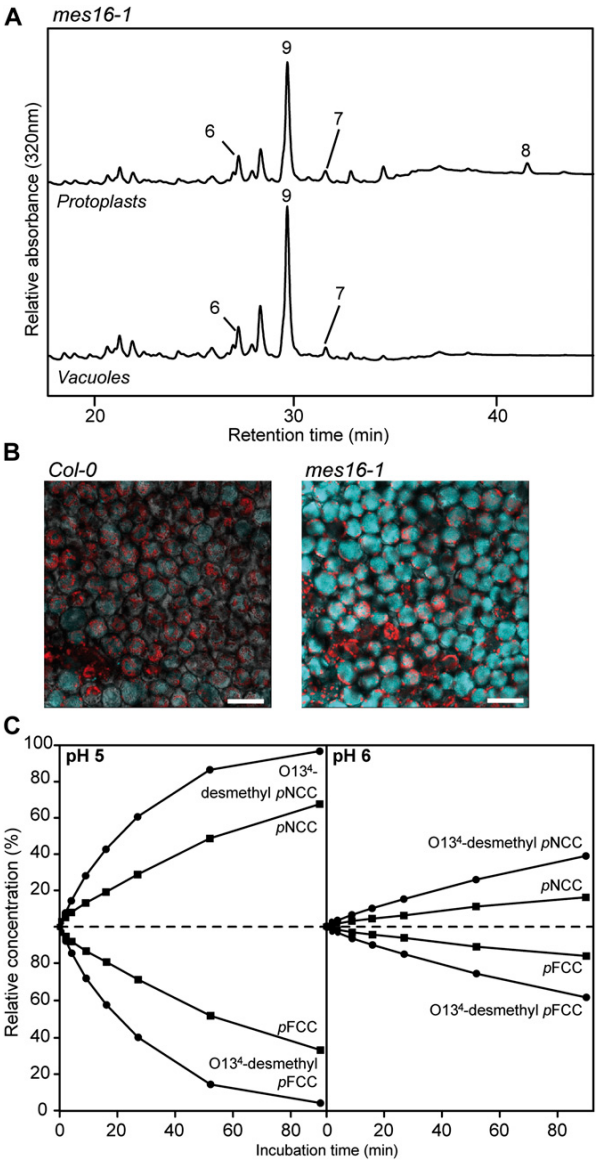

Figure 5. *mes16* mutants retain FCCs in the vacuoles. A, Protoplasts and vacuoles were isolated from *mes16-1*, and colorless catabolites were separated by HPLC as described in "Materials and Methods." For clarity, only a part of the HPLC traces is shown. For identification and peak numbering of FCCs and NCCs, see Table I. B, Palisade mesophyll of dark-induced leaves (4 d) of Col-0 and *mes16-1* observed with a laser scanning confocal microscope. FCC fluorescence was induced with an excitation wavelength of 355 nm, and the emission signal (blue) was recovered between 430 and 470 nm. Red is Chl autofluorescence. Bars = 50 μm. C, FCC-to-NCC isomerization assays performed with *p*FCC (black squares) or O13^4-desmethyl *p*FCC (black circles). Relative concentrations of FCCs and corresponding NCCs are plotted for pH 5 and 6. For more details, see "Materials and Methods." Calculated half-lives of FCCs are listed in Table II.

MES16 in the cytosol (Fig. 6A). Pheide *a* formation and further degradation to *p*FCC exclusively occur inside the chloroplast (Hörtensteiner, 2006); thus, only after export from the chloroplast are Chl degradation products accessible to MES16. Thus, the fact that Pheide *a* but not pyro-Pheide *a* was found in *pao1* (Fig. 6E) indicates that in this mutant, Pheide *a* accumulates inside the plastids and is not exported to the cytosol. In line with this is the chloroplast localization of MES16 in the *pao1* background, which enabled Pheide *a* demethylation (and decarboxylation; Fig. 6E). Interestingly, however, expressing MES16 in the chloroplast in the wild type did not alter the FCC/NCC catabolite pattern (i.e. no pyro-catabolites were formed; Supplemental Fig. S4), indicating that in a PAO-containing background, chloroplast-localized MES16 is unable to access Pheide and to convert it to pyro-Pheide. This may hint at the existence in chloroplasts of a metabolic channeling mechanism for Chl breakdown intermediates. Metabolic channeling and physical interaction have been shown for PAO and RCCR (Rodoni et al., 1997; Pruzinská et al., 2007), but these might also involve further (upstream) reactions. In such a scenario, lines that contain the entire chloroplast-located degradation machinery (e.g. *mes16-1* or the wild type) could shield Pheide *a* from chloroplast-targeted MES16. In contrast, in the *pao1* background, this intermediate is likely released from the degradation machinery and is accessible for chloroplast-localized MES16.

Recently, it was shown that the salicylic acid-binding protein 2 (SABP2) from tobacco (*Nicotiana tabacum*) is able to hydrolyze MeSA to salicylic acid (Forouhar et al., 2005). Since the MES proteins of Arabidopsis are homologous to SABP2, members of this family have been tested in vitro as possible hydrolases for methylesters of different plant hormones. All three members of subfamily 2, MES16, MES17, and MES18 (Fig. 1A), were shown to hydrolyze MeIAA, and MES16 also hydrolyzed MeJA, but not MeSA and the methylesters of two different gibberellic acids (Yang et al., 2008). In our inhibition studies, *p*FCC-hydrolyzing activity was inhibited to some extent by MeIAA but not by MeJA (Fig. 2E), confirming MeIAA to be a potential substrate of MES16. However, when analyzing *mes16* mutants (the identical alleles also used in our work) for auxin-related phenotypes, Yang et al. (2008) could not confirm a relation between MES16

Table II. *Half-lives of O13^4-desmethyl-pFCC and pFCC*

Sample	pH	$t_{1/2}$[a]	k[a]	R_2[b]
		min	*min*$^{-1}$	
*O*13^4-desmethyl-*p*FCC	5	18	−0.0382	0.9989
*p*FCC	5	57	−0.0122	0.9995
*O*13^4-desmethyl-*p*FCC	6	128	−0.0054	0.9981
*p*FCC	6	365	−0.0019	0.993

[a]Half-lives ($t_{1/2}$) and reaction rate constants (k) were determined using the following formula: $\ln[FCC]_t = \ln[FCC]_0 - kt$; $t_{1/2} = \ln(2)/k$. [b]Coefficient of determination of the linear regression of x = t (min) and $y = \ln[FCC]_t$.

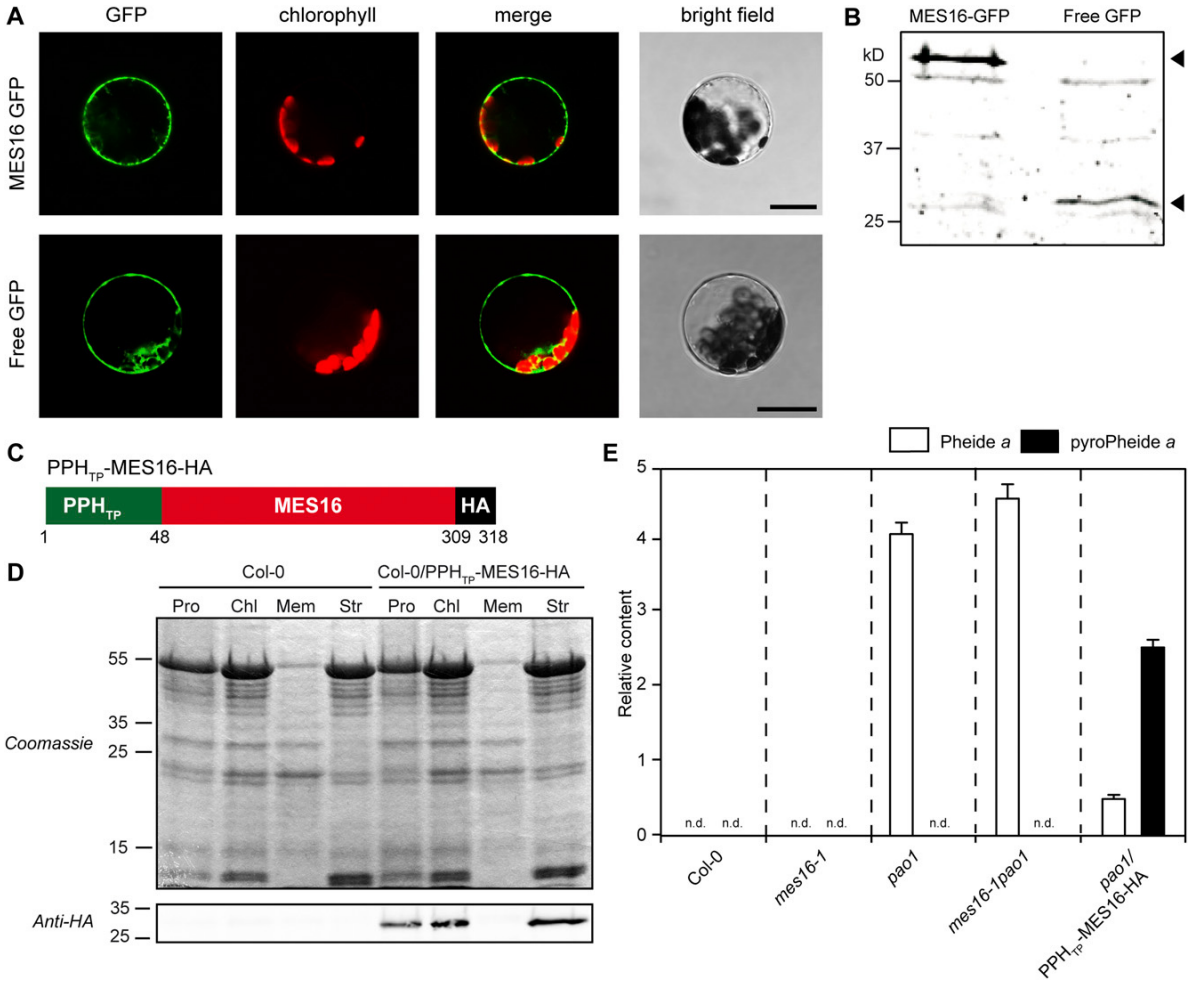

Figure 6. FCCs are the in vivo substrates of MES16. A, Transient expression of MES16-GFP and free GFP in Arabidopsis mesophyll protoplasts. GFP fluorescence (GFP) and Chl autofluorescence (chlorophyll) were examined by confocal laser scanning microscopy. The merge panels show overlays of GFP and autofluorescence. Bars = 20 μm. B, Anti-GFP immunoblotting of proteins from protoplasts expressing MES16-GFP and free GFP. The arrowheads indicate the predicted sizes of transiently expressed proteins. C, The chimeric construct used to target MES16 to the chloroplast. PPH$_{TP}$, Amino acids 1 to 48 from PPH, representing the chloroplasts transit peptide; HA, HA tag. D, Verification of MES16 targeting to the chloroplast. Leaves of Col-0 and Col-0/PPH$_{TP}$-MES16-HA were fractionated into protoplasts (Pro) and chloroplasts (Chl) and chloroplast subfractions (Mem, chloroplast membranes; Str, stroma). Gel loadings of protoplast and chloroplast fractions are based on equal amounts of chlorophyll. Anti-HA antibodies were used for detection of the chimeric protein. E, Quantification of Pheide *a* (white bars) and pyro-Pheide *a* (black bars) in dark-induced (5 d) Col-0, *mes16-1*, *pao1*, *mes16-1pao1*, and *pao1*/PPH$_{TP}$-MES16-HA. Values are means of three replicates, and error bars represent SD. n.d., Not detected.

activity and auxin function. In contrast, analysis of mutants deficient in MES17 demonstrated the capability of MES17 to hydrolyze MeIAA in vivo (Yang et al., 2008). On the other hand, neither MES17 nor MES18 exhibited FCC-demethylating activity both in vitro and in vivo (Supplemental Figs. S2 and S3). A predicted MES protein from maize (tentatively named ZmMES1) clustered together with Arabidopsis MES16 and RsPPD (Fig. 1A); however, all maize NCCs identified to date have an intact C13^2-carboxymethyl group, indicating that ZmMES1 is not involved in Chl breakdown in maize. In summary, these data imply that MES proteins of subfamily 2 have different functions and that function does not necessarily relate to the primary amino acid composition of these proteins. Furthermore, MES16 has a predominant (and possibly exclusive) role as an FCC methylesterase during Chl breakdown.

Demethylated Chl catabolites have so far only been found in a few species, raising the question about the significance of O13^4-demethylation. Interestingly, senescent *mes16* mutants exhibited a strong UV-excitable

fluorescence (Figs. 4 and 5), which was due to large increases of FCCs accumulating in the mutants. This resulted, at least in part, from slower FCC isomerization to the respective NCC in the presence of an intact $C13^2$-carboxymethylester compared with a free carboxylic acid group (Fig. 5C; Oberhuber et al., 2008). However, in contrast to Arabidopsis *mes16*, several plant species in which $O13^4$-demethylation has not been observed, such as *C. japonicum* or *Nicotiana rustica*, exclusively accumulate NCCs during leaf senescence (Curty and Engel, 1996; Oberhuber et al., 2003; Berghold et al., 2004). This is likely explained by differences in the vacuolar pH, which determines the velocity of FCC-to-NCC isomerization (Table II). Thus, whether a plant accumulates FCCs or NCCs might depend on the presence/absence of $O13^4$-demethylation and/or the vacuolar pH. Nevertheless, hypermodified FCCs, which are esterified at the C17-propionic acid side chain and therefore are not isomerized to NCCs (i.e. they persist as FCCs), have recently been identified in some senescing leaves and ripening banana fruits (Moser et al., 2009; Banala et al., 2010; Kräutler et al., 2010). The resulting strong fluorescence in these tissues might, as suggested for the bright colors of many autumnal leaves (Archetti and Brown, 2004), play an important ecological function (Moser et al., 2009). Noteworthy is the finding that the Arabidopsis Landsberg *erecta* (L*er*) ecotype exhibits a MES16 mutant phenotype (B. Christ and S. Hörtensteiner, unpublished data). Most probably, this is due to a single nucleotide polymorphism present in the L*er MES16* gene (http://polymorph-clark20.weigelworld.org/cgi-bin/retrieve_cds_snp.cgi), which alters a Val residue within the MES16 lipase motif (PROSITE motif 00120) that is fully conserved in all MES proteins (Yang et al., 2008) to Ala. Thus, L*er* likely is a natural mutant in MES16, and it will be interesting to examine in the future whether MES16 absence in this accession has any significance in an ecological context.

MATERIALS AND METHODS

Plant Material and Senescence Induction

Arabidopsis (*Arabidopsis thaliana*) Col-0 was used as the wild type. Ecotype Wassilewskija was also analyzed in experiments including *mes18-1* (Wassilewskija background). T-DNA insertion lines were from the following collections: SALK lines (Alonso et al., 2003): *AT4G16690-1* (*mes16-1*), SALK_139756; *AT4G16690-2* (*mes16-2*), SALK_151578; *AT4G37150-1* (*mes9-1*), SALK_030442; SAIL lines (Sessions et al., 2002): *AT3G10870-1* (*mes17-1*), SAIL_503_C03; GABI lines (Rosso et al., 2003): *AT5G10300-1* (*mes5-1*), GABI_453E01; FLAG lines (Balzergue et al., 2001): *AT5G58310-1* (*mes18-1*), FLAG_271B02. SALK and SAIL lines were obtained from the European Arabidopsis Stock Center. The GABI line was obtained from GABI Kat, Max Planck Institute for Plant Breeding Research. The FLAG line was obtained from the Arabidopsis Resource Centre for Genomics. Homozygous plants were identified by PCR using T-DNA-, transposon-, and gene-specific primers as listed in Supplemental Table S1. Likewise, a homozygous *mes16-1pao-1* double mutant was identified by PCR.

Plants were grown on soil either in short days (8 h of light/16 h of dark) under fluorescent light of 60 to 120 μmol photons m^{-2} s^{-1} at 22°C or in long days (16 h of light/8 h of dark) in a greenhouse with fluence rates of 100 to 200 μmol photons m^{-2} s^{-1} at 22°C. For senescence induction, leaves from 8-week-old (short-day) plants were excised and incubated in permanent darkness on wet filter paper for up to 10 d at ambient temperature.

Biocomputational Methods and Phylogenetic Analysis

Methylesterase homologs from canola (*Brassica napus*), barley (*Hordeum vulgare*), and maize (*Zea mays*) were identified by TBLASTN searches (Altschul et al., 1997) of MES16 with the est_others database of the National Center for Biotechnology Information (http://www.ncbi.nlm.nih.gov). EST sequences were conceptually translated. MES protein sequences were aligned and subjected to a maximum likelihood phylogenetic analysis using phylogeny.fr (http://www.phylogeny.fr/version2_cgi/index.cgi). Phylogeny.fr (Dereeper et al., 2008) employs MUSCLE for multiple sequence alignments, Gblocks for alignment curation, PhyML for phylogeny analysis, and TreeDyn for tree drawing and was used with the default settings. Bootstrap analysis was performed with 100 replicates.

GFP Fusion Protein Production and Confocal Microscopy

MES16 was amplified by PCR with the Expand High Fidelity PCR system (Roche Applied Science) using the primers listed in Supplemental Table S1, introducing *Sma*I/*Spe*I restriction sites at the ends. The PCR fragment was then cloned into the pGEM-T-easy vector (Promega) and, after *Sma*I/*Spe*I digestion, subcloned into pUC18-spGFP6 (Meyer et al., 2006), thereby producing a fusion of MES16 with the N terminus of GFP. Arabidopsis mesophyll protoplasts were isolated from 6-week-old short-day-grown Col-0 plants according to published procedures (Endler et al., 2006; Schelbert et al., 2009). Cell numbers were quantified with a Neubauer chamber and adjusted to a density of 2 to 3×10^6 protoplasts mL^{-1}. Protoplasts were transformed by 20% polyethylene glycol transformation (Meyer et al., 2006). Transformed cells were incubated for 48 h in the dark at room temperature before laser scanning confocal microscopic analysis (DM IRE2; Leica Microsystems). GFP fluorescence was imaged at an excitation wavelength of 488 nm, and the emission signal was recovered between 495 and 530 nm. Free GFP expressed from empty pUC18-spGFP6 was used as a control for cytosolic localization. Proteins of fractions corresponding to 1 to 2×10^6 protoplasts were precipitated with chloroform-methanol (Wessel and Flügge, 1984) and analyzed by SDS-PAGE and anti-GFP immunoblotting.

For confocal microscopy of leaves, the lower epidermis and spongy mesophyll were removed from senescent leaves of Col-0 and *mes16-1* using fine sandpaper. The palisade mesophyll was then observed with a laser scanning confocal microscope (TCS SP5; Leica Microsystems). FCC fluorescence was induced with an excitation wavelength of 355 nm, and the emission signal was recovered between 430 and 470 nm.

Targeting MES16 to the Chloroplast

A fusion protein consisting of the PPH transit peptide (amino acids 1–48; Schelbert et al., 2009), MES16, and an HA tag (PPH_{TP}-MES16-HA) was produced using a two-step PCR (Expand High Fidelity PCR system) with the primers listed in Supplemental Table S1. The PCR fragment was cloned into pGEM-T-easy (Promega) and, after digestion with *Eco*RI/*Hin*dIII, subcloned into pHannibal (Wesley et al., 2001). The pHannibal cassette containing the cauliflower mosaic virus 35S promoter, the fusion open reading frame, and an octopine synthase terminator was excised with *Not*I and introduced into *Not*I-restricted pGreen0179 (Hellens et al., 2000). Arabidopsis Col-0 and *pao-1* plants were transformed by the floral-dip method (Clough and Bent, 1998). Transformants were selected on hygromycin, and resistant T2 plants were used for further analysis. To verify that PPH_{TP}-MES16-HA was targeted to the chloroplasts, protoplasts were isolated from Col-0 and Col-0/PPH_{TP}-MES16-HA as described above. Chloroplasts were then isolated from protoplasts following published procedures (Kubis et al., 2008; Schelbert et al., 2009). Chl concentration was measured for each fraction as described below. Proteins from aliquots corresponding to 15 μg of Chl were precipitated with chloroform-methanol (Wessel and Flügge, 1984). In parallel, an aliquot of chloroplasts was fractionated into soluble and membrane fractions (Smith et al., 2002), and proteins were precipitated as well. Proteins from the different fractions were resolved by SDS-PAGE and analyzed by anti-HA immunoblotting.

RNA Isolation and RT-PCR

RNA was isolated using the RNeasy Plant kit (Qiagen). After DNA digestion with RQ1 DNase (Promega), first-strand cDNA was synthesized

using the Moloney murine leukemia virus reverse transcriptase (Promega). PCR was performed with a nonsaturating number of amplification cycles as shown in the figures using gene-specific primers as listed in Supplemental Table S1.

Heterologous Expression of MES Proteins and Activity Determination

MES5, *MES9*, *MES16*, and *MES17* cloned in pET28a (Vlot et al., 2008) were subcloned in pProEX Hta (Invitrogen) using *Eco*RI (*MES5*, *MES16*, and *MES17*) or *Eco*RI/*Xho*I (*MES9*) restriction sites. The *MES18* coding sequence was amplified by PCR (Expand High Fidelity PCR system) from clone U50042 (Arabidopsis Biological Resource Center) using the primers listed in Supplemental Table S1 and cloned into pProEX Hta via *Eco*RI. After sequencing, the plasmids were transformed into BL21-CodonPlus (DE3)-RIL (Stratagene). At an optical density at 600 nm of 0.6, protein expression was induced with 1.0 mM isopropylthio-β-galactoside and cells were grown at 30°C overnight. Cells were centrifuged and resuspended in 20 mM Tris-HCl, pH 8, complemented with a protease inhibitor cocktail (Complete; Roche Applied Science) before lysis with a high-pressure cell breaker (Constant Cell Disruption System; Constant Systems) at a pressure of 150 MPa. The cell lysates were examined by SDS-PAGE and anti-His immunoblotting to quantify relative levels of MES protein expression.

Standard *p*FCC assays with MES16 (total volume of 20 μL) consisted of 0.25 μg of crude protein extracts and 15 μM *p*FCC. Pheide assays contained 0.85 mM Pheide and 100 μg of crude protein extracts in a total volume of 30 μL. For assays with an NCC, CjNCC-1 (Moser et al., 2008) was used at 15 μM. After incubation at 25°C in darkness for different periods of time as indicated in the figures, the reactions were stopped by the addition of methanol (*p*FCC assay) or acetone (Pheide assay) to final concentrations of 60% or 50%, respectively. Crude protein extracts produced with empty pProEX Hta were used as controls. After centrifugation (2 min at 16,000*g*), samples were analyzed by HPLC as described below. For competition experiments, inhibitors were added to the *p*FCC assay at a final concentration of 1.5 mM (100×) for MeIAA, MeSA, and MeJA or 150 μM (10×) for Pheide. *p*FCC assays with MES5, MES9, MES17, and MES18 (total volume of 40 μL) consisted of 7.5 μM *p*FCC and a volume of *Escherichia coli* lysates containing an amount of recombinant protein equivalent to the amount of MES16 present in 0.25 μg of crude MES16 extract.

PAO and RCCR Extraction from Red Pepper and Synthesis of *p*FCC

PAO and RCCR were extracted from red pepper (*Capsicum annuum*) fruits as follows. Exocarp tissue was blended in a Sorvall mixer three times for 5 s each in a solution (2–3 mL g^{-1} fresh weight) containing 400 mM Suc, 50 mM Tris-MES, pH 8, 2 mM EDTA, 10 mM polyethylene glycol 4000, 5 mM dithiothreitol, and 5 mM L(+)-ascorbic acid. The homogenate was filtered through two layers of Miracloth and centrifuged (10 min at 10,000*g*). The pellet was resuspended (25 μL g^{-1} fresh exocarp tissue) in 25 mM Tris-MES, pH 8, 5 mM L(+)-ascorbic acid, and 1% (v/v) Triton X-100 and incubated during 30 min in the dark at 4°C on a shaking plate (15 rpm) to solubilize membrane proteins. After ultracentrifugation (1 h at 100,000*g*), aliquots of the supernatant containing RCCR and solubilized PAO were frozen in liquid nitrogen and stored at −80°C before use. *p*FCC was synthesized as described previously (Pruzinská et al., 2007). Briefly, assays contained 80% (v/v) PAO/RCCR extract from red pepper (see above), 0.5 mM Pheide (Hörtensteiner et al., 1995), 0.2 mg mL^{-1} ferrodoxin (Fd), and a Fd-reducing system consisting of 2 mM Glc-6-P, 1 mM NADPH, 1 milliunit μL^{-1} Glc-6-P dehydrogenase, 0.1 milliunit μL^{-1} Fd-NADPH-oxidoreductase, and 0.1 milliunit μL^{-1} catalase. After 1 h of incubation at 25°C, the reaction was terminated by the addition of methanol to a final concentration of 60% (v/v). The assays were then cleaned and concentrated using a C18-SepPak cartridge (Waters) prior to purification of *p*FCC by HPLC (see below). Pure *p*FCC fractions were stored in liquid nitrogen before use.

Vacuole Isolation

Arabidopsis mesophyll protoplasts were isolated from 6-week-old short-day-grown Col-0 and *mes16-1* plants after dark incubation of detached leaves for 4 d. Recovered protoplasts were digested in 10 volumes of lysis solution as described (Frelet-Barrand et al., 2008). The progression of vacuole release was continuously controlled using the microscope, and vacuoles were purified and concentrated by centrifugation (8 min at 1,400*g*) using a step gradient as follows: lower phase, 1 volume of lysate; middle phase, 1 volume of a 1:1 mixture of lysis solution and betaine buffer (0.4 M betaine, 30 mM potassium-gluconate, 20 mM HEPES-imidazole, pH 7.2, 1 mg mL^{-1} bovine serum albumin, and 1 mM dithiothreitol); upper phase, one-third volume of betaine buffer. Vacuoles were collected from the interface between the middle and upper phases. Contamination of Arabidopsis vacuoles with Chl was determined as described below. The activity of soluble vacuolar 3-*N*-acetylglucosaminidase was determined using *p*-nitrophenyl-*N*-acetyl-β-D-glucosaminide as described previously (Gao and Schaffer, 1999). Briefly, 10 μL of protoplast and vacuole fractions was incubated with 90 μL of 100 mM HEPES-KOH, pH 7.5, containing 3 mM *p*-nitrophenyl-*N*-acetyl-β-D-glucosaminide. The assay mixtures were incubated on a 96-well microtiter plate at room temperature, and the reaction was stopped by the addition of 160 μL of 1 M Na_2CO_3. The absorbance of formed *p*-nitrophenol was read with a plate reader spectrophotometer at 405 nm (Fusion Universal Microplate Analyzer; Packard). NCCs and FCCs of protoplast and vacuole fractions corresponding to equal activities of 3-*N*-acetylglucosaminidase were extracted with methanol and concentrated on a C18-SepPak cartridge prior to analysis by HPLC as described below for plant material.

Immunoblot Analysis and UV Analysis of Leaves

After separation by SDS-PAGE, proteins were transferred to nitrocellulose membranes according to standard procedures. Proteins were labeled with monoclonal antibodies against the poly-His tag (1:5,000) or GFP (1:2,000) or with polyclonal antibodies against the HA tag (1:5,000; all from Sigma). Thereafter, primary antibodies were labeled with horseradish peroxidase-conjugated secondary antibodies and proteins were visualized on a ChemiDoc XRS station (Bio-Rad) using the Immun-Star HRP Chemifluorescence kit (Bio-Rad). FCC fluorescence in senescent leaves of Col-0 and *mes16-1* was visualized under UV light (366 nm) with the ChemiDoc XRS setup.

Analysis of Chl and Chl Catabolites

HPLC Analysis of Pheide, O13^4-Desmethyl Pheide, and Pyro-Pheide, and Quantification of Chl

Pigments were extracted from liquid nitrogen-homogenized tissue during 2 h at −20°C in 10% (v/v) 0.2 M Tris-HCl, pH 8, in acetone precooled to –20°C (5 mL g^{-1} fresh weight). After two centrifugation steps (4 min, 16,000*g*, 4°C), supernatants were analyzed by reverse-phase HPLC as described (Pruzinská et al., 2005). The same conditions were used to analyze the products of in vitro MES assays with Pheide as substrate. Pigments were identified by their absorption spectra and quantified using peak areas at 665 nm. For Chl quantification, supernatants were analyzed spectrophotometrically (Strain et al., 1971).

Chl quantification of protoplast, chloroplast, and vacuole fractions was performed as follows. An aliquot of the fractions was 333-fold diluted with 20% (v/v) 20 mM Tris-HCl, pH 8, in acetone and mixed vigorously. After centrifugation for 1 min at 16,000*g*, Chl concentrations of the supernatants were determined spectrophotometrically according to Arnon et al. (1959).

Colorless Chl Catabolites

Plant material was ground in liquid nitrogen, and colorless catabolites were extracted with 3 volumes (w/v) of 50 mM phosphate buffer, pH 7: methanol (1:3, v/v). The reverse-phase HPLC system consisted of a C18 Hypersil ODS column (250 × 4.6 mm; Thermo Electron), which was developed with a gradient (flow rate of 1.0 mL min^{-1}) of solvent B (100% methanol) in solvent A (50 mM potassium phosphate, pH 7.0) as follows (all v/v): 20% to 60% in 30 min, 60% during 10 min, to 100% in 2 min, and 100% during 5 min.

For HPLC analysis of in vitro *p*FCC assays (esterase and isomerization assays), the column was developed with a gradient (flow rate of 1.0 mL min^{-1}) of solvent B in solvent A as follows (all v/v): 35% to 75% in 19 min, to 100% in 1 min, and 100% during 4 min.

Peak detection was performed with sequential monitoring using a PA-100 photodiode array detector (200–700 nm; Dionex) and a RF2000 fluorescence detector (excitation at 320 nm, emission at 450 nm; Dionex). Chl catabolites were identified by their absorption (FCCs and NCCs) and fluorescence (FCCs) properties. Relative amounts of FCCs and NCCs were determined using peak areas at 320 nm.

MS

For MS analysis, catabolite-containing HPLC fractions derived from MES16 enzyme assays or *mes16-1* leaf extracts were mixed with 1 volume of a saturated solution of 2,5-dihydroxybenzoic acid in acetonitrile and were spotted onto stainless-steel targets. MS was performed with an Ultraflex matrix-assisted laser-desorption ionization time of flight mass spectrometer (Bruker).

Matrix-assisted laser-desorption ionization time of flight MS data (percentage relative intensity, molecular formula, and type of ion) are as follows: *mes16*-FCC-1: 883.09 (33, $C_{41}H_{49}K_2N_4O_{13}$, $[M+2K]^+$), 845.13 (100, $C_{41}H_{50}K_1N_4O_{13}$, $[M+K]^+$), 807.16 (56, $C_{41}H_{51}N_4O_{13}$, $[M+H]^+$); *mes16*-FCC-2: 683.26 (45, $C_{35}H_{40}K_1N_4O_8$, $[M+K]^+$), 645.30 (100, $C_{35}H_{41}N_4O_8$, $[M+H]^+$); *mes16*-FCC-3: 667.23 (19, $C_{35}H_{40}K_1N_4O_7$, $[M+K]^+$), 629.25 (100, $C_{35}H_{41}N_4O_7$, $[M+H]^+$); *mes16*-NCC-1: 883.33 (16, $C_{41}H_{49}K_2N_4O_{13}$, $[M+2K]^+$), 845.36 (100, $C_{41}H_{50}K_1N_4O_{13}$, $[M+K]^+$), 807.38 (50, $C_{41}H_{51}N_4O_{13}$, $[M+H]^+$); O13^4-desmethyl *p*FCC: 647.14 (25, $C_{33}H_{37}K_2N_4O_5$, $[M+2K-CO_2]^+$), 615.22 (33, $C_{34}H_{39}N_4O_7$, $[M+H]^+$), 609.17 (80, $C_{33}H_{38}K_1N_4O_5$, $[M+1K-CO_2]^+$), 571.19 (100, $C_{33}H_{39}N_4O_5$, $[M+H-CO_2]^+$).

In Vitro FCC-to-NCC Isomerization

O13^4-desmethyl *p*FCC was produced from pure *p*FCC fractions using heterologously expressed MES16 and purified by HPLC. The isomerization assays consisted of 11.5 μM FCC (*p*FCC or O13^4-desmethyl *p*FCC) and 70 mM phosphate buffer, pH 5 or 6. Aliquots were taken after the incubation times indicated in Figure 5C, and isomerization was stopped by adding Tris-HCl, pH 8, to a concentration of 300 mM. Methanol was added to a final concentration of 35% (v/v) prior to analysis by HPLC as described above.

GenBank identification numbers for the DNA/protein sequences used in this work are as follows: Arabidopsis: AtMES1, 48310671 (AT2G23620); AtMES2, 15227863 (AT2G23600); AtMES3, 50198958 (AT2G23610); AtMES4, 34146844 (AT2G23580); AtMES5, 332004135 (AT5G10300); AtMES6, 330252371 (AT2G23550); AtMES7, 46402456 (AT2G23560); AtMES8, 330252376 (AT2G23590); AtMES9, 30017285 (AT4G37150); AtMES10, 332645146 (AT3G50440); AtMES11, 27808602 (AT3G29770); AtMES12, 332657411 (AT4G09900); AtMES13, 332192561 (AT1G26360); AtMES14, 94442411 (AT1G33990); AtMES15, 332196779 (AT1G69240); AtMES16, 332658384 (AT4G16690); AtMES17, 332641444 (AT3G10870); AtMES18, 332009649 (AT5G58310); AtMES19, 330252373 (AT2G23570); AtMES20, 332661358 (AT4G37140); PAO, 15230543 (AT3G44880); PPH, 15240707 (AT5G13800); canola: BnMES1, 151016294 (fragment); BnMES2, 151011122 (fragment); BnMES3, 125936604 (fragment); BnMES4, 151324766 (fragment); BnMES5, 242292656 (fragment); BnMES6, 150871604; BnMES7, 29690059 (fragment); barley: HvMES1, 60272487 (fragment); HvMES2, 94339163 (fragment); HvMES3, 24242376 (fragment); HvMES4, 24285085 (fragment); radish (*Raphanus sativus*): PPD, 122209128; maize: ZmMES1, 211364330 (fragment); ZmMES2, 211406694 (fragment); ZmMES3, 21481135 (fragment); ZmMES4, 149089611; ZmMES5, 78077695 (fragment); ZmMES6, 87153297 (fragment).

Supplemental Data

The following materials are available in the online version of this article.

Supplemental Figure S1. Coexpression network around *PAO*, *PPH*, *SGR*, *NYC1*, and *MES16*.

Supplemental Figure S2. Analysis of recombinant MES5, MES9, MES16, MES17, and MES18.

Supplemental Figure S3. Colorless catabolites occurring in *mes16-1* mutants during natural senescence and in mutants of other closely related MES family members after dark incubation.

Supplemental Figure S4. Colorless catabolites of Col-0/PPH_{TP}-MES16-HA.

Supplemental Table S1. List of primers used in this study.

ACKNOWLEDGMENTS

We thank Dr. Daniel F. Klessig at the Boyce Thompson Institute for Plant Research at Cornell University for providing *E. coli* expression clones (pET28a) for MES5, MES9, MES16, and MES17.

Received October 11, 2011; accepted December 3, 2011; published December 6, 2011.

LITERATURE CITED

Alonso JM, Stepanova AN, Leisse TJ, Kim CJ, Chen H, Shinn P, Stevenson DK, Zimmerman J, Barajas P, Cheuk R, et al (2003) Genome-wide insertional mutagenesis of *Arabidopsis thaliana*. Science **301:** 653–657

Altschul SF, Madden TL, Schäffer AA, Zhang JH, Zhang Z, Miller W, Lipman DJ (1997) Gapped BLAST and PSI-BLAST: a new generation of protein database search programs. Nucleic Acids Res **25:** 3389–3402

Archetti M, Brown SP (2004) The coevolution theory of autumn colours. Proc Biol Sci **271:** 1219–1223

Arnon DI, Whatley FR, Allen MB (1959) Photosynthesis by isolated chloroplasts. VIII. Photosynthetic phosphorylation and the generation of assimilatory power. Biochim Biophys Acta **32:** 47–57

Balzergue S, Dubreucq B, Chauvin S, Le-Clainche I, Le Boulaire F, de Rose R, Samson F, Biaudet V, Lecharny A, Cruaud C, et al (2001) Improved PCR-walking for large-scale isolation of plant T-DNA borders. Biotechniques **30:** 496–498, 502, 504

Banala S, Moser S, Müller T, Kreutz CR, Holzinger A, Lütz C, Kräutler B (2010) Hypermodified fluorescent chlorophyll catabolites: source of blue luminescence in senescent leaves. Angew Chem Int Ed Engl **49:** 5174–5177

Berghold J, Breuker K, Oberhuber M, Hörtensteiner S, Kräutler B (2002) Chlorophyll breakdown in spinach: on the structure of five nonfluorescent chlorophyll catabolites. Photosynth Res **74:** 109–119

Berghold J, Eichmüller C, Hörtensteiner S, Kräutler B (2004) Chlorophyll breakdown in tobacco: on the structure of two nonfluorescent chlorophyll catabolites. Chem Biodivers **1:** 657–668

Berghold J, Müller T, Ulrich M, Hörtensteiner S, Kräutler B (2006) Chlorophyll breakdown in maize: on the structure of two nonfluorescent chlorophyll catabolites. Monatsh Chem **137:** 751–763

Brown SB, Houghton JD, Hendry GAF (1991) Chlorophyll breakdown. *In* H Scheer, ed, Chlorophylls. CRC Press, Boca Raton, FL, pp 465–489

Clough SJ, Bent AF (1998) Floral dip: a simplified method for *Agrobacterium*-mediated transformation of *Arabidopsis thaliana*. Plant J **16:** 735–743

Curty C, Engel N (1996) Detection, isolation and structure elucidation of a chlorophyll *a* catabolite from autumnal senescent leaves of *Cercidiphyllum japonicum*. Phytochemistry **42:** 1531–1536

Dereeper A, Guignon V, Blanc G, Audic S, Buffet S, Chevenet F, Dufayard J-F, Guindon S, Lefort V, Lescot M, et al (2008) Phylogeny.fr: robust phylogenetic analysis for the non-specialist. Nucleic Acids Res **36:** W465–W469

Dodson G, Wlodawer A (1998) Catalytic triads and their relatives. Trends Biochem Sci **23:** 347–352

Endler A, Meyer S, Schelbert S, Schneider T, Weschke W, Peters SW, Keller F, Baginsky S, Martinoia E, Schmidt UG (2006) Identification of a vacuolar sucrose transporter in barley and Arabidopsis mesophyll cells by a tonoplast proteomic approach. Plant Physiol **141:** 196–207

Forouhar F, Yang Y, Kumar D, Chen Y, Fridman E, Park SW, Chiang Y, Acton TB, Montelione GT, Pichersky E, et al (2005) Structural and biochemical studies identify tobacco SABP2 as a methyl salicylate esterase and implicate it in plant innate immunity. Proc Natl Acad Sci USA **102:** 1773–1778

Frelet-Barrand A, Kolukisaoglu HU, Plaza S, Rüffer M, Azevedo L, Hörtensteiner S, Marinova K, Weder B, Schulz B, Klein M (2008) Comparative mutant analysis of Arabidopsis ABCC-type ABC transporters: AtMRP2 contributes to detoxification, vacuolar organic anion transport and chlorophyll degradation. Plant Cell Physiol **49:** 557–569

Gao Z, Schaffer AA (1999) A novel alkaline α-galactosidase from melon fruit with a substrate preference for raffinose. Plant Physiol **119:** 979–988

Gray J, Wardzala E, Yang M, Reinbothe S, Haller S, Pauli F (2004) A small family of LLS1-related non-heme oxygenases in plants with an origin amongst oxygenic photosynthesizers. Plant Mol Biol **54:** 39–54

Hellens RP, Edwards EA, Leyland NR, Bean S, Mullineaux PM (2000) pGreen: a versatile and flexible binary Ti vector for *Agrobacterium*-mediated plant transformation. Plant Mol Biol **42:** 819–832

Hilditch PI, Thomas H, Thomas BJ, Rogers LJ (1989) Leaf senescence in a non-yellowing mutant of *Festuca pratensis*: proteins of photosystem II. Planta **177:** 265–272

Hinder B, Schellenberg M, Rodoni S, Ginsburg S, Vogt E, Martinoia E,

Matile P, Hörtensteiner S (1996) How plants dispose of chlorophyll catabolites: directly energized uptake of tetrapyrrolic breakdown products into isolated vacuoles. J Biol Chem **271:** 27233–27236

Horie Y, Ito H, Kusaba M, Tanaka R, Tanaka A (2009) Participation of chlorophyll *b* reductase in the initial step of the degradation of light-harvesting chlorophyll *a*/*b*-protein complexes in *Arabidopsis*. J Biol Chem **284:** 17449–17456

Hörtensteiner S (2006) Chlorophyll degradation during senescence. Annu Rev Plant Biol **57:** 55–77

Hörtensteiner S (2009) Stay-green regulates chlorophyll and chlorophyll-binding protein degradation during senescence. Trends Plant Sci **14:** 155–162

Hörtensteiner S, Kräutler B (2011) Chlorophyll breakdown in higher plants. Biochim Biophys Acta **1807:** 977–988

Hörtensteiner S, Vicentini F, Matile P (1995) Chlorophyll breakdown in senescent cotyledons of rape, *Brassica napus* L.: enzymatic cleavage of phaeophorbide *a in vitro*. New Phytol **129:** 237–246

Hörtensteiner S, Wüthrich KL, Matile P, Ongania K-H, Kräutler B (1998) The key step in chlorophyll breakdown in higher plants: cleavage of pheophorbide *a* macrocycle by a monooxygenase. J Biol Chem **273:** 15335–15339

Joyard J, Ferro M, Masselon C, Seigneurin-Berny D, Salvi D, Garin J, Rolland N (2009) Chloroplast proteomics and the compartmentation of plastidial isoprenoid biosynthetic pathways. Mol Plant **2:** 1154–1180

Kräutler B (2008) Chlorophyll catabolites. *In* W Herz, H Falk, GW Kirny, RE Moore, C Tann, eds, Progress in the Chemistry of Organic Natural Products, Vol 89. Springer, Vienna, pp 1–43

Kräutler B, Banala S, Moser S, Vergeiner C, Müller T, Lütz C, Holzinger A (2010) A novel blue fluorescent chlorophyll catabolite accumulates in senescent leaves of the peace lily and indicates a split path of chlorophyll breakdown. FEBS Lett **584:** 4215–4221

Kräutler B, Hörtensteiner S (2006) Chlorophyll catabolites and the biochemistry of chlorophyll breakdown. *In* B Grimm, R Porra, W Rüdiger, H Scheer, eds, Chlorophylls and Bacteriochlorophylls: Biochemistry, Biophysics, Functions and Applications, Vol 25. Springer, Dordrecht, The Netherlands, pp 237–260

Kräutler B, Jaun B, Bortlik K-H, Schellenberg M, Matile P (1991) On the enigma of chlorophyll degradation: the constitution of a secoporphinoid catabolite. Angew Chem Int Ed Engl **30:** 1315–1318

Kubis SE, Lilley KS, Jarvis P (2008) Isolation and preparation of chloroplasts from *Arabidopsis thaliana* plants. Methods Mol Biol **425:** 171–186

Kusaba M, Ito H, Morita R, Iida S, Sato Y, Fujimoto M, Kawasaki S, Tanaka R, Hirochika H, Nishimura M, et al (2007) Rice NON-YELLOW COLORING1 is involved in light-harvesting complex II and grana degradation during leaf senescence. Plant Cell **19:** 1362–1375

Losey FG, Engel N (2001) Isolation and characterization of a urobilinogenoidic chlorophyll catabolite from *Hordeum vulgare* L. J Biol Chem **276:** 8643–8647

Matile P, Ginsburg S, Schellenberg M, Thomas H (1988) Catabolites of chlorophyll in senescing barley leaves are localized in the vacuoles of mesophyll cells. Proc Natl Acad Sci USA **85:** 9529–9532

Matile P, Schellenberg M (1996) The cleavage of pheophorbide *a* is located in the envelope of barley gerontoplasts. Plant Physiol Biochem **34:** 55–59

Matile P, Schellenberg M, Peisker C (1992) Production and release of a chlorophyll catabolite in isolated senescent chloroplasts. Planta **187:** 230–235

Meguro M, Ito H, Takabayashi A, Tanaka R, Tanaka A (2011) Identification of the 7-hydroxymethyl chlorophyll *a* reductase of the chlorophyll cycle in *Arabidopsis*. Plant Cell **23:** 3442–3453

Meyer A, Eskandari S, Grallath S, Rentsch D (2006) AtGAT1, a high affinity transporter for γ-aminobutyric acid in *Arabidopsis thaliana*. J Biol Chem **281:** 7197–7204

Morita R, Sato Y, Masuda Y, Nishimura M, Kusaba M (2009) Defect in non-yellow coloring 3, an α/β hydrolase-fold family protein, causes a stay-green phenotype during leaf senescence in rice. Plant J **59:** 940–952

Moser S, Müller T, Holzinger A, Lütz C, Jockusch S, Turro NJ, Kräutler B (2009) Fluorescent chlorophyll catabolites in bananas light up blue halos of cell death. Proc Natl Acad Sci USA **106:** 15538–15543

Moser S, Ulrich M, Müller T, Kräutler B (2008) A yellow chlorophyll catabolite is a pigment of the fall colours. Photochem Photobiol Sci **7:** 1577–1581

Mühlecker W, Kräutler B (1996) Breakdown of chlorophyll: constitution of nonfluorescing chlorophyll-catabolites from senescent cotyledons of the dicot rape. Plant Physiol Biochem **34:** 61–75

Mühlecker W, Ongania K-H, Kräutler B, Matile P, Hörtensteiner S (1997) Tracking down chlorophyll breakdown in plants: elucidation of the constitution of a 'fluorescent' chlorophyll catabolite. Angew Chem Int Ed Engl **36:** 401–404

Obayashi T, Hayashi S, Saeki M, Ohta H, Kinoshita K (2009) ATTED-II provides coexpressed gene networks for Arabidopsis. Nucleic Acids Res **37:** D987–D991

Oberhuber M, Berghold J, Breuker K, Hörtensteiner S, Kräutler B (2003) Breakdown of chlorophyll: a nonenzymatic reaction accounts for the formation of the colorless "nonfluorescent" chlorophyll catabolites. Proc Natl Acad Sci USA **100:** 6910–6915

Oberhuber M, Berghold J, Kräutler B (2008) Chlorophyll breakdown by a biomimetic route. Angew Chem Int Ed Engl **47:** 3057–3061

Park S-Y, Yu J-W, Park J-S, Li J, Yoo S-C, Lee N-Y, Lee S-K, Jeong S-W, Seo HS, Koh H-J, et al (2007) The senescence-induced staygreen protein regulates chlorophyll degradation. Plant Cell **19:** 1649–1664

Pruzinská A, Anders I, Aubry S, Schenk N, Tapernoux-Lüthi E, Müller T, Kräutler B, Hörtensteiner S (2007) In vivo participation of red chlorophyll catabolite reductase in chlorophyll breakdown. Plant Cell **19:** 369–387

Pruzinská A, Tanner G, Anders I, Roca M, Hörtensteiner S (2003) Chlorophyll breakdown: pheophorbide *a* oxygenase is a Rieske-type iron-sulfur protein, encoded by the *accelerated cell death 1* gene. Proc Natl Acad Sci USA **100:** 15259–15264

Pruzinská A, Tanner G, Aubry S, Anders I, Moser S, Müller T, Ongania K-H, Kräutler B, Youn J-Y, Liljegren SJ, et al (2005) Chlorophyll breakdown in senescent Arabidopsis leaves: characterization of chlorophyll catabolites and of chlorophyll catabolic enzymes involved in the degreening reaction. Plant Physiol **139:** 52–63

Ren GD, Zhou Q, Wu SX, Zhang YF, Zhang LG, Huang JR, Sun ZF, Kuai BK (2010) Reverse genetic identification of CRN1 and its distinctive role in chlorophyll degradation in *Arabidopsis*. J Integr Plant Biol **52:** 496–504

Rodoni S, Mühlecker W, Anderl M, Kräutler B, Moser D, Thomas H, Matile P, Hörtensteiner S (1997) Chlorophyll breakdown in senescent chloroplasts: cleavage of pheophorbide *a* in two enzymic steps. Plant Physiol **115:** 669–676

Rosso MG, Li Y, Strizhov N, Reiss B, Dekker K, Weisshaar B (2003) An *Arabidopsis thaliana* T-DNA mutagenized population (GABI-Kat) for flanking sequence tag-based reverse genetics. Plant Mol Biol **53:** 247–259

Sato Y, Morita R, Katsuma S, Nishimura M, Tanaka A, Kusaba M (2009) Two short-chain dehydrogenase/reductases, NON-YELLOW COLORING 1 and NYC1-LIKE, are required for chlorophyll *b* and light-harvesting complex II degradation during senescence in rice. Plant J **57:** 120–131

Schelbert S, Aubry S, Burla B, Agne B, Kessler F, Krupinska K, Hörtensteiner S (2009) Pheophytin pheophorbide hydrolase (pheophytinase) is involved in chlorophyll breakdown during leaf senescence in *Arabidopsis*. Plant Cell **21:** 767–785

Schenk N, Schelbert S, Kanwischer M, Goldschmidt EE, Dörmann P, Hörtensteiner S (2007) The chlorophyllases AtCLH1 and AtCLH2 are not essential for senescence-related chlorophyll breakdown in *Arabidopsis thaliana*. FEBS Lett **581:** 5517–5525

Schoch S, Vielwerth FX (1983) Chlorophyll degradation in senescent tobacco cell culture (*Nicotiana tabacum* var. "Samsun"). Z Pflanzenphysiol **110:** 309–317

Sessions A, Burke E, Presting G, Aux G, McElver J, Patton D, Dietrich B, Ho P, Bacwaden J, Ko C, et al (2002) A high-throughput *Arabidopsis* reverse genetics system. Plant Cell **14:** 2985–2994

Shimokawa K, Hashizume A, Shioi Y (1990) Pyropheophorbide *a*, a catabolite of ethylene-induced chlorophyll *a* degradation. Phytochemistry **29:** 2105–2106

Shioi Y, Tatsumi Y, Shimokawa K (1991) Enzymatic degradation of chlorophyll in *Chenopodium album*. Plant Cell Physiol **32:** 87–93

Shioi Y, Watanabe K, Takamiya K (1996) Enzymatic conversion of pheophorbide *a* to a precursor of pyropheophorbide *a* in leaves of *Chenopodium album*. Plant Cell Physiol **37:** 1143–1149

Smith D, Schnell D, Fitzpatrick L, Keegstra K (2002) In vitro analysis of chloroplast protein import. Curr Protoc Cell Biol **14:** 11.16.11–11.16.21

Strain HH, Cope BT, Svec WA (1971) Analytical procedures for the isolation, identification, estimation and investigation of the chlorophylls. Methods Enzymol **23:** 452–476

Suzuki T, Kunieda T, Murai F, Morioka S, Shioi Y (2005) Mg-dechelation activity in radish cotyledons with artificial and native substrates, Mg-chlorophyllin *a* and chlorophyllide *a*. Plant Physiol Biochem **43:** 459–464

Suzuki Y, Amano T, Shioi Y (2006) Characterization and cloning of the chlorophyll-degrading enzyme pheophorbidase from cotyledons of radish. Plant Physiol **140:** 716–725

Suzuki Y, Doi M, Shioi Y (2002) Two enzymatic reaction pathways in the formation of pyropheophorbide *a*. Photosynth Res **74:** 225–233

Suzuki Y, Shioi Y (1999) Detection of chlorophyll breakdown products in the senescent leaves of higher plants. Plant Cell Physiol **40:** 909–915

Suzuki Y, Soga K, Yoshimatsu K, Shioi Y (2008) Expression and purification of pheophorbidase, an enzyme catalyzing the formation of pyropheophorbide during chlorophyll degradation: comparison with the native enzyme. Photochem Photobiol Sci **7:** 1260–1266

Takamiya KI, Tsuchiya T, Ohta H (2000) Degradation pathway(s) of chlorophyll: what has gene cloning revealed? Trends Plant Sci **5:** 426–431

Tanaka R, Hirashima M, Satoh S, Tanaka A (2003) The Arabidopsis-accelerated cell death gene ACD1 is involved in oxygenation of pheophorbide a: inhibition of the pheophorbide a oxygenase activity does not lead to the "stay-green" phenotype in Arabidopsis. Plant Cell Physiol **44:** 1266–1274

Vlot AC, Liu PP, Cameron RK, Park SW, Yang Y, Kumar D, Zhou FS, Padukkavidana T, Gustafsson C, Pichersky E, et al (2008) Identification of likely orthologs of tobacco salicylic acid-binding protein 2 and their role in systemic acquired resistance in *Arabidopsis thaliana*. Plant J **56:** 445–456

Wesley SV, Helliwell CA, Smith NA, Wang MB, Rouse DT, Liu Q, Gooding PS, Singh SP, Abbott D, Stoutjesdijk PA, et al (2001) Construct design for efficient, effective and high-throughput gene silencing in plants. Plant J **27:** 581–590

Wessel D, Flügge UI (1984) A method for the quantitative recovery of protein in dilute solution in the presence of detergents and lipids. Anal Biochem **138:** 141–143

Wüthrich KL, Bovet L, Hunziker PE, Donnison IS, Hörtensteiner S (2000) Molecular cloning, functional expression and characterisation of RCC reductase involved in chlorophyll catabolism. Plant J **21:** 189–198

Yang Y, Xu R, Ma CJ, Vlot AC, Klessig DF, Pichersky E (2008) Inactive methyl indole-3-acetic acid ester can be hydrolyzed and activated by several esterases belonging to the AtMES esterase family of Arabidopsis. Plant Physiol **147:** 1034–1045

Ziegler R, Blaheta A, Guha N, Schönegge B (1988) Enzymatic formation of pheophorbide and pyropheophorbide during chlorophyll degradation in a mutant of *Chlorella fusca* Shiria et Kraus. J Plant Physiol **132:** 327–332

Zimmermann P, Hirsch-Hoffmann M, Hennig L, Gruissem W (2004) GENEVESTIGATOR: Arabidopsis microarray database and analysis toolbox. Plant Physiol **136:** 2621–2632

SUPPLEMENTAL INFORMATIONS

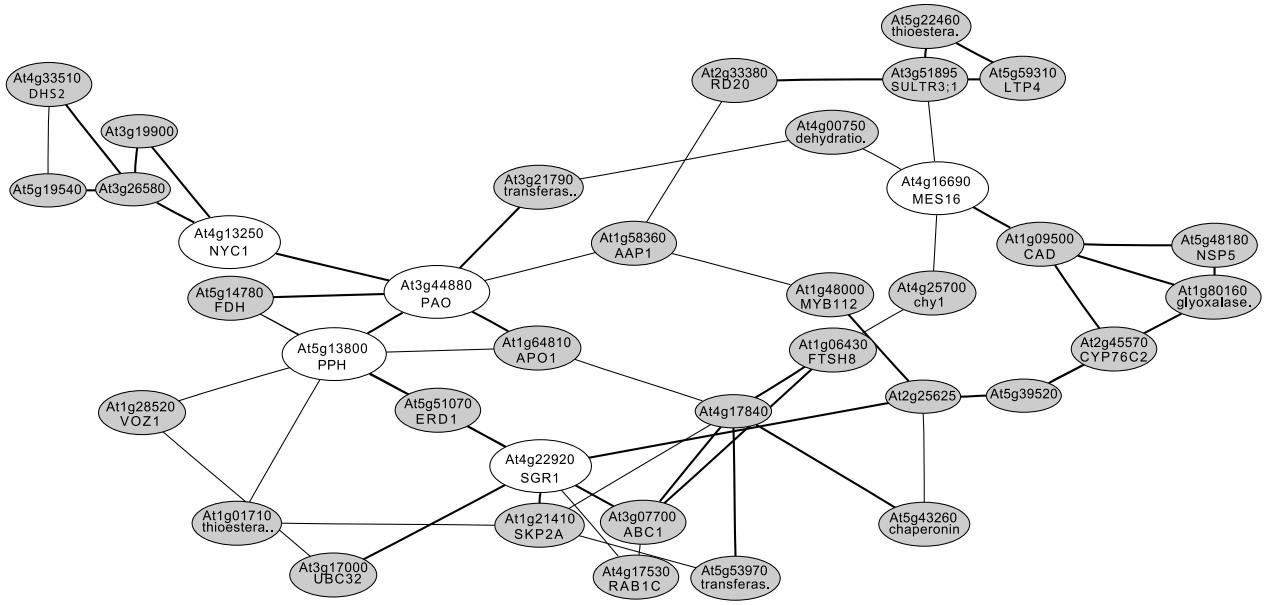

Supplemental Fig. 1.S1. Co-expression network around PAO, PPH, SGR, NYC1 and MES16. The ATTED-II NetworkDrawer tool (Obayashi et al., 2009) was used to generate the network with PAO (AT3G44880), PPH (AT5G13800), SGR (AT4G22920), NYC1 (AT4G13250) and MES16 (AT4G16690) as inputs.

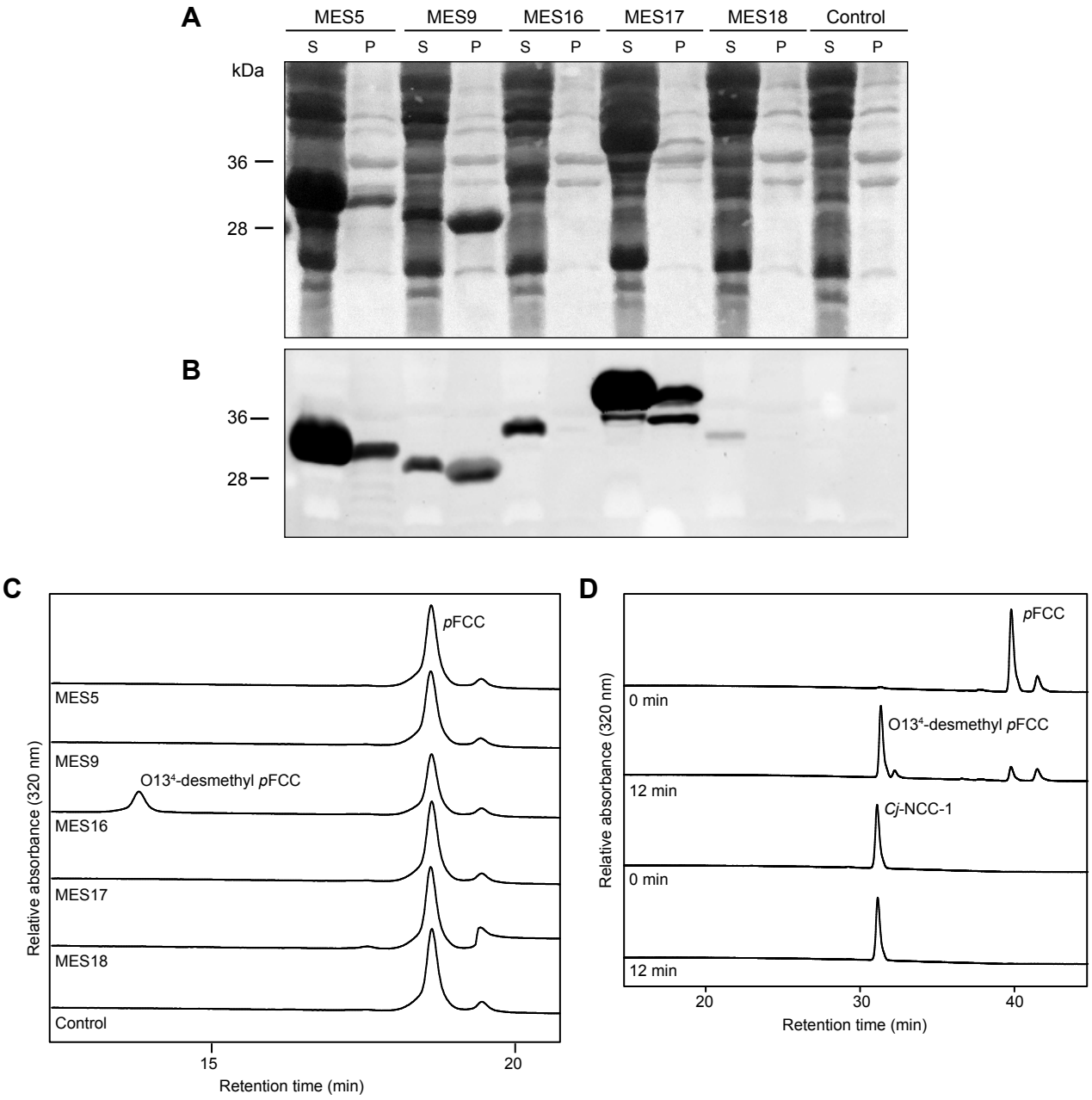

Supplemental Fig. 1.S2. Analysis of recombinant MES5, MES9, MES16, MES17 and MES18. A, Analysis of MES protein expression by SDS-PAGE followed by transfer to a nitrocellulose membrane and Ponceau S staining. Soluble (S) and unsoluble (P) proteins from equal cellular fractions were loaded in the gel. B, Detection of recombinant MES proteins by anti-His immunoblotting of the membrane showed in panel A. As control, an *E. coli* strain containing the empty vector was used. C, HPLC analysis of assays employing *E. coli* lysates expressing 6xHis-MES proteins with *p*FCC as substrate. Equivalent amount of recombinant proteins were used in the assays. Parts of HPLC traces at A_{320} after 12 min of incubation at 25°C are shown. D, Analysis of MES16 activity on *Cj*-NCC-1. Parts of HPLC traces at A_{320} after 0 and 12 min of incubation at 25°C are shown. *p*FCC was used as control. Note that the assays showed in panel D were analyzed by HPLC using the program described for plant extracts (see Materials and Methods).

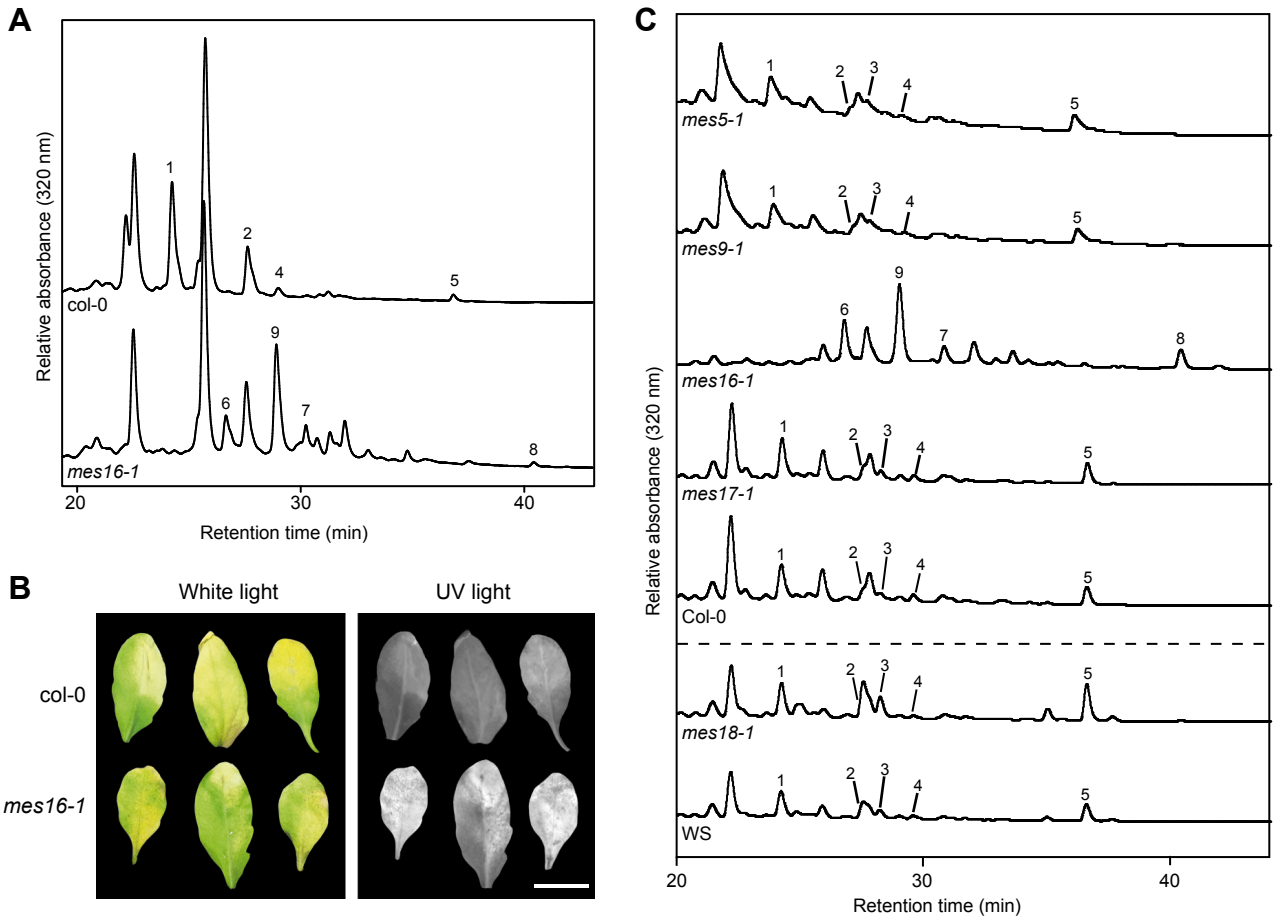

Supplemental Fig. 1.S3. Colorless catabolites occurring in *mes16-1* mutants during natural senescence and in mutants of other closely related MES family members after dark incubation. A, HPLC analysis of colorless catabolites of senescent leaves of Col-0 and *mes16-1* during natural senescence. B, Photographs of natural senescent Col-0 and *mes16-1* leaves under white light and UV light (366 nm). Bar = 1 cm. C, Colorless catabolites of *mes5-1*, *-9-1*, *-16-1*, *-17-1* and *-18-1* mutants after dark incubation (8 d for *mes5-1*, *-9-1*, *-16-1*, *-17-1*, background Col-0; 10 d for *mes18-1*, background WS). A and C, Catabolites were separated by HPLC as described in Materials and Methods. A_{320} was recorded. For clarity, only parts of the HPLC traces are shown in panels A and C. For identification and peak numbering of FCCs and NCCs see Table I.

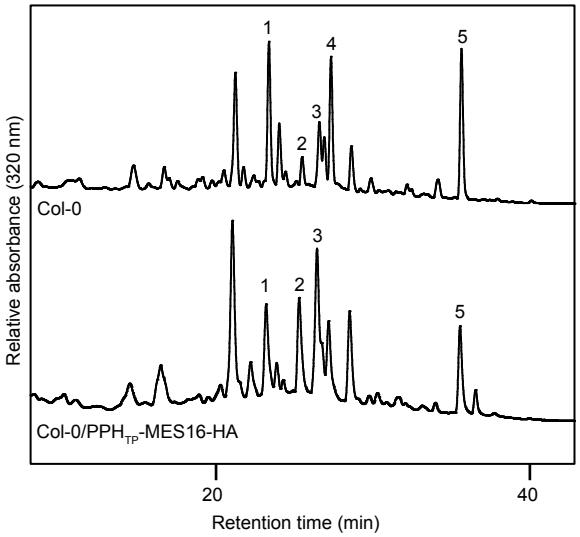

Supplemental Fig. 1.S4. Colorless catabolites of Col-0/*PPHTP-MES16-HA*. Colorless catabolites of dark-incubated (6 d) leaves of Col-0 and Col-0/*PPHTP-MES16-HA* plants were separated by HPLC as described in Materials and Methods. For clarity, only a part of the HPLC traces at A_{320} is shown. For identification and peak numbering of FCCs and NCCs, see Table I.

Supplemental Table 1.S1 : *List of primers used in this study*

GENE/ CONSTRUCT/ MUTANT	PRIMER NAME	SEQUENCE (5'->3')
	T-DNA confirmation	
mes16-1	MES16-1-RP	GTTGAAGAAAAGAAACCGCAC
	MES16-1-LP	CTGAGCCCGTAATTCACTTTG
mes16-2	MES16-2-RP	ACCTCATGTTGTCGTTCAAGG
	MES16-2-LP	CTAACATCGTCTTCGACTCCG
mes5-1	MES5-1-RP	TCATGAAGGCACGTCTTTACC
	MES5-1-LP	TTTTGTCTCACCTGCTTCCAC
mes9-1	MES9-1-RP	GTTTGACCTTGTACCAGCACC
	MES9-1-LP	CTTTGGAGGATTTCGCTAAGC
mes17-1	MES17-1-RP	CGAGTGCGATACAGAGATTCC
	MES17-1-LP	AAAACCAACAAAAGGCAATCC
mes18-1	MES18-1-RP	TTGTTGGGAGATTTTGTGGTC
	MES18-1-LP	TTTCATGAAGTTGTCAACACCTG
pao1	N14-RP	GGCTCACCTGACGCTTGGTTA
	N14-LP	CGACGGTGACAATTCAAAGGG
SALK T-DNA	LBb1.3	ATTTTGCCGATTTCGGAAC
SAIL T-DNA	LB2	GCTTCCTATTATATCTTCCCAAATTACCAATACA
GABI T-DNA	GABI-LB	CCCATTTGGACGTGAATGTAGACAC
FLAG T-DNA	FLAG_LB_TAG5	CTACAAATTGCCTTTTCTTATCGAC
	RT-PCR	
MES16	MES16_Ex1_S	TCACCGAAGCTCTTTGCAAG
	MES16_Ex3_AS	TTGAAGAAAAGAAACCGCACG
ACT2	ACT2-S	TGGAATCCACGAGACAACCTA
	ACT2-AS	TTCTGTGAACGATTCCTGGAC
SGR1	AtSGR1-S	TGGAGATGGGAACTTGTTGAA
	AtSGR1-AS	GCTAACGGTTGGAAAACAACA
PAO	ACD1-S	ACGGCATGGTAAGAGTCAGC
	ACD1-AS	AAACCAGCAAGAACCAGTCG
	Cloning MES16-GFP	
MES16	MES16-*Sma*I-S	TCCCCCGGGGAATGGGAGGAGAAGGTGGTGC
	MES16-*Spe*I-AS	CCACTAGTTCGTTGAAGAAAAGAAACCGCAC
	Cloning MES18 in pProEX Hta	
MES18	MES9-*Eco*RI-S	CCGGAATTCATGAGTGAGCATCATTTTGTG
	MES9-*Eco*RI-AS	CCGGAATTCTCAGGGAGAAAGAGATGAGG
	Cloning PPHTP-MES16-HA	
PPH transit peptide	PPH_TP-S	CGGAATTCATGGAGATAATCTCACTGAA
	PPH_TP-AS	CACCTTCTCCTCCTCCACTTCGAATCACAAGTC
MES16	MES16-S	GATTCGAAGTGGAGGAGGAGAAGG-TGGTGCTGA
	MES16_HA-AS	GAAGCTTTTAGGCATAGTCTGGGACGTCA-TATGGATATCGTTGAAGAAAAGAAACCG

2 - FCC DEFORMYLATION

Cytochrome P450 CYP89A9 is involved in the formation of major chlorophyll catabolites during leaf senescence in Arabidopsis thaliana.

Submitted to PNAS (2013-03-20)

This chapter is dedicated to the discovery of a new type of Chl catabolites in Arabidopsis. These catabolites have already been described in barley and Norway maple and are known as UCCs or NDCCs. NCCs and NDCCs differ on pyrrole ring A, where the side group at C^6 is a formyl group in NCCs and an oxo group in NDCCs. We demonstrate that NDCCs are the major Chl catabolites in Arabidopsis, accounting for more than 80% of all final Chl catabolites. We further identified cytochrome P450 CYP89A9 of Arabidopsis as being responsible for the oxidative deformylation of FCCs to FDCCs in the cytosol.To the best of our knowledge, the proposed reaction of CYP89A9, producing a γ-lactam upon deformylation of the α-formyl-pyrrole unit, is novel for cytochrome P450 enzymes.

Bastien Christ[1], Iris Süssenbacher[1], Simone Moser, Nicole Bichsel, Aurélie Egert, Thomas Müller, Bernhard Kräutler[2] and Stefan Hörtensteiner[2]

[1,2]These authors contributed equally to this work

INTRODUCTION

Senescence, the ultimate phase of leaf development in higher plants, is phenotypically defined by leaf yellowing, which results from the quantitative loss of chlorophyll (Chl). In many plant species, Chl has been shown to be broken down in a multi-step pathway to a group of structurally similar colorless linear tetrapyrroles, termed nonfluorescent Chl catabolites (NCCs) (Hörtensteiner and Kräutler, 2011; Kräutler and Matile, 1999; Moser et al., 2009b). NCCs are Chl *a*-derived formyloxobilin-type linear tetrapyrroles where the chlorin macrocycle is oxygenolytically opened in the so-called northern meso-position. Thereby, the C5-carbon atom bridging pyrrole rings A and B is retained as formyl group attached to ring B (Kräutler et al., 1991). This is in contrast to heme degradation by heme oxygenase, where the corresponding carbon atom is lost as CO, and biliverdin (a dioxobilin) is formed as degradation product (Unno et al., 2007).

The pathway of chlorophyll breakdown can be divided into two parts; early reactions that take place within senescing chloroplasts and that result in the formation of a colorless *primary* fluorescent Chl catabolite (*p*FCC) (Mühlecker et al., 1997). The reactions catalyzing Chl-to-*p*FCC conversion are commonly present in land plants and, therefore, represent the core part of the pathway. The intermediates of breakdown upstream of *p*FCC are considered potent phototoxins and metabolic channeling was proposed to occur among these early reactions to minimize the risk of phototoxicity (Kräutler and Matile, 1999). The key reaction of the pathway is catalyzed by pheophorbide *a* oxygenase (PAO), a plant-specific Rieske type monooxygenase, which catalyzes the already mentioned opening of the macrocycle of pheophorbide *a*, the Mg- and phytol-free intermediate of breakdown (Hörtensteiner et al., 1998; Pružinská et al., 2003). The product of the oxygenation reaction, red Chl catabolite (Kräutler et al., 1997), is reduced to *p*FCC by red Chl catabolite reductase (RCCR) in a stereo-specific manner. Thus, depending on the plant species as the source of RCCR one of two stereo-isomers, i.e. *p*FCC and *epi*-*p*FCC, are formed (Mühlecker et al., 2000, 1997; Pružinská et al., 2007).

The second part of the pathway of Chl breakdown is characterized by largely species-specific modification at different peripheral positions within *p*FCC, giving rise to modified FCCs (Moser et al., 2012; Pružinská et al., 2005) and *hypermodified* FCCs (see Fig. 2.S1; Hörtensteiner and Kräutler, 2011; Moser et al., 2008a). The reactions catalyzing these modifications occur in the cytosol, implying that *p*FCC is exported from the chloroplast. After import of modified FCCs into the vacuole, spontaneous nonenzymatic isomerization to respective NCCs occurs because of the acidic pH of the vacuolar sap (Oberhuber et al., 2003). Thus, it is commonly accepted now that peripheral modifications present in NCCs reflect modification reactions that occurred at the level of FCCs. In *Arabidopsis thaliana* (Arabidopsis), for example, five NCCs (*At*-NCCs) were identified that differ from each other at the $C7^1$, $C8^2$ and/or $O13^4$ position (R^1 R^2 and R^3 in Fig. 2.S1; Müller et al., 2006; Pružinská et al., 2005). The occurrence of different NCCs in a given plant species has been explained by the possibility that the corresponding variety of modified FCCs are imported to the vacuole; however, to date the affinities of the vacuolar transporters for such different FCCs have not been investigated.

As NCCs were found to accumulate in various senescent leaves, they were considered as the 'final' breakdown products of Chl, but the question whether they might be further metabolized in leaves was apparent (Ulrich et al., 2011). In senescent leaves of *Cercidiphyllum japonicum*, for example, a single NCC was estimated to represent more than 90% of the original Chl content (Curty and Engel, 1996), while for example the major NCC of spinach accounted for only 20% of the degraded Chl (Berghold et al., 2002). In several cases, additional presumed breakdown products of Chl were identified in senescent leaves, e.g. yellow- and pink-colored tetrapyrrolic catabolites, derived from the main NCC in *C. japonicum* (Fig. 2.S1; Moser et al., 2008b; Ulrich et al., 2011). In addition, two isomeric nonfluorescent dioxobilin-type Chl catabolites (NDCCs) were identified in barley. These were thought to be formed by unspecific oxidation events from *Hv*-NCC-1 (Losey and Engel, 2001), the major NCC in barley (Kräutler et al., 1991). Recently, a structurally similar NDCC was identified in naturally senescent leaves of Norway maple, representing about 50% of the Chl present

in green leaves, while NCCs were not detected (Müller et al., 2011). The molecular constitution of the maple NDCC was elucidated by spectroscopic means. These newer studies showed that NDCCs, rather than NCCs, are the major degradation products of Chl in some senescent leaves, and, in addition, they suggested that (N)DCCs were formed by still enigmatic, catabolic enzyme activities, rather than by non-physiological degradation events.

Here we show that also in the model plant *Arabidopsis thaliana* NDCCs, not NCCs, are the major breakdown products of Chl. We further identified cytochrome P450 monooxygenase CYP89A9 as being responsible for NDCC accumulation during Arabidopsis leaf senescence. Using a combination of genetic, biochemical and metabolic approaches, CYP89A9 was shown to catalyze a previously unknown deformylation reaction of FCC-type Chl breakdown intermediates. These findings reveal a novel basic transformation in the complex pathway of Chl breakdown that may not only be relevant in Arabidopsis, but might also occur in other plant species (Müller et al., 2011).

RESULTS

NDCCs are the major chlorophyll catabolites in Arabidopsis

To explore the possibility that, besides NCCs (Pružinská et al., 2005), NDCCs might accumulate in Arabidopsis, we re-analyzed senescent leaf extracts by HPLC. Like other NCCs, *At*-NCCs exhibit a characteristic absorption maximum at around 315 nm and equally strong absorption at 254 nm (Fig. 2.1A). When comparing Arabidopsis leaf extracts with detection at these two wavelengths, several fractions were identified that strongly absorbed at 254 nm but only weekly at 315 nm (Fig. 2.1C). At least five of these fractions showed absorption spectra (Fig. 2.1B; Fig. 2.S2A) that were described for the Norway maple NDCC (Müller et al., 2011), indicating that they could represent related NDCCs (*At*-NDCCs) in Arabidopsis.

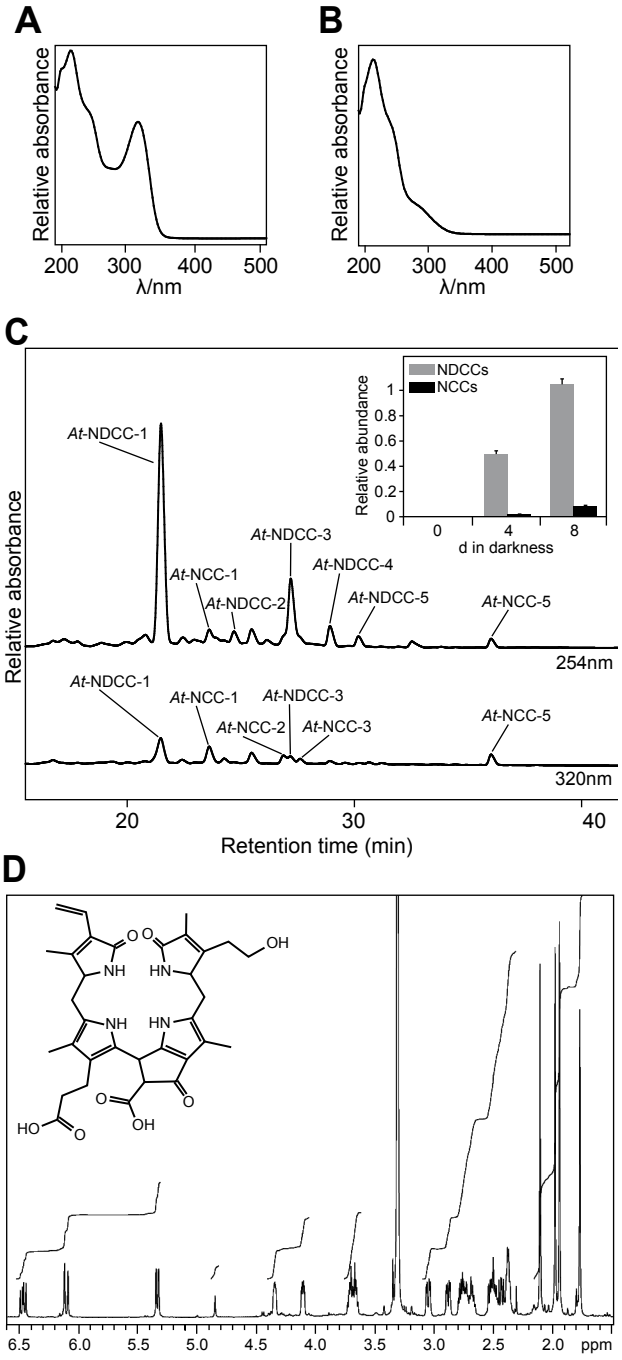

Fig. 2.1. NDCCs are the major catabolites in Arabidopsis. (*A*) UV absorption spectrum of *At*-NCC-1. (*B*) UV absorption spectra of *At*-NDCC-1. (*C*) Colorless catabolites of dark-incubated (8 d) leaves of Col-0 were separated by HPLC. A_{254} and A_{320} are shown. For clarity, only the relevant part of the HPLC traces is shown; inset, sums of NDCCs and NCCs accumulating during dark-induced senescence. Values are means of three replicates, and error bars represent SD. (*D*) 600 MHz ^{1}H-NMR spectrum of *At*-NDCC-1 (in CD_3OD, 283 K) and constitutional formula of *At*-NDCC-1.

The most polar, major NDCC from Arabidopsis (*At*-NDCC-1) was thoroughly analyzed by spectroscopic methods (for detailed spectroscopic data, see "Materials and Methods"). *At*-NDCC-1 was revealed to represent a dioxobilane-type NCC (see Fig. 2.1D, inset), as follows. The molecular formula of *At*-

NDCC-1 was determined as $C_{33}H_{38}N_4O_8$ by mass spectrometry (MS), by which the quasi-molecular ion $[C_{33}H_{38}N_4O_8+H]^+$ was observed at m/z = 619.3. In the ^1H NMR spectra of *At*-NDCC-1 (in CD_3OD, 10°C) (Fig. 2.1D), signals of all 30 exchange-inert carbon-bound hydrogen-atoms were observed. A singlet near 9 ppm was absent, which is a characteristic of the formyl hydrogen atom of NCCs (see e.g. (Kräutler et al., 1991)). Instead, a triplet at δ = 4.35 ppm and a multiplet at 4.11 ppm indicated hydrogen atoms at position C9 and C1, as are typical for NDCCs (see Fig. 2.1D; Müller et al., 2011).

Both NDCC and NCC abundances increased during the course of leaf senescence; however the amounts of NDCCs exceeded NCCs by a factor of about ten (inset in Fig. 2.1C). In addition, after 8 d of dark-induced senescence, NDCCs accounted for more than 75% of the degraded Chl, demonstrating them to represent the by far most abundant type of Chl catabolite in Arabidopsis.

CYP89A9 is required for NDCC accumulation in Arabidopsis

The identification of NDCCs as the major Chl catabolites in Arabidopsis asked for elucidating the mechanism of their formation. Two possible pathways were addressed; (i) formation from a chlorin-type substrate, such as Chl or pheophorbide, whose macrocycle could be opened by a heme oxygenase-like reaction, i.e. under the loss of the C5-carbon atom, or (ii) oxidative deformylation of the C5-formyl group present in FCCs and NCCs. We excluded the first possibility, because *pao1*, an Arabidopsis PAO mutant, retains large quantities of Chl during leaf senescence (Pružinská et al., 2005). If NDCC formation would involve an activity for chlorin ring cleavage that is distinct from PAO, degreening should not be blocked in *pao1*. Alternatively, PAO itself could exhibit a heme oxygenase-like activity; however, *in vitro* activity studies clearly demonstrated a specificity of PAO towards FCC formation (Hörtensteiner et al., 1995). To identify likely candidates for C5-deformylation, we tested whether cytochrome P450 monooxygenases (P450s) could be involved. P450s have been shown to catalyze a plethora of different reactions, including deformylation of C-bound formyl groups

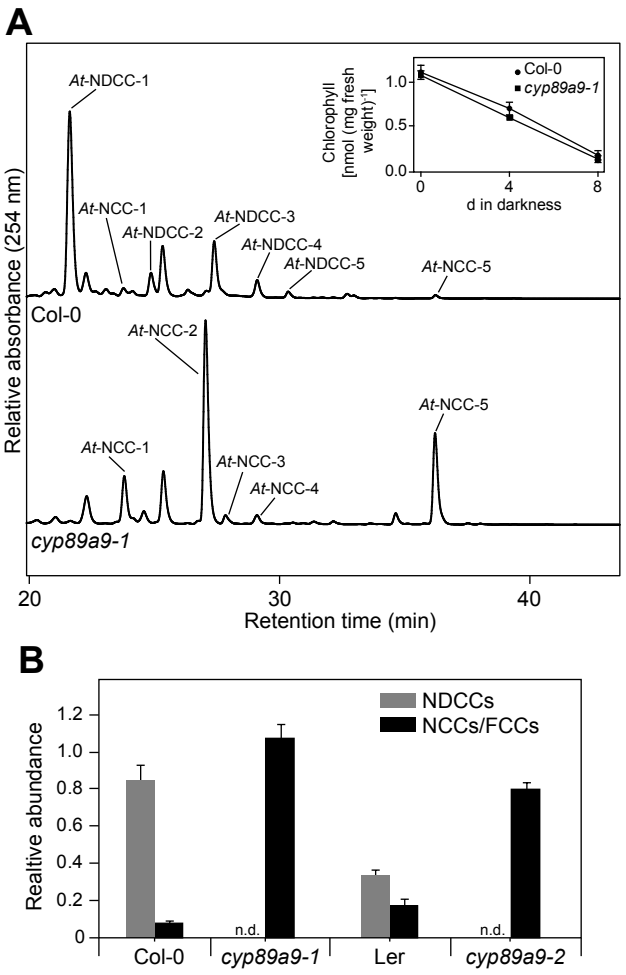

Fig. 2.2. Colorless catabolites accumulating in dark-incubated (8 d) leaves of *cyp89a9* mutants. (*A*) Colorless catabolites of Col-0 and *cyp89a9-1* were separated by HPLC. For clarity, only the relevant part of the A_{254} traces is shown. The inset shows Chl degradation of Col-0 and *cyp89a9-1* during dark-induced senescence. (*B*) NDCC and NCC abundance in Col-0, *cyp89a9-1*, Ler and *cyp89a9-2*. Values are means of three replicates, and error bars represent SD.

(Guengerich, 2001; Halkier, 1996). We exploited the ability of CO to effectively inhibit P450s (Schuler, 1996); when senescence was induced in detached leaves in an atmosphere composed of a 1:1 ratio (v/v) of CO and ambient air, the NDCC-to-NCC ratio was shifted to higher amounts of NCCs when compared to incubation at ambient air (Fig. 2.S3). This supported the idea that P450s could catalyze NDCC formation. Based on the fact that several genes encoding Chl catabolic enzymes are highly expressed in senescent rosette leaves, cauline leaves and petals and/or sepals (Pružinská et al., 2005; Zimmermann et al., 2004), we reasoned that the genes for P450s involved in NDCC formation could be similarly induced. Using the Genes Search Tool of the Genevestigator

platform (Zimmermann et al., 2004) and the above-mentioned tissues as targets, were found two P450 genes, *CYP89A9* and *CYP71B19*, among the first hundred genes that are similarly expressed (Table 2.S1). As expected, this gene list also contained *PAO*, *STAY-GREEN* and *PHEOPHYTINASE*, three senescence-regulated Chl catabolic genes. To analyze the potential role of the two P450 candidate genes, we characterized Chl breakdown in T-DNA insertion mutants that fail to express the respective full length gene transcripts (Fig. 2.S4A). These lines did not show any obvious visible phenotype during normal development and also upon senescence induction, Chl has degraded like in wild-type. During senescence,

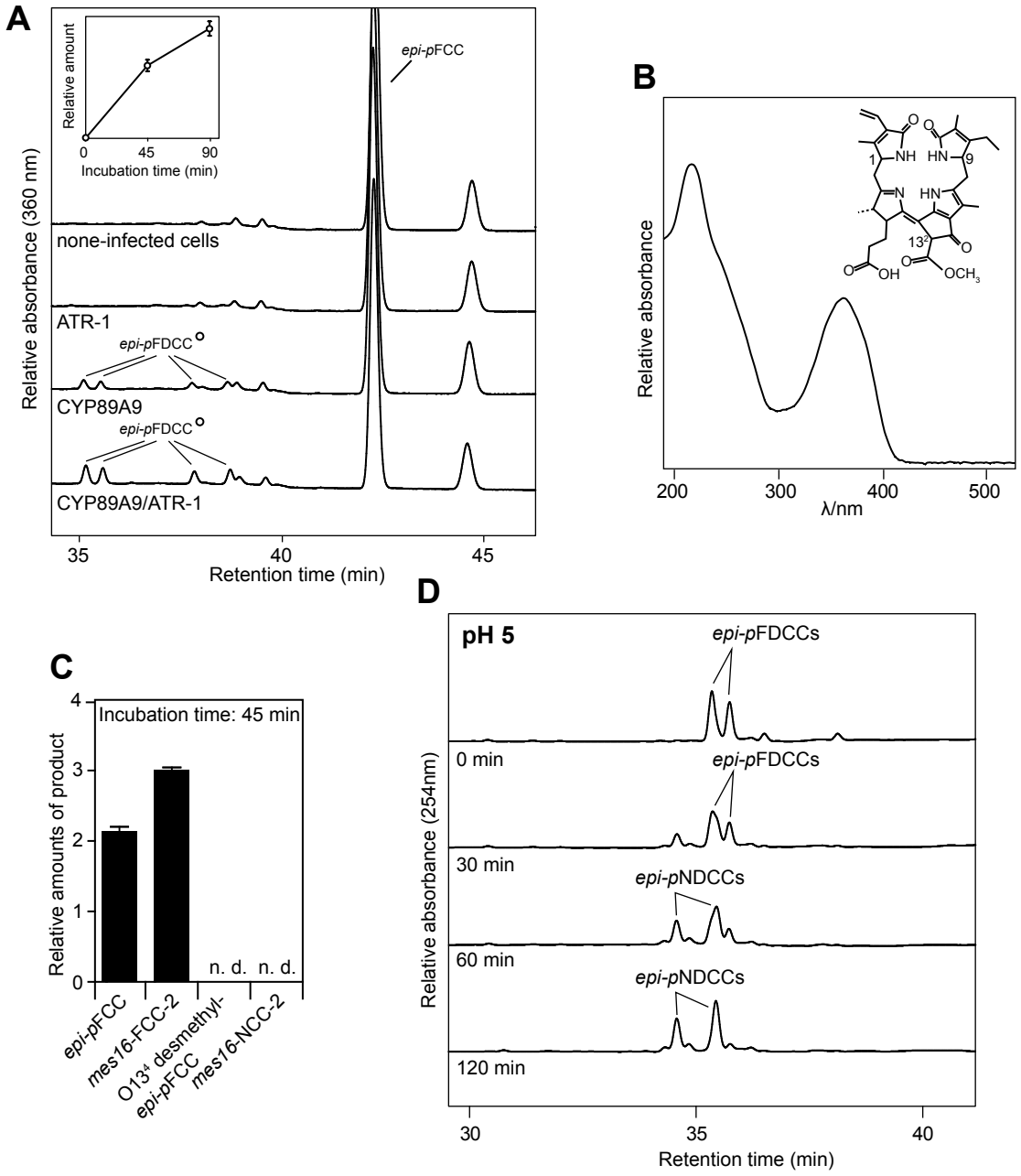

Fig. 2.3. Analysis of recombinant CYP89A9. (*A*) HPLC analysis of assays employing Sf9 microsomes expressing CYP89A9 and ATR1, and *epi-p*FCC as substrate. HPLC traces at A_{360} after 90 min of incubation at 28°C are shown. For clarity, only the part of the HPLC traces is shown. The inset shows the relative amounts of formed *epi-p*FDCCs. Values are means of three replicates. Error bars indicate SD. (*B*) UV absoption spectrum of *epi-p*FDCCs produced with recombinant CYP89A9 and chemical constitution of (*epi-*) *p*FDCCs. Relevant stereo-centers are labeled. (*C*) Substrate specificity of CYP89A9. Values are means of three replicates. Error bars indicate SD. (*D*) FDCC-to-NDCC isomerization assays. The two most polar *epi-p*FDCCs produced with recombinant CYP89A9 were incubated at pH 5 for up to 120 min and analyzed by HPLC. A_{254} is shown.

cyp71b19 mutants accumulated wild-type patterns of catabolites (Fig. 2.S4B) and were not considered further. By contrast, both investigated *cyp89a9* mutants did not accumulate NDCCs, but had more than 10-fold increased levels of NCCs (Fig. 2.2). In *cyp89a9-1*, NCCs accumulated up to 1.1 µmol per g fresh weight, which corresponded to more than 90% of degraded Chl. UV/Vis (Fig. 2.S2B) and MS analysis of the NCCs of *cyp89a9-1* (for MS data, see *SI Materials and Methods*) confirmed them to be identical to the NCCs found in the Col-0 wild-type (Pružinská et al., 2005). The *cyp89a9-2* mutation is in the Ler background and Ler has been shown to be a natural MES16 mutant (Christ et al., 2012). MES16 is responsible for demethylation of the $C13^2$-carboxymethyl group of FCCs. Because of this, the NDCC/NCC catabolite patterns differed between Col-0 and Ler (Fig. 2.2B; Fig. 2.S5A). In addition, $O13^4$-desmethyl FCCs that accumulate in *mes16* mutants (hence also in Ler) were shown to isomerize more slowly to the corresponding NCCs; i.e. these FCCs accumulate in senescent leaves, which, as a consequence, show strong fluorescence (Christ et al., 2012). To confirm that the catabolite pattern seen in *cyp89a9-2* is due to the absence of both CYP89A9 and MES16, we crossed *cyp89a9-1* with *mes16-1* (a MES16 mutant in Col-0 background). In this line, Chl catabolite patterns were identical to *cyp89a9-2* (Fig. 2.S5).

CYP89A9 is a fluorescent chlorophyll catabolite deformylase

The NDCC-deficiency of *cyp89a9* mutants indicated that CYP89A9 may catalyze their formation in wild-type plants. To analyze this hypothesis we tested *in vitro* activity of recombinant CYP89A9 expressed in Sf9 insect cells. FCCs were considered as likely substrates for CYP89A9, because, as shown for most P450 enzymes, CYP89A9 localized to the ER when expressed as a fusion with green fluorescent protein in Arabidopsis mesophyll protoplasts (Fig. 2.S6). P450 activity requires a P450 reductase; therefore, ATR1, one of the two Arabidopsis P450 reductases (Jensen and Moller, 2010), was expressed in Sf9 cells as well. Using *epi-p*FCC (Mühlecker et al., 2000) as substrate, four fractions of fluorescent compounds were obtained in a time-dependent manner in the presence of CYP89A9 (Fig. 2.3A). They exhibited identical spectra with a prominent absorption maximum at around 360 nm (Fig. 2.3B; Fig. 2.S2C). MS analysis (for MS data, see *SI Materials and Methods*) demonstrated these compounds to be isomers of a constitutionally uniform fluorescent DCC (FDCC) (Fig. 2.3B), which we termed *epi-p*FDCCs because they derived from *epi-p*FCC. They likely differ in the absolute configuration at $C13^2$ and C9 (see Fig. 2.3B); however, this was not further investigated. To test the substrate specificity of CYP89A9, assays were performed also with *mes16*-FCC-2 (*p*FCC with an additional hydroxyl group at $C8^2$) and the corresponding NCC, *mes16*-NCC-2 (Christ et al., 2012) (Fig. 2.3C). Only the FCC, but not the isomeric NCC, was converted by CYP89A9, supporting the specificity of CYP89A9 for FCCs. Under acidic conditions, the *epi-p*FDCCs isomerized into NDCCs (Fig. 2.3D; Fig. 2.S2D), indicating that *in vivo* formation of NDCCs from corresponding FDCCs might occur after their import into the vacuole.

FCC deformylation precedes FCC demethylation

During our analysis of CYP89A9 substrate specificity *in vitro* it turned out that the enzyme did not convert $O13^4$-demethylated *epi-p*FCC to the respective FDCC (Fig. 2.3D). This indicated that, although both CYP89A9 and MES16 act in the cytosol and therefore could compete for the same substrate *in vivo*, deformylation by CYP89A9 might precede catabolite demethylation by MES16. To investigate this in more detail, we used a line (Col-0/PPH_{TP}-MES16) in which MES16 was targeted to the chloroplast (Christ et al., 2012), i.e. demethylation was allowed to occur before FCC export to the cytosol. In this line, the NDCC-to-NCC ratio was significantly shifted towards more NCCs as compared to Col-0 (Fig. 2.4; Fig. 2.S7). This supports the idea that in Col-0 wild-type plants, CYP89A9 precedes MES16 action to a large extend leading to the formation of NDCCs, while only a small fraction of catabolites may be first demethylated, thus, ending in the formation of NCCs. Further evidence for this was obtained by CYP89A9 complementation tests in *cyp89a9* mutants. When analyzing the relative amounts of NDCCs and NCCs as a measure of complementation, absence of MES16 in the *mes16-1*/*cyp89a9-1* double mutant resulted in more efficient complementation compared to (the

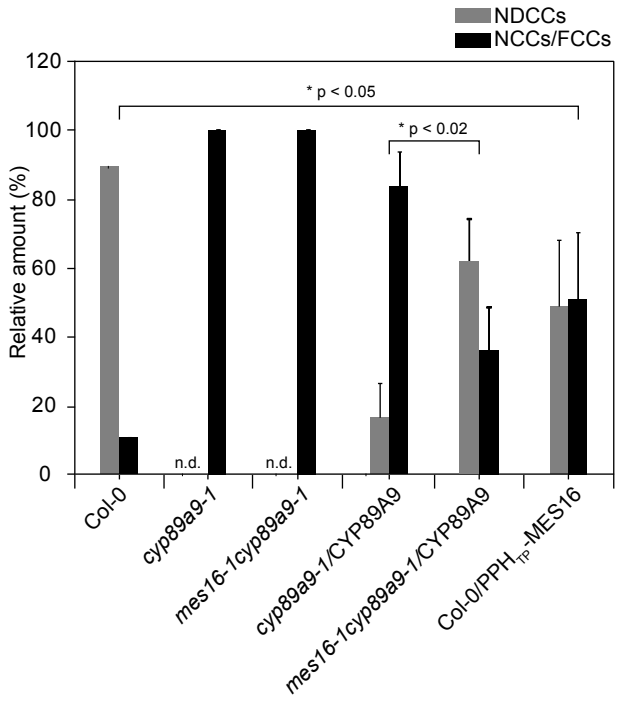

Fig. 2.4. FCC deformylation precedes FCC demethylation. Colorless catabolites accumulating in dark-incubated (7 d) leaves of Col-0, *cyp89a9-1*, *mes16-1cyp89a9-1*, *cyp89a9-1*/CYP89A9, *mes16-1cyp89a9-1*/CYP89A9 and Col-0/PPH$_{TP}$-MES16 were separated by HPLC. Relative amounts are means of N replicates (see below) and error bars represent SE. Col-0, *cyp89a9-1* and *cyp89a9-1mes16-1*, N=3; *cyp89a9-1*/CYP89A9 and Col-0/PPH$_{TP}$-MES16, N=6; *cyp89a9-1mes16-1*/CYP89A9, N=5. For the transgenic lines, replicates correspond to independent transformation events. The significance of differences between Col-0 and Col-0/PPH$_{TP}$-MES16 as well as between *cyp89a9-1*/CYP89A9 and *mes16-1cyp89a9-1*/CYP89A9 was determined using a one-tailed t test with Welch correction. n.d., not detected.

MES16-containing line) *cyp89a9-1* (Fig. 2.4).

DISCUSSION

NCCs are known since more than 20 years to represent colorless products of Chl breakdown during leaf senescence (Kräutler et al., 1991). They are seemingly end-products of a multistep-pathway (Hörtensteiner and Kräutler, 2011) which involves an acid-catalyzed isomerization of intermediary FCCs inside the vacuoles of senescing cells (Oberhuber et al., 2003). Both FCCs and NCCs are linear tetrapyrroles that can be classified as formyloxobilin-type tetrapyrroles, because the C5-carbon, bridging pyrrole rings A and B in Chl, is present as formyl group. Here we show that in Arabidopsis NCCs are only minor products of Chl breakdown and up to 90% of Chl is metabolized to a different type of catabolites termed here as dioxobilin-type Chl catabolites (DCCs). Compared to NCCs, nonfluorescent DCCs (NDCCs) miss the C5-carbon. In a few isolated reports, NDCCs were observed as presumed Chl degradation products (Djapic and Pavlovic, 2008; Djapic et al., 2009; Losey and Engel, 2001; Müller et al., 2011), but their way of formation remained unclear. Here we show that Arabidopsis CYP89A9 specifically deformylates FCCs to the corresponding FDCCs and, thus, defines the biochemical basis for the generation of DCCs (i.e. FDCC and NDCC) (Fig. 2.5).

The identification of NDCCs as major degradation products of Chl in Arabidopsis is intriguing, because structurally they are closely related to dioxobilins, which are known as products of heme degradation. Hence, regarding the structures of the main catabolites, Chl breakdown in Arabidopsis resembles heme degradation (Müller et al., 2011). Mechanistically, however, DCC formation totally differs from the latter. Heme oxygenase uses the iron-containing porphyrin, heme, as substrate for oxygenolytic ring opening and extrusion of the meso-carbon as CO. Thereby, the dioxobilin biliverdin is directly formed (Unno et al., 2007). By contrast, during Chl breakdown, PAO catalyzes chlorin ring opening of the metal-free breakdown intermediate pheophorbide *a* (Pružinská et al., 2003). Thereby, the C5-carbon is retained in FCCs and NCCs. The C5-carbon is only subsequently removed by oxidative deformylation of FCCs through the here discovered P450 monooxygenase, yielding dioxobilin-type FDCCs. In analogy to FCC-to-NCC isomerization (Oberhuber et al., 2003), FDCCs isomerize to NDCCs under acidic conditions (Fig. 2.4).

The key role of CYP89A9 in DCC formation is supported by the fact that *cyp89a9* mutants did not accumulate NDCCs, but contained proportionally higher quantities of NCCs (Fig. 2.2). This also implied that NDCCs and NCCs derive from a common source of precursors. Interestingly, although CYP89A9 specifically reacted with FCCs, it was not equally active towards different tested FCCs (Fig. 2.3). Thus, O13^4-desmethyl *epi-p*FCC was not deformylated, despite the fact that almost all NCCs (Pružinská et al., 2005) and also *At*-NDCC-1, structurally characterized here (Fig. 2.1), contain a free C13^2 carboxyl group. This indicates that CYP89A9 activity precedes demethylation by MES16 *in vivo*.

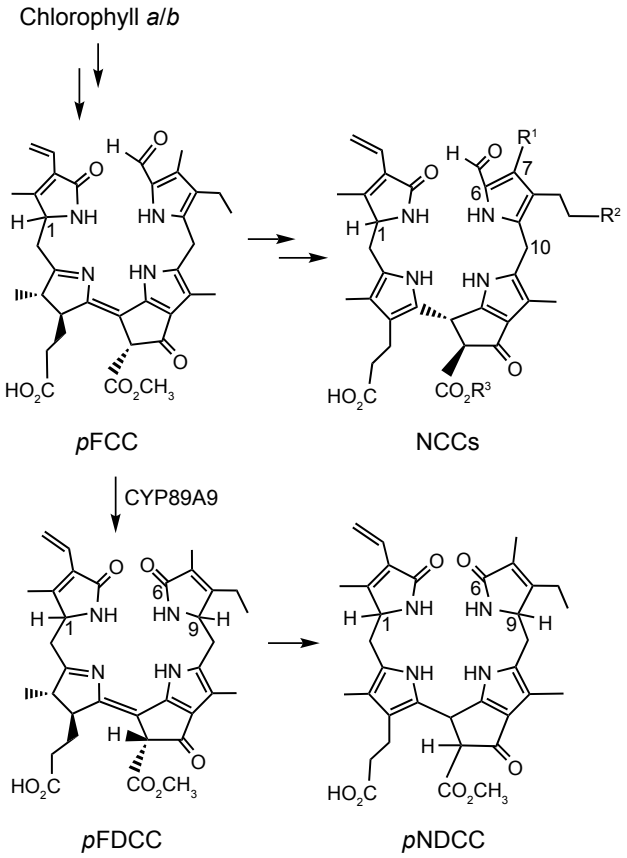

Fig. 2.5. Structural outline of Chl breakdown with representative key compounds. In Arabidopsis the primary fluorescent Chl catabolite is *p*FCC (the C-1 epimer of *epi*-*p*FCC), the degradation product of the Chls that is formed in the chloroplast. In addition, five nonfluorescent chlorophyll catabolites (NCCs) have been detected (with different groups R^1 to R^3; e.g. *At*-NCC-1: R^1 = CH_3, R^2 = O-*β*-glucopyranosyl, R^3 = H), which are derived from isomerization of the corresponding FCCs in the vacuole. Alternatively, as shown in this work, FCCs are converted by CYP89A9 to FDCCs, and the latter isomerize into corresponding NDCCs. As an example conversion of *p*FCC to *p*FDCC and further to *p*NDCC is depicted.

In agreement with this idea is the finding that wild-type plants, in which MES16 was targeted to the chloroplast and consequently FCCs demethylated before export from the organelle and exposure to ER-localized CYP89A9, exhibited a *cyp89a9*-mutant like phenotype, i.e. abundance of NCCs was increased largely (Fig. 2.4). There is increasing evidence in the literature that chloroplasts and the ER are associated through defined membrane contact sites (Andersson et al., 2007; Tan et al., 2011). Such contact sites have been shown to have an important function for lipid transfer between chloroplast and the ER and might involve protein-protein interaction between the partaking membranes. It is likely to assume that in regard to Chl breakdown, *p*FCC released from senescing chloroplasts might directly be transferred to ER-localized CYP89A9. Thus, NCCs found in wild-type might be the products of FCCs that 'escaped' CYP89A9 and were demethylated first.

Cytochrome P450 monooxygenases are among the largest gene families in plants with 245 members in Arabidopsis (Schuler et al., 2006). Based on phylogenetic relationships, CYP clans have been defined. CYP89A9 belongs to the highly divergent CYP71 clan, representing almost 50% of all known plant CYPs (Nelson and Werck-Reichhart, 2011). CYP71 clan members possess a great diversity of functions, including metabolism of amino acid derivatives, isoprenoids, alkaloids, fatty acids and hormones (Nelson and Werck-Reichhart, 2011). Our work extends the substrate spectrum of CYPs to linear tetrapyrroles, which to the best of our knowledge have not yet been considered CYP substrates. It remains unclear, however, whether CYP89-orthologs are involved in DCC-formation also in other plant species, which have been shown to produce them (Djapic and Pavlovic, 2008; Losey and Engel, 2001; Müller et al., 2011). Furthermore, functions for the six CYP89A9 paralogs of the CYP89 family present in Arabidopsis (Schuler et al., 2006) remain unknown. Based on the fact that *cyp89a9* mutants are devoid of any DCCs (Fig. 2.2), we assume that none of these paralogs is involved in FCC deformylation.

Chemically the conversion of FCCs to FDCCs is an oxidative deformylation. Several P450 are known that deformylate their substrates, thereby forming alkenes as products (Guengerich, 2001; Roberts et al., 1991). However, to the best of our knowledge, the proposed reaction of CYP89A9, producing a *γ*-lactam upon deformylation of an α-formyl-pyrrole unit, is unprecedented. In contrast to heme degradation, the by-product of the CYP89A9 reaction most probably is formate, which in plants can be metabolized either by formate dehydrogenase to CO_2 and H_2O (Li et al., 2002), or enter C1-metabolic pathways *via* conjugation to tetrahydrofolate (Chen et al., 1997). A result of the observed deformylation process is the new formation of a stereo-center at C9 of DCCs. It is most likely generated in a multi-step mechanism, thus allowing for the formation of two stereo-isomers at C9 (Fig. 2.3B). This explains the occurrence in *in vitro* CYP89A9 assays of several isomeric FDCCs

(Fig. 2.3A). C9-epimeric NDCCs were identified in senescent barley leaves (Losey and Engel, 2001). By contrast, Norway maple accumulates a single, stereochemically uniform NDCC (Müller et al., 2011), indicating that depending on the plant species and/or conditions, DCC formation might or might not be stereo-selective.

More than 20 years ago, the first NCC was identified in senescent barley leaves and characterized as a formyloxobilane-type tetrapyrrole (Kräutler et al., 1991). Since then an increasing number of NCCs was isolated from many different plant species (Hörtensteiner and Kräutler, 2011; Kräutler, 2008). By contrast, Norway maple was observed to accumulate one NDCC exclusively, but NCCs were absent (Müller et al., 2011), while in Arabidopsis, as shown here, both forms of catabolites occur simultaneously. Considering that P450-dependent reactions consume energy and absence of CYP89A9 activity in respective mutants does not cause an obvious phenotype that may indicate an important function for the plant, one may ask the question, why (for example) Arabidopsis specifically recruited CYP89A9 for (ultimately) NDCC formation, while other species can degrade Chl without such activity? Modifications of *p*FCC that occur at different peripheral positions increase its polarity. This is seen in reversed-phase HPLC, where all catabolites downstream of *p*FCC elute before *p*FCC. *At*-NDCC-1 is the most polar of all NDCCs and NCCs in Arabidopsis (Fig. 2.1B). Thus, it could be argued that CYP89A9, like other *p*FCC-modifying activities (Pružinská et al., 2005), helps to increase the polarity of catabolites, required for storage inside the vacuolar sap (Matile et al., 1988). In addition, it has been shown that Chl is broken down in order to detoxify this potentially phototoxic pigment when the photosynthetic machinery is dismantled during senescence (Hörtensteiner, 2004). Thus, a key feature of Chl breakdown is to abolish light absorption. In this respect, CYP89A9 activity is responsible for the loss of absorption around 320 nm, characteristic for the NCCs, and leaves behind colorless pigments that also display low light-absorption in the UV-A and UV-B ranges.

In summary, we have identified NDCCs as the major Chl catabolites in wild-type Arabidopsis, while NCCs, represent only a minor fraction. NDCCs are the products of acid-catalyzed isomerization from FDCCs. FDCCs are biosynthesized from FCCs by CYP89A9, a P450 enzyme of Arabidopsis, in an unprecedented oxidative deformylation reaction. Catabolite deformylation does not seem to occur in all plant species, but it remains to be shown how widely distributed NDCCs are as novel 'final' degradation products of Chl.

MATERIALS AND METHODS

Plant material and senescence induction

Arabidopsis thaliana ecotype Columbia-0 (Col-0) was used as the wild-type. Ecotype Landsberg erecta (Ler) was also analyzed in experiments including *cyp89a9-2* (Ler background). Ler is a natural mutant in the MES16 gene (Christ et al., 2012). T-DNA insertion lines were from the following collections: SALK lines (Alonso et al., 2003): *AT3G26170-2* (*cyp71b19-2*), SALK_149952; SAIL lines (Sessions et al., 2002): *AT3G26170-1* (*cyp71b19-1*), SAIL_1165_B02; JIC SM lines (Tissier et al., 1999): *AT3G03470-1* (*cyp89a9-1*), SM_3_39636; JIC GT lines (Sundaresan et al., 1995): *AT3G03470-2* (*cyp89a9-2*), GT_5_22744. SALK, SAIL, SM and GT lines were obtained from the European Arabidopsis Center, Nottingham, UK. Homozygous plants were identified by PCR using T-DNA-, transposon-, and gene-specific primers as listed in Supplemental Table II. Likewise, a homozygous *mes16-1cyp89a9-1* double mutant was identified by PCR.

Plants were grown on soil either in 8 h light:16 h dark (short-day) or 12 h light:12 h dark (12:12) photoperiods under fluorescent light of 60 to 120 µmol photons m^{-2} s^{-1} at 22°C or 16 h light:8 h dark (long-day) in a greenhouse with fluence rates of 100 to 200 µmol photons m^{-2} s^{-1} at 22°C. For senescence induction, leaves from eight-week-old (short-day) or five-week-old (12:12 and long-day) plants were excised and incubated in permanent darkness on wet filter paper for up to 8 d at ambient temperature. For dark incubation in CO atmosphere, leaves from short-day-grown Col-0 plants were excised and incubated for 5 d in glass containers containing 0, 50% and 100% (v/v) CO mixed with ambient air.

Biocomputational methods

Search for co-expressed genes in senescent rosette leaves, cauline leaves, petals and sepals was performed with the Gene Search Tool "Anatomy" of the Genevestigator platform (Zimmermann et al., 2004) using a limit of 100 genes.

GFP fusion protein production and confocal microscopy

CYP89A9 was amplified by PCR with the Expand High Fidelity PCR system (Roche Applied Science) from clone U67778 (Arabidopsis Biological Resource Center) using the primers listed in Supplemental Table II, introducing *Xma*I/*Nhe*I restriction sites at the ends. The PCR fragment was then cloned into the pGEM-T-easy vector (Promega) and after *Xma*I/*Nhe*I digest subcloned into pUC18-spGFP6 (Meyer et al., 2006), thereby producing a fusion of CYP89A9 with the N-terminus of GFP. Arabidopsis mesophyll protoplasts were isolated from six-week-old short-day-grown Col-0 plants according to published procedures (Endler et al., 2006; Schelbert et al., 2009). Cell numbers were quantified with a Neubauer chamber and adjusted to a density of 2-3 x 10^6 protoplasts mL^{-1}. CYP89A9-GFP was co-transformed with the ER marker BiP–RFP (Min et al., 2007) in protoplasts isolated from green or dark-induced senescent leaves (4-5 d) by 20% polyethylene glycol transformation (Meyer et al., 2006). Free GFP expressed from empty pUC18-spGFP6 was used as a control for cytosolic localization. Transformed cells were incubated for 24 h in the dark at room temperature before laser scanning confocal microscopic analysis (Leica TCS SP5, Leica Microsystems). GFP and RFP fluorescence were imaged at an excitation wavelength of 488 nm and 561 nm, respectively. The detection channel windows were set as follow: 495-530 nm (GFP), 593-619 nm (RFP) and 643-730 nm (Chl autofluorescence).

RNA isolation and RT-PCR

RNA was isolated using the RNeasy Plant kit (Qiagen) from green and dark-incubated leaves of plants grown in short-day photoperiod. After DNA digestion with RQ1 DNase (Promega), first strand cDNA was synthesized using the M-MLV Reverse Transcriptase (Promega). PCR was performed with a nonsaturating number of amplification cycles as shown in the Figures using gene-specific primers as listed in Supplemental Table II.

***epi-p*FCC, O13[4]-desmethyl *epi-p*FCC, *mes16*-FCC-2 and NCC preparation**

The preparation of *epi-p*FCC (from *Capsicum annuum* fruit extracts) is described elsewhere (Christ et al., 2012). O13[4]-desmethyl *epi-p*FCC was produced from *epi-p*FCC with MES16 (Christ et al., 2012). *mes16*-FCC-2 and *mes16*-NCC-2 were extracted from dark-incubated leaves (5 d) of *mes16-1cyp89a9-1* grown in 12:12 photoperiod in 50 mM phosphate buffer, pH 7/ methanol (1:3, v/v), concentrated using C18-SepPak cartridges (Waters) and purified by HPLC.

Heterologous expression of CYP89A9 and ATR-1, and activity determination

ATR1 and *CYP89A9* were amplified by PCR (Expand High Fidelity PCR system; Roche Applied Science) from clone pda02355 obtained from the RIKEN resource (Seki et al., 2002) and clone U67778 (Arabidopsis Biological Resource Center), respectively, using the primers listed in the Supplemental Table II and then cloned into pFastbac1 (Invitrogen) via *Eco*RI. *CYP89A9* and *ATR-1* were also cloned in pFastbac DUAL (Invitrogen) using *Kpn*I and *Eco*RI restriction sites, respectively, allowing simultaneous expression of the two genes with one bacmid. After sequencing, the constructs were used for the preparation of recombinant bacmid DNAs by transformation of *E. coli* strain DH10Bac (Invitrogen). Insect cell transfection and recombinant protein expression were conducted as outlined in the bac-to-bac manual (Invitrogen), using Sf9 cells grown in monolayer cultures. For expression of the recombinant proteins, Sf9 cells were maintained in BD BaculoGold™ TNM-FH Insect medium (BD Biosciences) supplemented with 200 mM 5-aminolevulinic acid and 200 mM ferrous sulfate to increase the low heme synthetic capacity of the insect cells (Saito et al., 2004). For preparation of microsomal fractions, infected cells were concentrated by centrifugation and re-suspended in lysis buffer consisting of 20 mM potassium phosphate, pH 7.3, 20% (v/v) glycerol, 1

mM EDTA, and 1 mM DTT complemented with a protease inhibitor cocktail (Complete; Roche Applied Science). The cells were homogenized on ice with a glass-Teflon homogenizer and cell debris were removed by centrifugation at 1'000*g* for 10 min. The supernatant was further centrifuged at 100,000*g* for 1 h. The pellet (microsomal fraction) was homogenized in lysis buffer with a syringe through a 0.5-mm-wide needle, frozen in liquid nitrogen and stored at -80°C until use.

Standard assays with CYP89A9 and ATR1 microsomes (total volume 100 µl) consisted of 40 µg of microsome proteins and 10 µM of substrate. After incubation at 28°C in darkness for different periods of time as indicated in Fig. 2.3, the reactions were stopped by the addition of methanol to a final concentration of 50%. After centrifugation (2 min at 16,000*g*), samples were analyzed by HPLC as described below. Microsomes produced with bacmids generated from pFastbac1 constructs were used for standard assays. None-infected cells or cells infected only with ATR1 bacmid were used as controls. For scaling up the standard assay to produce higher amounts of products obtained when using *epi-p*FCC as substrate, microsomes generated with the pFastbac DUAL construct were used. *epi-p*FDCCs were purified by HPLC prior to mass spectrometry analysis (see below).

Analysis of Chl and Chl catabolites

Quantification of Chl

Pigments were extracted from liquid nitrogen-homogenized tissue during 2 h at -20°C in 10% (v/v) 0.2 M Tris-HCl, pH 8 in acetone, pre-cooled to –20°C (5 mL g^{-1} fresh weight). After twice centrifugation (4 min, 16,000*g*, 4°C), supernatants were analyzed by spectrophotometry (Strain et al., 1971).

Colorless Chl catabolites

Plant material was ground in liquid nitrogen and colorless catabolites were extracted with 3 volumes (w/v) of 50 mM phosphate buffer (P-buffer), pH 7/methanol (1:3, v/v) and analyzed by HPLC as described (Christ et al., 2012).

Peak detection was performed with sequential monitoring using a PA-100 photodiode array detector (200–700 nm; Dionex Corporation) and a RF2000 fluorescence detector (excitation at 320 nm, emission at 450 nm; Dionex Corporation). Chl catabolites were identified by their absorption (FCCs, FDCCs, NCCs and NDCCs) and fluorescence (FDCCs and FCCs) properties. Relative amounts of FCCs, FDCCs, NCCs and NDCCs were determined by peak areas at 254 nm using the approximation that absorption at this wavelength is similar in the different types of catabolites. In addition, NCCs were quantified at 320 nm (Oberhuber et al., 2001).

***cyp89a9-1* and *mes16-1cyp89a-1* complementation**

CYP89A9 was amplified by PCR as described above and cloned via *Eco*RI/*Hin*dIII into pHannibal (Wesley et al., 2001). The pHannibal cassette containing CaMV 35S promoter, the CYP89A9 open reading frame and an OCS terminator was excised with *Not*I and introduced into *Not*I-restricted pGreen0179 (Hellens et al., 2000). Arabidopsis *cyp89a9-1* and *mes16-1cyp89a9-1* plants were transformed by the floral-dip method (Clough and Bent, 1998). Transformants were selected on hygromycin, and resistant T2 plants were used for further analysis.

***in vitro* FDCC-to-NDCC isomerization**

The isomerization assays consisted of 11.2 µM of purified *epi-p*FDCCs produced with recombinant CYP89A9 (see above) and 80 mM phosphate buffer, pH 5. Aliquots were taken after incubation times as indicated in Fig. 2.3E and isomerization was stopped by adding Tris-HCl, pH 8 to a concentration of 350 mM. Methanol was added to a final concentration of 35% (v/v) prior to analysis by HPLC as described above.

Mass spectrometry and NMR

Spectroscopy

UV/VIS Spectra: Hitachi U-3000 spectrophotometer; λ_{max} [nm] (ε_{rel}). CD Spectra: JASCO J715; $\lambda_{min/max}$ [nm] ($\Delta\varepsilon$). ^{1}H- and ^{13}C-NMR: Bruker UltraShield 600 MHz Avance II+ (δ ($C^{1}HD_2COD$) = 3.31 ppm, $\delta(^{13}CD_3OD)$ = 49.0 ppm]) (Gottlieb et al., 1997). Mass spectrometry: Finnigan MAT 95, electrospray ionzation (ESI) source, positive ion mode, 1.4 kV

spray voltage(*At*-DNCC-1); Finnigan LCQ classic, ESI source, positive ion mode, spray voltage 4.25 kV, solvent MeOH/H_2O (10 mM NH_4OAc) 1:1 (*v/v*); m/z (% intensity, type of ion).

HPLC

Hewlett Packard series 1100 HPLC-system, online degasser, Agilent quaternary pump, diode array detector (DAD) and fluorescent detector (FLD). *Analytical HPLC:* Injection loop 200 µL (Rheodyne valve); Phenomenex hyperclone ODS 5 µm 250 x 4.6 mm i.d. column (at room temperature) connected to Phenomenex ODS 4 x 3 mm i.d. pre-column was used with a flow rate 0.5 ml min^{-1}. Solvent A: MeOH, solvent B: P-buffer, pH 7; solvent composition (A/B, v/v) as a function of time: 0 – 5 min, 20/80; 5 – 55 min, 20/80 to 70/30; 55 – 60 min, 70/30 to 100/0; 60 – 70 min, 100/0; 70 – 75 min, 100/0 to 80/20; Separation of the four products of CYP89A9/ATR1 assay: Solvent A: MeOH, solvent B: 10 mM ammonium acetate buffer; solvent composition (A/B, v/v): 0 – 5 min, 30/70; 5 – 55 min, 30/70 to 65/35; 55 – 70 min, 65/35 to 75/25; 70 – 80 min, 75/25 to 100/0; 80 – 90 min,100/0; 90 – 95 min, 100/0 to 30/70. *Preparative HPLC:* Phenomenex HyperClone ODS 5 µm 250 x 21.2 mm i.d. column at room temperature protected with a Phenomenex ODS 10 mm x 5 mm i.d. pre-column was used with a flow rate of 5 ml min^{-1}. Solvent A: MeOH, solvent B: P-buffer, pH 7; solvent composition (A/B, v/v): 0 – 5 min, 25/75; 5 – 123 min, 25/75 to 38/62; 123 – 200 min, 38/62 to 64/36; 200 – 210 min, 64/36 to 100/0; 210 – 230 min, 100/0.

Spectroscopic characterization of At-NDCC-1

Senescent leaves (16.5 g) of Arabidopsis were ground in a mortar under liquid nitrogen, mixed with sea sand and extracted with 16 ml MeOH. The obtained slurry was filtrated through a Buchner funnel and the extraction with MeOH was repeated 7 times. The collected green extract (160 ml) was diluted with 30 ml P-buffer (pH 7) and washed twice with 160 ml n-hexane. The solution was reduced under vacuum to 70 ml, diluted with 600 ml P-buffer (pH 7) and filtrated. The mixture was loaded on a Sep-Pak Vac 20cc (5 g) C18 cartridge (Waters), washed with water (50 ml) and eluted with MeOH (15 ml). The solvent was removed under reduced pressure on a rotary evaporator. The crude product was dissolved in 800 µl methanol/P-buffer (50:50 v/v), diluted with 500 µL P-buffer and centrifuged for 5 min at 13 000 rpm. The clear brown solution was injected into the preparative HPLC. The *At*-NDCC-1-containing fraction was collected, diluted with 4 volumes of H_2O and applied to a Sep-Pak classic C18 cartridge. The *At*-NDCC-1 was obtained salt-free by washing with 20 ml H_2O and eluting with 5 ml MeOH. The solvents were removed in vacuum to give 0.770 mg of *At*-NDCC-1.

UV/Vis (MeOH, $6.9*10^{-4}$ M) λ_{max} (ε_{rel}): 288 sh (0.29), 239 sh (1.00), 221 (1.29); CD (MeOH, $6.9*10^{-4}$ M) $\lambda_{min/max}$ ($\Delta\varepsilon$): 311 (5.3), 284 (-26.4), 250 (7.1), 231 (17.1). ^{1}H-NMR (600 MHz CD_3OD, 283 K): δ [ppm] = 1.78 (s, CH_3 (7^1)), 1.95 (s, CH_3 (18^1)), 1.99 (s, CH_3 (2^1)), 2.11 (s, CH_3 (12^1)), 2.38 (m, CH_2 (17^2)), 2.45 (dd, J= 14.4/5.1 Hz, CH_A (20)), 2.50 (m, CH_A (8^1)), 2.54 (m, CH_A (10)), 2.69 (m, CH_A (17^1)), 2.75 (m, CH_B (17^1)), 2.78 (m, CH_B (8^1)), 2,89 (dd, J= 14.4/9.4 Hz, CH_B (20)), 3.05 (dd, J= 14.6/4.9 Hz, CH_B (10)), 3.66 (m, CH_A (8^2)), 3.70 (m, CH_B (8^2)), 4.11 (dd, J= 9.3/5.1 Hz, CH (1)), 4.34 (m, CH (9)), 4.84 (s, CH (15)), 5.33 (dd, J= 11.7/1.94 Hz, CH_A (3^2)), 6.09 (dd, J= 17.7/1.91 Hz, CH_B (3^2)), 6.46 (dd, J= 17.6/11.7 Hz, CH (3^1)); ^{13}C-NMR (150 MHz, CD_3OD, 283 K, ^{13}C-signal assignments from HSQC- & HMBC-experiments): δ [ppm] = 8.2 (7^1), 9.1 (18^1), 9.3 (12^1), 12.2 (2^1), 21.6 (17^1), 30.0 (10), 30.6 (20), 30.7 (8^1), 38.1 (15), 39.1 (17^2), 60.3 (9), 60.9 (8^2), 61.5 (1), 71.8 (13^2), 112.4 (12), 115.5 (18), 118.6 (3^2), 119.9 (17), 123.4 (19), 125.7 (16), 126.7 (3^1), 128.5 (3), 130.6 (7), 133.6 (11), 156.0 (8), 162.0 (14), 174.9 (4), 176.6 (6), 176.7 (13^3), 181.0 (17^3). ESI-MS: m/z (%) = 657.3 (33, $[M+K]^+$); 633.3 (10); 621.71 (6), 620.3 (35), 619.3 (100, $C_{33}H_{39}N_4O_8$, $[M+H]^+$); 613.3 (53, $[M-CO_2+K]^+$); 601.3 (31, $[M-H_2O+H]^+$); 575.3 (15, $[M-CO_2+H]^+$); 496.2 (26, $[M-C_7H_9NO$ (ring A)$+H]^+$; 478.2 (6, [M-ring A-$H_2O+H]^+$); 452.2 (32, $[M-CO_2$-ring A$+H]^+$).

Mass-spectrometric data of NCCs from cyp89a9-1

For MS analysis, five fractions containing NCCs from senescent leaf extracts of *cyp89a9-1* were isolated by HPLC, analyzed by ESI ionisation and tentatively identified with the known five *At*-NCCs (Müller et al., 2006; Pružinská et al., 2005).

ESI-MS: *At*-NCC-1: m/z (%) = 831.0 (39, $[M+K]^+$); 815.1 (52, $[M+Na]^+$); 795.1 (15), 794.1 (49), 793.2 (100, $C_{40}H_{49}N_4O_{13}$, $[M+H]^+$); 787.3 (4, $[M-CO_2+K]^+$); 779.1 (6, $[M-2H_2O+Na]^+$); 775.2 (14, $[M-H_2O+H]^+$); 771.3 (17, $[M-CO_2+Na]^+$); 749.1 (17, $[M-CO_2+H]^+$); 670.1 (5, $[M-C_7H_9NO$ (ring A)$+H]^+$); 631.2 (8, $[M-C_6H_{10}O_5$ (Gluc)$+H]^+$); 626.2 (6, $[M-CO_2$-ring A$+H]^+$); 613.2 (4, $[M-H_2O$-Gluc$+H]^+$); 587.1 (4, $[M-CO_2$-Gluc$+H]^+$); 479.2 (8). *At*-NCC-2: m/z (%) = 669.0 (17, $[M+K]^+$); 653.0 (15, $[M+Na]^+$); 633.1 (10), 632.2 (39), 631.1 (100, $C_{34}H_{39}N_4O_8$, $[M+H]^+$); 613.1 (29, $[M-H_2O+H]^+$); 609.2 (6, $[M-CO_2+Na]^+$); 587.1 (14, $[M-CO_2+H]^+$); 508.0 (4, [M-ring A$+H]^+$); 490.0 (4, $[M-H_2O$-ring A$+H]^+$); 464.1 (8, $[M-CO_2$-ring A$+H]^+$). *At*-NCC-3: m/z (%) = 669.0 (61, $[M+K]^+$); 653.1 (58, $[M+Na]^+$); 633.1 (15), 632.0 (36), 631.0 (100, $C_{34}H_{39}N_4O_8$, $[M+H]^+$); 613.1 (94, $[M-H_2O+H]^+$); 609.2 (26, $[M-CO_2+Na]^+$); 595.2 (45, $[M-2H_2O+H]^+$); 585.1 (13); 569.2 (54, $[M-H_2O-CO_2+H]^+$); 508.0 (7, [M-ring A$+H]^+$); 490.1 (9, $[M-H_2O$-ring A$+H]^+$); 472.0 (10, $[M-2H_2O$-ring A$+H]^+$); 464.1 (11, $[M-CO_2$-ring A$+H]^+$); 446.1 (11, $[M-H_2O-CO_2$-ring A$+H]^+$). *At*-NCC-4: m/z (%) = 845.1 (30, $[M+K]^+$); 829.2 (55, $[M+Na]^+$); 809.2 (24), 808.1 (44), 807.1 (100, $C_{41}H_{51}N_4O_{13}$, $[M+H]^+$); 793.3 (20); 775.2 (28, $[M-MeOH+H]^+$); 684.1 (12, [M-ring A$+H]^+$); 652.1 (4, [M-MeOH-ring A$+H]^+$); 645.1 (11, [M-Gluc$+H]^+$); 613.1 (7, [M-MeOH-Gluc$+H]^+$). *At*-NCC-5: m/z (%) = 653.0 (49, $[M+K]^+$); 637.1 (46, $[M+Na]^+$); 617.0 (12), 616.1 (36), 615.0 (100, $C_{34}H_{39}N_4O_7$, $[M+H]^+$); 597.2 (39, $[M-H_2O+H]^+$); 593.3 (54, $[M-CO_2+Na]^+$); 585.1 (13); 571.0 (20, $[M-CO_2+H]^+$); 492.00 (6, [M-ring A$+H]^+$); 474.1 (9, $[M-H_2O$-ring A$+H]^+$); 448.0 (15, $[M-CO_2$-ring A$+H]^+$).

Mass spectrometric data of epi-pFDCCs from CYP89A9/ATR1 assays with epi-pFCC as substrate

For MS analysis, the four products of the CYP89A9/ATR1 assay with *epi-p*FCC as substrate were isolated by HPLC and analyzed by ESI ionisation.

ESI MS: *epi-p*FDCC-1: m/z (%) = 677.1 (13, $[M+K+Na-H]^+$); 655.2 (19, $[M+K]^+$); 639.3 (24, $[M+Na]^+$); 619.2 (9), 618.1 (33), 617.1 (100, $C_{34}H_{41}N_4O_7$ $[M+H]^+$); 607.2 (6, $[M-MeOH+Na]^+$); 585.1 (19, $[M-MeOH+H]^+$; 559.2 (11); 519.2 (13); 492.1 (31, [M- $C_7H_{11}NO$ (ring B)$+H]^+$); 460.0 (5, [M-ring B-MeOH$+H]^+$); *epi-p*FDCC-2: m/z (%) = 677.1 (9, $[M+K+Na-H]^+$); 655.1 (16, $[M+K]^+$); 639.1 (24, $[M+Na]^+$); 619.1 (8), 618.1 (39), 617.1 (100, $[M+H]^+$); 585.1 (14, $[M-MeOH+H]^+$); 519.2 (4); 492.1 (13, [M-ring B$+H]^+$); 460.0 (4, [M-ring B-MeOH$+H]^+$); *epi-p*FDCC-3: m/z (%) = 677.1 (4, $[M+K+Na-H]^+$); 655.1 (14, $[M+K]^+$); 639.2 (16, $[M+Na]^+$); 619.1 (9), 618.1 (39), 617.1 (100, $[M+H]^+$); 585.1 (8, $[M-MeOH+H]^+$); 492.1 (9, [M-ring B$+H]^+$); *epi-p*FDCC-4: m/z (%) = 677.1 (4, $[M+K+Na-H]^+$); 655.1 (10, $[M+K]^+$); 639.1 (15, $[M+Na]^+$); 618.1 (9), 618.1 (39), 617.1 (100, $[M+H]^+$); 585.1 (8, $[M-MeOH+H]^+$); 492.1 (9, [M-ring B$+H]^+$).

SUPPLEMENTAL INFORMATIONS

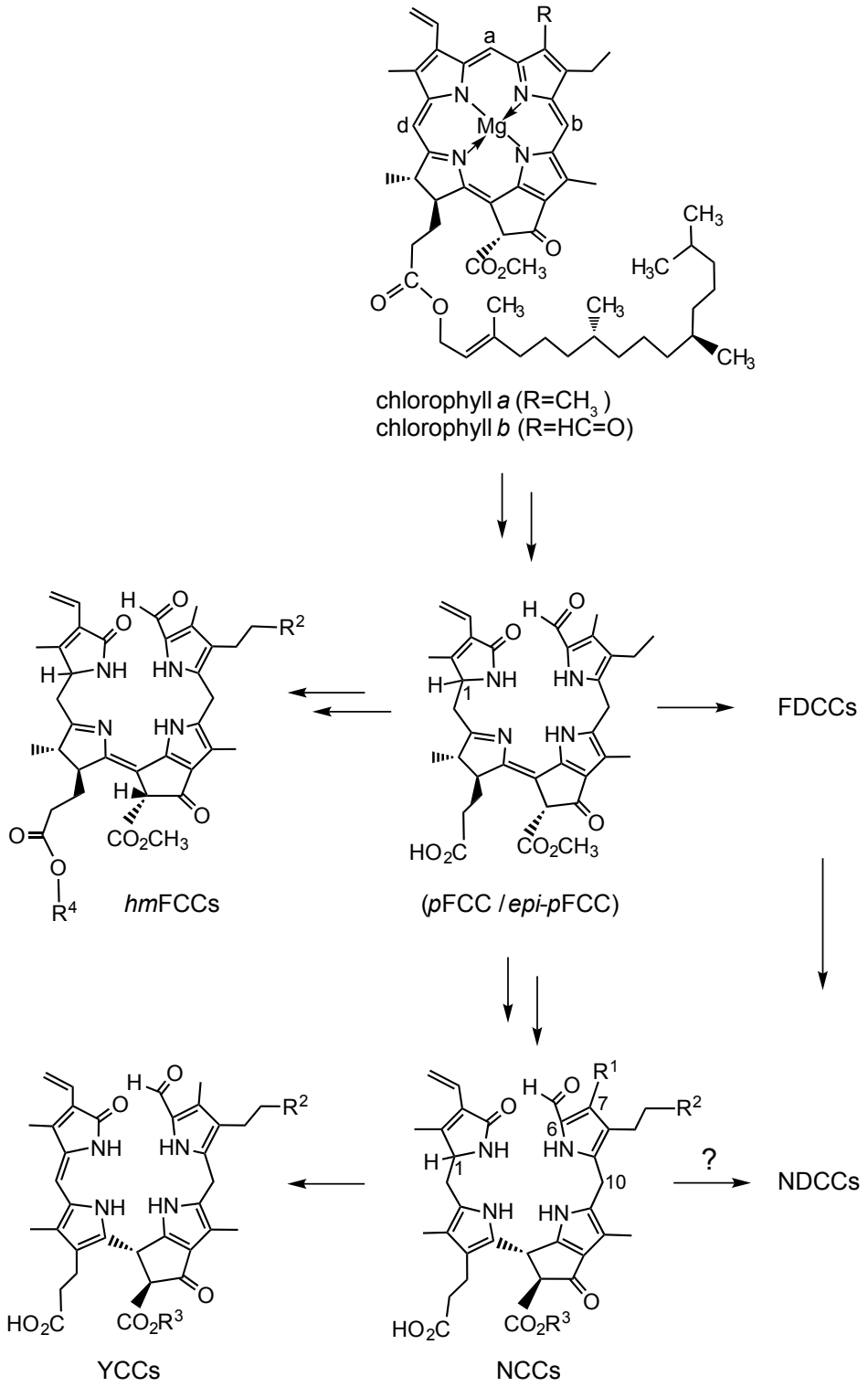

Fig. 2.S1. Overview on Chl degradation. Chls are degraded by a 'common pathway' inside the chloroplast to colorless and blue fluorescent '*primary*' FCCs (*p*FCC / *epi*-pFCC), which are processed further in a 'species-dependent pathway': basic transformations are the esterification at the propionate group to give persistent 'hypermodified' FCCs (*hm*FCCs, e.g. with R^2 = OH, R^4 = daucic acid, accumulating in peels of bananas; Moser et al., 2008a) or the modification at other side chains to give modified FCCs (in the cytosol), which isomerize in the vacuole to colorless, nonfluorescent catabolites (NCCs, e.g. with R^1 = CH_3, R^2 = OH, R^3 = H, as found in Arabidopsis; Ulrich et al., 2011). NCCs may be oxidized in senescent leaves to yellow Chl-catabolites (YCCs, e.g. R^2 = OH, R^3 = CH_3; Moser et al., 2008b). Alternatively, as shown here, deformylation of FCCs gives rise to FDCCs, dioxobilin-type catabolites, which isomerize to NDCCs in weakly acidic medium, as found in vacuoles (see Fig. 2.5).

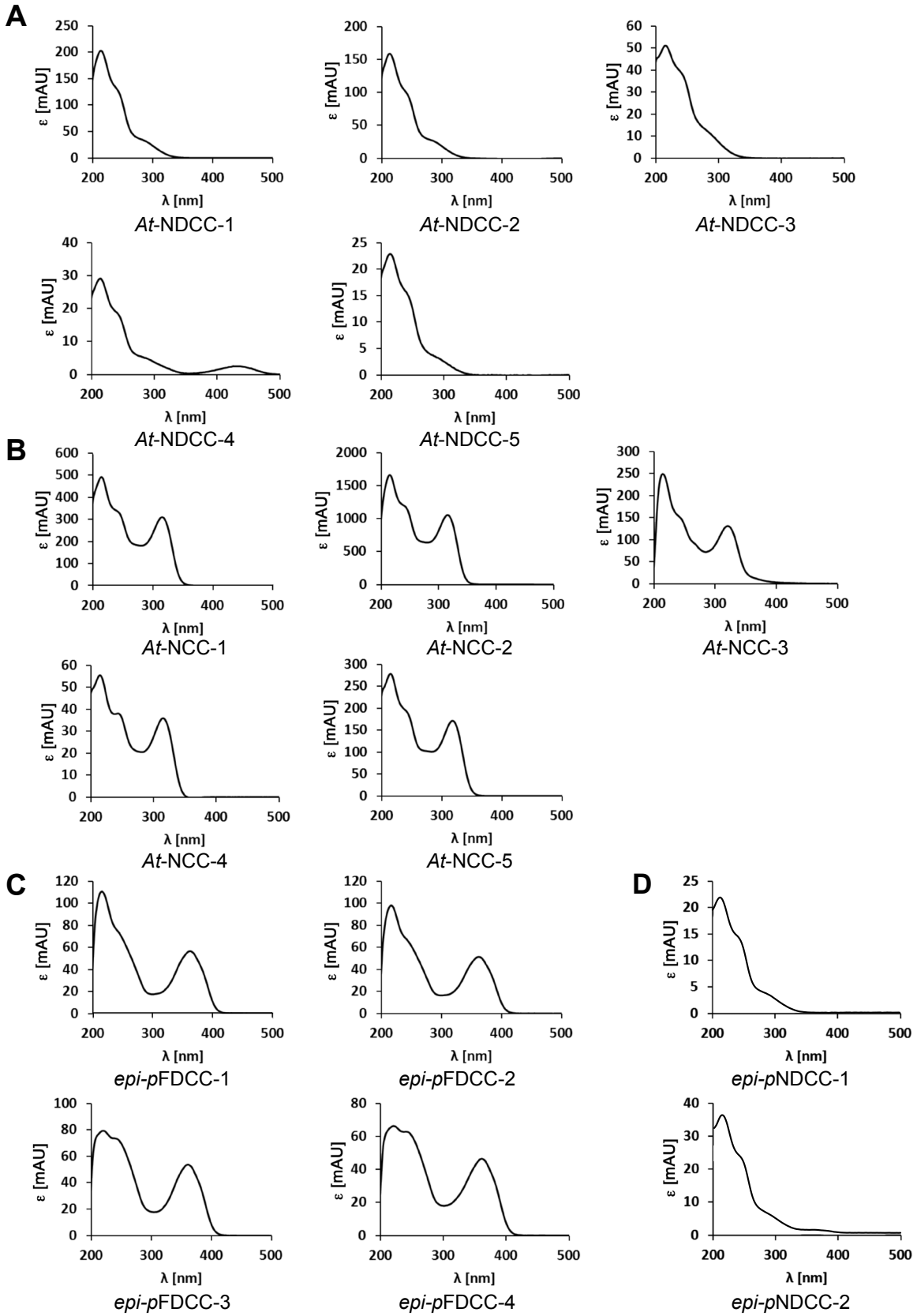

Fig. 2.S2. (*A*) On-line UV/Vis spectra of five *At*-NDCCs observed in senescent leaves of Arabidopsis. (*B*) On-line UV/Vis spectra of the five *At*-NCCs observed in senescent leaves of the Arabidopsis *cyp89a9-1* mutant. (*C*) On-line UV/Vis spectra of FDCCs observed as products of the assay with recombinant CYP89A9/ATR1 and using *epi-p*FCC as substrate. (*D*) On-line UV/Vis spectra of the epi-*p*NDCCs produced in vitro by isomerization of *epi-p*FDCCs at pH 5 (see text for further details).

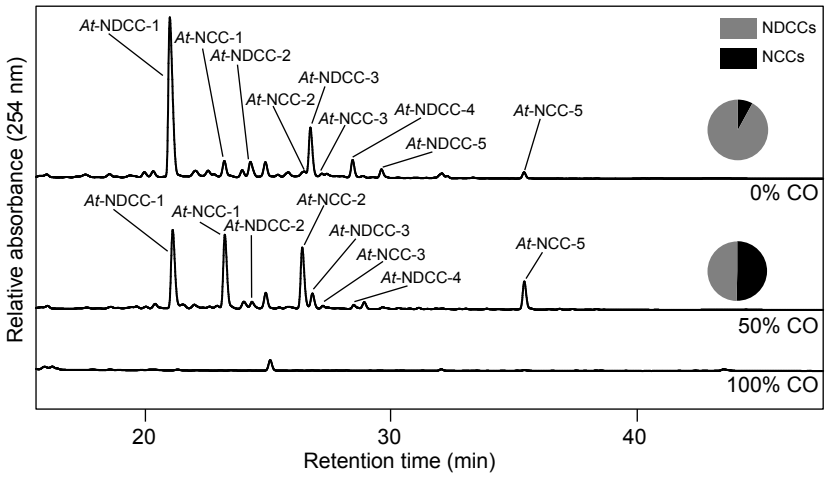

Fig. 2.S3. NDCC formation is inhibited by CO. Detached wild-type leaves were dark-incubated for 5 d in glass containers containing 0, 50% and 100% (v/v) CO mixed with ambient air. Colorless catabolites were analyzed by HPLC. HPLC traces at A_{254} are shown. Pie graphs depict the relative amounts of NDCCs and NCCs. In 100% CO atmosphere, Chl degradation was inhibited and no colorless catabolites were detected. For more details, see "Materials and Methods."

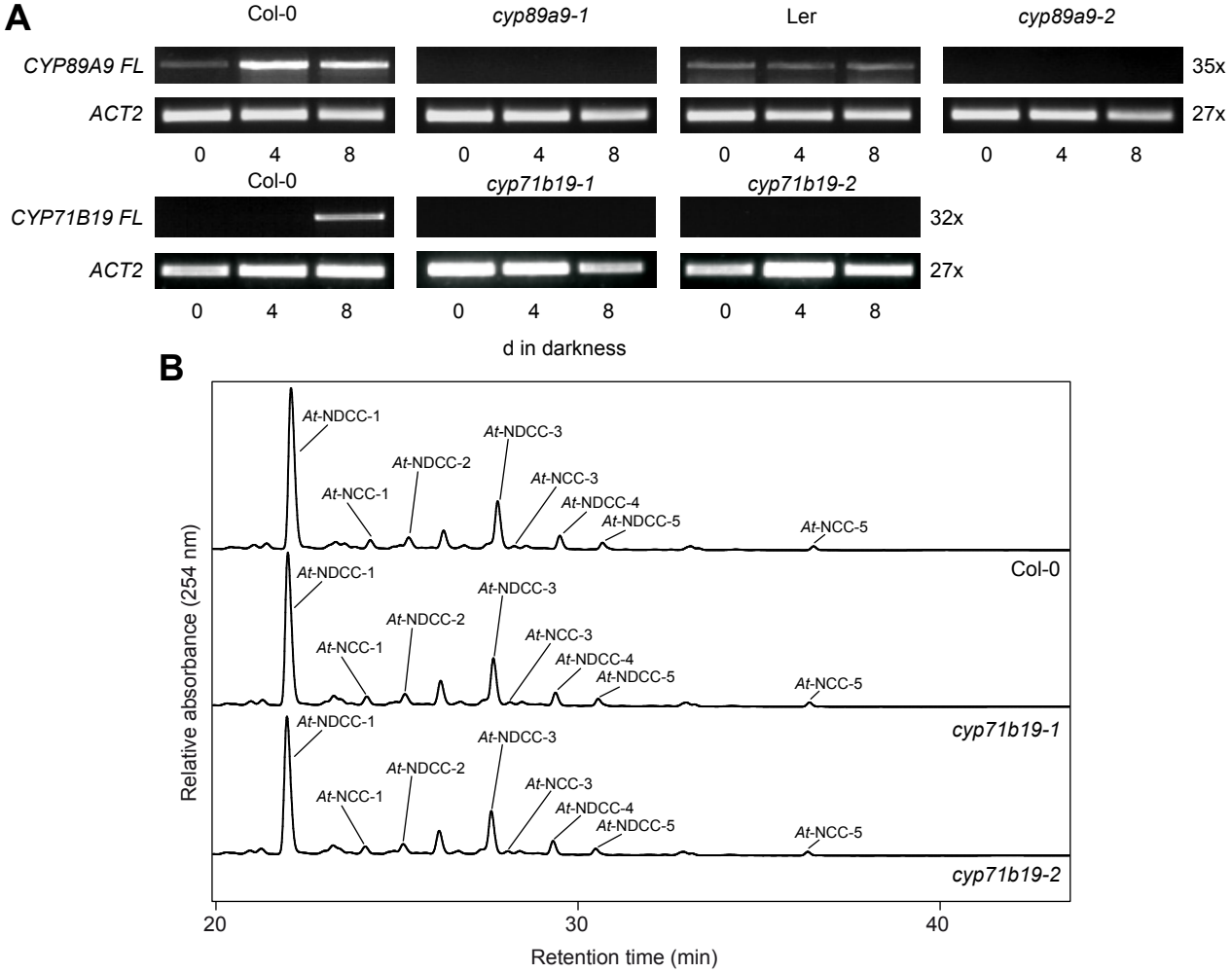

Fig. 2.S4. Analysis of gene expression in *cyp89a9* and *cyp71b19* mutants and colorless catabolites of *cyp71b19* mutants. (*A*) Analysis of gene expression during dark-induced senescence in *cyp89a9-1*, *cyp89a9-2*, *cyp71b19-1* and *cyp71b19-2*. Levels of *actin2* (*ACT2*) gene expression were used as control. Expression was analyzed with nonsaturating numbers of PCR cycles as shown at the right. PCR products were separated on agarose gels and visualized with ethidium bromide. (*B*) Colorless catabolites of dark-incubated (8 d) leaves of Col-0 and *cyp71b19* mutants were separated by HPLC. A_{254} is shown. For clarity, only the relevant part of the HPLC traces is shown.

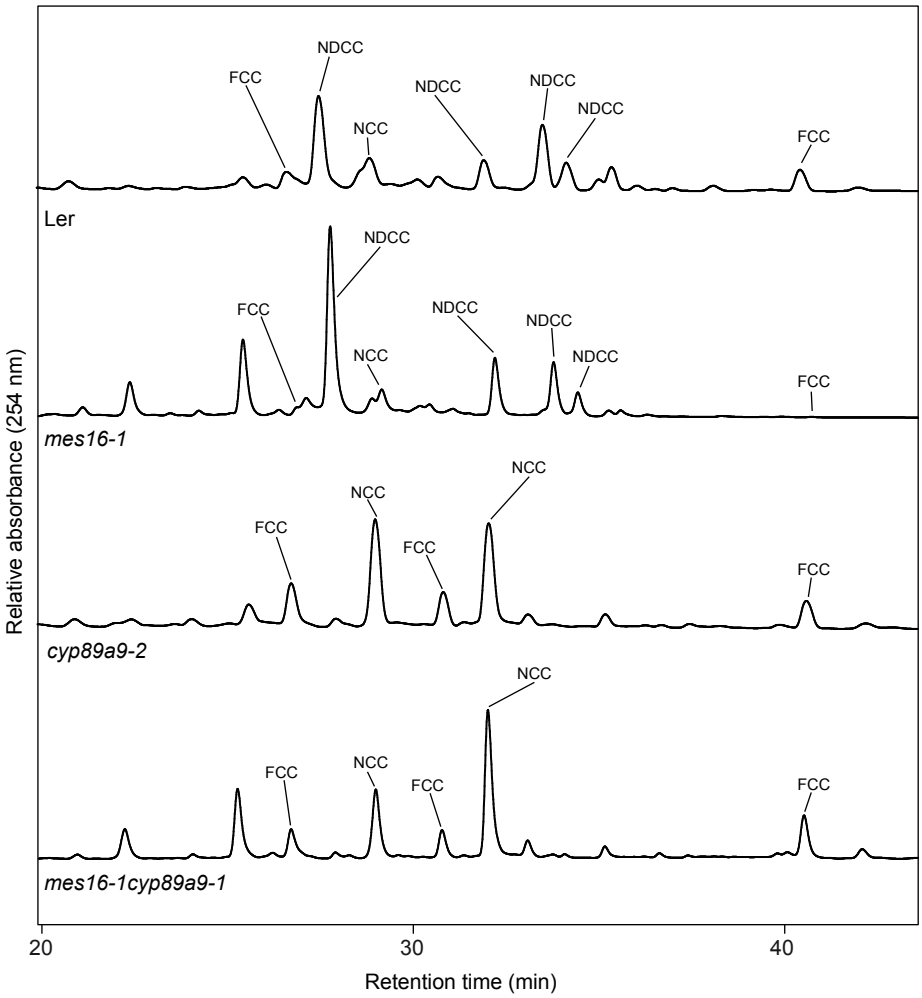

Fig. 2.S5. Analysis of the *cyp89a9-2* mutant in the Ler background, a natural *mes16* mutant. Colorless catabolites accumulating in dark-incubated (8 d) leaves of Ler, *mes16-1*, *cyp89a9-2* and *mes16-1cyp89a9-1* were separated by HPLC. A_{254} is shown. For clarity, only the relevant part of the HPLC traces is shown. Note that because of the absence of MES16, catabolite patterns are different from patterns in Col-0 (Christ et al., 2012). The catabolites in this figure were solely identified by their respective spectra.

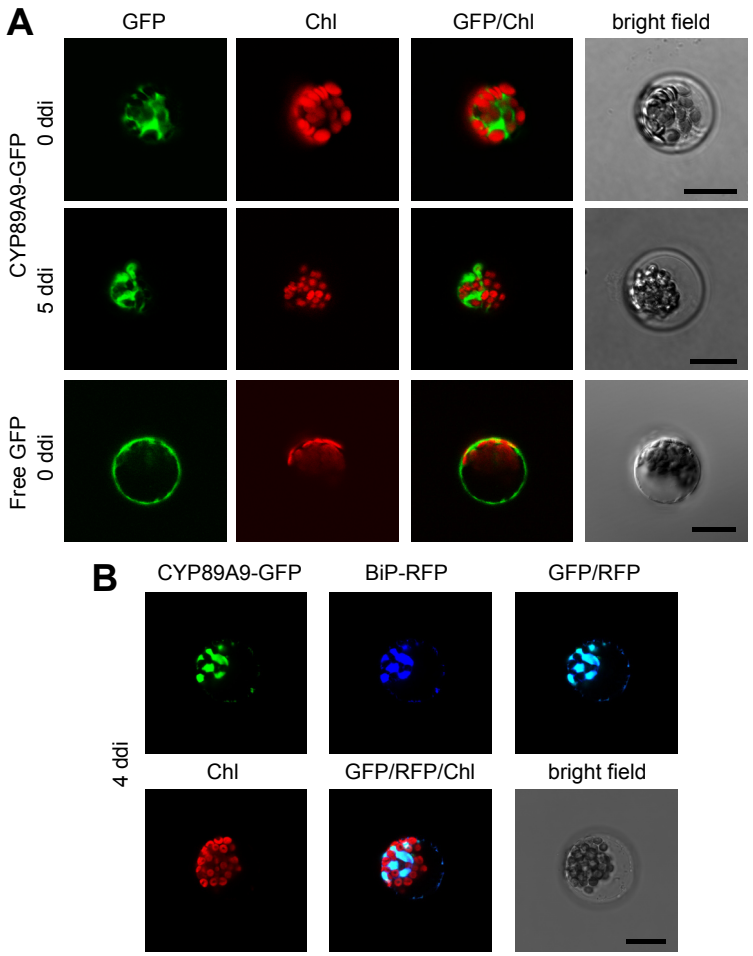

Fig. 2.S6. CYP89A9-GFP localizes to the ER in Arabidopsis mesophyll protoplasts. (*A*) Transient expression of CYP89A9-GFP and free GFP in protoplasts isolated from green (0 ddi) or senescent (5 ddi) leaves. (*B*) Colocalization of CYP89A9-GFP with BiP-RFP in protoplasts isolated from senescent (4 ddi) leaves. GFP, RFP and Chl autofluorescence (GFP, RFP and Chl) were examined by confocal laser scanning microscopy as described in "Materials and Methods". Different overlays of GFP, RFP and Chl autofluorescence signals are shown. Bars = 20 µm.

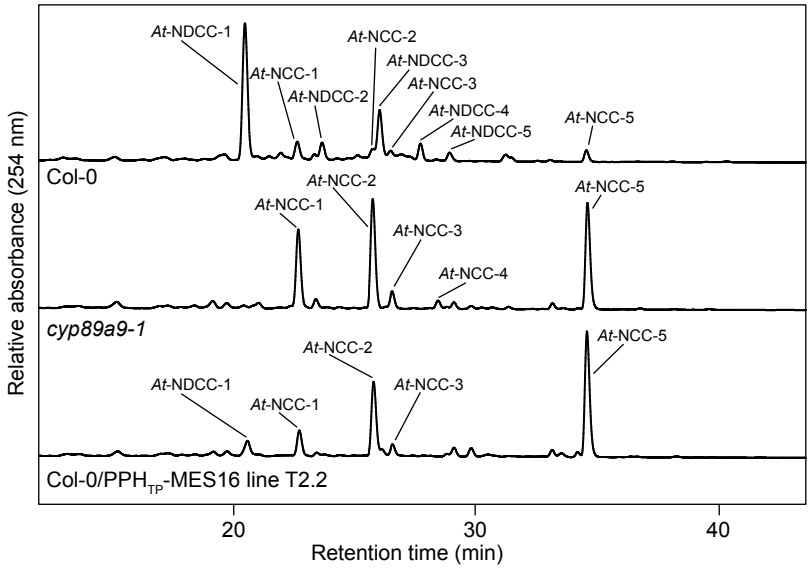

Fig. 2.S7. Colorless catabolites accumulating in dark-incubated (8 d) leaves of Col-0, *cyp89a9-1* and Col-0/PPHTP-MES16. Colorless catabolites were separated by HPLC. A_{254} is shown. For clarity, only the relevant part of the traces is shown.

Table 2.S1. Search for co-expressed genes in senescent leaves, cauline leaves, petals and sepals using the Genes Search Tool "Anatomy" of Genevestigator (Zimmermann et al. 2004).

ARRAY ELEMENT	LOCUS IDENTIFIER	ANNOTATION
267423_at	AT2G35060	KUP11 (K+ uptake permease 11); potassium ion transmembrane transporter
267076_at	AT2G41090	calmodulin-like calcium-binding protein, 22 kDa (CaBP-22)
266572_at	AT2G23840	HNH endonuclease domain-containing protein
266292_at	AT2G29350	SAG13 (Senescence-associated gene 13); oxidoreductase
266291_at	AT2G29320	tropinone reductase, putative / tropine dehydrogenase, putative
266078_at	AT2G40670	ARR16 (response regulator 16); transcription regulator/ two-component response regulator
265913_at	AT2G25625	similar to unnamed protein product [Vitis vinifera] (GB:CAO44157.1)
265698_at	AT2G32160	similar to unknown protein [Arabidopsis thaliana] (TAIR:AT2G32170.1); similar to unnamed protein product [Vitis vinifera] (GB:CAO64660.1); contains InterPro domain N2227-like (InterPro:IPR012901)
265151_at	AT1G51340	MATE efflux family protein
264901_at	AT1G23090	AST91 (SULFATE TRANSPORTER 91); sulfate transmembrane transporter
264899_at	AT1G23130	Bet v I allergen family protein
264636_at	AT1G65490	similar to unknown protein [Arabidopsis thaliana] (TAIR:AT1G65486.1)
264261_at	AT1G09240	nicotianamine synthase, putative
263478_at	AT2G31880	leucine-rich repeat transmembrane protein kinase, putative
262803_at	AT1G21000	zinc-binding family protein
262626_at	AT1G06430	FTSH8 (FtsH protease 8); ATP-dependent peptidase/ ATPase/ metallopeptidase/ zinc ion binding
262598_at	AT1G15260	similar to unknown protein [Arabidopsis thaliana] (TAIR:AT3G16070.1)
262281_at	AT1G68570	proton-dependent oligopeptide transport (POT) family protein
262232_at	AT1G68600	similar to unknown protein [Arabidopsis thaliana] (TAIR:AT1G25480.1); similar to unknown protein [Arabidopsis thaliana] (TAIR:AT2G17470.1); similar to unnamed protein product [Vitis vinifera] (GB:CAO42118.1); contains InterPro domain Protein of unknown function UPF0005 (InterPro:IPR006214)
261754_at	AT1G76130	AMY2/ATAMY2 (ALPHA-AMYLASE-LIKE 2); alpha-amylase
260933_at	AT1G02470	similar to unknown protein [Arabidopsis thaliana] (TAIR:AT1G02475.1); similar to unnamed protein product [Vitis vinifera] (GB:CAO40177.1); contains InterPro domain Streptomyces cyclase/dehydrase (InterPro:IPR005031)
260774_at	AT1G78290	serine/threonine protein kinase, putative

260419_at	AT1G69730	protein kinase family protein
260410_at	AT1G69870	proton-dependent oligopeptide transport (POT) family protein
260312_at	AT1G63880	disease resistance protein (TIR-NBS-LRR class), putative
260155_at	AT1G52870	peroxisomal membrane protein-related
260012_at	AT1G67865	unknown protein
260007_at	AT1G67870	glycine-rich protein
260004_at	AT1G67860	similar to unknown protein [Arabidopsis thaliana] (TAIR:AT1G67865.1)
259766_at	AT1G64360	unknown protein
259765_at	AT1G64370	unknown protein
259561_at	AT1G21250	WAK1 (CELL WALL-ASSOCIATED KINASE); kinase
259340_at	AT3G03870	similar to unknown protein [Arabidopsis thaliana] (TAIR:AT5G18130.2)
259129_at	AT3G02150	PTF1 (PLASTID TRANSCRIPTION FACTOR 1); transcription factor
259058_at	AT3G03470	CYP89A9 (cytochrome P450, family 87, subfamily A, polypeptide 9); oxygen binding
258925_at	AT3G10420	sporulation protein-related
258259_s_at	AT3G26820;AT3G26840	[AT3G26820, esterase/lipase/thioesterase family protein];[AT3G26840, esterase/lipase/thioesterase family protein]
257791_at	AT3G27110	peptidase M48 family protein
257634_s_at	AT3G26170;AT3G26180	[AT3G26170, CYP71B19 (cytochrome P450, family 71, subfamily B, polypeptide 19); oxygen binding];[AT3G26180, CYP71B20 (cytochrome P450, family 71, subfamily B, polypeptide 20); oxygen binding]
257611_at	AT3G26580	binding
257196_at	AT3G23790	AMP-binding protein, putative
256789_at	AT3G13672	seven in absentia (SINA) family protein
256497_at	AT1G31580	ECS1
256300_at	AT1G69490	NAP (NAC-LIKE, ACTIVATED BY AP3/PI); transcription factor
256168_at	AT1G51805	leucine-rich repeat protein kinase, putative
256008_s_at	AT1G34040;AT1G34060	[AT1G34040, alliinase family protein];[AT1G34060, alliinase family protein]
255795_at	AT2G33380	RD20 (RESPONSIVE TO DESSICATION 20); calcium ion binding
255630_at	AT4G00700	C2 domain-containing protein
255626_at	AT4G00780	meprin and TRAF homology domain-containing protein / MATH domain-containing protein
254833_s_at	AT4G12290;AT4G12280	[AT4G12290, copper amine oxidase, putative];[AT4G12280, copper amine oxidase family protein]
254764_at	AT4G13250	short-chain dehydrogenase/reductase (SDR) family protein

254691_at	AT4G17840	similar to unknown protein [Arabidopsis thaliana] (TAIR:AT2G35260.1); similar to hypothetical protein 40.t00061 [Brassica oleracea] (GB:ABD65174.1)
254574_at	AT4G19430	unknown protein
254564_at	AT4G19170	NCED4 (NINE-CIS-EPOXYCAROTENOID DIOXYGENASE 4)
254551_at	AT4G19840	ATPP2-A1 (Arabidopsis thaliana phloem protein 2-A1)
254305_at	AT4G22200	AKT2 (Arabidopsis K+ transporter 2); cyclic nucleotide binding / inward rectifier potassium channel
254299_at	AT4G22920	ATNYE1/NYE1 (NON-YELLOWING 1)
254189_at	AT4G24000	ATCSLG2 (Cellulose synthase-like G2); transferase/ transferase, transferring glycosyl groups
254178_at	AT4G23880	unknown protein
254174_at	AT4G24120	YSL1 (YELLOW STRIPE LIKE 1); oligopeptide transporter
254153_at	AT4G24450	ATGWD2/GWD3/PWD (PHOSPHOGLUCAN, WATER DIKINASE); ATP binding / kinase
254101_at	AT4G25000	AMY1/ATAMY1 (ALPHA-AMYLASE-LIKE); alpha-amylase
253911_at	AT4G27300	S-locus protein kinase, putative
253779_at	AT4G28490	HAESA (RECEPTOR-LIKE PROTEIN KINASE 5); ATP binding / kinase/ protein serine/threonine kinase
253382_at	AT4G33040	glutaredoxin family protein
253358_at	AT4G32940	GAMMA-VPE (Vacuolar processing enzyme gamma); cysteine-type endopeptidase
252648_at	AT3G44630	disease resistance protein RPP1-WsB-like (TIR-NBS-LRR class), putative
252485_at	AT3G46530	RPP13 (RECOGNITION OF PERONOSPORA PARASITICA 13); ATP binding
252462_at	AT3G47250	similar to unknown protein [Arabidopsis thaliana] (TAIR:AT3G47200.1); similar to unknown protein [Arabidopsis thaliana] (TAIR:AT3G47200.2); similar to unnamed protein product [Vitis vinifera] (GB:CAO15956.1); contains InterPro domain Protein of unknown function DUF247, plant (InterPro:IPR004158)
251591_at	AT3G57680	peptidase S41 family protein
251457_s_at	AT3G60970;AT3G60160	[AT3G60970, ATMRP15 (Arabidopsis thaliana multidrug resistance-associated protein 15)];[AT3G60160, ATMRP9 (Arabidopsis thaliana multidrug resistance-associated protein 9)]
251360_at	AT3G61210	embryo-abundant protein-related
251221_at	AT3G62550	universal stress protein (USP) family protein
251054_at	AT5G01540	lectin protein kinase, putative
250690_at	AT5G06530	ABC transporter family protein
250435_at	AT5G10380	zinc finger (C3HC4-type RING finger) family protein
250286_at	AT5G13320	PBS3 (AVRPPHB SUSCEPTIBLE 3)
250259_at	AT5G13800	hydrolase, alpha/beta fold family protein

250054_at	AT5G17860	CAX7 (CALCIUM EXCHANGER 7); calcium:sodium antiporter/ cation:cation antiporter
250028_at	AT5G18130	similar to unknown protein [Arabidopsis thaliana] (TAIR:AT3G03870.2); similar to unknown [Medicago truncatula] (GB:ABK28852.1)
249996_at	AT5G18600	glutaredoxin family protein
249860_at	AT5G22860	serine carboxypeptidase S28 family protein
249850_at	AT5G23240	DNAJ heat shock N-terminal domain-containing protein
249774_at	AT5G24150	SQP1 (Squalene monooxygenase 1)
249754_at	AT5G24530	oxidoreductase, 2OG-Fe(II) oxygenase family protein
249454_at	AT5G39520	similar to unknown protein [Arabidopsis thaliana] (TAIR:AT5G39530.1); similar to unnamed protein product [Vitis vinifera] (GB:CAO15021.1)
249377_at	AT5G40690	similar to unknown protein [Arabidopsis thaliana] (TAIR:AT2G41730.1); similar to unnamed protein product [Vitis vinifera] (GB:CAO14635.1)
249125_at	AT5G43450	2-oxoglutarate-dependent dioxygenase, putative
248566_s_at	AT5G49740;AT5G49730	[AT5G49740, ATFRO7/FRO7 (FERRIC REDUCTION OXIDASE 7); ferric-chelate reductase/ oxidoreductase];[AT5G49730, ATFRO6/FRO6 (FERRIC REDUCTION OXIDASE 6); ferric-chelate reductase/ oxidoreductase]
248153_at	AT5G54250	ATCNGC4 (DEFENSE, NO DEATH 2); calmodulin binding / cation channel/ cyclic nucleotide binding
247800_at	AT5G58570	unknown protein
247304_at	AT5G63850	AAP4 (amino acid permease 4); amino acid transmembrane transporter
246429_at	AT5G17450	heavy-metal-associated domain-containing protein / copper chaperone (CCH)-related
246335_at	AT3G44880	ACD1 (ACCELERATED CELL DEATH 1)
246302_at	AT3G51860	CAX3 (cation exchanger 3); cation:cation antiporter
245901_at	AT5G11060	KNAT4 (KNOTTED1-LIKE HOMEOBOX GENE 4); transcription factor
245501_at	AT4G15620	integral membrane family protein
245385_at	AT4G14020	rapid alkalinization factor (RALF) family protein
245353_at	AT4G16000	similar to unknown protein [Arabidopsis thaliana] (TAIR:AT4G15990.1)
245346_at	AT4G17090	CT-BMY (BETA-AMYLASE 3, BETA-AMYLASE 8); beta-amylase

Targets: senescent leaves, cauline leaves, petals and sepals. Limit: 100 genes. Rows with genes of interest are shaded in grey.

Table 2.S2. List of primers used in this study

GENE / MUTANT	PRIMER NAME	SEQUENCE (5'->3')
	T-DNA confirmation	
mes16-1	MES16-1-RP	GTTGAAGAAAAGAAACCGCAC
	MES16-1-LP	CTGAGCCCGTAATTCACTTTG
cyp89a9-1	CYP89A9-1-RP	TACGACAAATAAGCCCAATGG
	CYP89A9-1-LP	GCTCTGATGTGTTTCGGAGAG
cyp89a9-2	CYP89A9-2-RP	CTCACGATCTCCGAGTCACTC
	CYP89A9-2-LP	GCGTGGACCAAAATAAACAAG
cyp71b19-1	CYP71B19-1-RP	ATCGATGATGTCTTCGTGCTC
	CYP71B19-1-LP	CCACTAGACCATTGGCTTTTTC
cyp71b19-2	CYP71B19-2-RP	CCTCTCGGATATGCCTAAAGG
	CYP71B19-2-LP	CCAACTTTCTCTTCCCGAATC
SALK T-DNA	LBb1.3	ATTTTGCCGATTTCGGAAC
SAIL T-DNA	LB2	GCTTCCTATTATATCTTCCCAAATTACCAATACA
JIC SM T-DNA	Spm32	TACGAATAAGAGCG CCATTTTAGAGTGA
JIC GT T-DNA	Ds3-1	ACCCGACCGGATCGTATCGGT
	RT-PCR	
CYP89A9	CYP89A9_FL_S	TCGGAAACATCATCTGGCTTAA
	CYP89A9_FL_AS	GCTTTGAAAGGGTTTTTCATGACC
CYP71B19	CYP71B19_FL_S	TCTCATCACCTTCGTTTCGT
	CYP71B19_FL_AS	TCTTTATGTGTCATCCCATCAG
ACT2	ACT2-S	TGGAATCCACGAGACAACCTA
	ACT2-AS	TTCTGTGAACGATTCCTGGAC
	Cloning CYP89A9-GFP	
CYP89A9	CYP89A9-*Xma*I-S	TCCCCCCGGGATGGAGATCACCACTATC
	CYP89A9-*Nhe*I -AS	CTAGCTAGCCTTTCTCCTTGGATAAATATTTGC
	Cloning CYP89A9 and ATR-1 in pFastbac1 and pFastbac DUAL	
CYP89A9	*CYP89A9-Eco*RI-S	CCGGAATTCATGGAGATCACCACTATCAT
	*CYP89A9-Eco*RI-AS	CCGGAATTCTCACTTTCTCCTTGGATAAA
CYP89A9	*CYP89A9-Kpn*I-S	CGGGGTACCATGGAGATCACCACTATCATATTCC
	*CYP89A9- Kpn*I -AS	GCAAATATTTATCCAAGGAGAAAGTGAGGTACCCCG
ATR-1	*ATR-1 -Eco*RI-S	CCGGAATTCATGACTTCTGCTTTGTATGC

3 - FCC HYDROXYLATION

FCC hydroxylation in the stroma and transport of colorless chlorophyll catabolites across the chloroplast envelope

The results presented in the first section of this chapter demonstrate that C8^2-hydroxylation of *p*FCC occurs in the chloroplast. Furthermore, preliminary biochemical characterization of a putative hydroxylating activity present in isolated red bell pepper (*Capsicum annuum*) chromoplasts suggests that the C8^2-hydroxylation activity is located in the stroma and is dependent on electrons derived from G6P and/or NADPH. In the second section of this chapter, we present a novel method that allows investigation of the mechanism(s) of FCC transport across the chloroplast envelope in Arabidopsis. To perform FCC export assays, chloroplasts are isolated from senescent leaves of Arabidopsis and incubated with recombinant MES16, the enzyme responsible for FCC demethylation.

Bastien Christ, Maja Schellenberg and Stefan Hörtensteiner

INTRODUCTION

C8^2-hydroxylation of colorless Chl catabolites is the only modification which seems to be common to all higher plants (see Table I.1; Hörtensteiner, 2012). Indeed, all other FCC modifications appear to be species-specific. The nature and subcellular localization of the enzyme(s) responsible for C8^2-hydroxylation activity are unknown. Matile et al. (1992) could show that an FCC, that is more polar FCC than *p*FCC is produced by isolated gerontoplasts in barley (Matile et al., 1992). This polar FCC was later suggested to be C8^2-OH-*p*FCC but the chemical constitution of this catabolite has not been elucidated. The results presented in the first section of this chapter demonstrate that C8^2-hydroxylation of *p*FCC occurs in the chloroplast. HPLC analysis of colorless chlorophyll catabolites present in isolated gerontoplasts from senescent leaves of Arabidopsis reveals the presence of two FCCs. Coinjection experiments with previously characterized FCCs confirmed that the most polar FCC produced is C8^2-OH-*p*FCC and, thus, that hydroxylation of *p*FCC occurs within the chloroplast. Furthermore, preliminary biochemical characterization of a putative hydroxylating activity present in isolated red bell pepper (*Capsicum annuum*) chromoplasts suggests that the C8^2-hydroxylation activity is located in the stroma and is dependent on electrons derived from G6P and/or NADPH.

The second section of this chapter focuses on FCC transport across the chloroplast envelope in Arabidopsis. The export mechanism of Chl catabolites seems to be specific for open tetrapyrroles. Indeed, characterization of MES16, the enzyme demethylating FCCs in the cytosol of Arabidopsis, revealed that an export of Pheide from the chloroplasts of *pao1* is unlikely (see Chapter "1"; Christ et al., 2012). *In vitro*, MES16 can demethylate Pheide and convert it to pyroPheide but pyroPheide was not detected in *pao1*. However, when MES16 was mistargeted to the chloroplast using the PPH transit peptide, 75% of the Pheide accumulating in *pao1* was converted to PyroPheide (Christ et al., 2012; Schelbert et al., 2009). Furthermore, study of the subcellular localization in *acd2* mutant of RCC and RCC-like pigments, which are also open tetrapyrroles, revealed that these catabolites are exported from the chloroplast and mostly accumulate in the vacuole (Pružinská et al., 2007). Production and release of FCCs from isolated chloroplasts have already been described in the 1990s (Matile et al., 1992). Matile et al. (1992) could demonstrate that not only one, but two FCCs are produced by isolated gerontoplasts from barley. Incubation of barley gerontoplasts with ATP and G6P was shown to increase formation and export of these two FCCs. Notably, addition of only G6P in the assay enhanced the formation of both FCCs but not their release, indicating that ATP is required for FCC translocation across the chloroplast envelope. Here, we present a novel method that allows investigation of the mechanism(s) of FCC transport across the chloroplast envelope in Arabidopsis. To perform FCC export assays, chloroplasts are isolated from senescent leaves of Arabidopsis and incubated with recombinant MES16, the enzyme responsible for FCC demethylation (see Chapter "1"; Christ et al., 2012). During the assay, MES16 demethylates FCCs that are exported from the chloroplast. Direct HPLC analysis allows to distinguish between FCCs that remain within the chloroplast (methylated) and exported FCCs (demethylated) without the requirement of repurification of the organelles after the assay. Preliminary experiments performed with this method indicate that conditions of the assays must be optimized. Indeed, a major fraction of the chloroplasts lost their intactness during the assay. Nevertheless, these preliminary experiments already indicate that addition of ATP to the assay increases FCCs transport across the chloroplast envelope, as described earlier in barley (Matile et al., 1992).

MATERIALS AND METHODS

Plant material and growth conditions

Arabidopsis thaliana ecotype Columbia-0 (Col-0) was grown on soil in 8 h light:16 h dark (short-day) photoperiod under fluorescent light of 100 µmol photons m^{-2} s^{-1} at 22°C. For senescence induction, leaves were excised and incubated in permanent darkness on wet filter paper for 4-6 d at ambient temperature.

Chloroplast isolation

Chloroplasts were isolated in a two-step purification

procedure as described (Chapter "1"; Christ et al., 2012). Briefly, mesophyll protoplasts were released from dark-incubated leaves by cell wall digestion and purified using a Percoll gradient (Meyer et al., 2006). Then, pure protoplasts were lysed and chloroplasts were purified in a second Percoll gradient as described (Agne et al., 2009). Finally, chloroplasts were washed twice in HEPES/sorbitol buffer (330 mM sorbitol, 50 mM HEPES-KOH, pH 8). Isolated chloroplasts were analyzed for colorless catabolites by HPLC as described (Christ et al., 2012) or were used for FCC export assays (see below).

FCC export assays

The assays were performed with isolated chloroplasts from dark-induced leaves as described (Matile et al., 1992) with the following modifications. The leaves of 50 plants were used for one experiment. The assays (final volume 60 µl) consisted of 50 µl of Arabidopsis chloroplast suspension (chloroplast concentration was not determined), 25 µg of crude *E. coli* extract expressing MES16 (Christ et al., 2012), 5 mM Mg-ATP and 5 mM G6P. Before adding ATP and/or G6P to the assay (time "0 min" in Fig. 3.3), chloroplasts were incubated with recombinant MES16 for 10 min in the dark to allow demethylation of FCCs released from broken chloroplasts. The assays were started by the addition of ATP and/or G6P, incubated 60 min at room temperature in darkness and terminated by the addition of 60 µl methanol. The assays were then sonicated for 1 min in a sonication bath, centrifuged for 1 min at 16'000g to precipitate thylakoid membranes and proteins, and finally analyzed by HPLC as described (Christ et al., 2012).

Characterization of hydroxylation activity isolated from red bell pepper

Total proteins of red bell pepper chromoplasts were isolated as described (Christ et al., 2012). Chromoplast membrane proteins were isolated using the same procedure with the following modifications: exocarp tissue was blended in a grinding buffer depleted of sucrose (50 mM Tris-MES, pH 8, 2 mM EDTA, 10 mM polyethylene glycol 4000, 5 mM dithiothreitol, and 5 mM L(+)-ascorbic acid). Chromoplast membranes were washed twice by centrifugation (10 min at 10'000*g*) before membrane proteins were solubilized with 1% (v/v) Triton X-100. As indicated in Fig. 3.2, different *epi-p*FCC hydroxylation assays were performed using different combinations of the following components: 80% (v/v) of chromoplast protein extract, 20 µM purified *epi-p*FCC (Christ et al., 2012), 0.1 mU μL^{-1} Fd-NADPH-oxidoreductase (FNR), 0.2 mg mL^{-1} of ferredoxin (Fd), 1 mM NADPH, 1 mU μL^{-1} G6P dehydrogenase (GDH) and 2 mM G6P. After 30 min of incubation at 25°C, the assays were terminated by the addition of methanol to a final concentration of 60% (v/v) and analyzed by HPLC as described (Christ et al., 2012).

RESULTS

Hydroxylation of *p*FCC at $C8^2$ occurs within the chloroplast

Chloroplasts were isolated from senescent leaves of Arabidopsis and analyzed by HPLC (Fig. 3.1A). Two major peaks harbouring a typical FCC spectrum were identified. Due to its typical retention time (41-42 min), the most apolar FCC was considered to be *p*FCC. The structure of the most polar FCC (labelled FCC* in Fig. 3.1A) was determined by coinjection of chloroplast catabolite extract and isolated *mes16*-FCC-2 (Christ et al., 2012). FCC* and *mes16*-FCC-2 co-eluted as a single fraction when injected as a 1:1 (w/w) mixture, indicating that these two FCCs have the same constitution (Fig. 3.1B). This finding demonstrates that $C8^2$ hydroxylation of *p*FCC occurs within the Arabidopsis gerontoplasts. One could argue that proteins from other cellular compartments (such as ER membranes) could be carried over during chloroplast isolation and could be responsible for *p*FCC hydroxylation. However, preliminary experiments of incubation of intact isolated chloroplasts with recombinant MES16 (Fig. 3.3C, "0 min", see Materials and Methods), did not result in demethylation of *p*FCC and $C8^2$-OH-*p*FCC. This observation strongly indicates that *p*FCC hydroxylation occured within intact chloroplasts and was not due to co-purified extraplastidial enzymes that could derive from other cellular compartments.

Preliminary characterization of *p*FCC hydroxylation activity

An activity being potentially responsible for $C8^2$

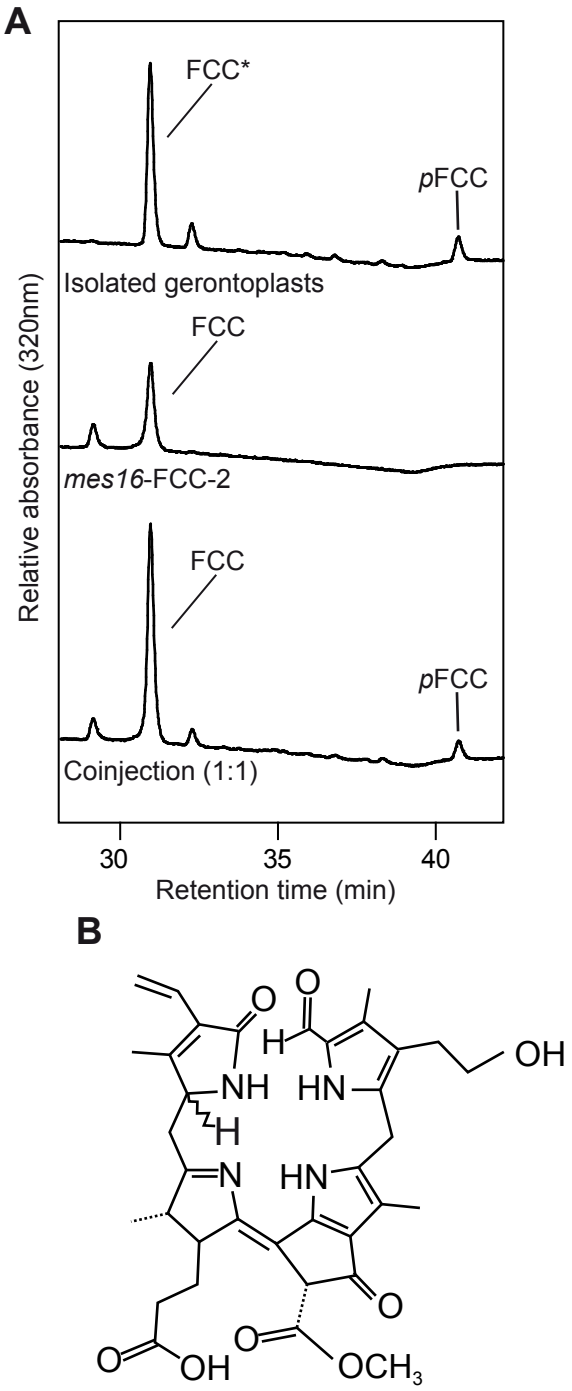

Fig. 3.1. C8[2] hydroxylation of Chl catabolites takes place within gerontoplasts. (*A*) Colorless Chl catabolite analysis of chloroplasts isolated from dark-induced leaves. To determine the identity of FCC* as C8[2]-OH-*p*FCC, coinjection was performed with *mes16*-FCC-2. For clarity, only a part of the HPLC traces at A_{320} is shown. (*B*) Chemical constitution of *mes16*-FCC-2 which is identical to C8[2]-OH-*p*FCC.

hydroxylation of *p*FCC was found to be present in red bell pepper chromoplasts (Fig. 3.2). Incubation of *epi-p*FCC with total chromoplast proteins led to the formation of a more polar FCC, labelled *epi-p*FCC* in Figure 2. The retention time of *epi-p*FCC* in our HPLC system strongly suggested it to be C8[2]-OH-*epi-p*FCC but this has not yet been confirmed. Preliminary experiments revealed that formation of epi-*p*FCC* was dependent on the presence of different cofactors (Fig. 3.2). Maximal activity was obtained with the addition of Fd, FNR, NADPH, GDH and G6P (Fig. 3.2, assay #1). Addition of only NADPH, GDH and G6P reduced the activity by 20% (assay #3) whereas addition of only Fd, alone or together with FNR, did not allow the formation of much *epi-p*FCC* (assay #2 and 4, respectively). Addition of NADPH or G6P alone led to around 20% of the activity obtained with all cofactors (assay #5 and 6, respectively). Finally, 40% of the maximal activity was reached by adding only GDH and G6P (assay #7). Interestingly, the activity responsible for *epi-p*FCC* formation seemed to be mostly lost when washed chromoplast membranes were used (assay #11). Collectively, these preliminary observations suggest that *epi-p*FCC*, which is most probably identical to C8[2]-OH-*epi-p*FCC, is formed by the activity of enzyme(s) present within the stroma of chromo- and chloroplasts or which is/are only weakly bound to plastid membranes. However, to confirm this hypothesis and exclude the involvement of chromoplast membrane protein(s) in the formation of *epi-p*FCC*, assays will have to be performed with stromal protein extract. Finally, even though not all cofactors combinations have been tested, the activity producing *epi-p*FCC* seems to require electrons derived from either NADPH or G6P.

A novel method to investigate FCC export from the chloroplast

Up to now, only one study has been published on Chl catabolite transport across the plastid envelope, which shows that the release of FCCs from isolated barley gerontoplasts is enhanced by external supply of ATP (Matile et al., 1992). Most chloroplast export assays, like other transport assays, require repurifying the organelles after incubation, a step which is critical due to the fragility of the chloroplast envelope. Attempts to repeat the FCC export assays described for Barley with Arabidopsis chloroplasts failed, most likely because of a loss of chloroplast intactness during the assay and/or the repurification step (data not shown). Instead, we tested a novel method for investigating

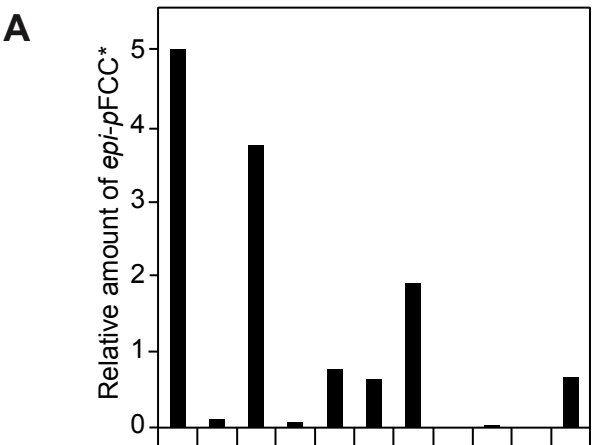

assay #	1	2	3	4	5	6	7	8	9	10	11
epi-*p*FCC	X	X	X	X	X	X	X	X			X
FNR	X	X							X		X
Fd	X	X		X					X		X
NADPH	X		X		X				X		X
GDH	X		X				X		X		X
G6P	X		X			X	X		X		X
Chro.	X	X	X	X	X	X	X	X	X	X	
Chro. mem.											X

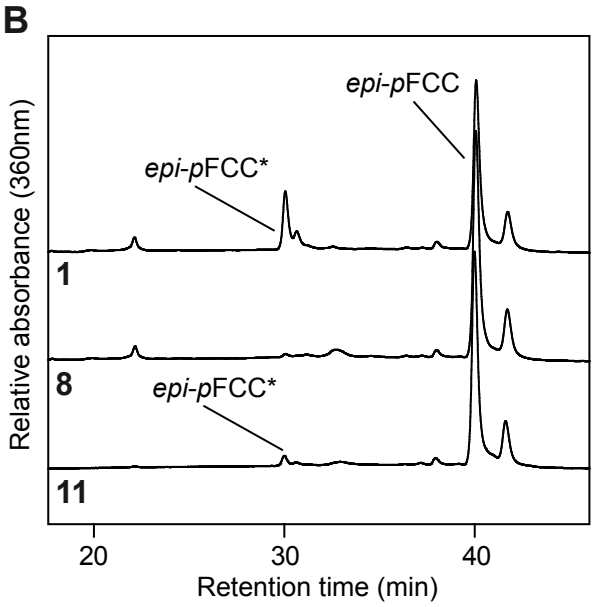

Fig. 3.2. Preliminary biochemical characterization of a putative C8² hydroxylation activity present in red bell pepper chromoplasts. (*A*) Assays employing total chromoplast proteins (#1-10) or chromoplast membrane proteins (#11) and different cofactors with *epi-p*FCC (i. e. the C1 epimer of pFCC) as substrate. Crosses (X) indicate the combination of cofactors used in the assays. (*B*) Selected HPLC analysis of assays from panel A (#1, 8 and 11). For clarity, only a part of the HPLC traces at A_{360} is shown.

FCC export from Arabidopsis chloroplast that makes use of recombinant MES16 (Christ et al., 2012). Isolated chloroplasts were incubated with MES16, ATP and/or G6P (Fig. 3.3A). During the incubation, MES16 demethylates FCCs that are exported from the chloroplast. We show that subsequent HPLC analysis allows, without any repurification step, to distinguish between FCCs that remained within the chloroplasts (methylated) and exported FCCs (demethylated) because of their different polarities (Fig. 3.3B). Analysis of in/out (methylated/demethylated) FCC ratios in our preliminary experiments revealed that Arabidopsis chloroplasts are rather instable during the assay (Fig. 3.3C). Indeed, the in/out FCC ratio decreased from about 22 at time "0 min" to 2 after 60 min of incubation without ATP or G6P. Even though more appropriate assay conditions have to be found to better maintain chloroplast intactness, these preliminary data already allowed to observe the effect of ATP on FCC export. Indeed, comparisons of in/out FCC ratios after incubation with only G6P (ratio = 1) or G6P and ATP (ratio = 0.5) suggest that ATP increases the release of FCCs from chloroplasts, as it was shown in barley (Matile et al., 1992).

DISCUSSION AND OUTLOOK

All higher plants seem to hydroxylate FCCs at C8² (Hörtensteiner, 2012). Up to now, the enzyme(s) responsible for C8² hydroxylation have not been identified. Moreover, apart from the observation that isolated gerontoplasts of barley produce a more polar FCC than *p*FCC, which was later speculated to be C8²-OH-*p*FCC, the subcellular localization of C8² hydroxylation remains unknown. Here, we characterized colorless Chl catabolites present in isolated chloroplasts of senescent leaves of Arabidopsis and could demonstrate that C8²-OH-*p*FCC is formed within the chloroplast (Fig. 3.1). From our experiments we can exclude the possibility that contaminations from other cellular compartments in the chloroplast preparation are responsible for *p*FCC C8² hydroxylation. Furthermore, our preliminary experiments indicate that this activity is present in the stroma of chromoplasts isolated from red bell pepper (Fig. 3.2). However, we cannot exclude the possibility that both soluble and membrane fractions are required simultaneously, like shown for the production of *p*FCC from Pheide *a* by PAO and RCCR

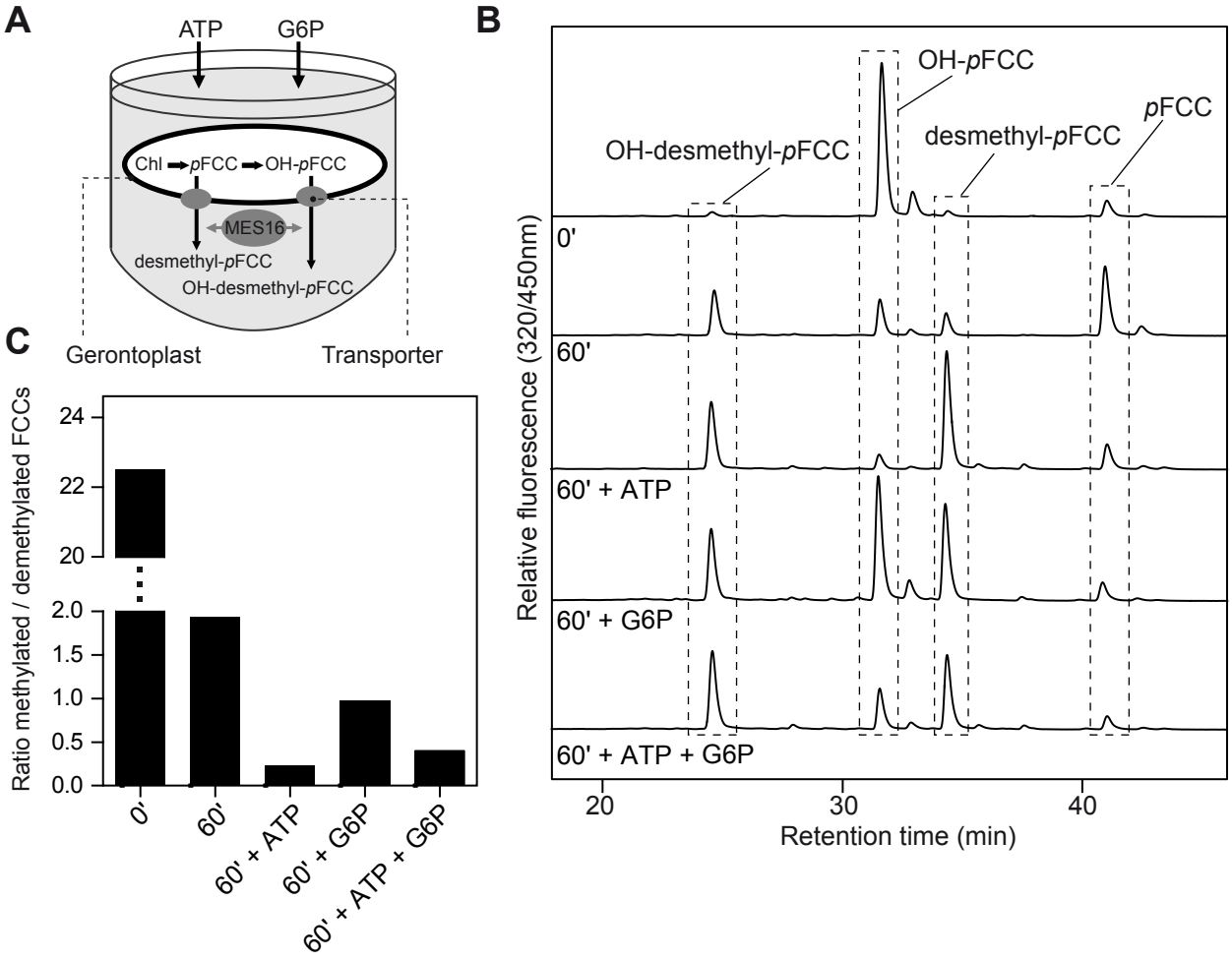

Fig. 3.3. Preliminary FCC export assays with isolated gerontoplasts and recombinant MES16. (*A*) Schematic description of the assay. (*B*) HPLC analysis of the assays after incubation. For clarity, only a part of the HPLC traces at F_{450} is shown. (*C*) Ratio between methylated (OH-*p*FCC and *p*FCC) and demethylated (OH-desmethyl-*p*FCC and desmethyl-*p*FCC) in the assays.

(Rodoni et al., 1997). In addition, our preliminary results indicate that the hydroxylation activity requires electrons derived from cofactors such as NADPH and G6P. Interestingly, Matile et al. (1992) described that incubation of isolated gerontoplasts from barley with G6P enhanced the formation of the most polar chloroplastic FCC, e. g. the putative $C8^2$-OH-*p*FCC. In Chapter "2", we found that progression of senescence in an atmosphere containing 50% CO inhibited CYP89A9, a cytochrome P450 responsible for NDCCs formation (Fig. 2.S3). However, other FCC modifications seemed not to be affect by CO, indicating that $C8^2$ hydroxylation of *p*FCC may not be due to the activity of cytochrome P450 enzyme, as suggested (Matile et al., 1999). However, cytochromes P450 belonging to the CYP74 family are known to display reduced affinity for carbon monoxide (Bak et al., 2011 and references therein). Furthermore, some of CYP74 family members, such as ALLENE OXIDE SYNTHASE (AOS), have been shown to be localized in the chloroplast (Vidi et al., 2006). This indicates that the involvement of cytochrome P450 enzyme(s) in $C8^2$ hydroxylation of *p*FCC cannot be completely excluded. Future experiments are demanded to obtain more information on the nature of *p*FCC $C8^2$ hydroxylation. The fact that the activity found in red bell pepper chromoplast is not lost by freezing (data not shown) will facilitate its (partial) purification and the subsequent identification of candidate proteins by mass spectrometry.

Apart from the production of two FCCs within isolated gerontoplasts of barley, Matile et al. (1992) could show that the release of these FCCs from the organelle was enhanced by the addition of ATP during the assay (Matile et al., 1992). FCC export

from the chloroplast seemed therefore to be an active mechanism. To the best of my knowledge, transporters for open tetrapyrroles at the chloroplast envelope have never been reported in the literature. Such transport mechanism is not only required during Chl breakdown for the export of *p*FCC and C8²-OH-*p*FCC. Indeed, the open tetrapyrrole phytochromobillin, the cofactor of phytochromes, is synthesized within the chloroplast and is exported to the cytosol by unknown mechanism(s) (Tanaka and Tanaka, 2007). Therefore, understanding FCC export from the chloroplast would probably also shed light on a crucial step of light sensing in higher plants. Here, we described a novel method that uses MES16 to characterize FCC export from isolated gerontoplasts (Fig. 3.3). Recombinant MES16 is incubated with isolated gerontoplasts of Arabidopsis and to demethylate released FCCs. Demethylation of FCCs induces a change in their polarity that can be monitored by direct HPLC analysis of crude export assay. This method avoids the repurification of chloroplasts after the export assay, which is critical due to the fragility of these organelles. Our preliminary experiments show that demethylated FCCs can be distinguished from methylated FCCs by HPLC. However, a major fraction of the chloroplasts loses its integrity during the export assay, indicating suboptimal assay conditions. Chloroplast intactness could be increased by modifying several factors such as decreasing temperature and time of incubation or adding sodium ascorbate and BSA as protectants to the HEPES/sorbitol buffer used during the assay. Furthermore, the osmolarity of the HEPES/sorbitol buffer, 330 mM, was optimized for chloroplasts isolated from green leaves of Arabidopsis (Kubis et al., 2008) and is probably not optimal for gerontoplasts. Despite the need for optimization, this novel method will be useful in the future to characterize FCC export in wild-type plant as well as in plant with suppressed expression of potential candidate genes. Interestingly, ABC transporters have been shown to transport diet-derived Pheide and protoporphyrin IX in mice (Jonker et al., 2002). Even though Pheide and protoporphyrin IX are porphyrins, it has been speculated, also because of the indication that FCC release is ATP-dependent, that ABC transporters located within the envelope could participate in the export of open tetrapyrroles like FCCs or phytochromobilin (Hörtensteiner, 2006). The fact that phytochromobilin transporters have not been identified during screens for mutants that are impaired in phytochrome-dependent light perception suggests that the transport open tetrapyrrole across the chloroplast envelope may be mediated by several transporters. This potential redundancy could challenge their reverse genetic identification using T-DNA insertion lines. Instead, the use of artificial microRNAs to simultaneously silence several genes (for an online tool, see WMD3, http://wmd3.weigelworld.org/cgi-bin/webapp.cgi) will be most probably of great help to identify open tetrapyrrole transporters of the chloroplast envelope. However, it cannot be excluded that FCCs and phytochromobilin are exported from the chloroplast by completely different mechanisms, independent of membrane transport proteins such as ABC transporters. Autophagy-dependent vesicle formation is known to occur at the chloroplast envelope and to be involved in Rubisco degradation (Wada et al., 2009). It could be hypothesized that such mechanisms could also be involved in FCC export, however, autophagy-deficient Arabidopsis plants accumulate the same profile of colorless Chl catabolites like wild-type (Shinya Wada, Bastien Christ and Stefan Hörtensteiner, unpublished data). Finally, SAVs, another type of vesicles derived from the chloroplast (Martínez et al., 2008), could play a role in open tetrapyrrole transport across the envelope. Unfortunately, the current lack of SAV-deficient mutant does not allow testing this hypothesis easily.

4 - CHLOROPHYLL BREAKDOWN DURING LEAF DESICCATION

Chlorophyll breakdown during desiccation of the resurrection plant *Xerophyta viscosa* (Baker): evidence for the involvement of the "PAO pathway"

Chl catabolites and breakdown mechanisms have only been described during senescence processes that ultimately lead to death of respective tissues. This study provides strong evidence that Chl breakdown during drought stress in the resurrection plant *X. viscosa* is mediated enzymatically by the "PAO pathway": PAO is up-regulated and several NCCs accumulate during leaf desiccation. These findings indicate that similar mechanisms, such as controlled and organized Chl breakdown, are used during leaf desiccation in resurrection plants and leaf senescence to maintain cell viability.

Bastien Christ[1], Aurélie Egert[1], Iris Süssenbacher, Berhard Kräutler, Stefan Hörtensteiner[2] and Shaun Peters[2]
[1,2] Theses authors contributed equally to this work

INTRODUCTION

In contrast to the majority of plants, resurrection or desiccation-tolerant plants are characterized by their ability to tolerate and survive extreme desiccation, withstanding the loss of up to 90-95% of the water of their vegetative tissues and subsequently resuming normal cellular metabolism within a short period when water is available (Farrant, 2000; Gaff and McGregor, 1979; Proctor and Tuba, 2002; Scott, 2000; Vicré et al., 2004). Desiccation tolerance entails cellular, biochemical, and molecular changes during dehydration (Vicré et al., 2004), including the synthesis of carbohydrates (Toldi et al., 2009; Whittaker et al., 2001), late embryogenesis-abundant proteins (Ingram and Bartels, 1996), antioxidants (Kranner et al., 2002; Mowla et al., 2002; Vicré et al., 2004), and volatile and non-volatile isoprenoids (Beckett et al., 2012).

Compared to homoiochlorophyllous plants, which during drying retain Chl and preserve the photosynthetic apparatus, poikilochlorophyllous *Xerophyta* species are plants that reversibly loose most of the Chl and dismantle the photosynthetic apparatus during dehydration (Sherwin and Farrant, 1996; Tuba et al., 1998, 1994). It was shown that in parallel to the loss of Chl, chloroplasts of *Xerophyta* species show grana dismantling, thylakoid vesiculation, and cessation of photosynthetic CO_2 assimilation and respiration (Collett et al., 2003; Gaff and McGregor, 1979; Ingle et al., 2008; Tuba et al., 1996). Chl breakdown during desiccation seems to be related to protection against ROS formation caused by overreduction of the electron transport chain (Farrant, 2000). This hypothesis is supported by the observation that *Xerophyta scabrida* preserves most of the Chl when dried in the dark but degrades Chl during desiccation under day/night growth conditions (Tuba et al., 1996). Upon rehydration, photochemical activity recovers rapidly in *Xerophyta* species (Farrant, 2000). Transition of xeroplasts (chloroplasts of dehydrated *Xerophyta* leaves) to photosynthetically active chloroplasts implies formation of grana, Chl biosynthesis, and light-dependent restoration of PSII photochemistry and CO_2 assimilation (Ingle et al., 2008; Pérez et al., 2011).

Up to now nothing is known about the mechanism of Chl degradation during dehydration of poikilochlorophyllous species. In this chapter, we investigated whether Chl degradation during desiccation in *Xerophyta viscosa* (*X. viscosa*) follows the well-described "PAO pathway", shown to be involved in leaf senescence and fruit ripening of higher plant species (see section ""; reviewed in Hörtensteiner and Kräutler, 2011; Hörtensteiner, 2012). Chl breakdown through this pathway starts with the removal of magnesium by MCS or MRP and the cleavage of the hydrophobic phytol moiety by PPH or CLH (Schelbert et al., 2009; Suzuki et al., 2005; Takamiya et al., 2000). In the subsequent step, PAO, a Rieske-type monooxygenase, and RCCR participate in the formation of *p*FCC (Mühlecker et al., 1997; Pružinská et al., 2007, 2003). *p*FCC, considered to be the first non-phototoxic Chl catabolite, is exported from the chloroplast (Hörtensteiner, 2006). Subsequently, FCCs are formed in the cytosol by species-specific modifications of *p*FCC at different positions and then imported into the vacuole where they are isomerized to NCCs (Hörtensteiner, 2012; Oberhuber et al., 2003). It was recently shown in Arabidopsis that tight interactions between the chloroplast-localized enzymes of the "PAO pathway" allow metabolite channeling, and thus controlled degradation of highly phototoxic Chl catabolites (Sakuraba et al., 2013, 2012b).

To date, Chl catabolites and breakdown mechanisms have only been described during senescence processes which ultimately lead to death of respective tissues (Hörtensteiner and Kräutler, 2011; Hörtensteiner, 2006). In poikilochlorophyllous species, Chl degradation has been suggested to be a result of photooxidation rather than of enzymatic processes (Proctor and Tuba, 2002; Tuba et al., 1996). Here, we provide strong evidence that Chl breakdown during drought stress in the resurrection plant *X. viscosa* is mediated enzymatically by the "PAO pathway": PAO is up-regulated and several NCCs accumulate during desiccation. Our study also includes the rehydration phase where we can show that the abundance of Chl breakdown products decreases in regreening leaves.

MATERIALS AND METHODS

Plant material

X. viscosa plants were propagated under greenhouse conditions as previously described (Peters et al., 2007). Plants used for water deficit experiments were grown in a controlled-environment chamber (16 h light with 130 µmol photons m^{-2} s^{-1} / 8 h dark, 25°C, 60% relative humidity) at the Institute of Plant Biology, University of Zürich, Switzerland.

Water deficit stress treatment

Water deficit stress was imposed on whole potted plants by withholding irrigation over a period of 16 d, at the end of which the relative water content (RWC) was determined to be 9%. Leaf samples were excised at regular intervals, immediately flash-frozen in liquid nitrogen, ground, freeze-dried and stored at -80 °C. Sampling times were determined by visual appraisal of the plant using leaf decoloration and folding as benchmarks, at which times the RWC of leaves was determined as previously described (Barrs and Weatherley, 1962; Peters et al., 2007). Pictures of leaf sections were taken with a digital camera at each sampling interval. Rehydration was conducted by watering the plants and sampling as described above.

Analysis of chlorophyll and chlorophyll catabolites

Chl was extracted from freeze-dried samples in 80% acetone and supernatants were analyzed spectrophotometrically (Strain et al., 1971). Colorless Chl catabolites (FCCs, NCCs) were extracted and analyzed by HPLC (setup "1") as previously described (Christ et al., 2012), except that freeze-dried samples were homogenized with 18 volumes (w/v) of 50 mM phosphate buffer, pH 7: methanol (1:3, v/v). Co-injection analysis was performed using another HPLC system (setup "2"; Dionex UltiMate 3000 system (pump and diode array detector)) equipped with a C18 ODS column (5 µm, 250 x 4.6 mm, Phenomenex), which was developed with a gradient (flow rate 0.5 mL min^{-1}) of solvent B (100% methanol) in solvent A (10 mM ammonium acetate buffer, pH 7.0) as follows: 38% during 2 min, 38% to 64% in 27 min, 64% to 100% in 3 min and 100% during 3 min. *Zm*-NCC-2 was prepared as described (Berghold, 2005).

For MS analysis, a *Xv*-NCC-3-containing fraction was isolated by HPLC using setup "2" (see above) and analyzed by electospray ionization mass spectrometry (ESI-MS; Finnigan LCQ classic, positive ion mode, spray voltage 4.25 kV). MS data for *Xv*-NCC-3 (percentage relative intensity, type of ions) are as follows: 883.2 (15, $[M-H+2K]^+$), 867.2 (13, $[M-H+Na+K]^+$), 845.2 (77, $[M+K]^+$), 829.3 (41, $[M+Na]^+$), 807.2 (100, $[M+H]^+$), 775.3 (33, $[M-MeOH+H]^+$), 684.2 (21, $[M-C_7H_9NO$ (ring A) $+H]^+$), 652.3 (6, [M-ring A-MeOH+H]$^+$), 645.20 (18, $[M-C_6H_{10}O_5$ (Gluc)+H]$^+$), 613.27 (14, [M-Gluc-MeOH+H]$^+$), 522.0 (5, [M-Gluc-ring A-M+H]$^+$), 490.0 (4, [M-Gluc-ring A-MeOH+H]$^+$).

Protein extraction and immunoblot analysis

Total leaf proteins were prepared as described (Ingle et al., 2005) with the following modifications. Total proteins were isolated from freeze-dried samples by homogenization in 15 volumes (w/v) of ice-cold extraction buffer (0.5 M Tris–HCl, pH 7.5, 10 mM EDTA, 1% (v/v) Triton X-100, 2% (v/v) 2-mercaptoethanol) complemented with a protease inhibitor cocktail (Complete; Roche Applied Science). Samples were centrifuged at 12'000g for 5 min and protein concentration of the supernatant determined using the Bradford Assay (Bio-Rad). Proteins were subsequently precipitated with chloroform-methanol (Wessel and Flügge, 1984) and analyzed by SDS-PAGE and immunoblotting as described (Pružinská et al., 2007; Schelbert et al., 2009). Fifteen micrograms of protein of each sample were loaded. The following antibodies were used: polyclonal antibodies against LHCb1 and PsbA (1:2000; AgriSera) and monoclonal antibodies against PAO (1:500; Gray et al., 2004).

RESULTS

Relative water content, chlorophyll content and leaf morphology

Changes in water content of *X. viscosa* during dehydration and rehydration is shown in Fig. 4.1A. Plants were dehydrated by withholding water and consequently the RWC dropped below 10% within 15

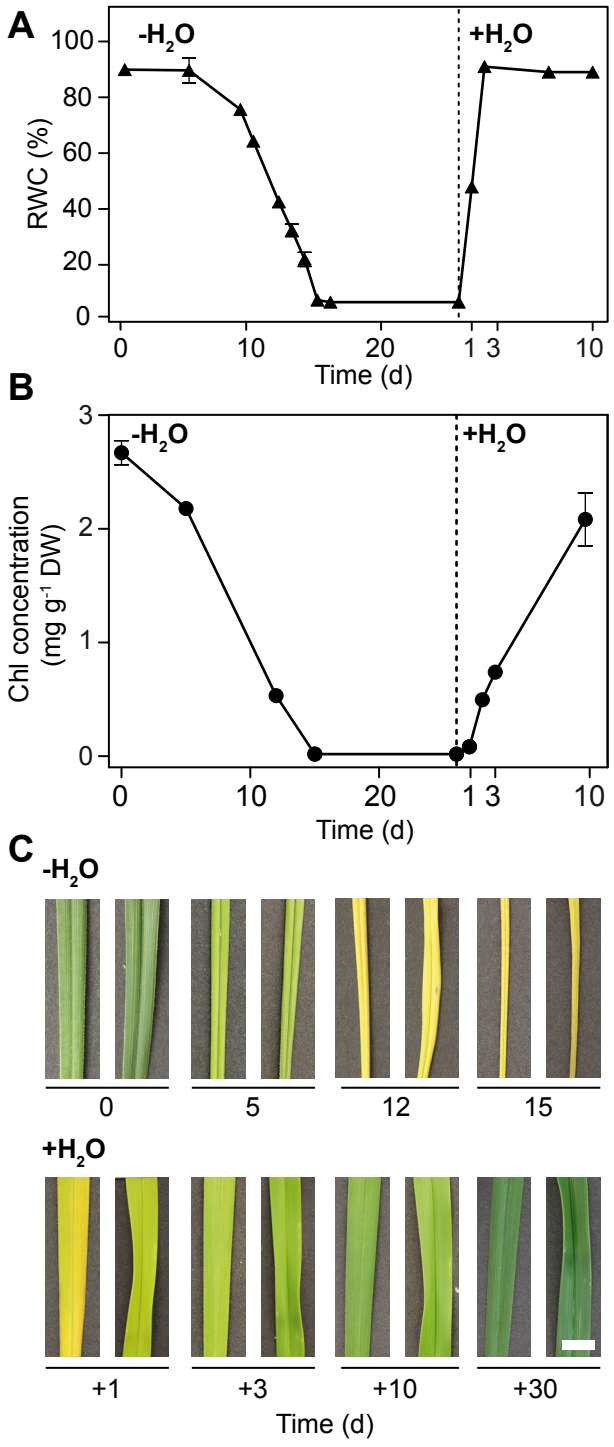

Figure 4.1. RWC (*A*), Chl (*B*) content and leaf morphology (*C*) of leaves of *X. viscosa* during dehydration (-H_2O) and rehydration periods (+H_2O). Data are mean values of a representative experiment with three replicates. Error bars indicate SD. In (*C*), leaf morphology and color during dehydration and rehydration periods were imaged using a digital camera. Bar = 0.5 cm.

d. During the rehydration period, the RWC increased rapidly and full turgor was reached after 3 d. *X. viscosa* has been described as a poikilochlorophyllous species (Farrant, 2000), i. e. dehydration induces Chl degradation. In our experiments, Chl was gradually degraded throughout desiccation leading to almost Chl-free dehydrated leaves (Fig. 4.1B). Chl biosynthesis was rapidly induced after rehydration and within 10 d 75% of the concentration prior to desiccation was reached. As a result of the loss of water and Chl, leaf morphology changed dramatically during the dehydration period (Fig. 4.1C). Leaves folded along their midribs and changed color from green to yellow due to Chl degradation and unmasking of other leaf pigments. During the recovery period, rehydration preceded Chl resynthesis, and therefore fully rehydrated leaves exhibited a transition phase between yellow and green color.

Changes in Rubisco, PsbA, LHCb1 and PAO expression

Total protein profiles of *X. viscosa* leaves were investigated during dehydration and rehydration by SDS-PAGE and Coomassie blue staining (Fig. 4.2A). The protein concentration (µg mg^{-1} DW) did not change significantly during dehydration and therefore the same amount of proteins of each sample (fifteen micrograms) was loaded on the gel. Levels of Rubisco large and small subunits, indicated with black arrowheads in Fig. 4.2A, stayed rather constant. However, immunoblot analysis revealed changes of the levels of thylakoid proteins involved in photosynthesis as already reported for poikilochlorophyllous *Xerophyta* species (Fig. 4.2B; Collett et al., 2004, 2003; Ingle et al., 2008, 2007; Pérez et al., 2011). Indeed, PsbA, a subunit of the core complex of PSII, was quantitatively degraded during dehydration and resynthesized during rehydration, similarly to Chl. The same pattern was observed for LHCb1, a component of the light-harvesting antennae of PSII.

To investigate whether Chl is broken down through the well-described "PAO pathway" (Hörtensteiner and Kräutler, 2011; Hörtensteiner, 2012), PAO protein levels were investigated during desiccation and rehydration (Fig. 4.2B). The level of PAO increased during dehydration, but decreased during rehydration; i. e. it was negatively correlated with the concentration of Chl. Surprisingly, the highest level of PAO was found after 1 d of rehydration.

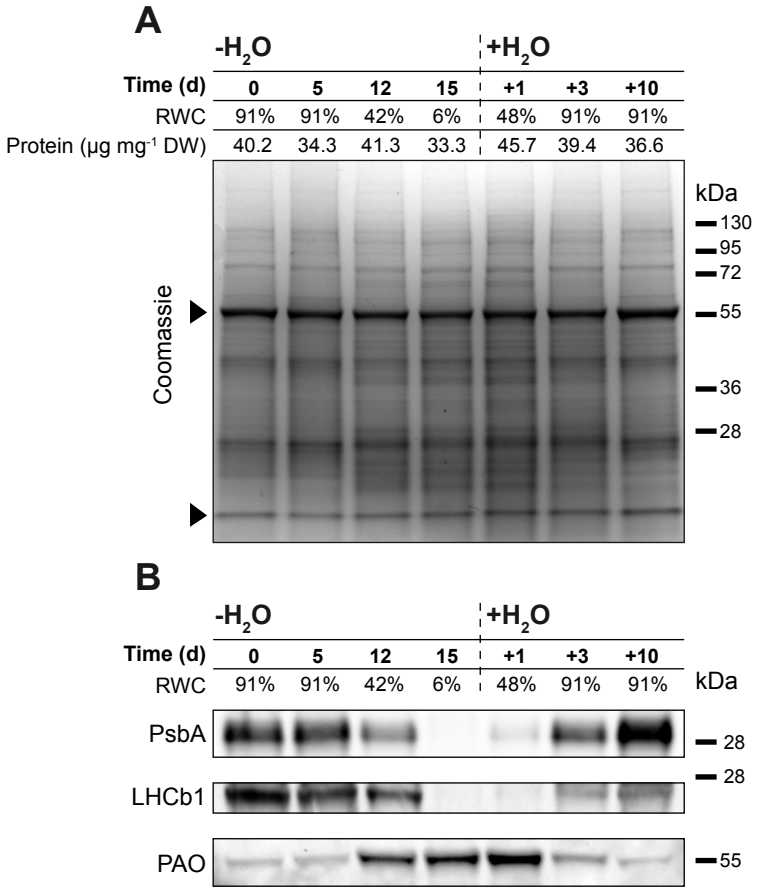

Figure 4.2. Analysis of protein in *X. viscosa* leaves during dehydration and rehydration periods. (*A*) Total leaf protein samples (15 µg) were separated by SDS-PAGE gel and stained with Coomassie blue. Rubisco large and small subunits are indicated with black arrowheads. (*B*) Analysis of PsbA, LHCb1 and PAO levels by immunoblotting. After SDS-PAGE as shown in panel *A*, proteins were transferred on a nitrocellulose membrane and visualized by immunoblotting using anti-PsbA, -LHCb1 and -PAO antibodies. For more details, see "Materials and Methods". Standard protein masses are given in kDa on the right.

Accumulation of NCCs during leaf desiccation of *Xeropyhta viscosa*

As shown above, the increase of PAO protein levels in leaves of *X. viscosa* during dehydration points to a possible involvement of the "PAO pathway" in the breakdown of Chl observed in this process. PAO is a key enzyme of the pathway because it opens the macrocycle of Pheide *a* and therefore determines the basic structure of all downstream linear catabolites (FCCs and NCCs) (Pružinská et al., 2003). In order to investigate the presence of such catabolites, samples were collected at different time points during the dehydration and rehydration phase and analyzed by reversed-phase HPLC (Fig. 4.3A). Spectral analysis of the resulting chromatograms allowed the identification of four fractions, tentatively named *Xv*-NCC-1 to -4, showing typical NCC absorbance properties. These fractions were absent before dehydration and accumulated increasingly in the leaves during dehydration and Chl degradation. After 10 d of subsequent rehydration, they had almost completely disappeared. In-depth analysis of the major fraction, *Xv*-NCC-3, by mass spectrometry revealed that this NCC has the same mass (m/z $[M+H^+]$ = 807.2; Fig. 4.3B) as *Zm*-NCC-2, an NCC described from *Zea mays* (Berghold, 2005). HPLC analysis of purified fractions showed that *Xv*-NCC-3 and *Zm*-NCC-2 exhibited the same retention time when analyzed independently and co-eluted as a single fraction when co-injected as a 1:1 (w/w) mixture (Fig. 4.3C). This observation strongly indicates that *Xv*-NCC-3 has the same constitution as *Zm*-NCC-2 (Fig. 4.3D; Berghold, 2005). *Xv*-NCC-3/*Zm*-NCC-2 contains a methyl group at the $O13^4$ position indicating the likely absence in *X. viscosa* of a homolog of the *Arabidopsis thaliana* MES16, responsible for the $O13^4$ demethylation (Christ et al., 2012). The $C8^2$-ethyl moiety of

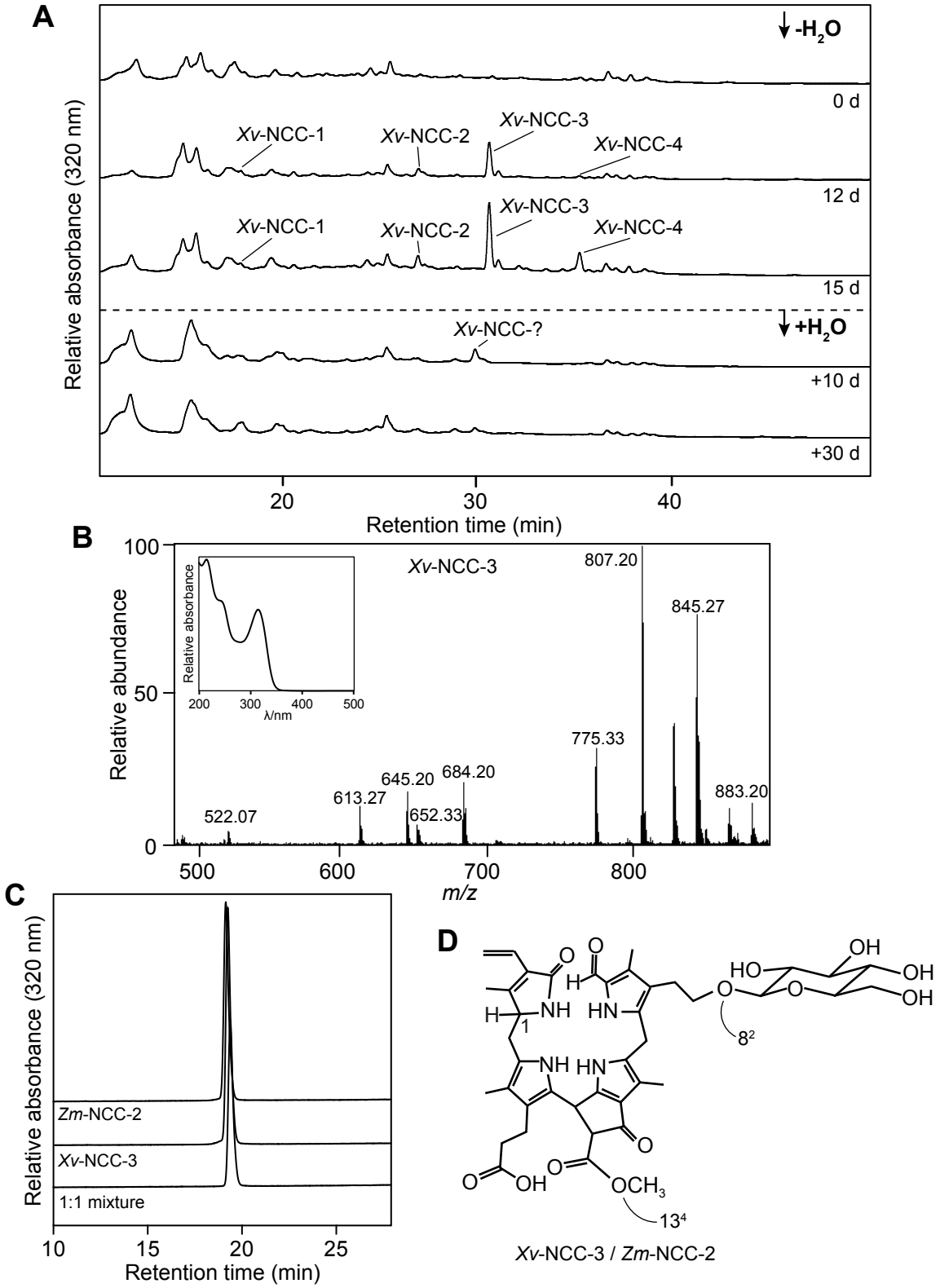

Figure 4.3. Colorless Chl catabolites of *X. viscosa* leaves during dessication and rehydration. (*A*) Colorless catabolites were separated using the HPLC setup "1" described in "Materials and Methods". A_{320} is shown. For clarity, only the relevant part of the HPLC traces is shown. (*B*) Mass and UV-vis spectra of *Xv*-NCC-3. For more details on MS data of *Xv*-NCC-3, see "Materials and Methods". UV-vis spectra of *Xv*-NCC-3 is shown in the inset. (*C*) HPLC co-injection of *Xv*-NCC-3 and *Zm*-NCC-2. Note that this experiment was performed with the HPLC setup "2" described in "Materials and Methods" and indicates that the two NCCs have the identical constitution. (*D*) Chemical structure of *Xv*-NCC-3/*Zm*-NCC-2. Relevant atoms are labeled.

Xv-NCC-3 is hydroxylated and subsequently glycosylated; respective modifications are also known to occur in *Arabidopsis thaliana, Brassica napus, Nicotiana rustica, Pyrus communis* and *Zea mays* (Hörtensteiner, 2012). In addition to providing structural constitution of *Xv*-NCC-3, co-injection with *Zm*-NCC-2 also revealed the stereoselectivity of *X. viscosa* RCCR. This enzyme reduces RCC produced by PAO to *p*FCC (Pružinská et al., 2007). Depending on the plant species, RCCR enzymes exhibit different stereospecificities in the reduction of the C20/C1 double bound of RCC and therefore yield one of the two possible C1-stereoisomers *p*FCC or epi-*p*FCC (Hörtensteiner, 2012). Thus, from the C1 stereochemistry of *Xv*-NCC-3, we can deduce that *Xv*-RCCR yields epi-*p*FCC like the RCCRs from *Zea mays*, *Nicotiana rustica*, *Spinacia oleracea* and *Cercidiphyllum japonicum* (Hörtensteiner, 2012).

DISCUSSION AND OUTLOOK

Leaf senescence is considered to be reversible until a point of no return (Thomas et al., 2003). Indeed, chloroplast-to-gerontoplast transition has been shown to be reversible in *Nicotiana rustica* (Zavaleta-Mancera et al., 1999a, 1999b). Shoot decapitation of senescing *Nicotiana rustica* plants leads to leaf regreening, an effect that is enhanced by cytokinin treatment. Leaf re-greening was shown to involve resynthesis of functional thylakoid membranes within gerontoplasts and not to be due to a *de novo* formation of chloroplasts. In this study, we focused on leaf de- and re-greening observed during dehydration of the resurrection plant *X. viscosa.* We hypothesized that similar reversible mechanisms for chloroplast dismantling are shared between age-dependent senescence of higher plants and leaf dehydration of resurrection plants. Poikilochlorophylly, e. g. Chl degradation during drought stress in resurrection plants, has long been described (Sherwin and Farrant, 1996; Tuba et al., 1998, 1994). Loss of Chl has been speculated to be the result of nonenzymatic photooxidation reactions (Proctor and Tuba, 2002; Tuba et al., 1996). However, the mechanism responsible for breakdown of Chl in poikilochlorophyllous species has never been investigated. Here, we demonstrate that during desiccation of *X. viscosa* Chl is degraded enzymatically via the "PAO pathway" (Hörtensteiner, 2012). Up-regulation of PAO (Fig. 4.2B), the enzyme that opens the Chl catabolite macrocycle, as well as accumulation of NCCs (Fig. 4.3) during dehydration clearly indicate that Chl degradation in resurrection plants follows the organized and regulated pathway already described for leaf and fruit senescence.

During leaf senescence, the "PAO pathway" detoxifies photoactive Chl catabolites and therefore increases cell viability. Indeed, suppression of PAO results in an accelerated cell death phenotype due to the accumulation of Pheide and does not allow the plant to undergo proper leaf senescence (Pružinská et al., 2003; Tanaka et al., 2003). Similarly, it can be assumed that Chl degradation in poikilochlorophyllous resurrection plants follows the regulated and organized "PAO pathway" in order to avoid ROS production by free Chl, and thus enhances survival during and after the desiccation period. Since Chl-apoprotein complex retention during desiccation would lead to the formation of ROS, it can be speculated that suppression of Chl breakdown in species such as *X. viscosa* would dramatically decrease their resurrection capacity. Homoiochlorophyllous resurrection plants, which retain large proportion of Chl during desiccation, have developed other protection mechanisms such as leaf folding, which has, among others, a light shading effect on Chl-apoprotein complexes. It is interesting to note that, as a general rule, desiccation-tolerant plants that have to face consecutive short periods of drought alternating with periods of water availability are homoiochlorophyllous. In contrast, resurrection plants such as several *Xerophyta* species, which stay desiccated for longer periods, are poikilochlorophyllous (Tuba et al., 1998). This observation indicates that benefits of degrading thylakoid components to avoid ROS production during long period of dehydration are higher than costs of their resynthesis during rehydration.

Parallel to Chl breakdown, PS core and antennae subunits are also degraded during desiccation of *X. viscosa* (Fig. 4.2B). Indeed, Chl *a* and *b* biosynthesis and degradation are known to be linked with PS assembly and disassembly due to the fact that Chl molecules are intimately integrated within PS subunits (Hörtensteiner, 2009; Nelson and Yocum, 2006; Tanaka and Tanaka, 2011). As a result, suppression

of genes involved in the first steps of Chl breakdown such as NYC1, NOL, SGR or PPH inhibits the degradation of several PS subunits. In addition to its detoxifying role, Chl degradation during leaf senescence is also thought to be a prerequisite for the degradation and remobilization of PS proteins, which represent a significant fraction of nitrogen present within mesophyll cells (Hörtensteiner and Feller, 2002). Moreover, the nitrogen contained in Rubisco, which accounts for 20–30% of total leaf nitrogen, is also remobilized during leaf senescence (Feller et al., 2008). The observation that Rubisco is not degraded during dehydration of *X. viscosa* (Fig. 4.2A) reveals that there are also major differences between leaf desiccation and senescence. It is reasonable to assume that leaf desiccation requires nitrogen remobilization for two reasons. The first one is that retention of Rubisco during dehydration of resurrection plant, in contrast to Chl-apoprotein complexes, does not have any toxic effect. The second reason is that resurrection plants do not remobilize leaf nitrogen to other organs during dehydration and therefore do not need to break down Rubisco.

The finding that the "PAO pathway" is involved during leaf desiccation in resurrection plants indicates that similar mechanisms are used during leaf desiccation in resurrection plants and leaf senescence to maintain cell viability, even though the main goals of these two process are different (survival and nutrient remobilization, respectively). Similarities such as Chl degradation through the "PAO pathway" are also found when comparing desiccation tolerance in resurrection plants and seed maturation. In most higher plants, drought tolerance is restricted to seeds. Seed maturation, similarly to leaf desiccation in resurrection plants, involves the accumulation of considerable quantities of non-reducing di- and oligosaccharides, compatible solutes and specific proteins such as the LATE EMBRYOGENESIS ABUNDANT PROTEINS (LEAs) and HEAT SHOCK PROTEINS (HSPs; Hoekstra et al., 2001). Interestingly, Chl degradation of cotyledons has been shown to occur during seed drying and is known to follow the "PAO pathway" (Chung et al., 2006; Nakajima et al., 2012; Weber et al., 2005). Furthermore, the germination capacity of matured seeds has been demonstrated to be inversely proportional to the Chl level (Jalink et al., 1998). Thus, suppression of Chl *b* to *a* conversion in Arabidopsis, which leads to Chl retention in cotyledons during seed drying, dramatically decrease seed germination capacity (Nakajima et al., 2012). In the future, it will be interesting to further investigate to which extent other senescence processes are involved during leaf desiccation and seed maturation. The following questions are of key importance: Is the overlap restricted to thylakoid and PSs degradation? How are typical senescence markers such as SAGs regulated during leaf desiccation and seed maturation? A wider approach should allow to answer these questions and to identify other similarities between leaf senescence, leaf desiccation in resurrection plants and seed maturation.

5 - RCCR MODULATES CELL DEATH

ACCELERATED CELL DEATH 2 suppresses mitochondrial oxidative bursts and modulates cell death in Arabidopsis

Published in Plant Journal (2011) 69: 589–600

This chapter presents further investigations on the role of RCCR in the protection against cell death. Specific targeting of RCCR to the mitochondria of *acd2* dramatically reduces RCC accumulation, cell death and mitochondrial ROS production. This rescue effect is dependent on the activity of RCCR since a mitochondria-targeted Glu154Ala variant of RCCR did not complement the cell death phenotype of *acd2*. Collectively, these *in vivo* data on RCCR function(s) provide evidence that this enzyme is involved in protection against pro-death molecules (such as RCC) in both chloroplast and mitochondria. These pro-death molecules, substrates of RCCR, are mobile within cells and have a major effect on mitochondria.

Gopal K. Pattanayak, Sujatha Venkataramani, Stefan Hörtensteiner, Lukas Kunz, Bastien Christ, Michael Moulin, Alison G. Smith, Yukihiro Okamoto, Hitoshi Tamiaki, Masakazu Sugishima and Jean T. Greenberg

REPRINT of Pattanayak GK, et al. (2012) Plant J 69: 589–600

the plant journal

SEB Society for Experimental Biology

The Plant Journal (2012) **69**, 589–600 doi: 10.1111/j.1365-313X.2011.04814.x

ACCELERATED CELL DEATH 2 suppresses mitochondrial oxidative bursts and modulates cell death in Arabidopsis

Gopal K. Pattanayak[1], Sujatha Venkataramani[1], Stefan Hortensteiner[2], Lukas Kunz[2], Bastien Christ[2], Michael Moulin[3,†], Alison G. Smith[3], Yukihiro Okamoto[4], Hitoshi Tamiaki[4], Masakazu Sugishima[5] and Jean T. Greenberg[1,*]

[1]*Department of Molecular Genetics and Cell Biology, The University of Chicago, Chicago, IL 60637, USA,*
[2]*Institute of Plant Biology, University of Zurich, CH-8008 Zurich, Switzerland,*
[3]*Department of Plant Sciences, University of Cambridge, Downing Street, Cambridge CB23EA, United Kingdom,*
[4]*Department of Bioscience and Biotechnology, Faculty of Science and Engineering, Ritsumeikan University, Kusatsu, Shiga 525-8577, Japan, and*
[5]*Department of Medical Biochemistry, Kurume University School of Medicine, Kurume 830-0011, Japan*

Received 9 August 2011; revised 4 October 2011; accepted 6 October 2011; published online 16 November 2011.
*For correspondence (fax +773 702 9270; e-mail jgreenbe@uchicago.edu).
†Present address: Plant Biochemistry and Physiology, BIVEG, University of Geneva-Science III, 1211 Geneva 4, Switzerland.

SUMMARY

The Arabidopsis ACCELERATED CELL DEATH 2 (ACD2) protein protects cells from programmed cell death (PCD) caused by endogenous porphyrin-related molecules like red chlorophyll catabolite or exogenous protoporphyrin IX. We previously found that during bacterial infection, ACD2, a chlorophyll breakdown enzyme, localizes to both chloroplasts and mitochondria in leaves. Additionally, *acd2* cells show mitochondrial dysfunction. In plants with *acd2* and *ACD2*$^+$ sectors, ACD2 functions cell autonomously, implicating a pro-death ACD2 substrate as being cell non-autonomous in promoting the spread of PCD. ACD2 targeted solely to mitochondria can reduce the accumulation of an ACD2 substrate that originates in chloroplasts, indicating that ACD2 substrate molecules are likely to be mobile within cells. Two different light-dependent reactive oxygen bursts in mitochondria play prominent and causal roles in the *acd2* PCD phenotype. Finally, ACD2 can complement *acd2* when targeted to mitochondria or chloroplasts, respectively, as long as it is catalytically active: the ability to bind substrate is not sufficient for ACD2 to function *in vitro* or *in vivo*. Together, the data suggest that ACD2 localizes dynamically during infection to protect cells from pro-death mobile substrate molecules, some of which may originate in chloroplasts, but have major effects on mitochondria.

Keywords: cell death, mitochondria, chloroplast, hydrogen peroxide, singlet oxygen, red chlorophyll catabolite.

INTRODUCTION

The Arabidopsis ACCELERATED CELL DEATH 2 (ACD2) protein, also known as red chlorophyll catabolite (RCC) reductase has multiple functions. *acd2* mutants were first identified as being compromised for cell death regulation because of their spontaneous spreading cell death phenotype (Greenberg *et al.*, 1994). Later, the ACD2 protein was identified as a component of the chlorophyll breakdown pathway (Rodoni *et al.*, 1997; Wuthrich *et al.*, 2000). In mature leaves, ACD2 localizes to chloroplasts, whereas in young seedlings and in roots, ACD2 is found in both chloroplasts (or plastids) and mitochondria (Mach *et al.*, 2001; Yao and Greenberg, 2006). After *Pseudomonas syringae* infection or protoporphyrin IX (PPIX) treatment of mature leaves, ACD2 is induced around cell death sites and is found in chloroplasts and mitochondria (Yao and Greenberg, 2006). As the mitochondrial form of ACD2 is larger than the chloroplast form, it is likely that unprocessed ACD2 is independently targeted to and processed in mitochondria and chloroplasts, respectively. Modulation of the levels of ACD2 strongly influences cell death caused by *P. syringae* and PPIX treatment: loss of ACD2 results in excessive cell death, whereas overproduction is cytoprotective (Greenberg *et al.*, 1994; Mach *et al.*, 2001; Yao *et al.*, 2004; Yao and Greenberg, 2006).

ACCELERATED CELL DEATH 2 is involved in the conversion of RCC, a chlorophyll degradation pathway intermediate,

to primary fluorescent chlorophyll catabolite (pFCC; Rodoni *et al.*, 1997; Wuthrich *et al.*, 2000). Details of the biochemical mechanism of ACD2 in the conversion of RCC to pFCC remain unclear; possibly ACD2 functions as a chaperone in the catalytic reaction that converts RCC to pFCC (Rodoni *et al.*, 1997; Wuthrich *et al.*, 2000; Oberhuber and Krautler, 2002; Pruzinska *et al.*, 2007). From the crystal structure of ACD2, it was hypothesized that glutamic acid 154 and aspartic acid 291 are the possible substrate binding and/or catalytic sites (Sugishima *et al.*, 2009, 2010). Excised leaves of *acd2* mutants accumulate RCC and RCC-like pigments after incubation in the dark for several days, which promotes their accumulation (Pruzinska *et al.*, 2007). Incubation in the dark also protects the pigments from light-induced fragmentation.

As compared with many other cell death mutants, the *acd2* mutant is somewhat unusual in that the cell death in each leaf starts spontaneously and propagates to consume the whole leaf (Greenberg *et al.*, 1994). The propagation of cell death lesions in the *acd1* mutant is similar to that in *acd2*; however, the onset of lesions in *acd2* occurs earlier in development compared with *acd1*. Cell death in *acd2* is light dependent and involves the production of hydrogen peroxide (H_2O_2; Mach *et al.*, 2001; Yao and Greenberg, 2006). Assuming some RCC/RCC-like pigments or that of other substrates can accumulate in light, their photo-activation may lead to singlet oxygen ($^1O_2$) production, which could also contribute to cell death. Indeed, RCC accumulation in dark-incubated *acd2* leaves is correlated with increased $^1O_2$ generation after leaves are exposed to light (Pruzinska *et al.*, 2007). Various chlorophyll precursors and their degradation intermediates also generate $^1O_2$ in light, which may contribute to cell death phenotypes in several mutants (Greenberg and Ausubel, 1993; Hu *et al.*, 1998; Ishikawa *et al.*, 2001; op den Camp *et al.*, 2003; Pruzinska *et al.*, 2003, 2007; Mur *et al.*, 2010).

Mitochondria play a key role in cellular metabolism and also are important players in the regulation of programmed cell death (PCD, Moller, 2001; Jones, 2000; Lam *et al.*, 2001). One of the early events in apoptotic cell death is the mitochondrial membrane permeability transition (MPT) that is induced by multiple independent pathways (Crompton, 1999; Moller, 2001), and occurs before cells exhibit apoptotic features (Arpagaus *et al.*, 2002; Tiwari *et al.*, 2002; Yao *et al.*, 2004). Although the release of cytochrome *c* has been documented during plant PCD (Balk and Leaver, 2001; Tiwari *et al.*, 2002), it is not always correlated with an MPT and cell death in plants (Yu *et al.*, 2002; Yao *et al.*, 2004). We previously characterized cell death events in *acd2* protoplasts, which die in response to light with an apoptotic morphology that includes chromatin condensation and the induction of DNA fragmentation (Yao *et al.*, 2004). The exogenous application of PPIX to *acd2* protoplasts accelerates cell death with apoptotic features. After exposure of *acd2* protoplasts to light, the mitochondria lose their membrane potential, accumulate H_2O_2, change their morphology and the cells finally die. Although *acd2* cells also accumulate H_2O_2 in chloroplasts, this later accumulating pool of H_2O_2 does not contribute to the induction of cell death (Yao and Greenberg, 2006).

Here, we address the possible reason and role, respectively, for spreading PCD and mitochondrial dysfunction in *acd2*, as well as the sites and mechanism of action of ACD2. Our data suggest an important role for the enzymatic activity of ACD2 in protecting mitochondria from substrate molecules that may move between organelles and cells, causing mitochondrial reactive oxygen species (ROS) that ultimately lead to cell death.

RESULTS

Disruption of the mitochondrial H_2O_2 partially suppresses cell death in *acd2*

As chloroplast-derived H_2O_2 does not contribute to the *acd2* cell death phenotype (Yao and Greenberg, 2006), the mitochondrial pool may be important. To test this, we increased the H_2O_2 scavenging capacity in *acd2* mitochondria by targeting the antioxidant enzymes thylakoid ascorbate peroxidase (tAPX; Jespersen *et al.*, 1997) and human catalase (HsCAT; Schriner *et al.*, 2005) to *acd2* mitochondria. As shown in Figure 1(a), using purified mitochondrial fractions from the *acd2*/m-tAPX and *acd2*/m-HsCAT plants, we detected m-tAPX and m-HsCAT proteins, respectively, along with the mitochondrial marker Peroxiredoxin II F (PRX II F; Finkemeier *et al.*, 2005). We did not detect HsCAT in chloroplasts (Figure S1), indicating that the targeting to mitochondria was robust (tAPX is normally present in chloroplasts; Jespersen *et al.*, 1997).

acd2/m-tAPX and *acd2*/m-HsCAT protoplasts showed very little mitochondrial H_2O_2 after exposure to light, as compared with *acd2* (Figure 1b). The mean fluorescence intensity (MFI) of the H_2O_2 indicator dye CM-H_2DCFDA in light-exposed cells in *acd2*/m-tAPX and *acd2*/m-CAT protoplasts was reduced compared with *acd2*, but was increased relative to wild-type protoplasts (Figure 1c). Reducing the mitochondrial H_2O_2 pool significantly improved the survival of *acd2* protoplasts exposed to light, although wild-type protoplasts still showed the best survival (Figure 1d). Additionally, in whole plants, reduction of mitochondrial H_2O_2 partially rescued the *acd2* cell death phenotype (Table S1).

Mitochondrial-derived $^1O_2$ correlates with the light-induced death of *acd2* cells

As the reduction in mitochondrial H_2O_2 did not completely rescue the *acd2* cell death phenotype, we assessed the contribution of other ROS. Superoxide levels were not different in *acd2* and wild-type protoplasts (Figure S2). However, $^1O_2$ accumulates in *acd2* leaves, possibly because of RCC accumulation (Pruzinska *et al.*, 2007). To discern whether RCC can

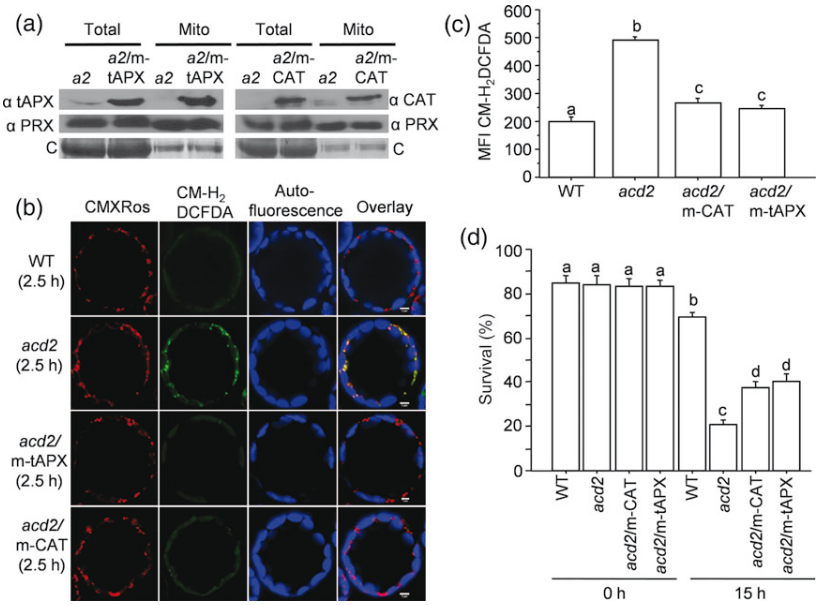

Figure 1. Targeting antioxidant enzymes to mitochondria increases the survival of *acd2* cells.
(a) Total proteins and mitochondrial proteins were isolated from *acd2* (*a2*), *a2*/m-tAPX and *a2*/m-CAT plants, and tAPX, catalase (CAT) and mitochondrial marker peroxiredoxin (PRX) II F proteins were detected by western blot analysis. tAPX and CAT were targeted to mitochondria in the *a2*/m-tAPX and *a2*/m-CAT plants, respectively; C, Coomassie staining of the membranes. This experiment was performed three times with similar results.
(b) Protoplasts isolated from 20-day-old plants were exposed to light for 2.5 h, and were then double-stained with CM-H_2DCFDA to detect H_2O_2 and CMXRos to mark mitochondria. Between 50 and 60 protoplasts were examined under a laser scanning confocal microscope (LSCM), and representative protoplasts are shown. Staining with CMXRos validated that the CM-H_2DCFDA-positive organelles were mitochondria. This experiment was performed three times with similar results.
(c, d) The mean fluorescence intensity (MFI) of CM-H_2DCFDA-stained protoplasts was determined using flow cytometry (c). Protoplasts were exposed to light for 15 h and the percentage (%) of surviving cells was determined by FDA staining (d). Results are from a single analysis that is representative of three independent experiments showing similar results. The error bars represent SDs (n = 3). Letters indicate different values using Fisher's protected least significant difference test (P < 0.004).

directly generate $^1O_2$ after light exposure, we made spin-trap electron paramagnetic resonance (EPR) spectroscopy measurements using 2,2,6,6-tetramethylpiperidine (TEMP) as an $^1O_2$ trap. Figure 2(a) shows the light-induced $^1O_2$ production from RCC (and PPIX, a positive control) as revealed from the EPR spectra of nitroxy radical 2,2,6,6-tetramethylpiperidine-1-oxyl (TEMPO), which is formed by the reaction of $^1O_2$ with TEMP. RCC or PPIX solutions incubated in the dark did not produce $^1O_2$ (Figure 2a). The TEMPO intensity increased in a time-dependent manner (Figure S3).

The cellular site of $^1O_2$ generation in protoplasts assessed by laser scanning confocal microscope after staining them with the fluorescent probe Singlet Oxygen Sensor Green (SOSG; Flors *et al.*, 2006; Gollmer *et al.*, 2011), co-localized with the mitochondrial marker, MitoTracker Red CMXRos, in *acd2* (Figure 2b). However, the SOSG signal in wild-type protoplasts was too low to detect a specific co-localization pattern. The SOSG MFI of light-exposed *acd2* protoplasts was also higher compared with wild-type protoplasts (Figure 2c). Chloroplast-generated $^1O_2$ can also contribute to cell death events (op den Camp *et al.*, 2003), a process suppressed by loss of chloroplast-localized executer proteins or by certain photoreceptors (Wagner *et al.*, 2004; Danon *et al.*, 2006; Lee *et al.*, 2007). However, mutations in executers or photoreceptors did not alter cell death in *acd2* (Figure S4). Thus, chloroplast-generated $^1O_2$ does not appear to contribute to the *acd2* PCD phenotype.

The application of vitamin B6 (Pyridoxine), a $^1O_2$ quencher (Bilski *et al.*, 2000; Danon *et al.*, 2005), significantly reduced the MFI of SOSG in protoplasts (Figure 2c), and resulted in the increased cell survival of *acd2* but not wild type (Figure 2d). The difference in the effect of B6 on survival probably results from the highly concentrated $^1O_2$ found in *acd2*, but not in wild-type mitochondria. B6 further increased the cell survival of *acd2*/m-tAPX also (Figure 2d). This indicates that both $^1O_2$ and H_2O_2 contribute to the *acd2* PCD phenotype. Interestingly, $^1O_2$ production in *acd2*/m-tAPX protoplasts, assessed by quantifying the SOSG MFI, was unchanged relative to *acd2* (Figure 2e). Similarly, the production of H_2O_2 by *acd2* in the presence of vitamin B6, assessed by quantifying the CM-H_2DCFDA MFI, was also unchanged relative to *acd2* alone (Figure 2f). Thus, $^1O_2$ and H_2O_2 are independently generated.

ACD2 targeted to chloroplasts or mitochondria reduces the *acd2* cell death phenotype

During pathogen and PPIX treatment, ACD2 shifts from chloroplast localization to both chloroplasts and mitochondria

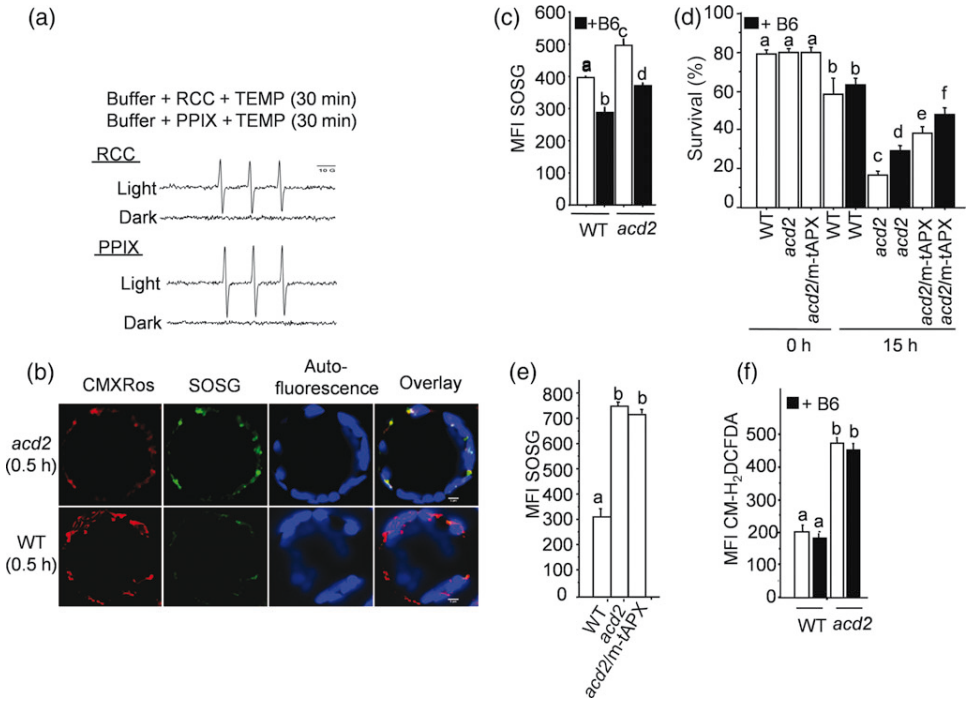

Figure 2. Singlet oxygen ($^1O_2$) production and its contribution to the *acd2* phenotype.
(a) $^1O_2$ formation from red chlorophyll catabolite (RCC) and protoporphyrin IX (PPIX) after light exposure as detected by spin-trap EPR measurement. The characteristic EPR spectrum represents the TEMPO formation; TEMPO was formed by the reaction of TEMP ($^1O_2$ trap) and $^1O_2$. Note there was no $^1O_2$ production from RCC or PPIX in the dark. Results are from a single analysis, representative of two independent experiments that showed similar results.
(b) Protoplasts were incubated with SOSG dye to detect $^1O_2$, exposed to light for 0.5 h and double stained with CMXRos. Images were assessed by laser scanning confocal microscope (LSCM). Note the strong SOSG (green) signal from *acd2* protoplasts after exposure to light, which overlapped with the CMXRos signals. This experiment was performed three times with similar results.
(c) The MFI of SOSG-stained protoplasts isolated from WT and *acd2* leaves in the absence and presence of vitamin B6 as measured by flow cytometry.
(d) Protoplasts were treated with and without vitamin B6 for 15 h under light. The percentage (%) of cell survival was determined by FDA staining. Note the cell viability of *acd2*/m-tAPX was further increased in the presence of B6.
(e) MFI of SOSG-stained protoplasts after light exposure (0.5 h).
(f) MFI of CM-H_2DCFDA-stained light-exposed (2.5 h) protoplasts in the presence and absence of vitamin B6. Results (c–f) are from a single analysis that is representative of three independent experiments showing similar results. The error bars represent SDs (n = 3). Letters indicate different values using Fisher's protected least significant difference (test (P < 0.002).

(Yao and Greenberg, 2006). This, along with the mitochondrial dysfunction of *acd2* cells, suggests a role for ACD2 in mitochondria and the possibility that pro-death ACD2 substrate molecules are mobile within and/or between cells. To understand this further, we targeted ACD2 solely to the mitochondria or to the chloroplasts of *acd2*. Using total protein, we detected ACD2 (Figure 3a), which was significantly increased in *acd2*/m-ACD2 and *acd2*/c-ACD2 plants relative to wild type. m-ACD2 and c-ACD2 were correctly targeted to chloroplasts and mitochondria, respectively (Figure 3a). Chloroplasts from the mitochondria-targeted plants (*acd2*/m-ACD2) and mitochondria from the chloroplast-targeted plants (*acd2*/c-ACD2) did not contain detectable levels of ACD2 (Figure 3a). The purity of the organelles was verified using mitochondria- and chloroplast-specific markers (Figure 3a).

The *acd2*/c-ACD2 plants displayed complete and stable rescue of the *acd2* cell death phenotype. Most *acd2*/m-ACD2 plants (>79% of plants) were also fully rescued. A minority of *acd2*/m-ACD2 plants showed cell death later in development relative to *acd2*, which was accompanied by reduced levels of ACD2 (Figure 3b; Table S2). (Some *acd2*/c-ACD2 lines had similar behavior to the *acd2*/m-ACD2 lines, but these were not characterized further.) It is unclear why ACD2 levels decreased with age in some transgenic lines. Light-exposed *acd2*/c-ACD2 and *acd2*/m-ACD2 protoplasts showed significantly higher cell viability (Figure 3c) and very little mitochondrial H_2O_2 and $^1O_2$ compared with *acd2* (Figure S5). Thus, c-ACD2 and m-ACD2 significantly rescued the *acd2* PCD phenotype and suppressed mitochondrial ROS.

Cytoprotective function of ACD2 in chloroplasts or mitochondria correlates with its enzymatic activity

Structural analysis of ACD2 indicates possible roles for Glu154 and Asp291 in substrate binding and/or enzyme

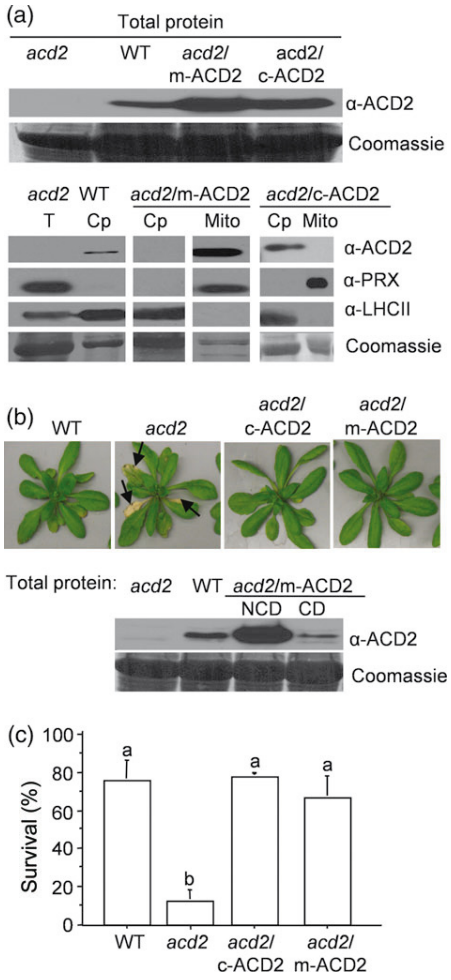

Figure 3. ACD2 either in mitochondria or in chloroplasts significantly suppresses the *acd2* cell death phenotype.
Transgenic *acd2* carrying ACD2 targeting to mitochondria (*acd2*/m-ACD2) or chloroplasts (*acd2*/c-ACD2) were generated and characterized. Experiments were performed with at least two independent transgenic lines per construct; data from representative lines are presented.
(a) The ACD2 level in total protein (T) extracts (upper panel) and in chloroplasts (Cp) and mitochondria (Mito) isolated from the indicated plants was detected by western blot analysis (lower panel). Organelle purity was assessed using antibodies against PRX II F and LHCII (chloroplasts). Signals of ACD2, PRX II F and LHC II for all samples are from single exposures of one continuous membrane. This experiment was performed three times with similar results.
(b) Phenotypes of 31-day-old plants of the indicated genotype. By day 31, about 20% of *acd2*/m-ACD2 showed a mild cell death phenotype (see text). ACD2 protein content in the healthy leaves of 21-day-old *acd2*/m-ACD2 plants that showed mild cell death (CD) and did not show cell death (NCD) on day 21 (lower panel). This experiment was performed three times with similar results.
(c) Protoplasts were exposed to light for 15 h and the percentage (%) of live cells was determined. This experiment was performed four times with similar results and the error bars represent SDs (n = 2). Letters indicate different values using Fisher's protected least significant difference test (P < 0.001).

catalysis (Sugishima *et al.*, 2009). Therefore, we tested whether the enzymatic activity and/or substrate binding is important for the cytoprotective role of ACD2. We generated a variant of ACD2 (ACD2**) in which both Glu154 (Glu154Ala; E154A) and Asp291 (Asp291His; D291H) residues were altered. Interestingly, RCC bound equally well to ACD2** and ACD2, as assessed by tryptophan fluorescence quenching (Figure 4a). In contrast, a coupled pheophorbide *a* oxygenase (PAO)/ACD2 enzyme assay using pheophorbide *a* as substrate with PAO isolated from bell pepper fruits and ACD2 variants indicated that ACD2** and the E154A variant completely lost their enzymatic activities, as no enzymatic product, pFCC, was produced (Figure 4b).

To discern the functional consequences of a loss of enzyme activity but not RCC binding, we targeted ACD2** to *acd2* chloroplasts (*acd2*/c-ACD2**) and mitochondria (*acd2*/m-ACD2**), respectively (Figure 5a). Targeting ACD2** either to chloroplasts or mitochondria did not alter the protoplast viability (Figure 5b) or the cell death initiation or progression relative to *acd2* in any of the 72 plants analyzed from each targeted line. Mitochondrial H_2O_2 and $^1O_2$ were also not altered in *acd2*/m-ACD2** or *acd2*/c-ACD2** compared with *acd2* (Figure S6). Thus, the cytoprotective function of ACD2 is dependent on its catalytic activity.

Targeting ACD2 to either chloroplasts or mitochondria reduces the accumulation of chlorophyll catabolites in *acd2*

Cell death in *acd2* correlates with the accumulation of RCC and RCC-like pigments, which can accumulate in dark-incubated leaves (Pruzinska *et al.*, 2007). The production of c-ACD2 or m-ACD2 in *acd2* resulted in reduced RCC in the dark-incubation assay, albeit c-ACD2 was more effective at reducing RCC than m-ACD2 (Figure 6a). In contrast, RCC levels were high in *acd2*/c-ACD2** and *acd2*/m-ACD2** plants that were not rescued (Figure 6a). The ability of m-ACD2 to cause reduced RCC accumulation probably results from the movement of RCC from chloroplasts to mitochondria (see Discussion).

Red chlorophyll catabolite is converted to non-fluorescent chlorophyll catabolite (NCC) isomers either enzymatically or non-enzymatically. The ratio of isomers is diagnostic of the mechanism of NCC formation. NCC3, NCC5 and their respective epimers (NCC3′ and NCC5′) occur in *acd2* leaves as a result of the non-enzymatic conversion of RCC (Pruzinska *et al.*, 2007). Complementation of *acd2* with ACD2 results in the loss of NCC3′ and NCC5′ (Pruzinska *et al.*, 2007). As shown in Figure 6(b), the ratios of NCC stereoisomers (NCC-3′/NCC-3; NCC-5′/NCC-5) were reduced in *acd2*/m-ACD2 and *acd2*/c-ACD2 plants, but not in the *acd2*/c-ACD2** and *acd2*/m-ACD2** plants (Figure 6c). Thus, ACD2 shows RCC reductase-like activity, which depends on the catalytic site, when targeted to either chloroplasts or mitochondria.

Genetic evidence that an ACD2 substrate(s) or a signal that induces the substrate can move between cells

Suppression of *acd2* PCD by mitochondria-targeted ACD2 is consistent with a pro-death ACD2 substrate migrating from

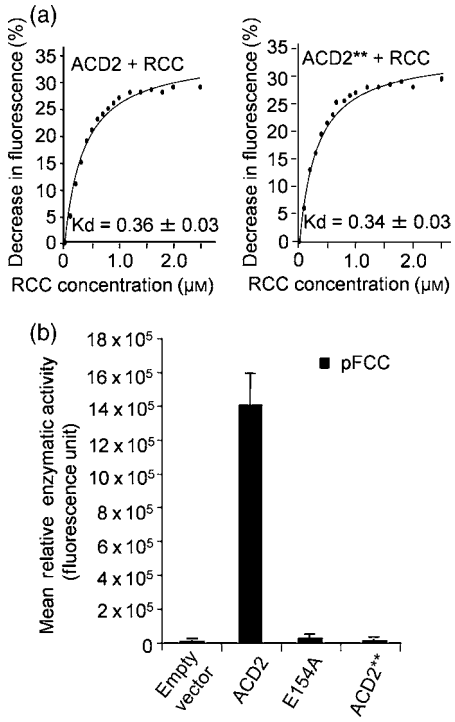

Figure 4. Biochemical characterization of ACD2.
(a) Quenching of endogenous fluorescence of purified wild-type ACD2$^{40–319}$ and ACD2**$^{40–319}$ (E154AD291H) protein, respectively, by red chlorophyll catabolite (RCC). The percentage (%) decrease in intrinsic fluorescence of the respective proteins caused by RCC binding was plotted against the concentration of RCC, and the K_d was found to be 0.36 ± 0.03 μM and 0.34 ± 0.03 μM, respectively. This experiment was performed twice with similar results.
(b) Activity of purified recombinant ACD2, ACD2** or ACD2E154A proteins was assessed in a coupled assay using purified pheophorbide *a* oxygenase (PAO) and co-factors (Pruzinska *et al.*, 2007), and primary fluorescent chlorophyll catabolite (pFCC) was measured by HPLC. As a negative control, the vector protein alone (pQE 30 in *Escherichia coli* M15) was used. Error bars represent SDs (n = 3). This experiment was performed twice with similar results.

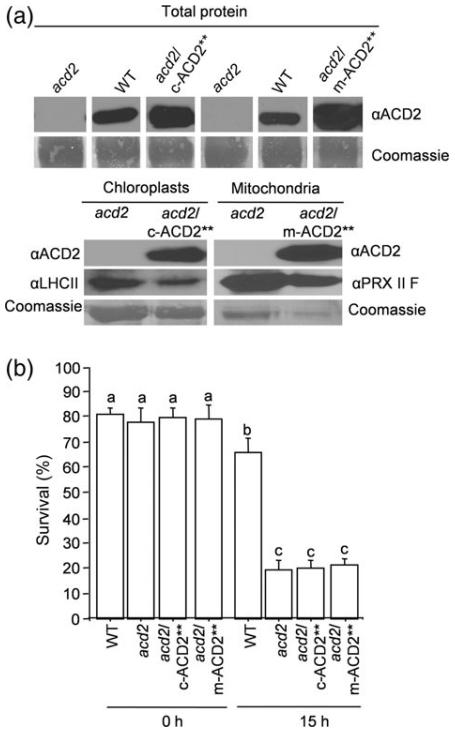

Figure 5. Targeting ACD2** to chloroplasts or mitochondria does not rescue the *acd2* cell death phenotype.
(a) The ACD2 level in total protein extracts (upper panel) and in chloroplasts and mitochondria isolated from the indicated plants was detected by western blot analysis (lower panel). Signals for ACD2 for chloroplast-targeted as well as for mitochondria-targeted plants, along with its controls, are from one continuous membrane (upper panel). Both chloroplast and mitochondrial organelle fractions were qualitatively checked by using chloroplast or mitochondria marker antibodies (LHC II and PRX II F, respectively; lower panel). This experiment was performed twice with similar results.
(b) Protoplasts were exposed to light for 15 h. The percentage (%) of surviving cells in the population was determined. This experiment was performed three times with similar results. The error bars represent SDs (n = 3). Bars with the same letters indicate the lack of differences in values using Fisher's protected least significant difference test test (P > 0.4).

chloroplasts to mitochondria. Possibly, such a pro-death ACD2 substrate(s) (or an inducer of such substrates) could also move from cell to cell, thereby explaining the spreading of the PCD phenotype in *acd2*. Alternatively, an ACD2 substrate might initiate cell death, but spreading might be caused by a separate mobile pro-death signal that indiscriminately affects *acd2* or *ACD2*$^+$ cells.

To distinguish between these possible models, we created mosaic plants with *acd2* sectors next to *ACD2*$^+$ sectors. We generated *acd2* seeds containing a cassette flanked by LOX recombination sites with *ACD2* linked to a gene encoding nuclear-localized GFP that could be excised by CRE recombinase after a transient heat shock (Figure S7a). *acd2* plants carrying this cassette were complemented (Figure S7b). Leaves that were not heat shocked showed GFP throughout the leaves (Figure 7a). A brief heat shock resulted in the creation of various sizes of random sectors lacking GFP, and hence ACD2 (Figure 7b). By visualizing the nuclear-localized GFP, we tracked the presence of ACD2 relative to regions of dying cells.

In 26 mosaic leaves, cell death from leaves on different plants started within a sector lacking ACD2 (Figure 7b), and spread rapidly to areas that lacked ACD2 (Figure 7c–f), but not to GFP$^+$/ACD2$^+$ sectors (Figure 7c–f). When a new lesion started it occurred in another sector that lacked GFP (and ACD2), and extended to cells that lacked GFP (Figure 7e,f). Mosaic leaves retained living cells even 5–7 days after the initiation of a lesion(s). In contrast, in 10 *acd2* leaves closely examined, cell death spread continuously in all directions once it started, and consumed the whole leaf within 3 days (Figure 7h–k). Thus ACD2 acts cell autonomously in whole leaves and can suppress the effects of possible mobile pro-PCD substrate molecules.

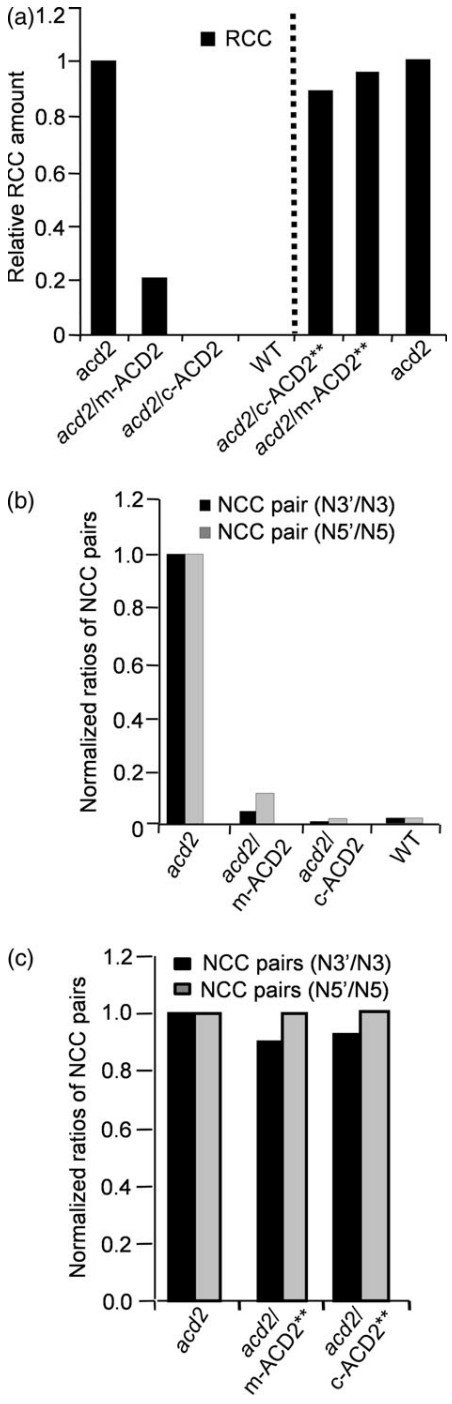

Figure 6. HPLC analysis of chlorophyll catabolites.
(a) Red chlorophyll catabolite (RCC) levels in extracts of detached leaves incubated for 4 days in the dark were quantified by HPLC. Note the relatively higher level of RCC that accumulated in *acd2* leaves. RCC was undetectable in wild-type and *acd2*/c-ACD2 leaves. The quantity of RCC was significantly decreased in *acd2*/m-ACD2 leaves. RCC levels were high in *acd2*/c-ACD2** and *acd2*/m-ACD2** leaves. RCC quantification in *acd2*/c-ACD2** and *acd2*/m-ACD2** leaves was performed separately from *acd2*/m-ACD2 and *acd2*/c-ACD2 extraction.
(b, c) Ratio of non-fluorescent chlorophyll catabolite (NCC) stereoisomers in *acd2*/c-ACD2 and *acd2*/m-ACD2 leaves or in *acd2*/c-ACD2** or *acd2*/m-ACD2** leaves normalized to the content in *acd2*. Note the ratios of NCC stereoisomers were significantly reduced in *acd2*/c-ACD2 and *acd2*/m-ACD2 plants, indicative of ACD2 activity in respective organelles (b). These experiments (a–c) were performed twice with similar results.

In planta PPIX levels are not affected in *acd2* plants even though PPIX binds to ACD2

Exogenous application of PPIX can initiate and accelerate the PCD events in *acd2* (Yao *et al.*, 2004; Yao and Greenberg, 2006). To test whether endogenous PPIX levels are modulated by ACD2, we analyzed its steady-state level in *acd2* leaves using HPLC. There was no difference in the levels of PPIX or other chlorophyll precursors in 15- or 20-day-old wild-type and *acd2* leaves (Figure 8a,b).

Interestingly, plants that over-express ACD2 show less PPIX-induced cell death (Yao and Greenberg, 2006). This might result from the direct binding of PPIX to ACD2. Indeed, recombinant ACD2 (Figure S8) binds to PPIX with a binding constant of 0.31 $\pm$ 0.02 μM (Figure 8c), as determined using a tryptophan fluorescence-quenching assay. Additionally, when ACD2 was purified from *Escherichia coli*, a fraction of the respective proteins already harbored bound PPIX (Figure S9). Thus, ACD2 might protect plants from PPIX by a mechanism that involves direct binding.

DISCUSSION

In leaves, ACD2 is predominantly a chloroplast-localized protein. However, a major consequence of its loss in *acd2* plants is manifested in the production of early mitochondrial ROS, which we showed here significantly contributes to cell death. The fact that infection induces ACD2 to localize to mitochondria as well as chloroplasts was a first hint that ACD2 may also function directly in mitochondria (Yao and Greenberg, 2006). Indeed, targeting ACD2 solely to mitochondria can largely rescue the *acd2* cell death phenotypes, mitochondrial ROS and the accumulation of the ACD2 substrate RCC. As targeting ACD2 solely in chloroplasts also rescues *acd2* phenotypes, we propose that the dynamic localization found in wild-type plants serves as a fail-safe mechanism to suppress spreading cell death during times of infection. In this 'fail-safe' model (Figure S10), infection causes the release of a pro-death ACD2 substrate(s) from chloroplasts. Most substrate molecules can be removed by ACD2 in chloroplasts, but some may escape chloroplasts and affect mitochondria through metabolite channeling or the close proximity of chloroplasts and mitochondria (Yao and Greenberg, 2006). By targeting some ACD2 to mitochondria during infection, the substrate molecules can be removed to minimize lethal bursts of $^1O_2$ and H_2O_2. A likely candidate for a pro-death ACD2 substrate is RCC, which we showed can produce light-dependent $^1O_2$ *in vitro*.

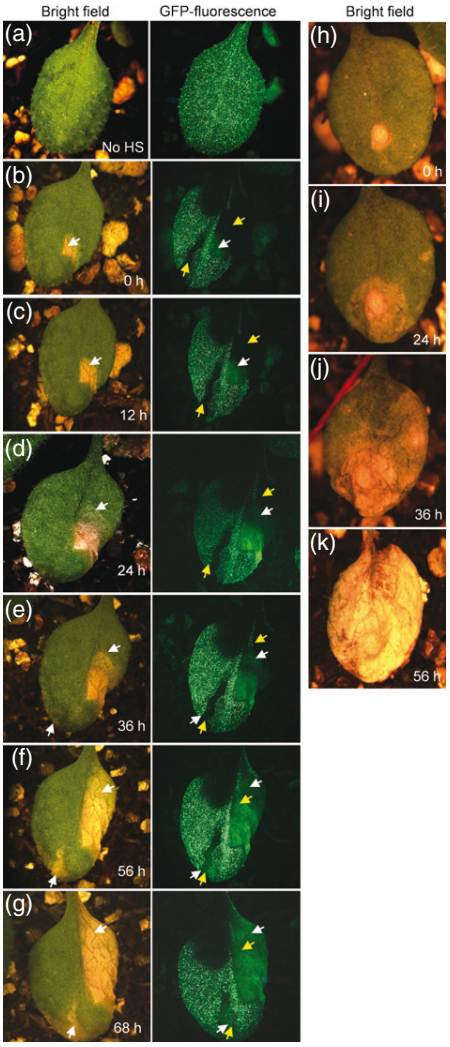

Figure 7. ACD2 acts cell autonomously in mosaic plants.
Homozygous *acd2* plants carrying both heat shock-inducible CRE recombinase and LOX recombination sites flanking genes encoding ACD2 and nuclear GFP were used to study cell death patterns. The initiation and spreading of cell death lesions were followed in single leaves over 10–12-h time intervals. This experiment was performed three times with similar results. Twenty-six leaves were analyzed. Lesions in panels 'b' and 'h' were arbitrarily assigned time 0 h.
(a) Non heat-shocked (No HS) control plants showed GFP throughout the leaf.
(b) Leaves showing GFP^- sectors after heat-shock treatment. The yellow arrows mark the GFP^- sector area. The white arrow marks the initiation of cell death. Note the cell death areas under the GFP channel gave autofluorescence that was lighter in color compared with GFP, and also lacked the nuclear localization seen with GFP fluorescence.
(c, d) Note the spreading of cell death lesions (follow the spreading of the lesion in the bright-field image and the autofluorescence area in the GFP^- sectors). However, the spreading of the lesion was contained in the area with GFP.
(e) A second lesion started in the other GFP^- sector (follow the white arrow in the bright field as well as the GFP channel).
(f, g) Spreading of the new lesion in the GFP^- sector (f). (g) Note that the leaf is alive after 68 h of light exposure.
(h–k) Initiation and spreading of cell death in *acd2*. Note that the cell death spreads continuously from its starting point to consume the whole leaf. Although panel (k) shows a completely dead leaf at 56 h, this leaf was dead by 48 h.

The above model invokes movement of an ACD2 substrate(s) out of chloroplasts, and requires that ACD2 has an enzymatic function in mitochondria. The movement of substrate is plausible, as RCC has been found in vacuoles (Pruzinska *et al.*, 2007), and the main early dysfunction in *acd2* occurs in mitochondria (Yao *et al.*, 2004; Yao and Greenberg, 2006). Mosaic analysis also supports the possibility that a pro-death ACD2 substrate is mobile. Cells containing ACD2 can stem the spread of cell death initiated in *acd2* cells of mosaic leaves, implying that a pro-death ACD2 substrate is mobile. However, we cannot rule out that *acd2* cells in fact produce a signal that moves to neighbors, where it then induces the ACD2 substrate. Our model is also consistent with the phenotype of ACD2-overexpressing plants. Such plants show reduced cell death spreading during infection, indicating that in wild-type plants the level of ACD2 is limiting (Yao and Greenberg, 2006).

An alternative 'threshold' model (Figure S10) can also explain our observation that ACD2 targeted to either chloroplasts or mitochondria rescues *acd2* mutants. In this model, different pro-death ACD2 substrates originate in both organelles. The accumulation of both substrates is necessary to trigger cell death by surpassing a pro-death threshold; therefore targeting ACD2 to either organelle can suppress cell death. This model does not rule out the possibility that substrates may migrate from one organelle to another. Indeed, RCC levels are reduced in ACD2 mitochondrial-targeted plants, implying that the RCC, which originates from chlorophyll in chloroplasts, can migrate from chloroplasts to mitochondria. We previously found that ACD2 is targeted to both mitochondria and plastids in roots. *acd2* root cells, which have no chlorophyll, also have mitochondrial ROS and show cell death (Yao and Greenberg, 2006), indicating there is likely to be at least one non-RCC substrate for ACD2, possibly arising from structurally similar bilin-derived molecules. Indeed, ACD2 is related to ferredoxin-dependent bilin reductases such as phytochromobilin reductase, and shares with them a few highly conserved amino acids (Frankenberg *et al.*, 2001). A prediction of this model is that mitochondrial-derived substrates should accumulate in *acd2*.

Distinguishing between these models will require the development of improved analytical and fractionation methods optimized for the analysis of metabolites that may be labile.

How might ACD2 protect mitochondria from chloroplast-derived substrate molecules? Considering its enzymatic mechanism in leaves, ACD2 converts RCC to pFCC without any co-factors to effect the transfer of electrons to RCC (Rodoni *et al.*, 1997; Wuthrich *et al.*, 2000). Instead, the electron transfer is thought to occur from ferredoxin (Oberhuber and Krautler, 2002). It is likely that ACD2 can use a mitochondrial ferredoxin to support the catalysis of RCC (or

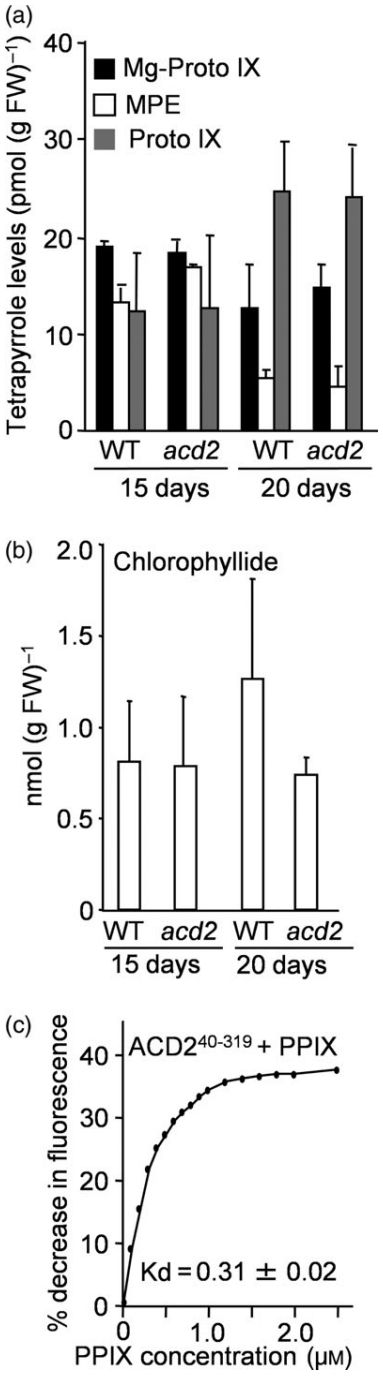

Figure 8. ACD2 does not affect the steady-state level of protoporphyrin IX *in planta*, although ACD2 binds to protoporphyrin IX *in vitro*.
Steady-state levels of chlorophyll precursors were measured from leaves of the wild type (WT) and *acd2* plants grown for 15 or 20 days. This experiment was performed twice with similar results. Error bars represent SDs (n = 2).
(a) Mg-protoporphyrin IX (Mg-Proto IX), Mg-protoporphyrin IX monomethyl ester (MPE) and protoporphyrin IX (PPIX) contents in WT and *acd2* plants.
(b) Chlorophyllide contents in WT and *acd2* plants.
(c) Quenching of ACD2 protein fluorescence by PPIX. The percentage (%) decrease in intrinsic fluorescence of purified ACD2 protein, resulting from PPIX binding, was plotted against the concentration of PPIX, and the K_d was found to be 0.31 ± 0.02 μM. This experiment was performed three times with similar results.

some other ACD2 substrate). The activity of ACD2 inside mitochondria correlates with the RCC reductase activity: its binding to RCC is not sufficient to rescue the PCD phenotype.

In addition to reducing RCC levels, ACD2 can protect against cell death and mitochondrial H_2O_2 induced by the exogenous application of PPIX (Yao and Greenberg, 2006). Interestingly, plants have a translocator in their mitochondrial outer membrane that can transport PPIX into mitochondria (Lindemann *et al.*, 2004). Additionally, PPIX treatment also induces mitochondrial targeting of ACD2 (Yao and Greenberg, 2006). We showed here that ACD2 can bind PPIX as well as its known substrate RCC. However, the loss of ACD2 does not affect steady-state levels of PPIX. ACD2 may affect the ability of PPIX to become photoactivated *in vivo*, similar to water-soluble chlorophyll binding protein, which binds to free chlorophyll molecules and reduces $^1O_2$ production (Schmidt *et al.*, 2003). Interestingly, recombinant ACD2 co-elutes with a small fraction of PPIX, which suggests the possibility of ACD2 binding to PPIX *in planta*. It is also possible that ACD2 may affect PPIX mobility after binding to it, which might lead to decreased ROS production inside mitochondria.

How might the accumulation or localized release of ACD2 substrate molecules contribute to cell death? Analysis of *acd2* mutant protoplasts has strongly implicated mitochondrial ROS as contributing to cell death. Interestingly, mitochondrial ROS occurs in at least two light-dependent waves, an early $^1O_2$ burst and a later, independently-generated, H_2O_2 burst. $^1O_2$ could result from the direct photoactivation of an ACD2 substrate; indeed, *in vitro* RCC can generate $^1O_2$. Although $^1O_2$ quenchers are present in plants they mainly reside in chloroplasts (Krieger-Liszkay and Trebst, 2006; Triantaphylides and Havaux, 2009), leaving mitochondria vulnerable. The generation of H_2O_2 might result from a different mechanism. Chlorophyll degradation intermediates may directly produce H_2O_2 inside the mitochondria by inhibiting the mitochondrial electron transport chain. Indeed, a pheophorbide *a* derivative inhibits the electron transport chain and produces H_2O_2 in a light-dependent manner in human cell lines (Kim *et al.*, 2004). The defense signal salicylic acid (SA) that accumulates in *acd2* plants (Greenberg *et al.*, 1994) may also contribute to H_2O_2 production. High SA can block mitochondrial electron transport flow, resulting in ROS production (Norman *et al.*, 2004).

Production of various kinds of ROS in different organelles may contribute to cell death through different pathways. Although *acd2* mutants accumulate chloroplastic H_2O_2, this H_2O_2 pool forms later than the mitochondrial pool and does not contribute to *acd2* cell death (Yao and Greenberg, 2006). Might other chloroplast ROS contribute to cell death in

acd2? A possible candidate could be $^1O_2$. However, no $^1O_2$ was detected in *acd2* chloroplasts. Additionally, triple mutants of *acd2 exe1 exe2* and *acd2 cry1 cry2* did not show cell death suppression, even though *exe1 exe2* and *cry1* mutations block cell death through chloroplast $^1O_2$ accumulation in *flu* mutants that accumulate a photo-activatable chlorophyll precursor (Wagner *et al.*, 2004; Danon *et al.*, 2006; Lee *et al.*, 2007).

In summary, this study highlights the involvement and importance of mitochondrial events in cell death control in plants, and suggests that the location of ROS within cells can cause cell death by different mechanisms.

EXPERIMENTAL PROCEDURES

Materials

All *Arabidopsis thaliana* plant materials used herein were in the Columbia background. *acd2-2*, *phyA-211*, *phyB*, *cry1* and *cry2* were described previously (Greenberg *et al.*, 1994; Lin *et al.*, 1995, 1998; Neff *et al.*, 1998). T-DNA insertion lines for *executer1* (*exe1*) and *executer2* (*exe2*) (SALK_002088 and SALK_012127, respectively) were obtained from the Arabidopsis Biological Resource Center (http://abrc.osu.edu). We generated and validated double and triple mutants carrying *acd2* and other mutants by crossing plants and using appropriate primers (Table S3). Plants were grown in soil [1:1 mix of C2 (Fafard, http://www.fafard.com) and Metromix 200 (Sun Gro Horticulture, http://www.sungro.com)] in a growth room with a light intensity of 288 μmoles photons m^{-2} s^{-1} (400 W metal halide and 400 W sodium bulbs) and a 16-h light/8-h dark photoperiod at 22 ± 2°C and 50–60% relative humidity.

The primers used in this study are shown in Table S3. PPIX-disodium salt was purchased from Frontier Scientific (http://www.frontiersci.com). TEMP, NATA (*N*-acetyltryptophanamide) and vitamin B6 (pyridoxine) was obtained from Sigma-Aldrich (http://www.sigmaaldrich.com). CM-H_2DCFDA (5- and 6-chloromethyl-2′,7′-dichlorodihydrofluorescein diacetate, acetyl ester), SOSG (singlet oxygen sensor green) and MitoTracker Red CMXRos (CMXRos) were obtained from Molecular Probes (http://www.invitrogen.com).

Generation of constructs and transgenic plants

The *At*tAPX cDNA (Jespersen *et al.*, 1997) lacking the chloroplast transit peptide sequences (78 aa; 234 bp) was PCR amplified from an Arabidopsis cDNA pool, restriction digested by *Bam*HI and *Eco*RI, and ligated into the pCB302-2 (Xiang *et al.*, 1999) vector under the control of the 35S promoter to generate the construct for mitochondrial targeting. The pCB302-2 vector carries the β-ATPase transit peptide sequence for mitochondria targeting (Xiang *et al.*, 1999). Similarly, the human catalase cDNA lacking the peroxisome-targeting signal was PCR amplified from the pCAGGS-catalase plasmid (Schriner *et al.*, 2005) using specific primers. The resulting PCR product was digested by *Sma*I and ligated into pCB302-2 to generate the construct for mitochondrial targeting. An ACD2 cDNA fragment lacking 39 amino acids of chloroplast transit peptide sequences ($ACD2^{40-319}$) and the point-mutated $ACD2^{40-319}$ (Glu154 > Ala154, and Asp291 > His291; see Appendix S1) fragments were PCR amplified from the pBI121-ACD2 plasmid (Mach *et al.*, 2001) using different pairs of primer sets. The resulting PCR products were digested with *Bam*HI and *Eco*RI and ligated into pCB302-1 or pCB302-2 to generate the constructs to target chloroplasts or mitochondria, respectively. The vector pCB302-1 carries the Rubisco small subunit transit peptide sequence for chloroplast targeting (Xiang *et al.*, 1999). Two sets of constructs were used for the mosaic analysis experiment (see Appendix S1). All constructs were introduced into *Agrobacterium* (GV3101), which were used to transform Arabidopsis using the floral-dip method (Clough and Bent, 1998). The homozygous lines were screened in the T_2 generation, confirmed by western blot analysis and used for further analysis.

Protoplast preparation, treatments and live imaging of ROS production

Leaf protoplasts were isolated in the dark from 20-day-old plants, exposed to light (100 μmoles photons m^{-2} s^{-1} at 22 ± 2°C), and the percentage of surviving protoplasts was determined by fluorescein diacetate (500 ng ml^{-1}) staining using a hemocytometer (Hausser Scientific Company, http://www.hausserscientific.com), as described by Yao *et al.* (2004).

Live imaging of ROS production from protoplasts

Confocal images were collected by using a laser-scanning confocal microscope (TCS SP2 AOBS; Leica, http://www.leica.com) with a 63× (numerical aperture 1.4) glycerol objective. After the light treatment, protoplasts were double stained with CMXRos (500 nM) and CM-H_2DCFDA (1 μM) to label the mitochondria and to detect the H_2O_2, respectively. For $^1O_2$ detection, protoplasts were incubated with the SOSG (100 μM) in the dark for 1 h, then washed with the protoplast suspension buffer and exposed to light for 30 min, double stained with CMXRos. The CM-H_2DCFDA and SOSG signals were visualized with excitation at 488 nm (emission: 498–532 nm). CMXRos signals were visualized with excitation at 543 nm (emission: 495–635 nm), and chloroplast autofluorescence (488 nm excitation) was visualized at 738–793 nm.

Flow cytometry

Flow cytometry (FACScan; BD Biosciences, http://www.bdbiosciences.com) was used to determine the mean fluorescence intensity (MFI) of cells stained with the fluorescent dyes H_2DCFDA and SOSG. A solid-state 488-nm laser was used for triggering and light scatter parameters. Forward scatter, which gives a rough estimate of cell size, and side scatter, which correlates with internal complexity/granularity, were both measured. From these parameters a 'live' gate was made to exclude cell debris. Light-treated protoplasts were incubated with 5 μM of H_2DCFDA and 100 μM of SOSG at room temperature (22°C) in the dark for 30 min and 1 h, respectively, washed twice with protoplast re-suspension solution and then subjected to flow analysis. Unstained protoplasts were used as autofluorescence controls. For each sample, 5000 protoplasts were gated and the MFI was measured using FLOWJO (Tree Star, http://www.treestar.com).

Cellular fractionation

Chloroplasts and mitochondria were isolated from 18–20-day-old Arabidopsis plants. Intact chloroplasts were purified using Percoll gradients as described by Lamppa (1995) with modification. Instead of one Percoll gradient, two Percoll gradients were run to purify the chloroplasts. Intact mitochondria were purified on Percoll gradients as described (Meyer and Millar, 2008). Organelle purity and/or contamination were assessed by western blot analysis using organelle-specific marker antibodies.

Protein extraction and western blot analysis

Protein extraction and western blot analysis were performed as described previously (Mach *et al.*, 2001; Appendix S1).

Binding assays

Intrinsic fluorescence measurements were performed at 22°C on a FluoroMax-3 spectrofluorimeter (Horiba, http://www.horiba.com), using an excitation wavelength of 296 nm. The emission spectra were collected from 310 to 460 nm. The proteins (ACD2 and ACD2**; 40–319 aa) were diluted to a concentration of 0.1 μM in a buffer containing 50 mM Na_2HPO_4 (pH 8.0) and 25 mM NaCl. Stock solutions of PPIX and RCC were prepared as described by Shepherd *et al.* (2007) and Sugishima *et al.* (2010). Quenching experiments with PPIX or RCC were performed by the addition of small aliquots of concentrated stock solutions to protein samples. To correct for the increased sample absorption caused by the increased concentration of pigments in the sample, we measured the influence of these compounds on the fluorescence emission of the model compound NATA (0.1 μM; λ_{ex} = 296 nm and λ_{em} = 332 nm) at each pigment concentration. The effect of pigments was linear with respect to concentration, and the relevant values were subtracted from those obtained with ACD2 and ACD2**. The data were analyzed as described by Solomaha and Palfrey (2005).

Pigment analysis

Chlorophyll biosynthetic intermediates, from leaves of wild-type and *acd2* plants, were extracted and the chromatographic separation was performed by HPLC as described by Papenbrock *et al.* (2000).

Excised leaves were incubated in dark for 4–5 days and their tetrapyrrolic chlorophyll catabolites were extracted, and chromatographic separation was performed by HPLC as described by Pruzinska *et al.* (2005, 2007).

Enzyme assays

The coupled PAO/ACD2 activity assay was performed as described by Hortensteiner *et al.* (1995), Wuthrich *et al.* (2000) and Pruzinska *et al.* (2005).

RCC synthesis

Red chlorophyll catabolite was synthesized and validated as described previously (Krautler *et al.*, 1997; Sugishima *et al.*, 2010).

Spin-trapping of $^1O_2$ by TEMP

Spin-trapping assays were performed in 10 mM sodium phosphate, pH 7.8, buffer with pigments (20 μM RCC, 5 μM of PPIX), 100 mM TEMP and methanol (ultrapure), in a final concentration of 3.5% (v/v). Samples were illuminated (350 μmol photons m^{-2} s^{-1}) for a given time and their EPR signals were measured with a Bruker ESP 300 spectrometer as described by Schmidt *et al.* (2003).

ACKNOWLEDGEMENTS

We thank Jocelyn Malamy, Gayle Lamppa, Eric Ottesen, Mark Shepherd, Robert M. Larkin, Christian Fankhauser, Junichi Taira and Greenberg lab members for helpful discussions. We thank Vytas Bindokas, Christine Labno, Ryan Duggan, Elena Solomaha and Eugene Barth for technical assistance. We thank Ron Mittler, Karl-Josef Dietz, Roberto Bassi, Peter Rabinovitch, Leslie E. Sieburth, Patricia Zambryski, Joanne Chory and Chentao Lin for reagents. This work was supported by grants from the United States Department of Agriculture (2006-35100-17265) and National Institutes of Health (R01 GM54292) to JTG, and by grants from the Swiss National Science Foundation and the Swiss National Center of Competence in Research Plant Survival to SH.

SUPPORTING INFORMATION

Additional Supporting Information may be found in the online version of this article:

Figure S1. Plants with HsCAT targeted to mitochondria do not accumulate HsCAT in chloroplasts.

Figure S2. Superoxide levels in *acd2* and wild-type protoplasts.

Figure S3. Singlet oxygen production by red chlorophyll catabolite (RCC).

Figure S4. Mutations in *executers* and photoreceptors do not affect the survival of light-treated *acd2* protoplasts.

Figure S5. ACD2 in mitochondria or chloroplasts significantly suppresses the ROS production in *acd2* protoplasts.

Figure S6. Targeting of ACD2** either to chloroplasts or mitochondria does not reduce ROS generation in *acd2* protoplasts.

Figure S7. Cre-Lox construct and characterization of the *acd2* transgenic plants.

Figure S8. Expression and purification of ACD2 from *Escherichia coli*.

Figure S9. PPIX is present in the methanol extract of recombinant $ACD2^{40–319}$.

Figure S10. How and where does ACD2 function to protect cells?

Table S1. Leaf cell death phenotype in *acd2*/m-tAPX and *acd2*/m-HsCAT plants.

Table S2. Impact of targeting ACD2 to different organelles on the cell death phenotype of *acd2*.

Table S3. Primers used in this study.

Appendix S1. Protein extraction and western blot analysis; purification of recombinant ACD2; generation of constructs and transgenic plants for mosaic analysis; superoxide levels in protoplasts isolated from wild-type and *acd2* leaves.

Please note: As a service to our authors and readers, this journal provides supporting information supplied by the authors. Such materials are peer-reviewed and may be re-organized for online delivery, but are not copy-edited or typeset. Technical support issues arising from supporting information (other than missing files) should be addressed to the authors.

REFERENCES

Arpagaus, S., Rawyler, A. and Braendle, R. (2002) Occurrence and characteristics of the mitochondrial permeability transition in plants. *J. Biol. Chem.* **277**, 1780–1787.

Balk, J. and Leaver, C. (2001) The PET1-CMS mitochondrial mutation in sunflower is associated with premature programmed cell death and cytochrome c release. *Plant Cell*, **13**, 1803–1818.

Bilski, P., Li, M.Y., Ehrenshaft, M., Daub, M. and Chignell, C.F. (2000) Vitamin B6 (pyridoxine) and its derivatives are efficient singlet oxygen quenchers and potential fungal antioxidants. *Photochem. Photobiol.* **71**, 129–134.

op den Camp, R.G., Przybyla, D., Ochsenbein, C. *et al.* (2003) Rapid induction of distinct stress responses after release of singlet oxygen in Arabidopsis. *Plant Cell*, **15**, 2320–2332.

Clough, S.J. and Bent, A.F. (1998) Floral dip: a simplified method for Agrobacterium-mediated transformation of *Arabidopsis thaliana*. *Plant J.* **16**, 735–743.

Crompton, M. (1999) The mitochondrial permeability transition pore and its role in cell death. *Biochem. J.* **341**, 233–249.

Danon, A., Miersch, O., Felix, G., Camp, R.G. and Apel, K. (2005) Concurrent activation of cell death-regulating signaling pathways by singlet oxygen in *Arabidopsis thaliana*. *Plant J.* **41**, 68–80.

Danon, A., Coll, N.S. and Apel, K. (2006) Cryptochrome-1-dependent execution of programmed cell death induced by singlet oxygen in *Arabidopsis thaliana*. *Proc. Natl Acad. Sci. USA*, **103**, 17036–17041.

Finkemeier, I., Goodman, M., Lamkemeyer, P., Kandlbinder, A., Sweetlove, L.J. and Dietz, K.J. (2005) The mitochondrial type II peroxiredoxin F is essential for redox homeostasis and root growth of *Arabidopsis thaliana* under stress. *J. Biol. Chem.* **280**, 12168–12180.

Flors, C., Fryer, M.J., Waring, J., Reeder, B., Bechtold, U., Mullineaux, P.M., Nonell, S., Wilson, M.T. and Baker, N.R. (2006) Imaging the production of

singlet oxygen in vivo using a new fluorescent sensor, Singlet Oxygen Sensor Green. *J. Exp. Bot.* **57**, 1725–1734.

Frankenberg, N., Mukougawa, K., Kohchi, T. and Lagarias, J.C. (2001) Functional genomic analysis of the HY2 family of ferridoxin-dependent bilin reductases from oxygenic photosynthetic organisms. *Plant Cell*, **13**, 965–978.

Gollmer, A., Arnbjerg, J., Blaikie, F.H., Pedersen, B.W., Breitenbach, T., Daasbjerg, K., Glasius, M. and Ogilby, P.R. (2011) Singlet Oxygen Sensor Green: photochemical behavior in solution and in a mammalian cell. *Photochem. Photobiol.* **87**, 671–679.

Greenberg, J.T. and Ausubel, F.M. (1993) Arabidopsis mutants compromised for the control of cellular damage during pathogenesis and aging. *Plant J.* **4**, 327–341.

Greenberg, J.T., Guo, A., Klessig, D.F. and Ausubel, F.M. (1994) Programmed cell death in plants, a pathogen-triggered response activated coordinately with multiple defense functions. *Cell*, **77**, 551–563.

Hortensteiner, S., Vicentini, F. and Matile, P. (1995) Chlorophyll breakdown in senescent cotyledons of rape, *Brassica napus* L.: enzymatic cleavage of pheophorbide *a in vitro*. *New Phytol.* **129**, 237–246.

Hu, G., Yalpani, N., Briggs, S.P. and Johal, G.S. (1998) A porphyrin pathway impairment is responsible for the phenotype of a dominant disease lesion mimic mutant of maize. *Plant Cell*, **10**, 1095–1105.

Ishikawa, A., Okamoto, H., Iwasaki, Y. and Asahi, T. (2001) A deficiency of coproporphyrinogen III oxidase causes lesion formation in Arabidopsis. *Plant J.* **27**, 89–99.

Jespersen, H.M., Kjaersgard, I.V., Ostergaard, L. and Welinder, K.G. (1997) From sequence analysis of three novel ascorbate peroxidase from *Arabidopsis thaliana* to structure, function and evolution of seven type of ascorbate peroxidase. *Biochem. J.* **326**, 305–310.

Jones, A. (2000) Does the plant mitochondria integrate cellular stress and regulate programmed cell death? *Trends Plant Sci.* **5**, 225–230.

Kim, C.S., Lee, C.H., Lee, P.H. and Han, S. (2004) Inactivation of mitochondrial electron transport by photosensitization of a pheophorbide *a* derivative. *Mol. Cells*, **17**, 347–352.

Krautler, B., Muhlecker, W., Anderl, M. and Gerlach, B. (1997) Breakdown of chlorophyll: partial synthesis of a putative intermediary catabolite. *Helv. Chim. Acta*, **80**, 1355–1362.

Krieger-Liszkay, A. and Trebst, A. (2006) Tocopherol is the scavenger of singlet oxygen produced by the triplet states of chlorophyll in the PSII reaction center. *J. Exp. Bot.* **57**, 1677–1684.

Lam, E., Kato, N. and Lawton, M. (2001) Programmed cell death, mitochondria and plant hypersensitive response. *Nature*, **411**, 848–853.

Lamppa, G.K. (1995) *In vitro* import of proteins into chloroplasts. In *Methods in Plant Molecular Biology* (Maliga, P., Klsessig, D.F., Cashmore, A.R., Gruissem, W. and Varner, J.E., eds). Plainview, NY: Cold Spring Harbor Lab Press, pp. 141–172.

Lee, K.P., Kim, C., Landgraf, F. and Apel, K. (2007) Executer1- and Executer 2-dependent transfer of stress-related signals from the plastid to nucleus of *Arabidopsis thaliana*. *Proc. Natl Acad. Sci. USA*, **104**, 10270–10275.

Lin, C., Robertson, D.E., Ahmad, M., Raibekas, A.A., Jorns, M.S., Dutton, P.L. and Cashmore, A.R. (1995) Association of flavin adenine dinucleotide with the Arabidopsis blue light receptor CRY1. *Science*, **269**, 968–970.

Lin, C., Yang, H., Guo, H., Mockler, T., Chen, J. and Cashmore, A.R. (1998) Enhancement of blue-light sensitivity of Arabidopsis seedlings by a blue light receptor cryptochrome 2. *Proc. Natl Acad. Sci. USA*, **95**, 2686–2690.

Lindemann, P., Koch, A., Degenhardt, B., Hause, G., Grimm, B. and Papadopoulos, V. (2004) A novel *Arabidopsis thaliana* protein is a functional peripheral-type benzodiazepine receptor. *Plant Cell Physiol.* **45**, 723–733.

Mach, J.M., Castillo, A.R., Hoogstraten, R. and Greenberg, J.T. (2001) The Arabidopsis accelerated cell death gene *ACD2* encodes red chlorophyll catabolite reductase and suppresses the spread of disease symptoms. *Proc. Natl Acad. Sci. USA*, **98**, 771–776.

Meyer, E.H. and Millar, A.H. (2008) Isolation of mitochondria from plant culture. *Methods Mol. Biol.* **425**, 163–169.

Moller, I.M. (2001) Plant mitochondria and oxidative stress: electron transport, NADPH turnover, and metabolism of reactive oxygen species. *Annu. Rev. Plant Physiol. Plant Mol. Biol.* **52**, 561–591.

Mur, L.A., Aubry, S., Mondhe, M. *et al.* (2010) Accumulation of chlorophyll catabolites photosensitizes the hypersensitive response elicited by *Pseudomonas syringae* in Arabidopsis. *New Phytol.* **188**, 161–174.

Neff, M.M., Neff, J.D., Chory, J. and Pepper, A.E. (1998) dCAPS, a simple technique for the genetic analysis of single nucleotide polymorphisms: experimental applications in *Arabidopsis thaliana* genetics. *Plant J.* **14**, 387–392.

Norman, C., Howell, K.A., Milar, A.H., Whelan, J.M. and Day, D.A. (2004) Salicylic acid is an uncoupler and inhibitor of mitochondrial electron transport. *Plant Physiol.* **134**, 492–501.

Oberhuber, M. and Krautler, B. (2002) Breakdown of chlorophyll: electrochemical bilin reduction provides synthetic access to fluorescent chlorophyll catabolites. *Chem. Bio. Chem.* **3**, 104–107.

Papenbrock, J., Mock, H., Tanaka, R., Kruse, E. and Grimm, B. (2000) Role of magnesium chelatase activity in the early steps of the tetrapyrrole biosynthetic pathway. *Plant Physiol.* **122**, 1161–1170.

Pruzinska, A., Anders, I., Tanner, G., Roca, M. and Hortensteiner, S. (2003) Chlorophyll breakdown: pheophorbide *a* oxygenase is a Rieske-type iron-sulfur protein, encoded by the accelerated cell death 1 gene. *Proc. Natl Acad. Sci. USA*, **100**, 15259–15264.

Pruzinska, A., Tanner, G., Aubry, S. *et al.* (2005) Chlorophyll breakdown in senescent Arabidopsis leaves: characterization of chlorophyll catabolites and of chlorophyll catabolic enzymes involved in the degreening reaction. *Plant Physiol.* **139**, 52–63.

Pruzinska, A., Anders, I., Aubry, S., Schenk, N., Tapernoux-Luthi, E., Muller, T., Krautler, B. and Hortensteiner, S. (2007) In vivo participation of red chlorophyll catabolite reductase in chlorophyll breakdown. *Plant Cell*, **19**, 369–387.

Rodoni, S., Muhlecker, W., Anderl, M., Krautler, B., Moser, D., Thomas, H., Matile, P. and Hortensteiner, S. (1997) Chlorophyll breakdown in senescent chloroplasts. Cleavage of pheophorbide a in two enzymic steps. *Plant Physiol.* **115**, 669–676.

Schmidt, K., Fufezan, C., Krieger-Liszkay, A., Satoh, H. and Paulsen, H. (2003) Recombinant water-soluble chlorophyll protein from *Brassica oleracea* var. Botrys binds various chlorophyll derivatives. *Biochemistry*, **42**, 7427–7433.

Schriner, S.E., Linford, N.J., Martin, G.M. *et al.* (2005) Extension of murine life span by overexpression of catalase targeted to mitochondria. *Science*, **308**, 1909–1911.

Shepherd, M., Heath, M.D. and Poole, R.K. (2007) NikA binds heme: a new role for an *Escherichia coli* periplasmic nickel-binding protein. *Biochemistry*, **46**, 5030–5037.

Solomaha, E. and Palfrey, H.C. (2005) Conformational changes in dynamin on GTP binding and oligomerization reported by intrinsic and extrinsic fluorescence. *Biochem. J.* **391**, 601–611.

Sugishima, M., Kitamori, Y., Noguchi, M., Kohchi, T. and Fukuyama, K. (2009) Crystal structure of red chlorophyll catabolite reductase: enlargement of the ferredoxin-dependent bilin reductase family. *J. Mol. Biol.* **389**, 376–387.

Sugishima, M., Okamoto, Y., Noguchi, M., Kohchi, T., Tamiaki, H. and Fukuyama, K. (2010) Crystal structures of the substrate-bound forms of red chlorophyll catabolite reductase: implications for site-specific and stereospecific reaction. *J. Mol. Biol.* **402**, 879–891.

Tiwari, B.S., Belenghi, B. and Levine, A. (2002) Oxidative stress increased respiration and generation of reactive oxygen species, resulting in ATP depletion, opening of mitochondrial permeability transition, and programmed cell death. *Plant Physiol.* **128**, 1271–1281.

Triantaphylides, C. and Havaux, M. (2009) Singlet oxygen in plants: production, detoxification and signaling. *Trends Plant Sci.* **14**, 219–228.

Wagner, D., Przybyla, D., op den Camp, R. *et al.* (2004) The genetic basis of singlet oxygen-induced stress responses of *Arabidopsis thaliana*. *Science*, **306**, 1183–1185.

Wuthrich, K.L., Bovet, L., Hunziker, P.E., Donnison, I.S. and Hortensteiner, S. (2000) Molecular cloning, functional expression and characterisation of RCC reductase involved in chlorophyll catabolism. *Plant J.* **21**, 189–198.

Xiang, C., Han, P., Lutziger, I., Wang, K. and Oliver, D.J. (1999) A mini binary vector series for plant transformation. *Plant Mol. Biol.* **40**, 711–717.

Yao, N. and Greenberg, J.T. (2006) Arabidopsis ACCELERATED CELL DEATH2 modulates programmed cell death. *Plant Cell*, **18**, 397–411.

Yao, N., Eisfelder, B., Marvin, J. and Greenberg, J.T. (2004) The mitochondrion—An organelle commonly involved in programmed cell death in *Arabidopsis thaliana*. *Plant J.* **40**, 596–610.

Yu, X., Perdue, T., Heimer, Y. and Jones, A. (2002) Mitochondrial involvement in tracheary element programmed cell death. *Cell Death Differ.* **9**, 189–198.

6 - RAFFINOSE DEGRADATION DURING COLD DEACCLIMATION

*At*DIN10: an alkaline α-galactosidase involved in chloroplastic raffinose degradation during cold stress deacclimation

Here, we present evidence that *At*DIN10 is involved in Raf degradation in the chloroplast during cold deacclimation. Our results demonstrate that *At*DIN10 is a chloroplast-localized alkaline α-galactosidase active on Raf and longer chain RFO members. Despite its homology to the rice α-galactosidase OsakαGal, which was shown to be involved in galactolipid degradation during senescence, we could not detect any activity of *At*DIN10 on DGDG. Furthermore, *atdin10* mutants degraded DGDG and MGDG as the wild-type during dark-induced senescence. By contrast, during cold deacclimation, *atdin10* mutants were unable to degrade Raf that accumulated in the chloroplast during the acclimation period.

Bastien Christ[1], Aurélie Egert[1], Stefan Hörtensteiner[2] and Shaun Peters[2]
[1,2] These authors contributed equally to this work

INTRODUCTION

During abiotic stress, plants are known to accumulate compatible solutes, also called osmoprotectants or osmolytes (Rhodes et al., 2004). They are non-toxic molecules that protect and stabilize cellular structures by interacting with membranes, protein complexes or enzymes (Bohnert et al., 1995; Yancey et al., 1982). Chemically, compatible solutes are generally grouped into three classes: (i) betaines, (ii) amino acids-like proline, and (iii) polyols (mannitol, sorbitol, etc.) and non-reducing sugars such as disaccharides (sucrose (Suc) and trehalose) and oligosaccharides (fructans and raffinose (Raf) family of oligosaccharides (RFO)) (Chen and Murata, 2008; Guy et al., 2008; Hare et al., 1998; Penna, 2003; Rontein et al., 2002; Shen et al., 1997; Tarczynski et al., 1993; Verbruggen and Hermans, 2008).

In this study, we focused on Raf catabolism, the most widely spread RFO in the plant kingdom which consists of two galactose (Gal) units linked to Suc via α-1,6-glycosidic linkages. Raf was shown to accumulate in seeds (for a review, see Peterbauer and Richter, 2001). In addition, leaves of Arabidopsis and *Ajuga reptans* have been shown to accumulate Raf during cold stress (Bachmann et al., 1994; Espinoza et al., 2010; Zuther et al., 2004). Raf is thought to be synthesized in the cytosol (Bachmann et al., 1994) and to be mostly transported to the vacuole (Bachmann and Keller, 1995). However, around 20% of total cellular Raf synthesized during cold stress has been shown to accumulate within chloroplasts (Heber, 1959; Santarius and Milde, 1977; Schneider and Keller, 2009). Chloroplastic Raf is thought to protect proteins and thylakoid membranes during stress and to play a role in scavenging ROS (Cacela and Hincha, 2006; Carpenter and Crowe, 1988; Hincha et al., 2003; Lineberger and Steponkus, 1980; Nishizawa et al., 2008). Indeed, suppression of RAF SYNTHASE (RafS) in Arabidopsis revealed that Raf is involved in PSII protection during freezing, corroborating the idea that Raf has a protective role (Knaupp et al., 2011).

Raf catabolism to Suc and Gal is thought to be mediated by acidic and alkaline α-galactosidases (Gao and Schaffer, 1999; Pennycooke et al., 2004, 2003; Peterbauer and Richter, 2001; Smart and Pharr, 1980). During seed imbibition, RFOs, such as Raf, have been shown to be degraded by α-galactosidases (Blöchl et al., 2008, 2007; Peterbauer and Richter, 2001). Even though down-regulation of an α-galactosidase has been shown to enhance freezing tolerance of petunia, little is known about RFO degradation in leaves during stress deacclimation (Pennycooke et al., 2003). In Arabidopsis, increase of alkaline and acidic α-galactosidase activities is correlated with a decrease of Raf amounts during cold stress recovery, suggesting that α-galactosidases play an important role in Raf degradation (Aurélie Egert, Shaun Peters and Felix Keller, unpublished data).

This study focuses on the analysis of Arabidopsis DARK INDUCIBLE 10 (*At*DIN10; AT5g20250), an alkaline α-galactosidase. *DIN* genes were first identified by their transcript up-regulation in cotyledons of radish seedlings that were transferred to the dark (Azumi and Watanabe, 1991; Nozawa et al., 1999). Arabidopsis *DIN* genes have also been identified by their up-regulation in dark-incubated and senescent leaves (Fujiki et al., 2001). Moreover, expression of several *DIN* genes seems to depend, at least in part, on cellular sugar levels. Indeed, exogenous application of sugar suppressed DIN2, 6, 9, 10 and 11 up-regulation during dark incubation of leaves, and sugar starvation triggered DIN1, 2, 3, 4, 6, 9 and 10 expression in Arabidopsis cell suspension cultures (Fujiki et al., 2001, 2000). Based on protein sequence, *At*DIN10 is similar to SEED IMBIBITION PROTEINS (SIPs), sharing 48% identity to the *Cicer arietum* SIP protein (X95875), and in Arabidopsis has two homologues, termed *At*SIP1 and *At*SIP2 (Fujiki et al., 2001). *At*SIP2 was shown to be an alkaline α-galactosidase with a substrate specificity for Raf (Peters et al., 2010). However, suppression of *At*SIP2 does not affect Raf degradation during cold deacclimation (Aurélie Egert, Shaun Peters and Felix Keller, unpublished data). Thus, *At*SIP2 has been proposed to participate in phloem unloading due to its apparent sink-specific expression pattern (Peters et al., 2010). *At*SIP1, which is specific for stachyose (Sta), an RFO tetrasaccharide, and galactinol (Gol), the galactosyl donor for the synthesis of raffinose, shows a similar expression pattern as *At*SIP2 but at a lower level (Aurélie Egert, Shaun Peters and Felix Keller, unpublished data). *At*SIP1 is thought to hydrolyze Sta in seeds during germination.

Here, we present evidence that *At*DIN10 is involved in Raf degradation in the chloroplast during cold deacclimation. *At*DIN10 localizes to the chloroplast, as predicted by the presence of a chloroplast transit peptide at its N-terminus. Recombinant expression in Sf9 insect cells reveals that *At*DIN10 is an alkaline α-galactosidase active on Raf and longer chain RFO members. Despite its homology to the rice α-galactosidase OsakαGal (Lee et al., 2009), which was shown to be involved in galactolipid degradation during senescence, we could not detect any activity of *At*DIN10 on DGDG. Furthermore, two T-DNA insertion lines for *At*DIN10 (*atdin10-1* and *-2*) degraded DGDG and MGDG as the wild-type during dark-induced senescence. In contrast, during cold deacclimation, *atdin10* mutants were unable to degrade Raf that accumulated in the chloroplast during the acclimation period. Collectively, these data indicate that *At*DIN10 is a stroma-localized α-galactosidase involved in Raf degradation during stress recovery.

MATERIAL AND METHODS

Plant material and growth conditions

Arabidopsis thaliana ecotype Columbia-0 (Col-0) was used as the wild type. T-DNA insertion lines were from the following collections: SALK lines (Alonso et al., 2003): *AT5g20250-1* (*atdin10-1*), SALK_130606; *AT5g20250-2* (*atdin10-2*), SALK_066490; *AT5g20250-3* (*atdin10-3*), SALK_035336. SALK lines were obtained from the European Arabidopsis Center, Nottingham, UK. Homozygous plants were identified by PCR using T-DNA specific primers designed with the iSect primers tool of the SALK Institute (http://signal.salk.edu/tdnaprimers.2.html).

Plants were grown on soil in 8 h light:16 h dark (short-day) photoperiods under fluorescent light of 100 µmol photons m^{-2} s^{-1} at 22°C. For senescence induction, leaves from eight-week-old plants were excised and incubated in permanent darkness on wet filter paper for up to 6 d at ambient temperature. For cold acclimation experiments, plants were grown at 21°C for 6 weeks, then acclimated for 7 d at 5°C and finally deacclimated for 7 d at 21°C.

GFP fusion protein analysis

*At*DIN10 was amplified by PCR from full-length cDNA clone pda08032 (RIKEN, Seki et al., 2002) with DIN10_speI_F (5'-GACTAGTATGGCGT-CACAGAGTTGCT-3') and DIN10_speI_R (5'-GACTAGTTAACTCAACTTGGATCAGATGA-3') primers using Expand High Fidelity polymerase (Roche). The PCR fragment was then cloned into the pGEM-T Easy vector and after *Spe*I restriction subcloned into pUC18-spGFP6 (Meyer et al., 2006), thereby producing an N-terminal fusion of *At*DIN10 with GFP. Arabidopsis mesophyll protoplasts were isolated from 6-week-old soil-grown plants as previously described (Christ et al., 2012). TIC110-GFP expressed from pCL60-TIC110-GFP (Schenk et al., 2007) was used as a control for inner chloroplast envelope localization (Felix Kessler, unpublished data; Schenk et al., 2007). Free GFP expressed from empty pUC18-spGFP6 was used as control for cytosolic localization.

Recombinant *At*DIN10 expression in Sf9 insect cells and activity determination

The *At*DIN10 cDNA clone pda08032 was amplified as described above using the coding sequence-specific primers DIN10fwd (5'-ATGACGATTAAACCGGCGGT-3') and DIN10rev (5´-TCATAACTCAACTTGGATC-3'). After cloning in the pGEM-T Easy, *At*DIN10 was subcloned into the pFastBac1 vector using *Not*I. Bacmid construction and expression of *At*DIN10 in Sf9 insect cells were conducted as outlined in the bac-to-bac manual (Invitrogen), using Sf9 cells grown in monolayer cultures. For expression of the recombinant proteins, Sf9 cells were maintained in BD BaculoGold™ TNM-FH Insect medium (BD Biosciences). 72 h after baculovirus infection, Sf9 cells were collected by centrifugation (500*g*, 5 min). Cell pellets were resuspended in 2 ml of extraction buffer (100 mM HEPES-KOH, pH 7.5, 5 mM $MgCl_2$, 1 mM EDTA, 10 mM DTT, 1 mM benzamidine, 1 mM PMSF, 0.05% (v/v) Triton X-100) and homogenized on ice using a Potter homogenizer connected to an electric drill. After centrifugation (12'000*g*, 4°C, 10 min), aliquots (100 µl) of clarified extracts were centrifuge-desalted by gel filtration (1'700*g*, 4°C, 2 min) through Sephadex G-25 fine columns (fine, final bed

volume of 2 ml). The pH optimum of *At*DIN10 was determined by incubating 20 µl of Sf9 crude extract with 20 µl of assay buffer (3 mM of the artificial substrates, para-nitrophenyl-α-D-galactopyranoside (pNPαGal) or pNPβGal, in 100 mM MES-KOH (pH 5.5-6.5), 100 mM HEPES-HCl (pH 7.0-8.0) or 100 mM Bicine-KOH buffer (pH 7.5-9.0)) at 30°C for 15 min. The specificity towards different substrates (Raf, Sta, verbascose (Ver), Gol, and melibiose (Mel)) was tested at 50 mM final concentrations at pH 8.0 and with an incubation of 1 h. DGDG and MGDG assays followed described methods (Dinur et al., 1984; Grossmann and Terra, 2001). Briefly, 1 mg of DGDG or MGDG (Materya LLC, Pleasant Gap, USA) was solubilized in 1 ml chloroform/methanol (2:1) solution containing 0.5% Triton X-100 and 0.12% taurocholate, followed by 10 min of vacuum drying and resuspension in 0.5 ml assay buffer (100 mM HEPES, pH 8) by 5 min of sonication. For assays, 20 µl of the protein crude extract (in 100 mM HEPES, pH 8, 5 mM $MgCl_2$, 1 mM EDTA, 20 mM DTT, 1 mM PMSF, 0.05% Triton X-100) were incubated with 20 µl of solubilized DGDG or MGDG (1 mg ml^{-1} final concentration) at 30°C for 1 h. All different assays were stopped by boiling the samples for 6 min. The extracts were then desalted and analyzed by HPLC as described (Peters and Keller, 2009; Peters et al., 2007).

Analysis of Raf in leaves and chloroplast samples

For cold acclimation and deacclimation experiments, Raf was extracted from crude leaf samples using an ethanol series as previously described (Peters and Keller, 2009; Peters et al., 2007) with minor modifications. 100 mg of fresh tissue was flash-frozen in liquid N_2 and ground prior to the extraction. Raf was extracted twice (per step) in a threestep sequential process, using 1 ml each of 80% EtOH, 50% EtOH and H_2O. Extractions were conducted at 80°C for 10 min and the tubes centrifuged at 15'000*g* (5 min, 4°C). Samples were then desalted and analyzed by HPLC.

Chloroplasts were isolated from acclimated and deacclimated plants using a Polytron homogenizer as described previously (Aronsson and Jarvis, 2011) with the following modifications. Chloroplasts were purified on a 40 / 85% Percoll gradient (40 or 85% Percoll (v/v), 300 mM sorbitol, 20 mM Tricine-KOH, pH 8.5, 5 mM $MgCl_2$, and 2.5 mM EDTA). After separation on the Percoll gradient, isolated chloroplasts were washed twice in HEPES-Sorbitol buffer (330 mM sorbitol , 50 mM HEPES-KOH, pH 8). Chloroplast intactness was estimated by phase-contrast microscopy and using the ferricyanide reducing assay (Lilley et al., 1975). Chloroplasts were broken by freeze-thaw cycles and debris was removed by centrifugation (4 min, 16'000g, 4°C). Supernatants were desalted prior to Raf content analysis by HPLC as described above. Chl content of leaf and chloroplast samples was determined as previously described, in order to express Raf content as µg Raf / µg Chl (Christ et al., 2012; Strain et al., 1971).

Analysis of galactolipids

Plant material was ground in liquid nitrogen and galactolipids were extracted with 10 volumes (w/v) of tetrahydrofuran. The extracts were centrifuged to remove cellular debris (4 min at 14'000*g*). Galactolipid content of the supernatants was analyzed using an LC-MS system consisting of an Acquity UPLC system (Waters) coupled to a Synapt G2 MS QTOF (Waters) equipped with an atmospheric pressure chemical ionization source as described (Martinis et al., 2011). Three major DGDGs (16:0-18:2, m/z = 915 $[M+H]^+$; 16:0-18:3, m/z = 913 $[M+H]^+$; 18:3-18:3, m/z = 935 $[M+H]^+$) and two major MGDGs (18:3-18:3, m/z = 773 $[M+H]^+$; 16:3-18:3, m/z = 745 $[M+H]^+$) were identified and relatively quantified.

RESULTS

***At*DIN10 is localized in the chloroplast**

ARAMEMNON only weakly predicts *At*DIN10 to be located in the chloroplast (http://aramemnon.botanik.uni-koeln.de/; Schwacke et al., 2003). However, alignment of the first 160 amino acids of *At*DIN10 with the N-terminal parts of its homologs *At*SIP1 and *At*SIP2 revealed the specific presence in *At*DIN10 of 95 amino acids at the N-terminus (Fig. 6.1A). To confirm that this *At*DIN10-specific N-terminal sequence is a chloroplast transit peptide, an *At*DIN10-GFP fusion construct was transiently transformed into Arabidopsis protoplasts and

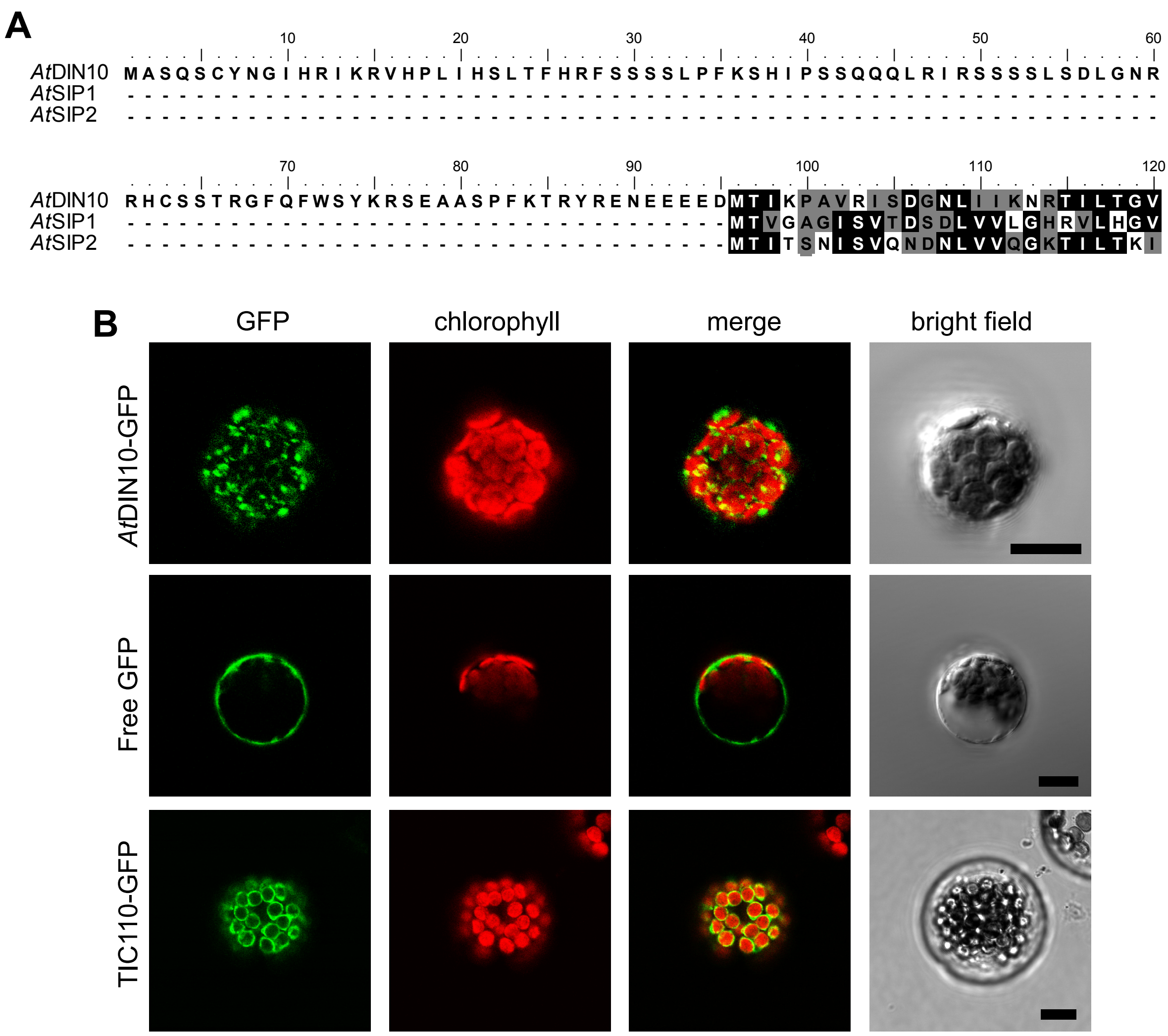

Fig. 6.1. *At*DIN10 localizes to the chloroplast. (A) Alignment of the first 120 amino acids of *At*DIN10 (AT5g20250) with the N-terminal parts of *At*SIP1 (AT1g55740) and *At*SIP2 (AT3g57520) protein sequences. Alignment was performed using the BioEdit software (http://www.mbio.ncsu.edu/bioedit/bioedit.html). (B) Transient expression in Arabidopsis mesophyll protoplasts of GFP fused in frame to the C-terminus of AtDIN10 (*At*DIN10-GFP). Free GFP was used as a cytosolic control and TIC110-GFP for chloroplast envelope localization. GFP fluorescence (GFP) and Chl autofluorescence (chlorophyll) were examined by confocal laser scanning microscopy. The merge panels show overlays of GFP and Chl autofluorescence. Bars = 10 µm.

analyzed by confocal microscopy (Fig. 6.1B). GFP fluorescence showed spots inside the chloroplast that largely co-localized with chlorophyll fluorescence, unlike free GFP (mainly found in the cytosol). By contrast, GFP fusion with translocon of the inner chloroplast envelope 110 (TIC110) showed distinct chlorophyll and GFP fluorescence signals as expected for a protein localized in the chloroplast envelope. From these results, together with the fact that ARAMEMNON predicts *At*DIN10 to be a soluble protein, we conclude that *At*DIN10 is most probably located in the chloroplast stroma.

_At_DIN10 is an alkaline α-galactosidase active on Raf and longer RFOs

Crude extracts of Sf9 cells infected with a baculovirus carrying *At*DIN10 cDNA were assayed for alkaline galactosidase activity with the artificial substrates pNPαGal and pNPβGal. *At*DIN10 showed an activity for the substrate pNPαGal (1.26 nkat mg^{-1} total protein, at pH 8) but did not hydrolyze the β-linked pNPGal variant (pNPβGal), indicating that *At*DIN10, like its homologues *At*SIP1 and -2, shows hydrolytic activity specifically on α-D-galactosidic linkages (Fig. 6.2A and B). The recombinant protein was active between pH 6.5 and pH 9 with maximum activity at pH 8, defining *At*DIN10 as an alkaline αGal (Fig. 6.2B).

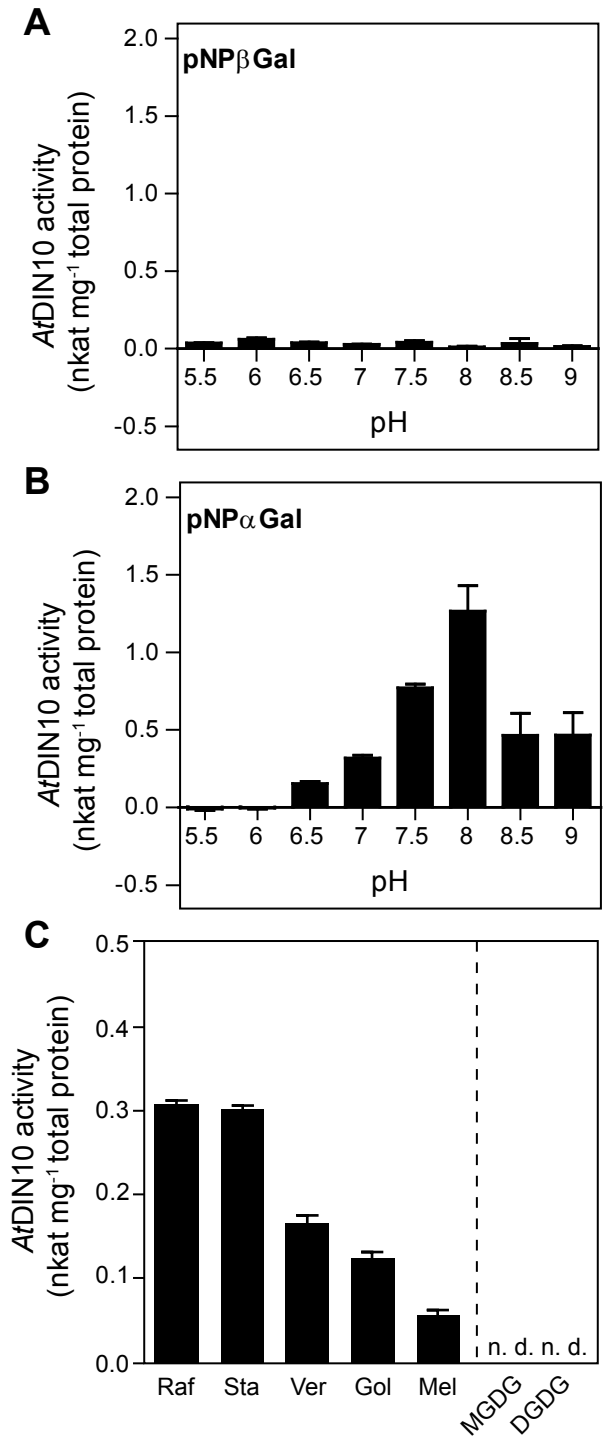

Fig. 6.2. Recombinant *At*DIN10 is active on various galacto-oligosaccharides but not on galactolipids. (*A*) A crude extract of Sf9 cells containing recombinant *At*DIN10 is not active on pNPβGal in the pH range of 5.5-8. (*B*) Crude extract of Sf9 containing recombinant *At*DIN10 displays a pH optimum of 8 with pNPαGal as substrate. (*C*) Recombinant *At*DIN10 protein activity on different substrates. Data are means ± SE of six replicates. n. d., not detected.

RafS activity was also investigated by incubating crude extracts with the appropriate substrates (100 mM Suc and 10 mM Gol), however *At*DIN10 did not exhibit RafS activity (data not shown). Subsequently, the substrate specificity of *At*DIN10 for various galacto-oligosaccharides and -lipids was determined (in HEPES buffer, pH 8). *At*DIN10 displayed good α-galactosidase activities toward a broad spectrum of α-1,6-galactosyl oligosaccharides with a preference for Raf (0.308 nkat mg^{-1} total protein) and Sta (0.299 nkat mg^{-1} total protein). However, all other tested oligosaccharide substrates, i.e. Mel (0.058 nkat mg^{-1} total protein), Ver (0.165 nkat mg^{-1} total protein) and Gol (0.126 nkat mg^{-1} total protein) were also hydrolyzed, albeit with lower activity (Fig. 6.2C). When tested with 1 mg ml^{-1} MGDG or DGDG, the most highly abundant galactolipids present in the chloroplast membranes, no activity was detected. This was expected for MGDG because it contains an endo-β-galactosidic linkage, but unexpected for DGDG which contains an endo-α-galactosidic linkage.

*At*DIN10 is not involved in galactolipid degradation

*At*DIN10 is the closest Arabidopsis homologue of rice OsakαGal, which has been suggested to be implicated in galactolipid degradation during leaf senescence (Lee et al., 2009). In order to investigate DGDG and MGDG degradation, galactolipid content in *atdin10-1* and *-2* during dark-induced senescence was analyzed by LC-MS (Fig. 6.3). The abundance of three MGDG and two major DGDG significantly decreased after 6 d of dark-inbucation similarly in wild-type plants and *atdin10* mutants. Together with the apparent inactivity of recombinant *At*DIN10 on DGDG and MGDG, these data strongly suggest that *At*DIN10 is not involved in galactolipid degradation during leaf senescence.

atdin10 mutants retain of Raf in the chloroplast during cold deacclimation

Due to the subcellular localization of *At*DIN10 and its *in vitro* activity on RFOs, we hypothesized that this α-galactosidase could be involved in Raf degradation within the chloroplast. Wild-type and *atdin10-1*, *-2* and *-3* were grown at 21°C for 6 weeks, acclimated

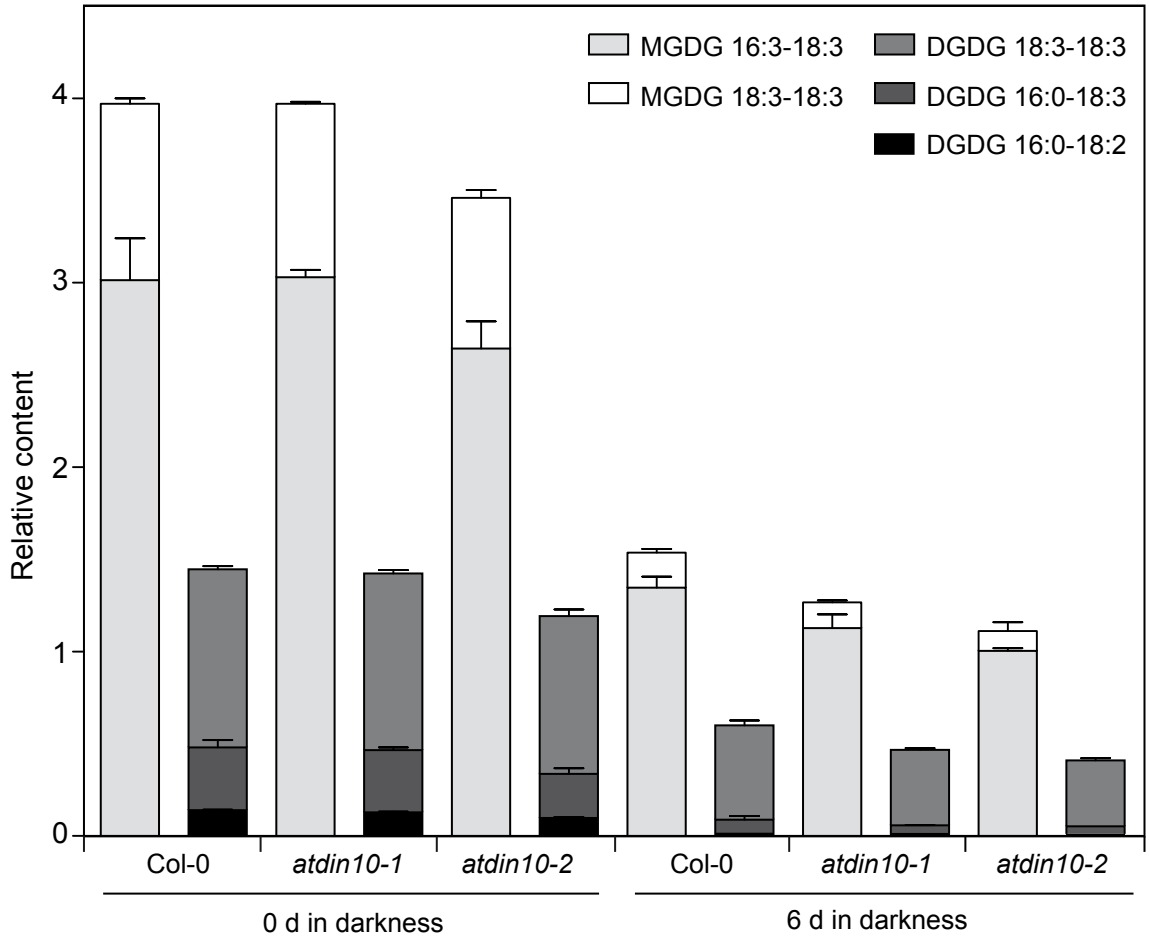

Fig. 6.3. *atdin10* mutants degrade galactolipids as wild-type during dark-induced senescence. Relative quantities of the major MGDGs and DGDGs of Col-0, *atdin10-1* and *din10-2* were determined by LC-MS as described in "Materials and Methods". Values are means of three replicates. Error bars indicate SD.

for 7 d at 5°C and finally deacclimated for 7 d at 21°C. Total Raf content of leaves was measured before and after acclimation, and after deacclimation (Fig. 6.4A). During cold acclimation, Raf concentrations increased similarly in wild-type and mutant plants. However, *atdin10* mutants appeared to retain more Raf than wild-type plants after the deacclimation phase (P-value = 0.0035). We further investigated the retention of Raf in *atdin10* mutants by quantifying Raf in isolated chloroplast and observed that *atdin10-1* is unable to degrade chloroplastic Raf during the deacclimation phase (Fig. 6.4B).

DISCUSSION AND OUTLOOK

Due to the homology of *At*DIN10 with the rice α-galactosidase OsakαGal, we originally hypothesized *At*DIN10 to be involved in the degradation of DGDG (Lee et al., 2009). However, unlike silencing of OsakαGal in rice, we found that suppression of *At*DIN10 in Arabidopsis does not affect galactolipid degradation during leaf senescence (Fig. 6.3). In addition to wild-type galactolipid degradation, *atdin10* mutants do not display any delay in leaf senescence which would result in a stay-green phenotype during dark-incubation (data not shown). Together with these findings, the inactivity of recombinant *At*DIN10 on galactolipids *in vitro* corroborate the idea that *At*DIN10, in contrast to its rice homologue, is not involved in galactolipid degradation. Nevertheless, we cannot exclude the possibility that *At*DIN10 acts downstream of galactolipases during galactolipid breakdown. Indeed, the first step of galactolipid degradation has also been proposed to involve galactolipases rather than galactosidases (see Fig. I.2.; Bhalla and Dalling, 1984; Kaniuga and Gemel, 1984). Thus, it could be speculated that *At*DIN10 might hydrolyze digalactosyl glycerol produced from DGDG by galactolipases. Analysis of digalactosyl glycerol degradation during leaf senescence of

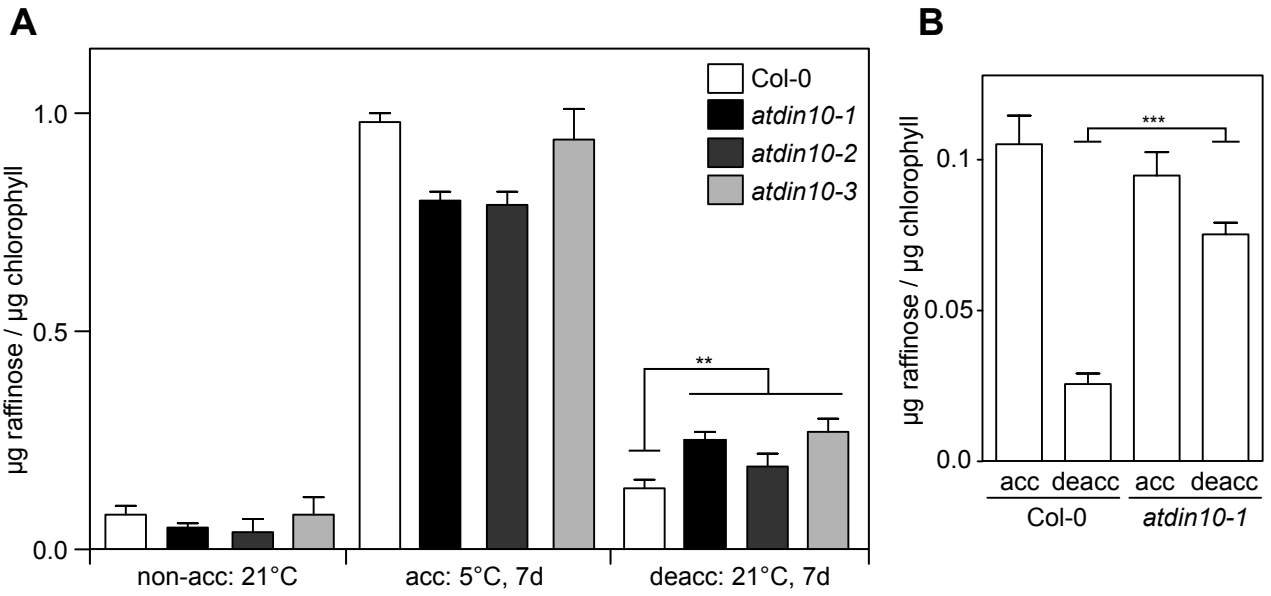

Fig. 6.4. *atdin10* mutants retain Raf in the chloroplast during cold deacclimation. (*A*) Raf content in leaves of *atdin10* mutants was analyzed by HPLC before and after cold acclimation (non-acc and acc, respectively), and after cold deacclimation (deacc). (*B*) Raf content in chloroplasts isolated from cold acclimated and deacclimated leaves of Col-0 and *atdin10-1*. The asteriks indicate the significance of the differences after deacclimation between leaf Raf content of Col-0 and atdin10 mutants (panel A, p-value = 0.0035) and between Raf content of chloroplast isolated from Col-0 and atdin10-1 (panel B, p-value < 0.0001), as determined using a two-tailed t-test. Values are means of three biological replicates. Error bars indicate SD.

atdin10 mutants and analysis of recombinant *At*DIN10 activity on digalactosyl glycerol *in vitro* are needed to corroborate or reject this hypothesis.

In vitro, recombinant *At*DIN10 was not active on galactolipid but, in contrast, could hydrolyze molecules also containing Gal moiety bound in a α-1,6-linkage such as Raf and longer RFOs (Fig. 6.2C). Raf has been shown to (partially) accumulate in the chloroplast during cold acclimation (Knaupp et al., 2011; Schneider and Keller, 2009). As a consequence, suppression of *At*DIN10 led to minor but significant retention of Raf at the whole leaf level during cold deacclimation (Fig. 6.4A). We further provide evidence that this partial retention of Raf in leaves of *atdin10* mutants is due to an almost complete retention of Raf within the chloroplast after cold deacclimation (Fig. 6.4B). Thus, these data indicate that *At*DIN10 is the major enzyme involved in Raf degradation within the chloroplast. Due to the fact that Raf accumulating in chloroplasts represents only a minor fraction of total Raf content of the leaf, *At*DIN10 suppression does not dramatically affect total Raf degradation (Fig. 6.4A and B; Schneider and Keller, 2009). During cold acclimation, Raf is thought to be synthesized in the cytosol and then partially imported into the chloroplast by a, up to date unknown, Raf transporter (Schneider and Keller, 2009). However, our data suggest that, during cold deacclimation, Raf is degraded to sucrose and galactose by *At*DIN10 within the chloroplast and not exported and degraded in other cellular compartments.

In future experiments, it will be interesting to investigate if *At*DIN10 expression is correlated with Raf content of chloroplasts. Indeed, there are good indications in publicly available gene expression data that *At*DIN10 is down-regulated during cold acclimation (Zimmermann et al., 2004). If this expression pattern can be confirmed, overexpression of *At*DIN10 should prevent Raf accumulation during cold acclimation. Furthermore, it can be speculated that *atdin10* mutants would hyperaccumulate Raf in the chloroplast after successive cold acclimation and deacclimation cycles.

The role of RFO catabolism during stress deacclimation remains unclear. Why do plants not permanently accumulate RFOs? One hypothesis is that the energy stored in RFOs is not negligible. The plant could therefore profit from remobilizing these sugars during stress deacclimation. Another reason for RFO catabolism may be that RFO retention

under non-stress conditions could decrease plant metabolism. RFOs are thought to protect cellular components during stresses by direct interaction with membranes and proteins. Interestingly, suppression of RafS, which completely abolish Raf synthesis, does not diminish freezing tolerance in Arabidopsis, indicating that Raf is not essential for basic freezing tolerance or cold acclimation of Arabidopsis (Zuther et al., 2004). However, during chilling, Raf was shown to protect PSs, which are sensitive to cold temperatures (Knaupp et al., 2011; Winfield et al., 2010). It can be imagined that the interaction between RFOs and chloroplast components could inhibit or decrease certain biochemical processes, e.g. photosynthesis, and lead to a decrease of metabolism under non-stress conditions. Therefore, suppression of *At*DIN10 in *atdin10* mutants and consequent Raf accumulation in the chloroplast after successive cold stress periods could negatively affect plant growth and fitness. This hypothesis has to be investigated in future experiments.

CONCLUSION AND OUTLOOK

This chapter summarises the new findings of my PhD thesis and exposes open questions in colorless chlorophyll catabolite modifications. What is the nature of FCC hydroxylation, glucosylation and hypermodification activities? What is/are the role(s) of FCC modifications? What about the by-products of FCC modifications? How are colorless Chl catabolites transported within the cell. Is there a close interaction between ER and the chloroplast envelope during leaf senescence? Different experiments are proposed to further understand FCC modifications during chlorophyll breakdown.

GENERAL SUMMARY OF MY THESIS

The main focus of my PhD thesis was the investigation of the modifications of colorless Chl catabolites occurring during Chl breakdown. Together with the group of Prof. Bernhard Kräutler (Innsbruck), we could identify and characterize Arabidopsis MES16 and CYP89A9, two enzymes involved in FCC modification and thus significantly increase our knownledge on Chl breakdown. Chapter "1" describes the characterization of MES16, a methyl esterase involved in FCC demethylation at O13^4. Surprisingly, we found that MES16 increases the rate of FCC-to-NCC isomerization in the vacuole. Indeed, suppression of MES16 in *mes16* mutants led to the retention of methylated FCCs in the vacuole, whereas wild-type plants accumulated mostly demethylated NCCs. As a result of the retention of fluorescent catabolites, senescent leaves of *mes16* mutants were fluorescing under UV light. In Chapter "2", we demonstrate that the major Chl catabolites in Arabidopsis are not NCCs, as previously believed, but NDCCs, which represent more than 90% of the Chl present in green leaves. NCCs and NDCCs differ at pyrrole ring A, where the side group at C6 is a formyl group in NCCs and an oxo group in NDCCs. Furthermore, cytochrome P450 CYP89A9 was identified as being responsible for the conversion of FCCs into FDCCs within the cytosol. To the best of our knowledge, the proposed reaction of CYP89A9, producing a γ-lactam upon deformylation of the α-formyl-pyrrole unit, is novel for cytochrome P450 enzymes. Finally, the results presented in the first part of Chapter "3" provide evidence that C8^2 hydroxylation of FCCs occurs within chloroplasts of Arabidopsis. Furthermore, preliminary experiments show that the enzyme(s) responsible for this modification might be purifiable from red bell pepper chromoplasts. In the same chapter, we describe a novel method, for characterizing FCC transport across the chloroplast envelope, which makes use of recombinant MES16. The model depicted in Figure C.1 illustrates the new findings on FCC modifications in Arabidopsis provided by my thesis.

In the frame of my PhD, I also collaborated with other research groups on three different projects. In Chapter "4", together with Dr. Shaun Peters (Stellenbosch) and Prof. Berhard Kräutler (Innsbruck), we provide evidence that Chl is degraded during dessication of the resurrection plant *X. viscosa* through the "PAO pathway". This study indicates that organized and controlled degradation of phototoxic Chl catabolites is not only required for nutrient remobilization during leaf senescence but also for plant survival during and after leaf dessication of resurrection plants. We also collaborated with Prof. Jean T. Greenberg (Chicago) to better understand the function of RCCR, the enzyme that reduces RCC to *p*FCC. This study, presented in Chapter "5", indicates that RCCR is involved in the protection against pro-death molecules, such as RCC, in both chloroplasts and mitochondria. Finally, new findings on *At*DIN10, an α-galactosidase localized in the chloroplast, are presented in Chapter 6 (in collaboration with Dr. Shaun Peters). Originally studied as being potentially involved in galactolipid degradation during leaf senescence, we found that *At*DIN10 is in fact involved in chloroplastic Raf degradation during cold deacclimation.

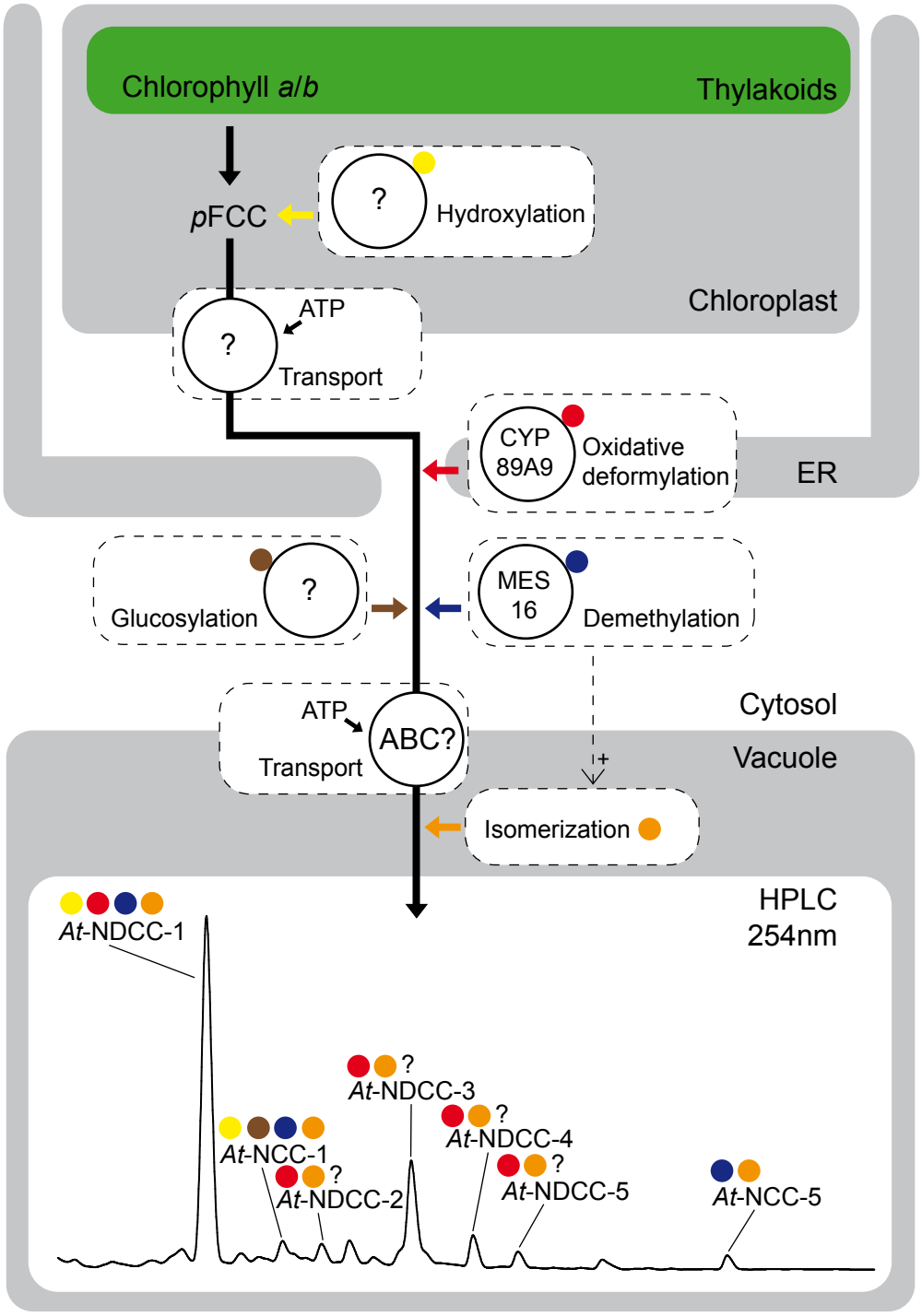

Figure C.1. Model for FCC modifications in Arabidopsis during Chl breakdown. Degradation of colored Chl catabolites at the thylakoid membrane leads to the release of *p*FCC into the stroma. *p*FCC is then hydroxylated in the chloroplast and translocated across the envelope by unknown active mechanism(s). Close interaction between ER and the chloroplast envelope allows the oxidative deformylation of most FCCs to fluorescent dioxobilane-type Chl catabolites (FDCCs). FCCs and FDCCs are then further modified by demethylation and glucosylation in the cytosol before their import into the acidic vacuole where they are isomerized to nonfluorescent Chl catabolites (NCCs and NDCCs). Relative amounts of major colorless Chl catabolites accumulating in the vacuole can be estimated from the HPLC trace representing an extract from yellow leaves of wild-type Arabidopsis. The colored dots represent the different modifications of the colorless catabolites. The exact chemical constitution of *At*-NDCC-2 to -5 is unknown.

OPEN QUESTIONS IN FCC MODIFICATIONS

FCC hydroxylation, glucosylation and hypermodification activities

The enzyme(s) responsible for $C8^2$ hydroxylation of *p*FCC within gerontoplasts remain(s) unknown. Preliminary experiments presented in Chapter "3" will help in the future to further investigate this FCC modification, which is common to all higher plants. Partial purification of the activity detected in red bell pepper chromoplasts followed by mass spectrometry analysis seems a reasonable strategy to identify candidate protein(s) responsible for $C8^2$ hydroxylation. In some species such as Arabidopsis, tobacco and oilseed rape, the $C8^2$ hydroxyl group of FCCs appears to be subsequently malonylated and/or glucosylated (see Table I.1; Berghold et al., 2004; Hörtensteiner, 1998; Pružinská et al., 2005). The molecular nature of these activities is unknown, although a malonyltransferase activity has been partially purified from oilseed rape (Hörtensteiner, 1998). Arabidopsis UGTs are known to catalyze the addition of a sugar group to hydroxyl groups of target molecules by formation of a glycosidic bond (Osmani et al., 2009; Paquette et al., 2003). It can therefore be imagined that one or several of the 120 cytosol-localized UGTs in Arabidopsis (Paquette et al., 2003) are responsible for the addition of glucose to $C8^2$-OH-FCCs in Arabidopsis. All Arabidopsis UGTs have been cloned for recombinant expression in *E. coli* (Lim et al., 2003). Thus, a good strategy to identify candidates for FCC glucosylation would be assays with heterologously expressed UGTs using $C8^2$-OH-*p*FCC as substrate. Finally, identification of the enzymes that hypermodify FCCs, i. e. react with the $C17^3$ carboxyl group, in banana and other related taxa is also of interest. Due to a lack of genomic resources for these species, the identification of these enzymes should be performed by partial purification of the activities and subsequent analysis by mass spectrometry. Once identified, these enzymes could be used to hypermodify and consequently stabilize FCCs in other plant species that do not retain FCCs. This could allow to investigate if FCCs have indeed physiological and/or ecological role(s) (see below).

What is/are the role(s) of FCC modifications?

Retention of FCCs in *mes16* mutants and lack of NDCC formation in *cyp89a9* mutants does not seem to affect plant growth and leaf senescence, i.e. no phenotype was observed in *mes16, cyp89a9* and *mes16cyp89a9* mutants during vegetative growth and Chl *a* and *b* are degraded in these mutants as in wild-type plants during leaf senescence. Thus, the role(s) of FCC modification remain(s) unclear. One hypothesis is that FCC modifications could participate in the detoxification of Chl catabolites. As it can be seen in Figure C.2, the first steps of degradation produce phototoxic catabolites and FCC modifications could lead to a further decrease of the light absorption capacity of the catabolites. Indeed, demethylation of FCCs increases the rate of isomerization to nonfluorescent catabolites in the vacuole and, thus, facilitates the loss of their 360 nm absorption peak (see Chapter "1"). Furthermore, FDCC formation by CYP89A9 results in the loss of the C5-formyl group of FCCs and, consequently, of the 320 nm absorption peak. The reason why we did not observe any phenotype in *mes16* and *cyp89a9* mutants could arise from the fact that our mutants were grown under controlled, UV-limited conditions. It can be speculated that under sun-light conditions leaf senescence could be affected if are retained colorless Chl catabolites that absorb light between 300 and 380 nm (Fig. C.2). This hypothesis could be tested by growing these mutants under natural or artificial UV-B-containing light conditions. Besides reducing the light absorption capacity of colorless Chl catabolites, modifications of FCC side chains increase their polarity. This observation corroborates the idea that FCC modification directly participates to Chl catabolite detoxification. Indeed, sequential hydroxylation and glucosylation are known to participate in the detoxification of various molecules such as xenobiotics by increasing their polarity (Dosnon-Olette et al., 2011; Pedras et al., 2001). Therefore, relocation of FCCs from the chloroplast into the vacuole is probably facilitated by an increase in the solubility of the catabolites. Identification of the enzyme(s) responsible for FCC hydroxylation, together with the knowledge on FCC demethylation and oxidative deformylation provided in my thesis could help testing if FCC modification has indeed a physiological role. It would be of interest to study leaf

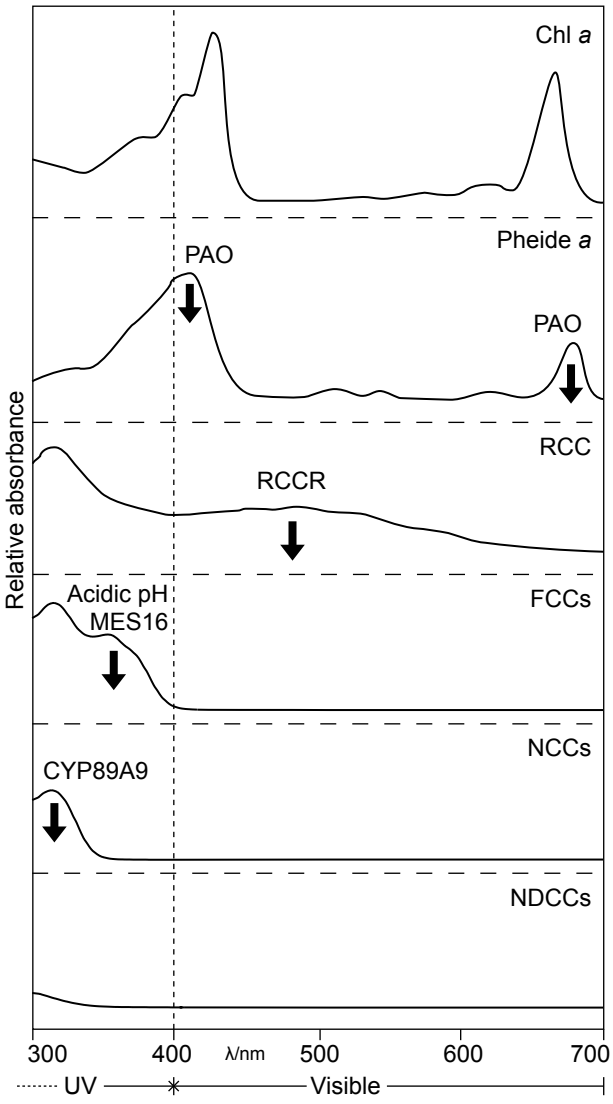

Figure C.2. Schematic representation of the loss of absorption capacity of different Chl catabolites during Chl breakdown. The enzymes having a direct influence on UV/Vis spectra of the Chl catabolites are shown. The UV/Vis spectra are schematically drawn. Relative absorptions between different catabolites cannot be compared.

senescence in Arabidopsis plants that are deficient in all FCC modifications and thus accumulate only *p*FCC and *p*NCC during Chl breakdown.

Why do FCC modifications occur in a species-specific manner? One hypothesis is that FCCs could have ecological functions. On one hand, plants such as Arabidopsis appear to avoid FCC accumulation. On the other, permanent FCC accumulation has been shown to occur in leaves and fruits of banana and other related taxa (Hörtensteiner and Kräutler, 2011; Kräutler et al., 2010; Moser et al., 2009a). Furthermore, while humans are not sensitive to blue light between 400-500 nm, other animals, such as insects, are known to possess blue photoreceptors having a maximal sensitivity around 450 nm (Briscoe and Chittka, 2001). It is therefore reasonable to assume that some insects are able to detect the blue fluorescence emitted by FCCs around 450 nm. In the case of species such as banana, which naturally retain FCCs, these fluorescent catabolites may play a role in beneficial interactions with insects such as pollinations or be a signal of fruit ripening for bigger animals contributing to seed dispersal. Other plant species may benefit from the further conversion of FCCs into NCCs/NDCCs because herbivores might be able to link FCC fluorescence of senescent leaves with reduced plant fitness at this late developmental stage. Thus, by facilitating FCC-to-NCC isomerization MES16 could, for instance, avoid the attraction of herbivores by the plant during nutrient relocation and seed maturation. Chapters "1" and "2" present the characterization of Arabidopsis mutants, which accumulate different relative FCC amounts during senescence (*mes16*, *mes16cyp89a9*) and which could be used in future experiments to investigate if insects can indeed detect FCC fluorescence.

By-products of FCC modifications

During leaf senescence, one mole of degraded Chl leads to the production of one mole of colorless catabolites. In addition, FCC modifications appear to lead to the formation of by-products. Even if it has not been experimentally shown, Chl catabolite demethylation (MES16) and oxidative deformylation (CYP89A9) are thought to produce methanol and formate, respectively (Fig. C.3). The amount of Chl catabolites produced during leaf senescence is about 1 µmol per gram fresh weight. If we assume that MES16 demethylates and CYP89A9 deformylates 100% of the Chl catabolites, we can estimate that Chl breakdown is responsible for the formation of 1 µmol of methanol and 1 µmol of formate per gram fresh weight, amounts that are not negligible. Methanol is known to be produced in leaves by processes such as pectin and lignin degradation and to be metabolized by C1-metabolism via production of formate or to exit the leaf via the stomata (Fall and Benson, 1996; Gout et al., 2000; Igamberdiev et al., 1999). Although stomata are thought to be open during the late stages of senescence (Zhang and Gan, 2012), it can still be imagined that methanol partially accumulates within

the leaves and has physiological effect(s). Indeed, in rice, methanol formation during leaf senescence has been connected to tryptophan biosynthesis through induction of the transcription factor WRKY14 (Kang et al., 2011b). Tryptophan biosynthesis has been shown to promote serotonin production, which in turn delays leaf senescence (Kang et al., 2009). Furthermore, exogenous application of methanol modulates the expression of hundreds of genes involved in multiple detoxification and signaling pathways (Downie et al., 2004). It could therefore be interesting to investigate the contribution of Chl catabolite demethylation to the total production of methanol during leaf senescence. Indeed, if methanol has also regulatory effect(s) during senescence in Arabidopsis, it could be argued that FCC demethylation can indirectly regulate gene expression. However, this hypothesis is unlikely because *mes16* mutants do not show any accelerated or delayed leaf senescence phenotype.

In leaves, formate is known to be the by-product of photorespiration and fermentation pathways, and possibly the product of direct CO_2 reduction in chloroplasts (Igamberdiev et al., 1999). As mentioned above, formate could also be formed from methanol generated by pectin and lignin degradation, and potentially also by FCC demethylation. In theory, FCC-to-FDCC conversion by CYP89A9 should also contribute to the formation of formate in senescent leaves. Because formate is less volatile than methanol, it has to be metabolized within senescing leaves. Two routes for formate utilization have been described in plants (Igamberdiev et al., 1999). The first one is mediated by FORMATE DEHYDROGENASE (FDH) which converts formate to CO_2 (Li et al., 2000; Olson et al., 2000). Although overexpression of FDH in Arabidopsis has been shown to increase tolerance to exogenous application of formate, the role of FDH in leaves remains unknown (Li et al., 2002). Interestingly, Arabidopsis FDH seems to be co-expressed with Chl catabolic enzymes (Fig. C.4), indicating that the enzyme could have a role during leaf senescence. To the best of my knowledge, accumulation of formate in *fdh* mutants has never been reported in the literature. Furthermore, Arabidopsis *fdh* mutants do not show any accumulation of formate during dark-induced leaf senescence (Bastien Christ and Stefan Hörtensteiner, unpublished data). The non-accumulation of formate in *fdh* mutants could

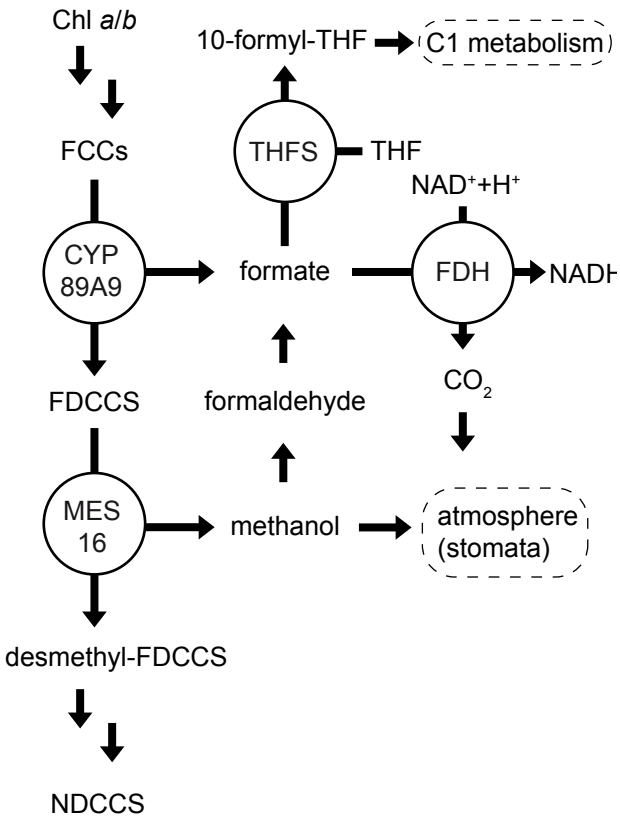

Figure C.3. By-products of FCC modifications. Demethylation by MES16 and oxidative deformylation by CYP89A9 of FCCs produce methanol and formate, respectively. Methanol and formate are thought to be directly or indirectly released into the atmosphere or metabolized by C1-metabolism. See text for more information.

arise from a compensation effect of a second route of formate utilization. Indeed, formate can be condensed with tetrahydrofolate (THF) to produce formyl-THF by the action of 10-FORMYL-THF SYNTHETASE (SYN or THFS; Igamberdiev et al., 1999). Formyl-THF is then further used for serine and methionine biosynthesis. Nothing is known the THFS of Arabidopsis, which is a single copy gene. Thus, it would be of interest to suppress both routes of formate metabolism in Arabidopsis by crossing an *fdh* and *thfs* mutant. If, as expected, *fdhthfs* double mutants accumulate formate, it will be possible to investigate the contribution of FCC modification to formate production during leaf senescence.

Transport of colorless Chl catabolites

Understanding the transport of FCCs across the chloroplast envelope is not only of interest to better understand leaf senescence but also for research on other open tetrapyrroles such as phytochromobilin,

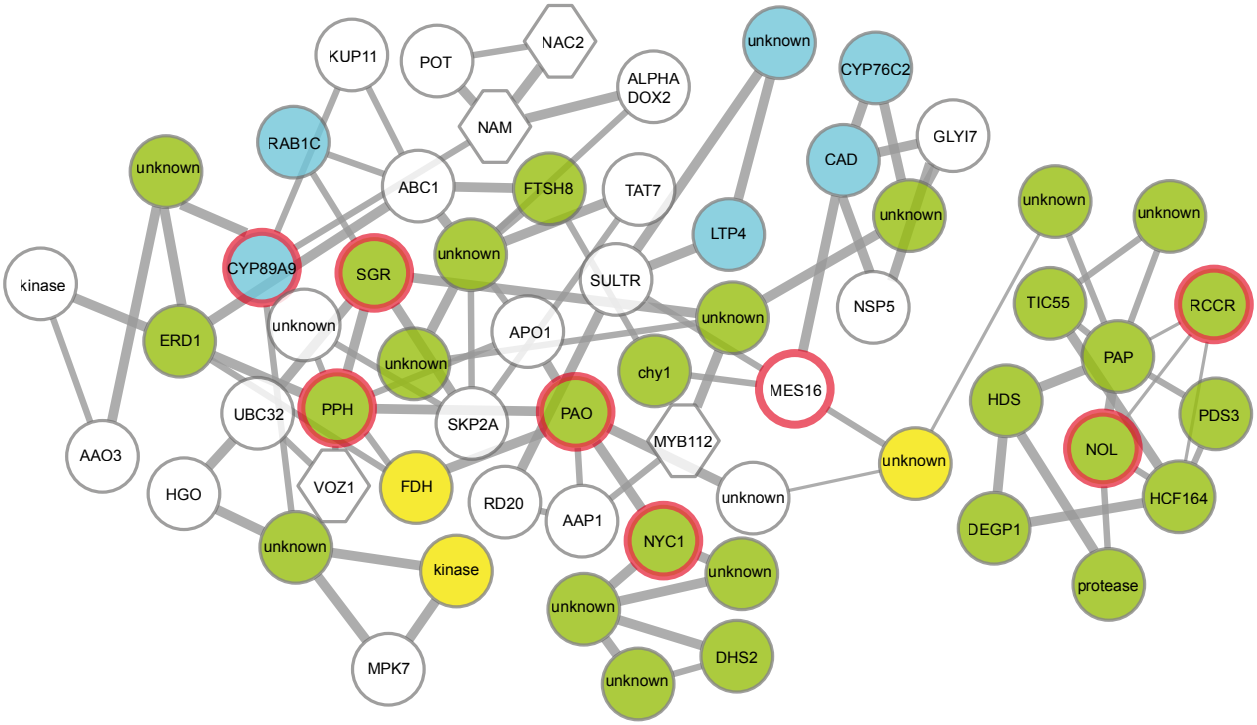

Figure C.4. Co-expression network around *SGR*, *PPH*, *PAO*, *RCCR*, *NYC1*, *NOL*, *MES16* and *CYP89A9* (red circles). The ATTED-II NetworkDrawer tool (Obayashi et al., 2009) was used to generate the network (using all available experiments). Predicted or confirmed localization: green, chloroplasts; yellow, mitochondria; blue; secretory pathway; white, cytosol and others. Enzymes are depicted by circles and transcription factors by hexagons.

the chromophore of phytochromes. Besides the observation that export of FCCs from the chloroplast seems to be ATP-dependent, suggesting that it is an active mechanism, nothing is known about open tetrapyrrole transport within the plant cell (Chapter "3"; Matile et al., 1992). As already discussed in Chapter "3", it can be speculated that ABC transporters are responsible for this transport. To elaborate strategies for the identification of FCC transporter(s), it might be helpful to anticipate the phenotype(s) that would result from the suppression of FCC export from the chloroplast. Massive accumulation of *p*FCC and C8^2-OH-*p*FCC within the stroma during leaf senescence could affect upstream enzymatic steps of Chl degradation and potentially lead to the accumulation of colored Chl catabolites such as RCC, Pheide or Phein. Furthermore, if FCC export from the chloroplast is also involved in the transport of phytochromobillin, its suppression could affect red light perception due to the lack of active phytochromes (Franklin and Quail, 2010). Interestingly, mutations in *AtNAP1,* i.e. *long after far-red* 6 (*laf6*) and *7-hydroxymethyl Chl a 1* (*hmc1*) lead to reduced responsiveness toward continuous far-red light and accumulation of Pheide during Chl breakdown (Møller et al., 2001; Nagane et al., 2010). *AtNAP1* encodes a protein that has homology with soluble ABC transporters as well as with prokaryotic sulfur (SUF) system subunits (Sanchez-Fernandez et al., 2001; Xu et al., 2005). In addition, *At*NAP1 is known to be up-regulated during leaf senescence and to be localized in the chloroplast. Even though *At*NAP1 was proposed to have a role in Fe-S cluster formation (Xu et al., 2005), the phenotype of *laf6* and *hmc1* mutants suggest that this soluble protein might also interact with membrane protein(s) localized within the chloroplast inner membrane and participate in the transport of open tetrapyrroles. This hypothesis can be easily tested using *laf6* and *hmc1* mutants. Indeed, Nagane et al. (2010) mentioned that Pheide accumulation in senescent leaves of *hmc1* represents only 40% of the degraded Chl but they did not analyze Chl catabolites downstream of Pheide. The accumulation of colorless Chl catabolites such as NCCs and NDCCs in *laf6* and *hmc1* would indicate that Pheide accumulation is due to lower activity of PAO caused by deficiency in Fe-S cluster formation, as proposed by Nagane et al. (2010). However, accumulation of *p*FCC and C8^2-OH-*p*FCC would rather suggest that *At*NAP1 is involved in

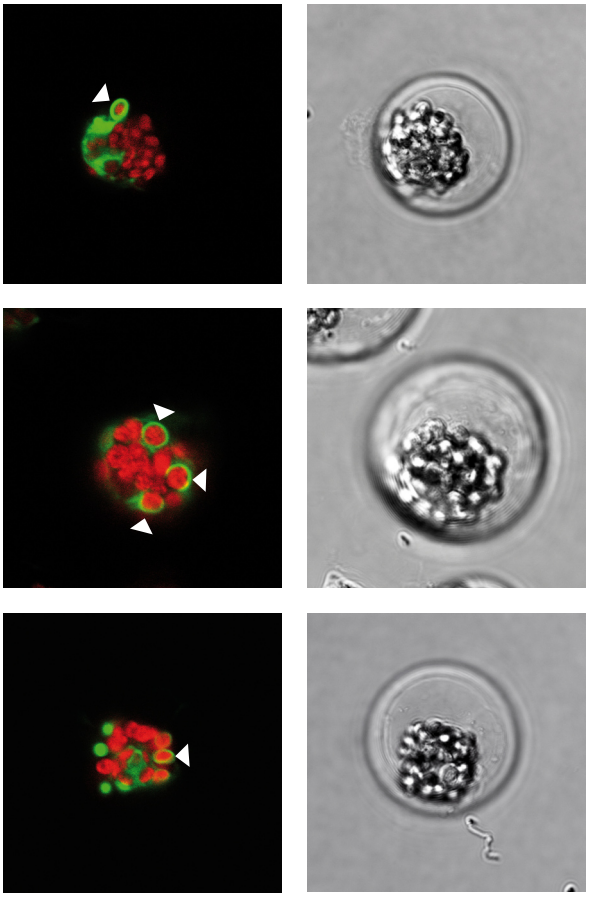

Figure C.5. ER localized CYP89A9-GFP partially interacts with chloroplasts in senescent Arabidopsis mesophyll protoplasts (white arrowheads). Transient expression of CYP89A9-GFP in protoplasts isolated from senescent (5 DDI) leaves was examined by confocal laser scanning microscopy as described in Chapter 2. First column, overlay of GFP and Chl autofluorescence signals; Second column, transmission image.

open tetrapyrrole transport across the chloroplast envelope.

Import of FCCs from the cytosol into the vacuole is better understood than their transport across the chloroplast envelope. *At*MRP2 and *At*MRP3, two members of the multidrug resistance–associated protein (MRP) subfamily of ABC transporters, have been shown to be capable of importing colorless catabolites *in vitro* (Lu et al., 1998; Tommasini et al., 1998). However, mutant plants deficient in FCC transport across the tonoplast have never been isolated. Redundancy between vacuolar ABC members could render their reverse genetic identification using T-DNA insertion lines difficult. Instead, the use of artificial microRNAs to simultaneously silence several genes (for an online tool, see WMD3, http://wmd3.weigelworld.org/cgi-bin/webapp.cgi) will be most probably of great help for their identification. Furthermore, methods described in my thesis allow, if needed, screening of numerous plant lines. Indeed, retention of FCCs in the cytosol of senescent leaves caused by the suppression of tonoplast FCC transport systems can be detected by HPLC. In addition, as for *mes16* mutants, it may be possible to visualize FCC accumulation at the whole-leaf level under UV light (Chapter "1", Fig. 4).

Interaction between ER and the chloroplast envelope during leaf senescence

In Chapter "2", we demonstrate that FDCC formation by CYP89A9 precedes FCC demethylation by MES16 *in vivo*. This observation, together with the fact that CYP89A9 is located at the ER, suggests a close interaction between ER and chloroplast in senescent leaves. This idea is corroborated by the finding that CYP89A9-GFP fusion, which co-localizes with an ER marker, partially surrounds chloroplasts when transformed in protoplasts isolated from senescent leaves (Fig. C.5, Bastien Christ and Stefan Hörtensteiner, unpublished data). It can therefore be speculated that ER and chloroplasts interact and create membrane contact sites during senescence, as it was shown in green leaves for lipid trafficking (Andersson et al., 2007). Furthermore, it can be speculated that proteins involved in FCC export from the chloroplast and CYP89A9 co-localize at these membrane contact sites. It has been proposed that these membrane contact sites are mediated by protein-protein interactions (Andersson et al., 2007). Therefore, it could even be possible that CYP89A9 specifically interacts with the putative FCC transport system. A method has been develop to isolate these plastid-associated ER membranes in green leaves (Andersson et al., 2007), which could be used in the future to investigate ER-chloroplast interaction during senescence.

CONCLUSIVE REMARKS

Delaying the onset of leaf senescence has been described as a good strategy for increasing crop productivity (Thomas and Howarth, 2000). Indeed, the yield record in corn was obtained with a Type A or B functional stay-green mutant. Suppression of Chl degradation only leads to cosmetic Type C or Type D stay-green phenotypes, which do not increase plant fitness but rather accelerates cell death and seed germination. Nonetheless, understanding Chl breakdown during leaf senescence, fruit ripening and other developmental processes or stress responses is not only of interest to increase our fundamental knowledge, but it can also improve post-harvest storage. Indeed, loss of the green color due to senescence in vegetables such as broccoli decreases their commercial value. Besides open questions about FCC modifications and transport (see above sections), several other aspects of Chl breakdown by the "PAO pathway" need further investigations. For instance, although SGR and Chl catabolic enzymes have been shown to interact with LHCII subunits and SGR has been implicated in the destabilization of Chl-apoprotein complexes during senescence, its mechanism of action remains to be defined. SGR LHCII. Furthermore, it is unknown if the same mechanism is involved in the degradation of Chl from PSI. It cannot be excluded that PSI degradation (partially) differs from the one of PSII. Recent studies, showing that SGR has other functions besides its role during Chl breakdown could be helpful to better understand the role(s) of this protein. The mechanism involved in Chl demetalation also remains unknown. Whether it involves an MRP, MCS and/or simply changes in the chloroplast pH of the stroma still needs to be demonstrated. The *in vivo* role of CLHs, proteins that are highly active on Chl *in vitro*, is still unclear. A collective consideration of key studies on CLHs points to their involvement during stress responses against various biotic and abiotic stresses, and not during age-dependent leaf senescence. Chl degradation is a highly controlled process. This is seen by protein-protein interactions during the first steps of the pathway that allows metabolic channelling of phototoxic catabolites (Sakuraba et al., 2013, 2012) and by the high co-regulation of Chl catabolic gene expression (Fig. C.4). However, the mechanism(s) of transcriptional regulation of Chl breakdown remain(s) unknown. Interestingly, overexpression of a single Chl catabolic enzyme results in an increased rate of degradation in the whole pathway (Sakuraba et al., 2012). Finally, another very interesting research area in Chl breakdown is to better understand how cell death is triggered by the accumulation of Chl catabolites in mutant such as *acd1* and *acd2*. Interestingly, cell death in *acd1* is not mediated through a singlet oxygen signaling pathway involving EXECUTER proteins and therefore seems to involve different, unknown mechanisms (Stefan Hörtensteiner, unpublished data).

Chl breakdown is part of the chloroplast-to-gerontoplast transition, which also involves processes such as lipid and protein degradation. The introduction of my thesis reveals that many aspects of chloroplast dismantling such as degradation of galactolipids, photosystem subunits and Rubisco remain unclear. Moreover, trafficking of degradation products across the chloroplast envelope during leaf senescence has been completely overlooked. Even though chromoplast proteome analyses have been published (Barsan et al., 2012, 2010; Siddique et al., 2006; Zeng et al., 2011), a coupled analysis of the Arabidopsis gerontoplast proteome and metabolome, would surely be helpful to better understand the fascinating transdifferentiation of chloroplasts to gerontoplasts.

REFERENCES

A

Agne B, Infanger S, Wang F, Hofstetter V, Rahim G, Martin M, Lee DW, Hwang I, Schnell D, Kessler F (2009) A TOC159 import receptor mutant, defective in hydrolysis of GTP, supports preprotein import into chloroplasts. J Biol Chem **284**: 8670–8679

Aida M, Ishida T, Fukaki H, Fujisawa H, Tasaka M (1997) Genes involved in organ separation in Arabidopsis: an analysis of the cup-shaped cotyledon mutant. Plant Cell **9**: 841–857

Alonso JM, Stepanova AN, Leisse TJ, Kim CJ, Chen H, Shinn P, Stevenson DK, Zimmermann J, Barajas P, Cheuk R, et al (2003) Genome-wide insertional mutagenesis of Arabidopsis thaliana. Science **301**: 653–657

Anderson MM, McCarty RE, Zimmer EA (1974) The role of galactolipids in spinach chloroplast lamellar membranes I. Partial purification of a bean leaf galactolipid lipase and its action on subchloroplast particles. Plant Physiol **53**: 699–704

Andersson MX, Goksör M, Sandelius AS (2007) Optical manipulation reveals strong attracting forces at membrane contact sites between endoplasmic reticulum and chloroplasts. J Biol Chem **282**: 1170–1174

Apel K, Hirt H (2004) Reactive oxygen species: metabolism, oxidative stress, and signal transduction. Annu Rev Plant Biol **55**: 373–399

Armstead I, Donnison I, Aubry S, Harper J, Hörtensteiner S, James C, Mani J, Moffet M, Ougham H, Roberts L, et al (2007) Cross-species identification of Mendel's I locus. Science **315**: 73

Aronsson H, Jarvis RP (2011) Rapid isolation of Arabidopsis chloroplasts and their use for in vitro protein import assays. *In* RP Jarvis, ed, Chloroplast research in Arabidopsis. Humana Press, pp 281–305

Aubry S, Mani J, Hörtensteiner S (2008) Stay-green protein, defective in Mendel's green cotyledon mutant, acts independent and upstream of pheophorbide a oxygenase in the chlorophyll catabolic pathway. Plant Mol Biol **67**: 243–256

Austin JR, Frost E, Vidi PA, Kessler F, Staehelin LA (2006) Plastoglobules are lipoprotein subcompartments of the chloroplast that are permanently coupled to thylakoid membranes and contain biosynthetic enzymes. Plant Cell **18**: 1693–1703

Ay N, Irmler K, Fischer A, Uhlemann R, Reuter G, Humbeck K (2009) Epigenetic programming via histone methylation at WRKY53 controls leaf senescence in Arabidopsis thaliana. Plant J **58**: 333–346

Azoulay-Shemer T, Harpaz-Saad S, Cohen-Peer R, Mett A, Spicer V, Lovat N, Krokhin O, Brand A, Gidoni D, Standing KG, et al (2011) Dual N- and C-terminal processing of citrus chlorophyllase precursor within the plastid membranes leads to the mature enzyme. Plant Cell Physiol **52**: 70–83

Azumi Y, Watanabe A (1991) Evidence for a senescence-associated gene induced by darkness. Plant Physiol **95**: 577–583

B

Bachmann M, Keller F (1995) Metabolism of the raffinose family oligosaccharides in leaves of Ajuga reptans L. (Inter- and Intracellular Compartmentation). Plant Physiol **109**: 991–998

Bachmann M, Matile P, Keller F (1994) Metabolism of the raffinose family oligosaccharides in leaves of Ajuga reptans L. (Cold acclimation, translocation, and sink to source transition: discovery of chain elongation enzyme). Plant Physiol **105**: 1335–1345

Baena-Gonzalez E, Rolland F, Thevelein JM, Sheen J (2007) A central integrator of transcription networks in plant stress and energy signalling. Nature **448**: 938–U10

Bak S, Beisson F, Bishop G, Hamberger B, Höfer R, Paquette S, Werck-Reichhart D (2011) Cytochromes P450. Arabidopsis Book. doi: 10.1199/tab.0144

Balazadeh S, Kwasniewski M, Caldana C, Mehrnia M, Zanor MI, Xue GP, Mueller-Roeber B (2011) ORS1, an H2O2-responsive NAC transcription factor, controls senescence in Arabidopsis thaliana. Mol Plant **4**: 346–360

Balazadeh S, Riaño-Pachón DM, Mueller-Roeber B (2008) Transcription factors regulating leaf senescence in Arabidopsis thaliana. Plant Biol **10 (Suppl. 1)**: 63–75

Balazadeh S, Wu A, Mueller-Roeber B (2010) Salt-triggered expression of the ANAC092-dependent senescence regulon in Arabidopsis thaliana. Plant Signal Behav **5**: 733–735

Banala S, Moser S, Müller T, Kreutz CR, Holzinger A, Lütz C, Kräutler B (2010) Hypermodified fluorescent chlorophyll catabolites: source of blue luminescence in senescent leaves. Angew Chem Int Ed **49**: 5174–5177

Barrs H, Weatherley P (1962) A re-examination of the relative turgidity technique for estimating water deficits in leaves. Aust J Biol Sci **15**: 413–428

Barry CS, McQuinn RP, Chung MY, Besuden A, Giovannoni JJ (2008) Amino acid substitutions in homologs of the STAY-GREEN protein are responsible for the green-flesh and chlorophyll retainer mutations of tomato and pepper. Plant Physiol **147**: 179–187

Barsan C, Sanchez-Bel P, Rombaldi C, Egea I, Rossignol M, Kuntz M, Zouine M, Latché A, Bouzayen M, Pech J-C (2010) Characteristics of the tomato chromoplast revealed by proteomic analysis. J Exp Bot **61**: 2413–2431

Barsan C, Zouine M, Maza E, Bian W, Egea I, Rossignol M, Bouyssie D, Pichereaux C, Purgatto E, Bouzayen M, et al (2012) Proteomic analysis of chloroplast-to-chromoplast transition in tomato reveals metabolic shifts coupled with disrupted thylakoid biogenesis machinery and elevated energy-production components. Plant Physiol **160**: 708–725

Beckett M, Loreto F, Velikova V, Brunetti C, Di Ferdinando M, Tattini M, Calfapietra C, Farrant JM (2012) Photosynthetic limitations and volatile and non-volatile isoprenoids in the poikilochlorophyllous resurrection plant Xerophyta humilis during dehydration and rehydration. Plant Cell Environ **35**: 2061–2074

Benedetti CE, Arruda P (2002) Altering the expression of the chlorophyllase gene ATHCOR1 in transgenic Arabidopsis caused changes in the chlorophyll-to-chlorophyllide ratio. Plant Physiol **128**: 1255–1263

Berghold J (2005) Chemische und biochemische Untersuchungen zum Chlorophyllabbau. PhD. Univ. Innsbruck, Innsbruck

Berghold J, Breuker K, Oberhuber M, Hörtensteiner S, Kräutler B (2002) Chlorophyll breakdown in spinach: on the structure of five nonfluorescent chlorophyll catabolites. Photosynth Res **74**: 109–119

Berghold J, Eichmüller C, Hörtensteiner S, Kräutler B (2004) Chlorophyll breakdown in tobacco: on the structure of two nonfluorescent chlorophyll catabolites. Chem Biodivers **1**: 657–668

Berghold J, Müller T, Ulrich M, Hörtensteiner S, Kräutler B (2006) Chlorophyll breakdown in maize: on the structure of two nonfluorescent chlorophyll catabolites. Monatsh Chem **137**: 751–763

Besagni C, Kessler F (2013) A mechanism implicating plastoglobules in thylakoid disassembly during senescence and nitrogen starvation. Planta **237**: 463–470

Besson-Bard A, Pugin A, Wendehenne D (2008) New insights into nitric oxide signaling in plants. Annu Rev Plant Biol **59**: 21–39

Bhalerao R, Keskitalo J, Sterky F, Erlandsson R, Bjorkbacka H, Birve SJ, Karlsson J, Gardestrom P, Gustafsson P, Lundeberg J, et al (2003) Gene expression in autumn leaves. Plant Physiol **131**: 430–442

Bhalla PL, Dalling MJ (1984) Characteristics of a β-galactosidase associated with the stroma of chloroplasts prepared from mesophyll protoplasts of the primary leaf of wheat. Plant Physiol **76**: 92–95

Blöchl A, Peterbauer T, Hofmann J, Richter A (2008) Enzymatic breakdown of raffinose oligosaccharides in pea seeds. Planta **228**: 99–110

Blöchl A, Peterbauer T, Richter A (2007) Inhibition of raffinose oligosaccharide breakdown delays germination of pea seeds. J Plant Physiol **164**: 1093–1096

Block MA, Dorne AJ, Joyard J, Douce R (1983) Preparation and characterization of membrane fractions enriched in outer and inner envelope membranes from spinach chloroplasts. II. Biochemical characterization. J Biol Chem **258**: 13281–13286

Bohnert H, Nelson D, Jensen R (1995) Adaptations to environmental stresses. Plant Cell **7**: 1099–1111

Bopp M (1996) The origin of developmental physiology of plants in Germany. Int J Dev Biol **40**: 89–92

Brandis A, Vainstein A, Goldschmidt EE (1996) Distribution of chlorophyllase among components of chloroplast membranes in Citrus sinensis organs. Plant Physiol Bioch **34**: 49–54

Bréhélin C, Kessler F (2008) The plastoglobule: a bag full of lipid biochemistry tricks. Photochem Photobiol **84**: 1388–1394

Briscoe AD, Chittka L (2001) The evolution of color vision in insects. Annu Rev Entomol **46**: 471–510

Brusslan JA, Rus Alvarez-Canterbury AM, Nair NU, Rice JC, Hitchler MJ, Pellegrini M (2012) Genome-wide evaluation of histone methylation changes associated with leaf senescence in Arabidopsis. PLoS One. doi: 10.1371/journal.pone.0033151

Bryant DA, Frigaard N-U (2006) Prokaryotic photosynthesis and phototrophy illuminated. Trends Microbiol **14**: 488–496

Buchanan-Wollaston V (1997) The molecular biology of leaf senescence. J Exp Bot **48**: 181–199

Buchanan-Wollaston V, Earl S, Harrison E, Mathas E, Navabpour S, Page T, Pink D (2003) The molecular analysis of leaf senescence - a genomics approach. Plant Biotechnol J **1**: 3–22

Buchanan-Wollaston V, Page T, Harrison E, Breeze E, Lim PO, Nam HG, Lin JF, Wu SH, Swidzinski J, Ishizaki K, et al (2005) Comparative transcriptome analysis reveals significant differences in gene expression and signalling pathways between developmental and dark/starvation-induced senescence in Arabidopsis. Plant J **42**: 567–585

Büchert AM, Civello PM, Martínez GA (2011) Characterization of Mg-dechelating substance in senescent and pre-senescent Arabidopsis thaliana leaves. Biol Plant **55**: 75–82

Burg SP (1968) Ethylene, plant senescence and abscission 1. Plant Physiol **43**: 1503–1511

C

Cacela C, Hincha DK (2006) Monosaccharide composition, chain length and linkage type influence the interactions of oligosaccharides with dry phosphatidylcholine membranes. BBA-Biomembranes **1758**: 680–691

Cao J, Jiang F, Sodmergen, Cui K (2003) Time-course of programmed cell death during leaf senescence in Eucommia ulmoides. J Plant Res **116**: 7–12

Carpenter JF, Crowe JH (1988) The mechanism of cryoprotection of proteins by solutes. Cryobiology **25**: 244–255

Chen LF, Chan SY, Cossins EA (1997) Distribution of folate derivatives and enzymes for synthesis of 10-formyltetrahydrofolate in cytosolic and mitochondrial fractions of pea leaves. Plant Physiol **115**: 299–309

Chen M, Schliep M, Willows RD, Cai ZL, Neilan BA, Scheer H (2010) A red-shifted chlorophyll. Science **329**: 1318–1319

Chen THH, Murata N (2008) Glycinebetaine: an effective protectant against abiotic stress in plants. Trends Plant Sci **13**: 499–505

Chen W, Provart NJ, Glazebrook J, Katagiri F, Chang H-S, Eulgem T, Mauch F, Luan S, Zou G, Whitham SA, et al (2002) Expression profile matrix of Arabidopsis transcription factor genes suggests their putative functions in response to environmental stresses. Plant Cell **14**: 559–574

Chen XM (2010) Small RNAs - secrets and surprises of the genome. Plant J **61**: 941–958

Chew AGM, Bryant DA (2007) Chlorophyll biosynthesis in bacteria: the origins of structural and functional diversity. Annu Rev Microbiol **61**: 113–129

Chiba A, Ishida H, Nishizawa NK, Makino A, Mae T (2003) Exclusion of ribulose-1,5-bisphosphate carboxylase/oxygenase from chloroplasts by specific bodies in naturally senescing leaves of wheat. Plant Cell Physiol **44**: 914–921

Chory J, Nagpal P, Peto CA (1991) Phenotypic and genetic analysis of det2, a new mutant that affects light-regulated seedling development in Arabidopsis. Plant Cell **3**: 445–459

Christ B, Schelbert S, Aubry S, Süssenbacher I, Müller T, Kräutler B, Hörtensteiner S (2012) MES16, a member of the methylesterase protein family, specifically demethylates fluorescent chlorophyll catabolites during chlorophyll breakdown in Arabidopsis. Plant Physiol **158**: 628–641

Chuck G, O'Connor D (2010) Small RNAs going the distance during plant development. Curr Opin Plant Biol **13**: 40–45

Chung DW, Pružinská A, Hörtensteiner S, Ort DR (2006) The role of pheophorbide a oxygenase expression and activity in the canola green seed problem. Plant Physiol **142**: 88–97

Clough SJ, Bent AF (1998) Floral dip: a simplified method for Agrobacterium-mediated transformation of Arabidopsis thaliana. Plant J **16**: 735–743

Clouse SD, Sasse JM (1998) Brassinosteroids: essential regulators of plant growth and development. Annu Rev Plant Phys **49**: 427–451

Collett H, Butowt R, Smith J, Farrant J, Illing N (2003) Photosynthetic genes are differentially transcribed during the dehydration-rehydration cycle in the resurrection plant, Xerophyta humilis. J Exp Bot **54**: 2593–2595

Collett H, Shen A, Gardner M, Farrant JM, Denby KJ, Illing N (2004) Towards transcript profiling of desiccation tolerance in Xerophyta humilis: construction of a normalized 11 k X. humilis cDNA set and microarray expression analysis of 424 cDNAs in response to dehydration. Physiol Plantarum **122**: 39–53

Corpas FJ, Barroso JB, Carreras A, Quirós M, León AM, Romero-Puertas MC, Esteban FJ, Valderrama R, Palma JM, Sandalio LM, et al (2004) Cellular and subcellular localization of endogenous nitric oxide in young and senescent pea plants. Plant Physiol **136**: 2722–2733

Curty C, Engel N (1996) Detection, isolation and structure elucidation of a chlorophyll a catabolite from autumnal senescent leaves of Cercidiphyllum japonicum. Phytochemistry **42**: 1531–1536

Czarnecki O, Grimm B (2012) Post-translational control of tetrapyrrole biosynthesis in plants, algae, and cyanobacteria. J Exp Bot **63**: 1675–1687

D

DellaPenna D, Pogson BJ (2006) Vitamin synthesis in plants: tocopherols and carotenoids. Annu Rev Plant Biol **57**: 711–738

Delorme VG, McCabe PF, Kim DJ, Leaver CJ (2000) A matrix metalloproteinase gene is expressed at the boundary of senescence and programmed cell death in cucumber. Plant Physiol **123**: 917–927

Deprost D, Yao L, Sormani R, Moreau M, Leterreux G, Nicolaï M, Bedu M, Robaglia C, Meyer C (2007) The Arabidopsis TOR kinase links plant growth, yield, stress resistance and mRNA translation. EMBO Rep **8**: 864–870

Deruère J, Römer S, D' Harlingue A, Backhaus RA, Kuntz M, Camara B (1994) Fibril assembly and carotenoid overaccumulation in chromoplasts: a model for supramolecular lipoprotein structures. Plant Cell **6**: 119–133

Dinur T, Grabowski GA, Desnick RJ, Gatt S (1984) Synthesis of a fluorescent derivative of glucosyl ceramide for the sensitive determination of glucocerebrosidase activity. Anal Biochem **136**: 223–234

Djapic N, Pavlovic M (2008) Chlorophyll catabolite from Parrotia persica autumnal leaves. Rev Chim **59**: 878–882

Djapic N, Pavlovic M, Arsovski S, Vujic G (2009) Chlorophyl biodegradation product from Hamamelis virginiana autumnal leaves. Rev Chim **60**: 398–402

Donnison IS, Gay AP, Thomas H, Edwards KJ, Edwards D, James CL, Thomas AM, Ougham HJ (2007) Modification of nitrogen remobilization, grain fill and leaf senescence in maize (Zea mays) by transposon insertional mutagenesis in a protease gene. New Phytol **173**: 481–494

Van Doorn WG (2008) Is the onset of senescence in leaf cells of intact plants due to low or high sugar levels? J Exp Bot **59**: 1963–1972

Van Doorn WG, Woltering EJ (2004) Senescence and programmed cell death: substance or semantics? J Exp Bot **55**: 2147–2153

Dörmann P, Benning C (2002) Galactolipids rule in seed plants. Trends Plant Sci **7**: 112–118

Dosnon-Olette R, Schröder P, Bartha B, Aziz A, Couderchet M, Eullaffroy P (2011) Enzymatic basis for fungicide removal by Elodea canadensis. Environ Sci Pollut Res **18**: 1015–1021

Downie A, Miyazaki S, Bohnert H, John P, Coleman J, Parry M, Haslam R (2004) Expression profiling of the response of Arabidopsis thaliana to methanol stimulation. Phytochemistry **65**: 2305–2316

E

Eckhardt U, Grimm B, Hörtensteiner S (2004) Recent advances in chlorophyll biosynthesis and breakdown in higher plants. Plant Mol Biol **56**: 1–14

Ellis CM, Nagpal P, Young JC, Hagen G, Guilfoyle TJ, Reed JW (2005) AUXIN RESPONSE FACTOR1 and AUXIN RESPONSE FACTOR2 regulate senescence and floral organ abscission in Arabidopsis thaliana. Development **132**: 4563–4574

Endler A, Meyer S, Schelbert S, Schneider T, Weschke W, Peters SW, Keller F, Baginsky S, Martinoia E, Schmidt UG (2006) Identification of a vacuolar sucrose transporter in barley and Arabidopsis mesophyll cells by a tonoplast proteomic approach. Plant Physiol **141**: 196–207

Espineda CE, Linford AS, Devine D, Brusslan JA (1999) The AtCAO gene, encoding chlorophyll a oxygenase, is required for chlorophyll b synthesis in Arabidopsis thaliana. Proc Natl Acad Sci USA **96**: 10507–10511

Espinoza C, Degenkolbe T, Caldana C, Zuther E, Leisse A, Willmitzer L, Hincha DK, Hannah MA (2010) Interaction with diurnal and circadian regulation results in dynamic metabolic and transcriptional changes during cold acclimation in Arabidopsis. PLoS ONE **5**: e14101

Eulgem T, Somssich IE (2007) Networks of WRKY transcription factors in defense signaling. Curr Opin Plant Biol **10**: 366–371

Even-Chen Z, Itai C (1975) The role of abscisic acid in senescence of detached tobacco leaves. Physiol Plantarum **34**: 97–100

F

Fall R, Benson AA (1996) Leaf methanol — the simplest natural product from plants. Trends Plant Sci **1**: 296–301

Fan L, Zheng S, Wang X (1997) Antisense suppression of phospholipase D alpha retards abscisic acid- and ethylene-promoted senescence of postharvest Arabidopsis leaves. Plant Cell **9**: 2183–96

Farrant JM (2000) A comparison of mechanisms of desiccation tolerance among three angiosperm resurrection plant species. Plant Ecology **151**: 29–39

Feller U, Anders I, Mae T (2008) Rubiscolytics: fate of Rubisco after its enzymatic function in a cell is terminated. J Exp Bot **59**: 1615–1624

Finkelstein RR, Rock CD (2002) Abscisic acid biosynthesis and response. Arabidopsis Book. doi: 10.1199/tab.0058

Fischer AM (2012) The complex regulation of senescence. CRC Cr Rev Plant Sci **31**: 124–147

Fletcher RA, Osborne DJ (1966) Gibberellin as a regulator of protein and ribonucleic acid synthesis during senescence of leaf cells of Taraxacum officinale. Can J Bot **44**: 739–745

Foyer CH, Noctor G (2005) Redox homeostasis and antioxidant signaling: a metabolic interface between stress perception and physiological responses. Plant Cell **17**: 1866–1875

Franklin KA, Quail PH (2010) Phytochrome functions in Arabidopsis development. J Exp Bot **61**: 11–24

Frye CA, Tang D, Innes RW (2001) Negative regulation of defense responses in plants by a conserved MAPKK kinase. Proc Natl Acad Sci USA **98**: 373–378

Fujiki Y, Ito M, Nishida I, Watanabe A (2000) Multiple signaling pathways in gene expression during sugar starvation. Pharmacological analysis of DIN gene expression in suspension-cultured cells of Arabidopsis. Plant Physiol **124**: 1139–1148

Fujiki Y, Yoshikawa Y, Sato T, Inada N, Ito M, Nishida I, Watanabe A (2001) Dark-inducible genes from Arabidopsis thaliana are associated with leaf senescence and repressed by sugars. Physiol Plantarum **111**: 345–352

G

Gaff DF, McGregor GR (1979) The effect of dehydration and rehydration on the nitrogen content of various fractions from resurrection plants. Biol Plant **21**: 92–99

Gan S, Amasino RM (1995) Inhibition of leaf senescence by autoregulated production of cytokinin. Science **270**: 1986–1988

Gantt E (1981) Phycobilisomes. Ann Rev Plant Physio **32**: 327–347

Gao Z, Schaffer AA (1999) A novel alkaline a-galactosidase from melon fruit with a substrate preference for raffinose. Plant Physiol **119**: 979–988

Gepstein S, Thimann KV (1980) Changes in the abscisic acid content of oat leaves during senescence. Proc Natl Acad Sci USA **77**: 2050–2053

Gierloff-Emden HG, Buchroithner MF (1989) Fernerkundungskartographie mit Satellitenaufnahmen. 1. Allgemeine Grundlagen und Anwendungen. Deuticke

Ginsburg S, Matile P (1993) Identification of catabolites of chlorophyll porphyrin in senescent rape cotyledons. Plant Physiol **102**: 521–527

Ginsburg S, Schellenberg M, Matile P (1994) Cleavage of chlorophyll-porphyrin. Requirement for reduced ferredoxin and oxygen. Plant Physiol **105**: 545–554

Goldthwaite JJ, Laetsch WM (1968) Control of senescence in Rumex leaf discs by gibberellic acid. Plant Physiol **43**: 1855–1858

Golldack D, Popova OV, Dietz K-J (2002) Mutation of the matrix metalloproteinase At2-MMP inhibits growth and causes late flowering and early senescence in Arabidopsis. J Biol Chem **277**: 5541–5547

Gottlieb HE, Kotlyar V, Nudelman A (1997) NMR chemical shifts of common laboratory solvents as trace impurities. J Org Chem **62**: 7512–7515

Gout E, Aubert S, Bligny R, Rébeillé F, Nonomura AR, Benson AA, Douce R (2000) Metabolism of methanol in plant cells. Carbon-13 nuclear magnetic resonance studies. Plant Physiol **123**: 287–296

Van der Graaff E, Schwacke R, Schneider A, Desimone M, Flugge UI, Kunze R (2006) Transcription analysis of Arabidopsis membrane transporters and hormone pathways during developmental and induced leaf senescence. Plant Physiol **141**: 776–792

Gray J, Janick-Bruckner D, Bruckner B, Close PS, Johal GS (2002) Light-dependent death of maize lls1 cells is mediated by mature chloroplasts. Plant Physiol **130**: 1894–1907

Gray J, Wardzala E, Yang M, Reinbothe S, Haller S, Pauli F (2004) A small family of LLS1-related non-heme oxygenases in plants with an origin amongst oxygenic photosynthesizers. Plant Mol Biol **54**: 39–54

Grbić V, Bleecker AB (1995) Ethylene regulates the timing of leaf senescence in Arabidopsis. Plant J **8**: 595–602

Greenberg JT, Ausubel FM (1993) Arabidopsis mutants compromised for the control of cellular damage during pathogenesis and aging. Plant J **4**: 327–341

Grossmann GA, Terra WR (2001) α-Galactosidases from the larval midgut of Tenebrio molitor (Coleoptera) and Spodoptera frugiperda (Lepidoptera). Comp Biochem Phys B **128**: 109–122

Guengerich FP (2001) Common and uncommon cytochrome P450 reactions related to metabolism and chemical toxicity. Chem Res Toxicol **14**: 611–650

Guo F-Q, Crawford NM (2005) Arabidopsis NITRIC OXIDE SYNTHASE1 is targeted to mitochondria and protects against oxidative damage and dark-induced senescence. Plant Cell **17**: 3436–3450

Guo Y, Cai Z, Gan S (2004) Transcriptome of Arabidopsis leaf senescence. Plant Cell Environ **27**: 521–549

Guo Y, Gan S (2006) AtNAP, a NAC family transcription factor, has an important role in leaf senescence. Plant J **46**: 601–612

Guy C, Kaplan F, Kopka J, Selbig J, Hincha DK (2008) Metabolomics of temperature stress. Physiol Plantarum **132**: 220–235

H

Halkier BA (1996) Catalytic reactivities and structure/function relationships of cytochrome P450 enzymes. Phytochemistry **43**: 1–21

Hara-Nishimura I, Hatsugai N, Nakaune S, Kuroyanagi M, Nishimura M (2005) Vacuolar processing enzyme: an executor of plant cell death. Curr Opin Plant Biol **8**: 404–408

Hare PD, Cress WA, Van Staden J (1998) Dissecting the roles of osmolyte accumulation during stress. Plant Cell Environ **21**: 535–553

Harpaz-Saad S, Azoulay T, Arazi T, Ben-Yaakov E, Mett A, Shiboleth YM, Hörtensteiner S, Gidoni D, Gal-On A, Goldschmidt EE, et al (2007) Chlorophyllase is a rate-limiting enzyme in chlorophyll catabolism and is posttranslationally regulated. Plant Cell **19**: 1007–1022

Hatsugai N, Kuroyanagi M, Yamada K, Meshi T, Tsuda S, Kondo M, Nishimura M, Hara-Nishimura I (2004) A plant vacuolar protease, VPE, mediates virus-induced hypersensitive cell death. Science **305**: 855–858

He K, Gou X, Yuan T, Lin H, Asami T, Yoshida S, Russell SD, Li J (2007) BAK1 and BKK1 regulate brassinosteroid-dependent growth and brassinosteroid-independent cell-death pathways. Curr Biol **17**: 1109–1115

He P, Osaki M, Takebe M, Shinano T, Wasaki J (2005) Endogenous hormones and expression of senescence-related genes in different senescent types of maize. J Exp Bot **56**: 1117–1128

He Y, Fukushige H, Hildebrand DF, Gan S (2002) Evidence supporting a role of jasmonic acid in Arabidopsis leaf senescence. Plant Physiol **128**: 876–884

He Y, Gan S (2002) A gene encoding an acyl hydrolase is involved in leaf senescence in Arabidopsis. Plant Cell **14**: 805–815

Heber U (1959) Beziehungen zwischen der Größe von Chloroplasten und ihrem Gehalt an löslichen Eiweißen und Zuckern im Zusammenhang mit dem Frostresistenzproblem. Protoplasma **51**: 284–298

Hellens R, Edwards EA, Leyland NR, Bean S, Mullineaux PM (2000) pGreen: a versatile and flexible binary Ti vector for Agrobacterium-mediated plant transformation. Plant Mol Biol **42**: 819–832

Herring JW and D (2000) NASA Earth Observatory. http://earthobservatory.nasa.gov/Features/MeasuringVegetation/measuring_vegetation_2.php

Hincha DK, Zuther E, Heyer AG (2003) The preservation of liposomes by raffinose family oligosaccharides during drying is mediated by effects on fusion and lipid phase transitions. BBA-Biomembranes **1612**: 172–177

Hinderhofer K, Zentgraf U (2001) Identification of a transcription factor specifically expressed at the onset of leaf senescence. Planta **213**: 469–473

Hirashima M, Satoh S, Tanaka R, Tanaka A (2006) Pigment shuffling in antenna systems achieved by expressing prokaryotic chlorophyllide a oxygenase in Arabidopsis. J Biol Chem **281**: 15385–15393

Hirashima M, Tanaka R, Tanaka A (2009) Light-independent cell death induced by accumulation of pheophorbide a in Arabidopsis thaliana. Plant Cell Physiol **50**: 719–729

Hoekstra FA, Golovina EA, Buitink J (2001) Mechanisms of plant desiccation tolerance. Trends Plant Sci **6**: 431–438

Holden M (1961) The breakdown of chlorophyll by chlorophyllase. Biochem J **78**: 359–364

Van der Hoorn RAL (2008) Plant Proteases: from phenotypes to molecular mechanisms. Annu Rev Plant Biol **59**: 191–223

Horie Y, Ito H, Kusaba M, Tanaka R, Tanaka A (2009) Participation of chlorophyll b reductase in the initial step of the degradation of light-harvesting chlorophyll a/b-protein complexes in Arabidopsis. J Biol Chem **284**: 17449–17456

Hörtensteiner S (2009) Stay-green regulates chlorophyll and chlorophyll-binding protein degradation during senescence. Trends Plant Sci **14**: 155–162

Hörtensteiner S (2006) Chlorophyll degradation during senescence. Annu Rev Plant Biol **57**: 55–77

Hörtensteiner S (1998) NCC malonyltransferase catalyses the final step of chlorophyll breakdown in rape (Brassica napus). Phytochemistry **49**: 953–956

Hörtensteiner S (2004) The loss of green color during chlorophyll degradation - a prerequisite to prevent cell death? Planta **219**: 191–194

Hörtensteiner S (2012) Update on the biochemistry of chlorophyll breakdown. Plant Mol Biol 1–13

Hörtensteiner S, Feller U (2002) Nitrogen metabolism and remobilization during senescence. J Exp Bot **53**: 927–937

Hörtensteiner S, Kräutler B (2011) Chlorophyll breakdown in higher plants. Biochem Biophys Acta **1807**: 977–988

Hörtensteiner S, Rodoni S, Schellenberg M, Vicentini F, Nandi OI, Qiu Y-L, Matile P (2000) Evolution of chlorophyll degradation: the significance of RCC reductase. Plant Biol **2**: 63–67

Hörtensteiner S, Vicentini F, Matile P (1995) Chlorophyll breakdown in senescent cotyledons of rape, Brassica napus L.: enzymatic cleavage of phaeophorbide a in vitro. New Phytol **129**: 237–246

Hörtensteiner S, Wüthrich KL, Matile P, Ongania K-H, Kräutler B (1998) The key step in chlorophyll breakdown in higher plants. Cleavage of pheophorbide a macrocycle by a monooxygenase. J Biol Chem **273**: 15335–15339

I

Igamberdiev AU, Bykova NV, Kleczkowski LA (1999) Origins and metabolism of formate in higher plants. Plant Physiol Bioch **37**: 503–513

Inada N, Sakai A, Kuroiwa H, Kuroiwa T (1998) Three-dimensional analysis of the senescence program in rice (Oryza sativa L.) coleoptiles. Investigations of tissues and cells by fluorescence microscopy. Planta **205**: 153–64

Ingle RA, Collett H, Cooper K, Takahashi Y, Farrant JM, Illing N (2008) Chloroplast biogenesis during rehydration of the resurrection plant Xerophyta humilis: parallels to the etioplast–chloroplast transition. Plant Cell Environ **31**: 1813–1824

Ingle RA, Schmidt UG, Farrant JM, Thomson JA, Mundree SG (2007) Proteomic analysis of leaf proteins during dehydration of the resurrection plant Xerophyta viscosa. Plant Cell Environ **30**: 435–446

Ingle RA, Smith JAC, Sweetlove LJ (2005) Responses to nickel in the proteome of the hyperaccumulator plant Alyssum lesbiacum. Biometals **18**: 627–641

Ingram J, Bartels D (1996) The molecular basis of dehydration tolerance in plants. Annu Rev Plant Phys **47**: 377–403

Ischebeck T, Zbierzak AM, Kanwischer M, Dörmann P (2006) A salvage pathway for phytol metabolism in Arabidopsis. J Biol Chem **281**: 2470–2477

Ishida H, Wada S (2009) Autophagy of whole and partial chloroplasts in individually darkened leaves A unique system in plants? Autophagy **5**: 736–737

Ishida H, Yoshimoto K, Izumi M, Reisen D, Yano Y, Makino A, Ohsumi Y, Hanson MR, Mae T (2008) Mobilization of rubisco and stroma-localized fluorescent proteins of chloroplasts to the vacuole by an ATG gene-dependent autophagic process. Plant Physiol **148**: 142–155

Iturraspe J, Moyano N, Frydman B (1995) A new 5-formylbilinone as the major chlorophyll a catabolite in tree senescent leaves. J Org Chem **60**: 6664–6665

Izumi M, Wada S, Makino A, Ishida H (2010) The autophagic degradation of chloroplasts via Rubisco-containing bodies is specifically linked to leaf carbon status but not nitrogen status in Arabidopsis. Plant Physiol **154**: 1196–1209

J

Jakob-Wilk D, Holland D, Goldschmidt EE, Riov J, Eyal Y (1999) Chlorophyll breakdown by chlorophyllase: isolation and functional expression of the Chlase1 gene from ethylene-treated Citrus fruit and its regulation during development. Plant J **20**: 653–661

Jalink H, Van der Schoor R, Frandas A, Van Pijlen JG, Bino RJ (1998) Chlorophyll fluorescence of Brassica oleracea seeds as a non-destructive marker for seed maturity and seed performance. Seed Sci Res **8**: 437–443

Jansson S, Thomas H (2008) Senescence: developmental program or timetable? New Phytol **179**: 575–579

Jensen K, Moller BL (2010) Plant NADPH-cytochrome P450 oxidoreductases. Phytochemistry **71**: 132–141

Jiang H, Li M, Liang N, Yan H, Wei Y, Xu X, Liu J, Xu Z, Chen F, Wu G (2007) Molecular cloning and function analysis of the stay green gene in rice. Plant J **52**: 197–209

Jiménez A, Hernández JA, Pastori G, Río LA del, Sevilla F (1998) Role of the ascorbate-glutathione cycle of mitochondria and peroxisomes in the senescence of pea leaves. Plant Physiol **118**: 1327–1335

Jin Y, Ni D-A, Ruan Y-L (2009) Posttranslational elevation of cell wall invertase activity by silencing its inhibitor in tomato delays leaf senescence and increases seed weight and fruit hexose level. Plant Cell **21**: 2072–2089

Jing HC, Anderson L, Sturre MJG, Hille J, Dijkwel PP (2007) Arabidopsis CPR5 is a senescence-regulatory gene with pleiotropic functions as predicted by the evolutionary theory of senescence. J Exp Bot **58**: 3885–3894

Jing HC, Hebeler R, Oeljeklaus S, Sitek B, Stühler K, Meyer HE, Sturre MJG, Hille J, Warscheid B, Dijkwel PP (2008) Early leaf senescence is associated with an altered cellular redox balance in Arabidopsis cpr5/old1 mutants. Plant Biol **10**: 85–98

Jing HC, Hille J, Dijkwel PP (2003) Ageing in plants: conserved strategies and novel pathways. Plant Biol **5**: 455–464

Jing HC, Schippers JHM, Hille J, Dijkwel PP (2005) Ethylene-induced leaf senescence depends on age-related changes and OLD genes in Arabidopsis. J Exp Bot **56**: 2915–2923

Jing HC, Sturre MJG, Hille J, Dijkwel PP (2002) Arabidopsis onset of leaf death mutants identify a regulatory pathway controlling leaf senescence. Plant J **32**: 51–63

John I, Drake R, Farrell A, Cooper W, Lee P, Horton P, Grierson D (1995) Delayed leaf senescence in ethylene-deficient ACC-oxidase antisense tomato plants - molecular and physiological analysis. Plant J **7**: 483–490

Jonker JW, Buitelaar M, Wagenaar E, Van der Valk MA, Scheffer GL, Scheper RJ, Plösch T, Kuipers F, Oude Elferink RPJ, Rosing H, et al (2002) The breast cancer resistance protein protects against a major chlorophyll-derived dietary phototoxin and protoporphyria. Proc Natl Acad Sci USA **99**: 15649–15654

Jossier M, Bouly J-P, Meimoun P, Arjmand A, Lessard P, Hawley S, Grahame Hardie D, Thomas M (2009) SnRK1 (SNF1-related kinase 1) has a central role in sugar and ABA signalling in Arabidopsis thaliana. Plant J **59**: 316–328

K

Kang J, Park J, Choi H, Burla B, Kretzschmar T, Lee Y, Martinoia E (2011a) Plant ABC transporters. Arabidopsis Book **9**: e0153

Kang K, Kim Y-S, Park S, Back K (2009) Senescence-induced serotonin biosynthesis and its role in delaying senescence in rice leaves. Plant Physiol **150**: 1380–1393

Kang K, Park S, Natsagdorj U, Kim YS, Back K (2011b) Methanol is an endogenous elicitor molecule for the synthesis of tryptophan and tryptophan-derived secondary metabolites upon senescence of detached rice leaves. Plant J **66**: 247–257

Kaniuga Z, Gemel J (1984) Galactolipase activity and free fatty acid levels in chloroplasts: novel approach to characteristics of chilling sensitivity of plants. FEBS Lett **171**: 55–58

Kaniuga Z, Sączyńska V, Miśkiewicz E, Garstka M (1999) Degradation of leaf polar lipids during chilling and post-chilling rewarming of Zea mays genotypes reflects differences in their response to chilling stress. The role of galactolipase. Acta Physiol Plant **21**: 45–56

Kariola T, Brader G, Li J, Palva ET (2005) Chlorophyllase 1, a damage control enzyme, affects the balance between defense pathways in plants. Plant Cell **17**: 282–294

Kato Y, Murakami S, Yamamoto Y, Chatani H, Kondo Y, Nakano T, Yokota A, Sato F (2004) The DNA-binding protease, CND41, and the degradation of ribulose-1,5-bisphosphate carboxylase/oxygenase in senescent leaves of tobacco. Planta **220**: 97–104

Kato Y, Sakamoto W (2010) New insights into the types and function of proteases in plastids. *In* Kwang W. Jeon, ed, International Review of Cell and Molecular Biology. Academic Press, pp 185–218

Kato Y, Yamamoto Y, Murakami S, Sato F (2005) Post-translational regulation of CND41 protease activity in senescent tobacco leaves. Planta **222**: 643–651

Keech O (2011) The conserved mobility of mitochondria during leaf senescence reflects differential regulation of the cytoskeletal components in Arabidopsis thaliana. Plant Signal Behav **6**: 147–150

Keech O, Pesquet E, Ahad A, Askne A, Nordvall D, Vodnala SM, Tuominen H, Hurry V, Dizengremel P, Gardeström P (2007) The different fates of mitochondria and chloroplasts during dark-induced senescence in Arabidopsis leaves. Plant Cell Environ **30**: 1523–1534

Keech O, Pesquet E, Gutierrez L, Ahad A, Bellini C, Smith SM, Gardestrom P (2010) Leaf senescence is accompanied by an early disruption of the microtubule network in Arabidopsis. Plant Physiol **154**: 1710–1720

Kim E-H, Li X-P, Razeghifard R, Anderson JM, Niyogi KK, Pogson BJ, Chow WS (2009a) The multiple roles of light-harvesting chlorophyll a/b-protein complexes define structure and optimize function of Arabidopsis chloroplasts: A study using two chlorophyll b-less mutants. BBA-Bioenergetics **1787**: 973–984

Kim HJ, Ryu H, Hong SH, Woo HR, Lim PO, Lee IC, Sheen J, Nam HG, Hwang I (2006) Cytokinin-mediated control of leaf longevity by AHK3 through phosphorylation of ARR2 in Arabidopsis. Proc Natl Acad Sci USA **103**: 814–819

Kim JH, Woo HR, Kim J, Lim PO, Lee IC, Choi SH, Hwang D, Nam HG (2009b) Trifurcate feed-forward regulation of age-dependent cell death involving miR164 in Arabidopsis. Science **323**: 1053–1057

Kim JI, Murphy AS, Baek D, Lee S-W, Yun D-J, Bressan RA, Narasimhan ML (2011) YUCCA6 over-expression demonstrates auxin function in delaying leaf senescence in Arabidopsis thaliana. J Exp Bot **62**: 3981–3992

Kleffmann T, Russenberger D, Von Zychlinski A, Christopher W, Sjolander K, Gruissem W, Baginsky S (2004) The Arabidopsis thaliana chloroplast proteome reveals pathway abundance and novel protein functions. Curr Biol **14**: 354–362

Knaupp M, Mishra KB, Nedbal L, Heyer AG (2011) Evidence for a role of raffinose in stabilizing photosystem II during freeze–thaw cycles. Planta **234**: 477–486

Kong ZS, Li MN, Yang WQ, Xu WY, Xue YB (2006) A novel nuclear-localized CCCH-type zinc finger protein, OsDOS, is involved in delaying leaf senescence in rice. Plant Physiol **141**: 1376–1388

Kranner I, Beckett RP, Wornik S, Zorn M, Pfeifhofer HW (2002) Revival of a resurrection plant correlates with its antioxidant status. Plant J **31**: 13–24

Kräutler B (2008) Chlorophyll catabolites. *In* W Herz, H Falk, GW Kirny, RE Moore, C Tann, eds, Progress in the Chemistry of Organic Natural Products. Springer, Vienna, pp 1–43

Kräutler B, Banala S, Moser S, Vergeiner C, Müller T, Lütz C, Holzinger A (2010) A novel blue fluorescent chlorophyll catabolite accumulates in senescent leaves of the peace lily (Spathiphyllum wallisii) and indicates a divergent path of chlorophyll breakdown. FEBS Lett **584**: 4215–4221

Kräutler B, Jaun B, Bortlik K-H, Schellenberg M, Matile P (1991) On the enigma of chlorophyll degradation: the constitution of a secoporphinoid catabolite. Angew Chem Int Ed **30**: 1315–1318

Kräutler B, Matile P (1999) Solving the riddle of chlorophyll breakdown. Acc Chem Res **32**: 35–43

Kräutler B, Mühlecker W, Anderl M, Gerlach B (1997) Breakdown of chlorophyll: partial synthesis of a putative intermediary catabolite. Helvetica Chimica Acta **80**: 1355–1362

Kubis SE, Lilley KS, Jarvis P (2008) Isolation and preparation of chloroplasts from Arabidopsis thaliana plants. Methods Mol Biol **425**: 171–186

Kusaba M, Ito H, Morita R, Iida S, Sato Y, Fujimoto M, Kawasaki S, Tanaka R, Hirochika H, Nishimura M, et al (2007) Rice NON-YELLOW COLORING1 is involved in light-harvesting complex II and grana degradation during leaf senescence. Plant Cell **19**: 1362–1375

L

Lara MEB, Garcia MCG, Fatima T, Ehness R, Lee TK, Proels R, Tanner W, Roitsch T (2004) Extracellular invertase is an essential component of cytokinin-mediated delay of senescence. Plant Cell **16**: 1276–1287

Lee IC, Hong SW, Whang SS, Lim PO, Nam HG, Koo JC (2011) Age-dependent action of an ABA-inducible receptor kinase, RPK1, as a positive regulator of senescence in Arabidopsis leaves. Plant Cell Physiol **52**: 651–662

Lee RH, Hsu JH, Huang HJ, Lo SF, Chen SCG (2009) Alkaline alpha-galactosidase degrades thylakoid membranes in the chloroplast during leaf senescence in rice. New Phytol **184**: 596–606

Li R, Moore M, Bonham-Smith PC, King J (2002) Overexpression of formate dehydrogenase in Arabidopsis thaliana resulted in plants tolerant to high concentrations of formate. J Plant Physiol **159**: 1069–1076

Li R, Ziola B, King J (2000) Purification and characterization of formate dehydrogenase from Arabidopsis thaliana. J Plant Physiol **157**: 161–167

Li XP, Gan R, Li PL, Ma YY, Zhang LW, Zhang R, Wang Y, Wang NN (2006) Identification and functional characterization of a leucine-rich repeat receptor-like kinase gene that is involved in regulation of soybean leaf senescence. Plant Mol Biol **61**: 829–844

Lilley RM, Fitzgerald MP, Rienits KG, Walker DA (1975) Criteria of intactness and the photosynthetic activity of spinach chloroplast preparations. New Phytol **75**: 1–10

Lim E-K, Baldauf S, Li Y, Elias L, Worrall D, Spencer SP, Jackson RG, Taguchi G, Ross J, Bowles DJ (2003) Evolution of substrate recognition across a multigene family of glycosyltransferases in Arabidopsis. Glycobiology **13**: 139–145

Lim PO, Kim HJ, Gil Nam H (2007) Leaf senescence. Annu Rev Plant Biol **58**: 115–136

Lin JF, Wu SH (2004) Molecular events in senescing Arabidopsis leaves. Plant J **39**: 612–628

Lineberger RD, Steponkus PL (1980) Cryoprotection by glucose, sucrose, and raffinose to chloroplast thylakoids 1. Plant Physiol **65**: 298–304

Lippold F, Dorp K vom, Abraham M, Hölzl G, Wewer V, Yilmaz JL, Lager I, Montandon C, Besagni C, Kessler F, et al (2012) Fatty acid phytyl ester synthesis in chloroplasts of Arabidopsis. Plant Cell **24**: 2001–2014

Liu Y, Bassham DC (2012) Autophagy: pathways for self-eating in plant cells. Annu Rev Plant Biol **63**: 215–237

Losey FG, Engel N (2001) Isolation and characterization of a urobilinogenoidic chlorophyll catabolite from Hordeum vulgare L. J Biol Chem **276**: 27233–27236

Lu Y-P, Li Z-S, Drozdowicz Y-M, Hörtensteiner S, Martinoia E, Rea PA (1998) AtMRP2, an Arabidopsis ATP binding cassette transporter able to transport glutathione S-conjugates and chlorophyll catabolites: functional comparisons with AtMRP1. Plant Cell **10**: 267–282

Lucinski R, Misztal L, Samardakiewicz S, Jackowski G (2011) The thylakoid protease Deg2 is involved in stress-related degradation of the photosystem II light-harvesting protein Lhcb6 in Arabidopsis thaliana. New Phytol **192**: 74–86

Lundquist PK, Poliakov A, Bhuiyan NH, Zybailov B, Sun Q, Van Wijk KJ (2012) The functional network of the Arabidopsis plastoglobule proteome based on quantitative proteomics and genome-wide coexpression analysis. Plant Physiol **158**: 1172–1192

Luo Z, Zhang J, Li J, Yang C, Wang T, Ouyang B, Li H, Giovannoni J, Ye Z (2013) A STAY-GREEN protein SlSGR1 regulates lycopene and β-carotene accumulation by interacting directly with SlPSY1 during ripening processes in tomato. New Phytol **198(2)**: 442–452

M

Ma W, Smigel A, Walker RK, Moeder W, Yoshioka K, Berkowitz GA (2010) Leaf senescence signaling: the Ca2+-conducting Arabidopsis cyclic nucleotide gated channel2 acts through nitric oxide to repress senescence programming. Plant Physiol **154**: 733–743

Mach JM, Castillo AR, Hoogstraten R, Greenberg JT (2001) The Arabidopsis-accelerated cell death gene ACD2 encodes red chlorophyll catabolite reductase and suppresses the spread of disease symptoms. Proc Natl Acad Sci USA **98**: 771–776

Makino A, Osmond B (1991) Effect of nitrogen nutrition on nitrogen partitioning between chloroplasts and mitochondria in pea and wheat. Plant Physiol **96**: 355–362

Martínez DE, Costa ML, Gomez FM, Otegui MS, Guiamet JJ (2008) "Senescence-associated vacuoles" are involved in the degradation of chloroplast proteins in tobacco leaves. Plant J **56**: 196–206

Martinis J, Kessler F, Glauser G (2011) A novel method for prenylquinone profiling in plant tissues by ultra-high pressure liquid chromatography-mass spectrometry. Plant Methods **7**: 23

Masuda T, Takamiya K (2004) Novel insights into the enzymology, regulation and physiological functions of light-dependent protochlorophyllide oxidoreductase in angiosperms. Photosyth Res **81**: 1–29

Matile P, Ginsburg S, Schellenberg M, Thomas H (1988) Catabolites of chlorophyll in senescing barley leaves are localized in the vacuoles of mesophyll cells. Proc Natl Acad Sci USA **85**: 9529–9532

Matile P, Hörtensteiner S, Thomas H (1999) Chlorophyll degradation. Annu Rev Plant Physio **50**: 67–95

Matile P, Hörtensteiner S, Thomas H, Kräutler B (1996) Chlorophyll breakdown in senescent leaves. Plant Physiol **112**: 1403–1409

Matile P, Schellenberg M, Peisker C (1992) Production and release of a chlorophyll catabolite in isolated senescent chloroplasts. Planta **187**: 230–235

Matile P, Schellenberg M, Vicentini F (1997) Localization of chlorophyllase in the chloroplast envelope. Planta **201**: 96–99

Matos AR, D' Arcy-Lameta A, França M, Pêtres S, Edelman L, Kader J-C, Zuily-Fodil Y, Pham-Thi AT (2001) A novel patatin-like gene stimulated by drought stress encodes a galactolipid acyl hydrolase. FEBS Lett **491**: 188–192

Mayer H (1930) Untersuchungen über die Chlorophyllase. Planta **11**: 294–330

Mecey C, Hauck P, Trapp M, Pumplin N, Plovanich A, Yao J, He SY (2011) A critical role of STAYGREEN/ Mendel's I locus in controlling disease symptom development during Pseudomonas syringae pv tomato infection of Arabidopsis. Plant Physiol **157**: 1965–1974

Meguro M, Ito H, Takabayashi A, Tanaka R, Tanaka A (2011) Identification of the 7-hydroxymethyl chlorophyll a reductase of the chlorophyll cycle in Arabidopsis. Plant Cell **23**: 3442–3453

Mendel G (1866) Versuche über Pflanzenhybriden. Verh Naturforsch Ver Brünn **4**: 3–47

Meskauskiene R, Nater M, Goslings D, Kessler F, Op den Camp R, Apel K (2001) FLU: a negative regulator of chlorophyll biosynthesis in Arabidopsis thaliana. Proc Natl Acad Sci USA **98**: 12826–12831

Meyer A, Eskandari S, Grallath S, Rentsch D (2006) AtGAT1, a high affinity transporter for g-aminobutyric acid in Arabidopsis thaliana. J Biol Chem **281**: 7197–7204

Miao Y, Laun T, Zimmermann P, Zentgraf U (2004) Targets of the WRKY53 transcription factor and its role during leaf senescence in Arabidopsis. Plant Mol Biol **55**: 853–867

Miao Y, Zentgraf U (2010) A HECT E3 ubiquitin ligase negatively regulates Arabidopsis leaf senescence through degradation of the transcription factor WRKY53. Plant J **63**: 179–188

Miao Y, Zentgraf U (2007) The antagonist function of Arabidopsis WRKY53 and ESR/ESP in leaf senescence is modulated by the jasmonic and salicylic acid equilibrium. Plant Cell **19**: 819–830

Min MK, Kim SJ, Miao Y, Shin J, Jiang L, Hwang I (2007) Overexpression of Arabidopsis AGD7 causes relocation of golgi-localized proteins to the endoplasmic reticulum and inhibits protein trafficking in plant cells. Plant Physiol **143**: 1601–1614

Mishina TE, Lamb C, Zeier J (2007) Expression of a nitric oxide degrading enzyme induces a senescence programme in Arabidopsis. Plant Cell Environ **30**: 39–52

Miyashita H, Ikemoto H, Kurano N, Adachi K, Chihara M, Miyachi S (1996) Chlorophyll d as a major pigment. Nature **383**: 402–402

Mochizuki N, Brusslan JA, Larkin R, Nagatani A, Chory J (2001) Arabidopsis genomes uncoupled 5 (GUN5) mutant reveals the involvement of Mg-chelatase H subunit in plastid-to-nucleus signal transduction. Proc Natl Acad Sci USA **98**: 2053–2058

Mochizuki N, Tanaka R, Grimm B, Masuda T, Moulin M, Smith AG, Tanaka A, Terry MJ (2010) The cell biology of tetrapyrroles: a life and death struggle. Trends Plant Sci **15**: 488–498

Møller IM, Jensen PE, Hansson A (2007) Oxidative modifications to cellular components in plants. Annu Rev Plant Biol **58**: 459–481

Møller SG, Kunkel T, Chua NH (2001) A plastidic ABC protein involved in intercompartmental communication of light signalling. Genes Dev **15**: 90–103

Moore B, Zhou L, Rolland F, Hall Q, Cheng W-H, Liu Y-X, Hwang I, Jones T, Sheen J (2003) Role of the Arabidopsis glucose sensor HXK1 in nutrient, light, and hormonal signaling. Science **300**: 332–336

Morita R, Sato Y, Masuda Y, Nishimura M, Kusaba M (2009) Defect in non-yellow coloring 3, an α/β hydrolase-fold family protein, causes a stay-green phenotype during leaf senescence in rice. Plant J **59**: 940–952

Morris K, MacKerness SA, Page T, John CF, Murphy AM, Carr JP, Buchanan-Wollaston V (2000) Salicylic acid has a role in regulating gene expression during leaf senescence. Plant J **23**: 677–685

Moser S, Müller T, Ebert MO, Jockusch S, Turro NJ, Kräutler B (2008a) Blue luminescence of ripening bananas. Angew Chem Int Ed **47**: 8954–8957

Moser S, Müller T, Holzinger A, Lutz C, Jockusch S, Turro NJ, Kräutler B (2009a) Fluorescent chlorophyll catabolites in bananas light up blue halos of cell death. Proc Natl Acad Sci USA **106**: 15538–15543

Moser S, Müller T, Holzinger A, Lütz C, Kräutler B (2012) Structures of chlorophyll catabolites in bananas (Musa acuminata) reveal a split path of chlorophyll breakdown in a ripening fruit. Chem Eur J **18**: 10873–10885

Moser S, Müller T, Oberhuber M, Kräutler B (2009b) Chlorophyll catabolites - Chemical and structural footprints of a fascinating biological phenomenon. Eur J Org Chem 21–31

Moser S, Ulrich M, Müller T, Kräutler B (2008b) A yellow chlorophyll catabolite is a pigment of the fall colours. Photochem Photobiol Sci **7**: 1577–1581

Mowla SB, Thomson JA, Farrant JM, Mundree SG (2002) A novel stress-inducible antioxidant enzyme identified from the resurrection plant Xerophyta viscosa Baker. Planta **215**: 716–726

Mühlecker W, Kräutler B (1996) Breakdown of chlorophyll: constitution of nonfluorescing chlorophyll-catabolites from senescent cotyledons of the dicot rape. Plant Physiol Biochem **34**: 61–75

Mühlecker W, Kräutler B, Moser D, Matile P, Hörtensteiner S (2000) Breakdown of chlorophyll: a fluorescent chlorophyll catabolite from sweet pepper (Capsicum annuum). Helv Chim Acta **83**: 278–286

Mühlecker W, Ongania K-H, Kräutler B, Matile P, Hörtensteiner S (1997) Tracking down chlorophyll breakdown in plants: elucidation of the constitution of a “fluorescent” chlorophyll catabolite. Angew Chem Int Ed **36**: 401–404

Müller T, Moser S, Ongania K-H, Pružinská A, Hörtensteiner S, Kräutler B (2006) A divergent path of chlorophyll breakdown in the model plant Arabidopsis thaliana. ChemBioChem **7**: 40–42

Müller T, Rafelsberger M, Vergeiner C, Kräutler B (2011) A dioxobilane as product of a divergent path of chlorophyll breakdown in Norway Maple. Angew Chem Int Ed **50**: 10724–10727

Müller T, Ulrich M, Ongania KH, Kräutler B (2007) Colorless tetrapyrrolic chlorophyll catabolites found in ripening fruit are effective antioxidants. Angew Chem Int Ed **46**: 8699–8702

Mur LAJ, Aubry S, Mondhe M, Kingston-Smith A, Gallagher J, Timms-Taravella E, James C, Papp I, Hörtensteiner S, Thomas H, et al (2010) Accumulation of chlorophyll catabolites photosensitizes the hypersensitive response elicited by Pseudomonas syringae in Arabidopsis. New Phytol **188**: 161–174

N

Nagane T, Tanaka A, Tanaka R (2010) Involvement of AtNAP1 in the regulation of chlorophyll degradation in Arabidopsis thaliana. Planta **231**: 939–949

Nagatani A (2010) Phytochrome: structural basis for its functions. Curr Opin Plant Biol **13**: 565–570

Nakagawara E, Sakuraba Y, Yamasato A, Tanaka R, Tanaka A (2007) Clp protease controls chlorophyll b synthesis by regulating the level of chlorophyllide a oxygenase. Plant J **49**: 800–809

Nakajima S, Ito H, Tanaka R, Tanaka A (2012) Chlorophyll b reductase plays an essential role in maturation and storability of Arabidopsis seeds. Plant Physiol **160**: 261–273

Nakatogawa H, Suzuki K, Kamada Y, Ohsumi Y (2009) Dynamics and diversity in autophagy mechanisms: lessons from yeast. Nat Rev Mol Cell Bio **10**: 458–467

Navabpour S, Morris K, Allen R, Harrison E, A-H-Mackerness S, Buchanan-Wollaston V (2003) Expression of senescence-enhanced genes in response to oxidative stress. J Exp Bot **54**: 2285–2292

Nelson D, Werck-Reichhart D (2011) A P450-centric view of plant evolution. Plant J **66**: 194–211

Nelson N, Yocum CF (2006) Structure and function of photosystems I and II. Annu Rev Plant Biol **57**: 521–565

Nishizawa A, Yabuta Y, Shigeoka S (2008) Galactinol and raffinose constitute a novel function to protect plants from oxidative damage. Plant Physiol **147**: 1251–1263

Noh YS, Amasino RM (1999) Identification of a promoter region responsible for the senescence-specific expression of SAG12. Plant Mol Biol **41**: 181–94

Noodén LD, Kahanak GM, Okatan Y (1979) Prevention of monocarpic senescence in soybeans with auxin and cytokinin: an antidote for self-destruction. Science **206**: 841–843

Nozawa A, Ito M, Hayashi H, Watanabe A (1999) Dark-induced expression of genes for asparagine synthetase and cytosolic glutamine synthetase in radish cotyledons is dependent on the growth stage. Plant Cell Physiol **40**: 942–948

O

Obayashi T, Hayashi S, Saeki M, Ohta H, Kinoshita K (2009) ATTED-II provides coexpressed gene networks for Arabidopsis. Nucleic Acids Res **37**: D987–D991

Oberhuber M, Berghold J, Breuker K, Hörtensteiner S, Kräutler B (2003) Breakdown of chlorophyll: a nonenzymatic reaction accounts for the formation of the colorless "nonfluorescent" chlorophyll catabolites. Proc Natl Acad Sci USA **100**: 6910–6915

Oberhuber M, Berghold J, Mühlecker W, Hörtensteiner S, Kräutler B (2001) Chlorophyll breakdown - on a nonfluorescent chlorophyll catabolite from spinach. Helv Chim Acta **84**: 2615–2627

Oh SA, Park J-H, Lee GI, Paek KH, Park SK, Nam HG (1997) Identification of three genetic loci controlling leaf senescence in Arabidopsis thaliana. Plant J **12**: 527–535

Oka M, Shimoda Y, Sato N, Inoue J, Yamazaki T, Shimomura N, Fujiyama H (2012) Abscisic acid substantially inhibits senescence of cucumber plants (Cucumis sativus) grown under low nitrogen conditions. J Plant Physiol **169**: 789–796

Okushima Y, Mitina I, Quach HL, Theologis A (2005) AUXIN RESPONSE FACTOR 2 (ARF2): a pleiotropic developmental regulator. Plant J **43**: 29–46

Olinares PDB, Kim J, Van Wijk KJ (2011) The Clp protease system; a central component of the chloroplast protease network. BBA-Bioenergetics **1807**: 999–1011

Olson, Skavdahl, Ramberg, Osterman, Markwell (2000) Formate dehydrogenase in Arabidopsis thaliana: characterization and possible targeting to the chloroplast. Plant Sci **159**: 205–212

Ono K, Hashimoto H, Katoh S (1995) Changes in the number and size of chloroplasts during senescence of primary leaves of wheat grown under different conditions. Plant Cell Physiol **36**: 9–17

Ono Y, Wada S, Izumi M, Makino A, Ishida H (2013) Evidence for contribution of autophagy to Rubisco degradation during leaf senescence in Arabidopsis thaliana. Plant Cell Environ n/a–n/a

Osmani SA, Bak S, Møller BL (2009) Substrate specificity of plant UDP-dependent glycosyltransferases predicted from crystal structures and homology modeling. Phytochemistry **70**: 325–347

Oster U, Tanaka R, Tanaka A, Rudiger W (2000) Cloning and functional expression of the gene encoding the key enzyme for chlorophyll b biosynthesis (CAO) from Arabidopsis thaliana. Plant J **21**: 305–310

Otegui MS, Noh YS, Martinez DE, Vila Petroff MG, Andrew Staehelin L, Amasino RM, Guiamet JJ (2005) Senescence-associated vacuoles with intense proteolytic activity develop in leaves of Arabidopsis and soybean. Plant J **41**: 831–844

P

Paquette S, Møller BL, Bak S (2003) On the origin of family 1 plant glycosyltransferases. Phytochemistry **62**: 399–413

Park JH, Oh SA, Kim YH, Woo HR, Nam HG (1998) Differential expression of senescence-associated mRNAs during leaf senescence induced by different senescence-inducing factors in Arabidopsis. Plant Mol Biol **37**: 445–54

Park S-Y, Yu J-W, Park J-S, Li J, Yoo S-C, Lee N-Y, Lee S-K, Jeong S-W, Seo HS, Koh H-J, et al (2007) The senescence-induced STAYGREEN protein regulates chlorophyll degradation. Plant Cell **19**: 1649–1664

Parthier B (1988) Gerontoplasts - the yellow end in ontogenesis of chloroplasts. Endocyt Cell Res **5**: 163–190

Pattanayak GK, Venkataramani S, Hortensteiner S, Kunz L, Christ B, Moulin M, Smith AG, Okamoto Y, Tamiaki H, Sugishima M, et al (2012) ACCELERATED CELL DEATH 2 suppresses mitochondrial oxidative bursts and modulates cell death in Arabidopsis. Plant J **69**: 589–600

Pedras MSC, Zaharia IL, Gai Y, Zhou Y, Ward DE (2001) In planta sequential hydroxylation and glycosylation of a fungal phytotoxin: avoiding cell death and overcoming the fungal invader. Proc Natl Acad Sci USA **98**: 747–752

Penna S (2003) Building stress tolerance through over-producing trehalose in transgenic plants. Trends Plant Sci **8**: 355–357

Pennycooke JC, Jones ML, Stushnoff C (2003) Down-regulating α-galactosidase enhances freezing tolerance in transgenic petunia. Plant Physiol **133**: 901–909

Pennycooke JC, Vepachedu R, Stushnoff C, Jones ML (2004) Expression of an α-galactosidase gene in petunia is upregulated during low-temperature deacclimation. J Amer Soc Hort Sci **129**: 491–496

Peoples MB, Dalling MJ (1988) The interplay between proteolysis and amino acid metabolism during senescence and nitrogen allocation. *In* LD Noodén, AC Leopold, eds, Senescence and Aging in Plants. Academic Press, San Diego, USA, pp 181–217

Pérez P, Rabnecz G, Laufer Z, Gutiérrez D, Tuba Z, Martínez-Carrasco R (2011) Restoration of photosystem II photochemistry and carbon assimilation and related changes in chlorophyll and protein contents during the rehydration of desiccated Xerophyta scabrida leaves. J Exp Bot **62**: 895–905

Peterbauer T, Richter A (2001) Biochemistry and physiology of raffinose family oligosaccharides and galactosyl cyclitols in seeds. Seed Sci Res **11**: 185–197

Peters S, Egert A, Stieger B, Keller F (2010) Functional identification of Arabidopsis ATSIP2 (At3g57520) as an alkaline α-galactosidase with a substrate specificity for raffinose and an apparent sink-specific expression pattern. Plant Cell Physiol **51**: 1815–1819

Peters S, Keller F (2009) Frost tolerance in excised leaves of the common bugle (Ajuga reptans L.) correlates positively with the concentrations of raffinose family oligosaccharides (RFOs). Plant Cell Environ **32**: 1099–1107

Peters S, Mundree SG, Thomson JA, Farrant JM, Keller F (2007) Protection mechanisms in the resurrection plant Xerophyta viscosa (Baker): both sucrose and raffinose family oligosaccharides (RFOs) accumulate in leaves in response to water deficit. J Exp Bot **58**: 1947–1956

Philosoph-Hadas S, Hadas E, Aharoni N (1993) Characterization and use in ELISA of a new monoclonal antibody for quantitation of abscisic acid in senescing rice leaves. Plant Growth Regul **12**: 71–78

Piller L, Abraham M, Dörmann P, Kessler F, Besagni C (2012) Plastid lipid droplets at the crossroads of prenylquinone metabolism. J Exp Bot **63**: 1609–1618

Pontier D, Gan S, Amasino RM, Roby D, Lam E (1999) Markers for hypersensitive response and senescence show distinct patterns of expression. Plant Mol Biol **39**: 1243–1255

Procházková D, Wilhelmová N (2007) Leaf senescence and activities of the antioxidant enzymes. Biol Plant **51**: 401–406

Proctor MCF, Tuba Z (2002) Poikilohydry and homoihydry: antithesis or spectrum of possibilities? New Phytol **156**: 327–349

Pružinská A, Anders I, Aubry S, Schenk N, Tapernoux-Lüthi E, Müller T, Kräutler B, Hörtensteiner S (2007) In vivo participation of red chlorophyll catabolite reductase in chlorophyll breakdown. Plant Cell **19**: 369–387

Pružinská A, Anders I, Tanner G, Roca M, Hörtensteiner S (2003) Chlorophyll breakdown: pheophorbide a oxygenase is a Rieske-type iron-sulfur protein, encoded by the accelerated cell death 1 gene. Proc Natl Acad Sci USA **100**: 15259–15264

Pružinská A, Tanner G, Aubry S, Anders I, Moser S, Müller T, Ongania K-H, Kräutler B, Youn J-Y, Liljegren SJ, et al (2005) Chlorophyll breakdown in senescent Arabidopsis leaves: characterization of chlorophyll catabolites and of chlorophyll catabolic enzymes involved in the degreening reaction. Plant Physiol **139**: 52–63

Pudelski B, Kraus S, Soll J, Philippar K (2010) The plant PRAT proteins – preprotein and amino acid transport in mitochondria and chloroplasts. Plant Biol **12**: 42–55

Q

Quiles MJ, García C, Cuello J (1995) Differential effects of abscisic acid and methyl jasmonate on endoproteinases in senescing barley leaves. Plant Growth Regul **16**: 197–204

Quirino BF, Noh YS, Himelblau E, Amasino RM (2000) Molecular aspects of leaf senescence. Trends Plant Sci **5**: 278–282

Quirino BF, Normanly J, Amasino RM (1999) Diverse range of gene activity during Arabidopsis thaliana leaf senescence includes pathogen-independent induction of defense-related genes. Plant Mol Biol **40**: 267–78

R

Raab S, Drechsel G, Zarepour M, Hartung W, Koshiba T, Bittner F, Hoth S (2009) Identification of a novel E3 ubiquitin ligase that is required for suppression of premature senescence in Arabidopsis. Plant J **59**: 39–51

Reape TJ, McCabe PF (2008) Apoptotic-like programmed cell death in plants. New Phytol **180**: 13–26

Ren G, An K, Liao Y, Zhou X, Cao Y, Zhao H, Ge X, Kuai B (2007) Identification of a novel chloroplast protein AtNYE1 regulating chlorophyll degradation during leaf senescence in Arabidopsis. Plant Physiol **144**: 1429–1441

Ren GD, Zhou Q, Wu SX, Zhang YF, Zhang LG, Huang JR, Sun ZF, Kuai BK (2010) Reverse genetic identification of CRN1 and its distinctive role in chlorophyll degradation in Arabidopsis. J Integr Plant Biol **52**: 496–504

Rhodes D, Nadolska-Orczyk A, Rich PJ (2004) Salinity, osmolytes and compatible solutes. *In* A Läuchli, U Lüttge, eds, Salinity: Environment - Plants - Molecules. Springer Netherlands, pp 181–204

Richards DE, King KE, Ait-ali T, Harberd NP (2001) How gibberellin regulates plant growth and development: a molecular genetic analysis of gibberellin signaling. Annu Rev Plant Phys **52**: 67–88

Riefler M, Novak O, Strnad M, Schmülling T (2006) Arabidopsis cytokinin receptor mutants reveal functions in shoot growth, leaf senescence, seed size, germination, root development, and cytokinin metabolism. Plant Cell **18**: 40–54

Del Rio LA, Sandalio LM, Altomare DA, Zilinskas BA (2003) Mitochondrial and peroxisomal manganese superoxide dismutase: differential expression during leaf senescence. J Exp Bot **54**: 923–933

Robatzek S, Somssich IE (2001) A new member of the Arabidopsis WRKY transcription factor family, AtWRKY6, is associated with both senescence- and defence-related processes. Plant J **28**: 123–133

Robatzek S, Somssich IE (2002) Targets of AtWRKY6 regulation during plant senescence and pathogen defense. Genes Dev **16**: 1139–1149

Roberts ES, Vaz ADN, Coon MJ (1991) Catalysis by cytochrome P-450 of an oxidative reaction in xenobiotic aldehyde metabolism: Deformylation with olefin formation. Proc Natl Acad Sci USA **88**: 8963–8966

Roberts IN, Caputo C, Criado MV, Funk C (2012) Senescence-associated proteases in plants. Physiol Plant **145**: 130–139

Rockwell NC, Su Y-S, Lagarias JC (2006) Phytochrome structure and signaling mechanisms. Annu Rev Plant Biol **57**: 837–858

Rodoni S, Mühlecker W, Anderl M, Kräutler B, Moser D, Thomas H, Matile P, Hörtensteiner S (1997) Chlorophyll breakdown in senescent chloroplasts. Cleavage of pheophorbide a in two enzymic steps. Plant Physiol **115**: 669–676

Rojo E, Zouhar J, Carter C, Kovaleva V, Raikhel NV (2003) A unique mechanism for protein processing and degradation in Arabidopsis thaliana. Proc Natl Acad Sci USA **100**: 7389–7394

Rontein D, Basset G, Hanson AD (2002) Metabolic engineering of osmoprotectant accumulation in plants. Metab Eng **4**: 49–56

Rushton PJ, Torres JT, Parniske M, Wernert P, Hahlbrock K, Somssich IE (1996) Interaction of elicitor-induced DNA-binding proteins with elicitor response elements in the promoters of parsley PR1 genes. EMBO J **15**: 5690–5700

S

Sacher JA (1957) Relationship between auxin and membrane-integrity in tissue senescence and abscission. Science **125**: 1199–1200

Saga Y, Tamiaki H (2012) Demetalation of chlorophyll pigments. Chem Biodivers **9**: 1659–1683

Saito S, Hirai N, Matsumoto C, Ohigashi H, Ohta D, Sakata K, Mizutani M (2004) Arabidopsis CYP707A encodes (+)-abscisic 8'-acid-hydroxylase, a key enzyme in the oxidative catabolism of abscisic Acid. Plant Physiol **134**: 1439–1449

Sakuraba Y, Balazadeh S, Tanaka R, Mueller-Roeber B, Tanaka A (2012a) Overproduction of Chl b retards senescence through transcriptional reprogramming in Arabidopsis. Plant Cell Physiol **53**: 505–517

Sakuraba Y, Kim Y-S, Yoo S-C, Hörtensteiner S, Paek N-C (2013) 7-Hydroxymethyl chlorophyll a reductase functions in metabolic channeling of chlorophyll breakdown intermediates during leaf senescence. Biochem Bioph Res Co **430**: 32–37

Sakuraba Y, Schelbert S, Park S-Y, Han S-H, Lee B-D, Andrès CB, Kessler F, Hörtensteiner S, Paek N-C (2012b) STAY-GREEN and chlorophyll catabolic enzymes interact at light-harvesting complex II for chlorophyll detoxification during leaf senescence in Arabidopsis. Plant Cell **24**: 507–18

Sakuraba Y, Tanaka R, Yamasato A, Tanaka A (2009) Determination of a chloroplast degron in the regulatory domain of chlorophyllide a oxygenase. J Biol Chem **284**: 36689–36699

Sakuraba Y, Yokono M, Akimoto S, Tanaka R, Tanaka A (2010) Deregulated chlorophyll b synthesis reduces the energy transfer rate between photosynthetic pigments and induces photodamage in Arabidopsis thaliana. Plant Cell Physiol **51**: 1055–1065

Sanchez-Fernandez R, Davies TGE, Coleman JOD, Rea PA (2001) The Arabidopsis thaliana ABC protein superfamily, a complete inventory. J Biol Chem **276**: 30231–30244

Santarius KA, Milde H (1977) Sugar compartmentation in frost-hardy and partially dehardened cabbage leaf cells. Planta **136**: 163–166

Sato Y, Moria R, Katsuma S, Nishimura M, Tanaka A, Kusaba M (2009) Two short-chain dehydrogenase/reductases, NON-YELLOW COLORING 1 and NYC1-LIKE, are required for chlorophyll b and light-harvesting complex II degradation during senescence in rice. Plant J **57**: 120–131

Scheer H (2006) An overview of chlorophylls and bacteriochlorophylls: biochemistry, biophysics, functions and applications. *In* B Grimm, R Porra, W Rüdiger, H Scheer, eds, Chlorophylls and Bacteriochlorophylls: Biochemistry, Biophysics, Functions and Applications. Springer, Dordrecht, The Netherlands, pp 1–26

Schelbert S, Aubry S, Burla B, Agne B, Kessler F, Krupinska K, Hörtensteiner S (2009) Pheophytin pheophorbide hydrolase (pheophytinase) is involved in chlorophyll breakdown during leaf senescence in Arabidopsis. Plant Cell **21**: 767–785

Schellenberg M, Matile P, Thomas H (1990) Breakdown of chlorophyll in chloroplasts of senescent barley leaves depends on ATP. J Plant Physiol **136**: 564–568

Schellenberg M, Matile P, Thomas H (1993) Production of a presumptive chlorophyll catabolite in vitro: requirement for reduced ferredoxin. Planta **191**: 417–420

Schenk N, Schelbert S, Kanwischer M, Goldschmidt EE, Dörmann P, Hörtensteiner S (2007) The chlorophyllases AtCLH1 and AtCLH2 are not essential for senescence-related chlorophyll breakdown in Arabidopsis thaliana. FEBS Lett **581**: 5517–5525

Scherl M, Müller T, Kräutler B (2012) Chlorophyll catabolites in senescent leaves of the lime tree (Tilia cordata). Chem Biodivers **9**: 2605–2617

Schippers JHM, Jing H-C, Hille J, Dijkwel PP (2007) Developmental and hormonal control of leaf senescence. *In* S Gan, ed, Annual Plant Reviews Volume 26: Senescence Processes in Plants. Blackwell Publishing Ltd, pp 145–170

Schippers JHM, Nunes-Nesi A, Apetrei R, Hille J, Fernie AR, Dijkwel PP (2008) The Arabidopsis onset of leaf death5 mutation of quinolinate synthase affects nicotinamide adenine dinucleotide biosynthesis and causes early ageing. Plant Cell **20**: 2909–2925

Schliep M, Cavigliasso G, Quinnell RG, Stranger R, Larkum AWD (2013) Formyl group modification of chlorophyll a: a major evolutionary mechanism in oxygenic photosynthesis. Plant Cell Environ **36**: 521–527

Schneider T, Keller F (2009) Raffinose in chloroplasts is synthesized in the cytosol and transported across the chloroplast envelope. Plant Cell Physiol **50**: 2174–2182

Schuler MA (1996) Plant cytochrome P450 monooxygenases. Critical Rev Plant Sci **15**: 235–284

Schuler MA, Duan H, Bilgin M, Ali S (2006) Arabidopsis cytochrome P450s through the looking glass: a window on plant biochemistry. Phytochem Rev **5**: 205–237

Schwacke R, Schneider A, Van der Graaff E, Fischer K, Catoni E, Desimone M, Frommer WB, Flügge U-I, Kunze R (2003) ARAMEMNON, a novel database for Arabidopsis integral membrane proteins. Plant Physiol **131**: 16–26

Scott P (2000) Resurrection plants and the secrets of eternal leaf. Ann Bot **85**: 159–166

Seki M, Narusaka M, Kamiya A, Ishida J, Satou M, Sakurai T, Nakajima M, Enju A, Akiyama K, Oono Y, et al (2002) Functional annotation of a full-length Arabidopsis cDNA collection. Science **296**: 141–145

Sessions A, Burke E, Presting G, Aux G, McElver J, Patton D, Dietrich B, Ho P, Bacwaden J, Ko C, et al (2002) A high-throughput Arabidopsis reverse genetics system. Plant Cell **14**: 2985–94

Shan X, Wang J, Chua L, Jiang D, Peng W, Xie D (2011) The role of Arabidopsis Rubisco activase in jasmonate-induced leaf senescence. Plant Physiol **155**: 751–764

Shen B, Jensen RG, Bohnert HJ (1997) Mannitol protects against oxidation by hydroxyl radicals. Plant Physiol **115**: 527–532

Sherwin HW, Farrant JM (1996) Differences in rehydration of three desiccation-tolerant angiosperm species. Ann Bot **78**: 703–710

Shimoda Y, Ito H, Tanaka A (2012) Conversion of chlorophyll b to chlorophyll a precedes magnesium dechelation for protection against necrosis in Arabidopsis. Plant J **72**: 501–511

Shioi Y, Tomita N, Tsuchiya T, Takamiya K (1996a) Conversion of chlorophyllide to pheophorbide by Mg-dechelating substance in extracts of Chenopodium album. Plant Physiol Biochem **34**: 41–47

Shioi Y, Watanabe K, Takamiya K (1996b) Enzymatic conversion of pheophorbide a to a precursor of pyropheophorbide a in leaves of Chenopodium album. Plant Cell Physiol **37**: 1143–1149

Shoji K, Addicott FT, Swets WA (1951) Auxin in relation to leaf blade abscission. Plant Physiol **26**: 189–191

Siddique MA, Grossmann J, Gruissem W, Baginsky S (2006) Proteome analysis of bell pepper (Capsicum annuum L.) chromoplasts. Plant Cell Physiol **47**: 1663–1673

Simeonova E, Sikora A, Charzyńska M, Mostowska A (2000) Aspects of programmed cell death during leaf senescence of mono- and dicotyledonous plants. Protoplasma **214**: 93–101

Smallwood M, Knox JP, Bowles DJ (1996) Membranes: specialized functions in plants. BIOS Scientific Publishers

Smart EL, Pharr DM (1980) Characterization of α-galactosidase from cucumber leaves 1. Plant Physiol **66**: 731–734

Souer E, Van Houwelingen A, Kloos D, Mol J, Koes R (1996) The NO APICAL MERISTEM gene of Petunia is required for pattern formation in embryos and flowers and is expressed at meristem and primordia boundaries. Cell **85**: 159–170

Spassieva S, Hille J (2002) A lesion mimic phenotype in tomato obtained by isolating and silencing an Lls1 homologue. Plant Sci **162**: 543–549

Strain HH, Cope BT, Svec WA (1971) Analytical procedures for the isolation, identification, estimation and investigation of the chlorophylls. Methods Enzymol **23**: 452–476

Sugishima M, Kitamori Y, Noguchi M, Kohchi T, Fukuyama K (2009) Crystal structure of red chlorophyll catabolite reductase: enlargement of the ferredoxin-dependent bilin reductase family. J Mol Biol **389**: 376–387

Sugishima M, Okamoto Y, Noguchi M, Kohchi T, Tamiaki H, Fukuyama K (2010) Crystal structures of the substrate-bound forms of red chlorophyll catabolite reductase: implications for site-specific and stereospecific reaction. J Mol Biol **402**: 879–891

Sun T, Gubler F (2004) Molecular mechanism of gibberellin signaling in plants. Annu Rev Plant Biol **55**: 197–223

Sundaresan V, Springer P, Volpe T, Haward S, Jones JDG, Dean C, Ma H, Martienssen R (1995) Patterns of gene-action in plant development revealed by enhancer trap and gene trap transposable elements. Genes Dev **9**: 1797–1810

Suzuki T, Kunieda T, Murai F, Morioka S, Shioi Y (2005) Mg-dechelation activity in radish cotyledons with artificial and native substrates, Mg-chlorophyllin a and chlorophyllide a. Plant Physiol Biochem **43**: 459–464

Suzuki T, Shioi Y (2002) Re-examination of Mg-dechelation reaction in the degradation of chlorophylls using chlorophyllin a as substrate. Photosynth Res **74**: 217–223

Suzuki Y, Amano T, Shioi Y (2006) Characterization and cloning of the chlorophyll-degrading enzyme pheophorbidase from cotyledons of radish. Plant Physiol **140**: 716–725

Suzuki Y, Doi M, Shioi Y (2002) Two enzymatic reaction pathways in the formation of pyropheophorbide a. Photosynth Res **74**: 225–233

Suzuki Y, Shioi Y (1999) Detection of chlorophyll breakdown products in the senescent leaves of higher plants. Plant Cell Physiol **40**: 909–915

Suzuki Y, Tanabe K, Shioi Y (1999) Determination of chemical oxidation products of chlorophyll and porphyrin by high-performance liquid chromatography. J Chromatogr **A. 839**: 85–91

Swartzberg D, Hanael R, Granot D (2011) Relationship between hexokinase and cytokinin in the regulation of leaf senescence and seed germination. Plant Biol **13**: 439–444

T

Takahashi Y, Berberich T, Yamashita K, Uehara Y, Miyazaki A, Kusano T (2004) Identification of tobacco HIN1 and two closely related genes as spermine-responsive genes and their differential expression during the tobacco mosaic virus-induced hypersensitive response and during leaf- and flower-senescence. Plant Mol Biol **54**: 613–622

Takamiya K, Tsuchiya T, Ohta H (2000) Degradation pathway(s) of chlorophyll: what has gene cloning revealed? Trends Plant Sci **5**: 426–431

Tan B-C, Joseph LM, Deng W-T, Liu L, Li Q-B, Cline K, McCarty DR (2003) Molecular characterization of the Arabidopsis 9-cis epoxycarotenoid dioxygenase gene family. Plant J **35**: 44–56

Tan XL, Wang QY, Tian BX, Zhang HA, Lu DL, Zhou J (2011) A Brassica napus lipase locates at the membrane contact sites involved in chloroplast development. Plos One. doi: 10.1371/journal.pone.0026831

Tanaka A, Ito H, Tanaka R, Tanaka NK, Yoshida K, Okada K (1998) Chlorophyll a oxygenase (CAO) is involved in chlorophyll b formation from chlorophyll a. Proc Natl Acad Sci USA **95**: 12719–12723

Tanaka R, Hirashima M, Satoh S, Tanaka A (2003) The Arabidopsis-accelerated cell death gene ACD1 is involved in oxygenation of pheophorbide a: inhibition of pheophorbide a oxygenase activity does not lead to the "stay-green" phenotype in Arabidopsis. Plant Cell Physiol **44**: 1266–1274

Tanaka R, Kobayashi K, Masuda T (2011) Tetrapyrrole metabolism in Arabidopsis thaliana. Arabidopsis Book 9. doi: 10.1199/tab.0145

Tanaka R, Koshino Y, Sawa S, Ishiguro S, Okada K, Tanaka A (2001) Overexpression of chlorophyllide a oxygenase (CAO) enlarges the antenna size of photosystem II in Arabidopsis thaliana. Plant J **26**: 365–373

Tanaka R, Tanaka A (2007) Tetrapyrrole biosynthesis in higher plants. Annu Rev Plant Biol **58**: 321–346

Tanaka R, Tanaka A (2011) Chlorophyll cycle regulates the construction and destruction of the light-harvesting complexes. BBA-Bioenergetics **1807**: 968–976

Tanaka R, Tanaka A (2005) Effects of chlorophyllide a oxygenase overexpression on light acclimation in Arabidopsis thaliana. Photosynth Res **85**: 327–340

Tang D, Christiansen KM, Innes RW (2005) Regulation of plant disease resistance, stress responses, cell death, and ethylene signaling in Arabidopsis by the EDR1 protein kinase. Plant Physiol **138**: 1018–1026

Tang Y, Li M, Chen Y, Wu P, Wu G, Jiang H (2011) Knockdown of OsPAO and OsRCCR1 cause different plant death phenotypes in rice. J Plant Physiol **168**: 1952–1959

Tarczynski MC, Jensen RG, Bohnert HJ (1993) Stress protection of transgenic tobacco by production of the osmolyte mannitol. Science **259**: 508–510

Thomas H (2013a) Photosynthesis in senescence. SenEssence, http://www.sidthomas.net/SenEssence/Genes/photosynthesis.htm

Thomas H (2013b) Senescence, ageing and death of the whole plant. New Phytol **197**: 696–711

Thomas H, Howarth CJ (2000) Five ways to stay green. J Exp Bot **51**: 329–337

Thomas H, Ougham HJ, Wagstaff C, Stead AD (2003) Defining senescence and death. J Exp Bot **54**: 1127–1132

Thomas H, Stoddart JL (1980) Leaf senescence. Ann Rev Plant Physiol **31**: 83–111

Thompson JE, Froese CD, Madey E, Smith MD, Hong Y (1998) Lipid metabolism during plant senescence. Prog Lipid Res **37**: 119–141

Tissier AF, Marillonnet S, Klimyuk V, Patel K, Torres MA, Murphy G, Jones JD (1999) Multiple independent defective suppressor-mutator transposon insertions in Arabidopsis: a tool for functional genomics. Plant Cell **11**: 1841–1852

Toldi O, Tuba Z, Scott P (2009) Vegetative desiccation tolerance: is it a goldmine for bioengineering crops? Plant Sci **176**: 187–199

Tommasini R, Vogt E, Fromenteau M, Hörtensteiner S, Matile P, Amrhein N, Martinoia E (1998) An ABC transporter of Arabidopsis thaliana has both glutathione-conjugate and chlorophyll catabolite transport activity. Plant J **13**: 773–780

Tripathy BC, Sherameti I, Oelmüller R (2010) Siroheme. Plant Signal Behav **5**: 14–20

Tsuchiya T, Ohta H, Okawa K, Iwamatsu A, Shimada H, Masuda T, Takamiya K (1999) Cloning of chlorophyllase, the key enzyme in chlorophyll degradation: finding of a lipase motif and the induction by methyl jasmonate. Proc Natl Acad Sci USA **96**: 15362–15367

Tuba Z, Lichtenthaler HK, Csintalan Z, Nagy Z, Szente K (1996) Loss of chlorophylls, cessation of photosynthetic CO2 assimilation and respiration in the poikilochlorophyllous plant Xerophyta scabrida during desiccation. Physiol Plant **96**: 383–388

Tuba Z, Lichtenthaler HK, Csintalan Z, Nagy Z, Szente K (1994) Reconstitution of chlorophylls and photosynthetic CO2 assimilation upon rehydration of the desiccated poikilochlorophyllous plant Xerophyta scabrida (Pax). Planta **192**: 414–420

Tuba Z, Protor CF, Csintalan Z (1998) Ecophysiological responses of homoiochlorophyllous and poikilochlorophyllous desiccation tolerant plants: a comparison and an ecological perspective. Plant Growth Regul **24**: 211–217

U

Ueda J, Kato J (1979) Isolation and identification of a senescence-promoting substance from Wormwood (Arthemisia absinthium L.). Plant Physiol **66**: 246–249

Ülker B, Mukhtar MS, Somssich IE (2007) The WRKY70 transcription factor of Arabidopsis influences both the plant senescence and defense signaling pathways. Planta **226**: 125–137

Ulrich M, Moser S, Muller T, Krautler B (2011) How the colourless "nonfluorescent" chlorophyll catabolites rust. Chem Eur J **17**: 2330–2334

Unno M, Matsui T, Ikeda-Saito M (2007) Structure and catalytic mechanism of heme oxygenase. Nat Prod Rep **24**: 553–570

V

Valentin HE, Lincoln K, Moshiri F, Jensen PK, Qi Q, Venkatesh TV, Karunanandaa B, Baszis SR, Norris SR, Savidge B, et al (2006) The Arabidopsis vitamin E pathway gene5-1 mutant reveals a critical role for phytol kinase in seed tocopherol biosynthesis. Plant Cell **18**: 212–224

Vanstraelen M, Benková E (2012) Hormonal interactions in the regulation of plant development. Annu Rev Cell Dev Bi **28**: 463–487

Verbruggen N, Hermans C (2008) Proline accumulation in plants: a review. Amino Acids **35**: 753–759

Vert G, Nemhauser JL, Geldner N, Hong F, Chory J (2005) Molecular mechanisms of steroid hormone signaling in plants. Annu Rev Cell Dev Bi **21**: 177–201

Vianello A, Zancani M, Peresson C, Petrussa E, Casolo V, Krajňáková J, Patui S, Braidot E, Macrì F (2007) Plant mitochondrial pathway leading to programmed cell death. Physiol Plant **129**: 242–252

Vicentini F, Iten F, Matile P (1995) Development of an assay for Mg-dechelatase of oilseed rape cotyledons, using chlorophyllin as the substrate. Physiol Plant **94**: 57–63

Vicré M, Farrant JM, Driouich A (2004) Insights into the cellular mechanisms of desiccation tolerance among angiosperm resurrection plant species. Plant Cell Environ **27**: 1329–1340

Vidi PA, Kanwischer M, Baginsky S, Austin JR, Csucs G, Dörmann P, Kessler F, Brehelin C (2006) Tocopherol cyclase (VTE1) localization and vitamin E accumulation in chloroplast plastoglobule lipoprotein particles. J Biol Chem **281**: 11225–11234

W

Wada S, Ishida H, Izumi M, Yoshimoto K, Ohsumi Y, Mae T, Makino A (2009) Autophagy plays a role in chloroplast degradation during senescence in Individually darkened leaves. Plant Physiol **149**: 885–893

Waditee-Sirisattha R, Shibato J, Rakwal R, Sirisattha S, Hattori A, Nakano T, Takabe T, Tsujimoto M (2011) The Arabidopsis aminopeptidase LAP2 regulates plant growth, leaf longevity and stress response. New Phytol **191**: 958–969

Wagner R, Aigner H, Pruzinska A, Jankanpaa HJ, Jansson S, Funk C (2011) Fitness analyses of Arabidopsis thaliana mutants depleted of FtsH metalloproteases and characterization of three FtsH6 deletion mutants exposed to high light stress, senescence and chilling. New Phytol **191**: 449–458

Wang Z-Y, Bai M-Y, Oh E, Zhu J-Y (2012) Brassinosteroid signaling network and regulation of photomorphogenesis. Annu Rev Genet **46**: 701–724

Weaver LM, Froehlich JE, Amasino RM (1999) Chloroplast-targeted ERD1 Protein declines but its mRNA increases during senescence in Arabidopsis. Plant Physiol **119**: 1209–1216

Weber H, Borisjuk L, Wobus U (2005) Molecular physiology of legume seed development. Annu Rev Plant Biol **56**: 253–279

Wesley SV, Helliwell CA, Smith NA, Wang M, Rouse DT, Liu Q, Gooding PS, Singh SP, Abbot D, Stoutjesdijk PA, et al (2001) Construct design for efficient, effective and high-throuput gene silencing in plants. Plant J **27**: 581–590

Wessel D, Flügge UI (1984) A method for the quantitative recovery of protein in dilute solution in the presence of detergents and lipids. Anal Biochem **138**: 141–143

Whittaker A, Bochicchio A, Vazzana C, Lindsey G, Farrant J (2001) Changes in leaf hexokinase activity and metabolite levels in response to drying in the desiccation□tolerant species Sporobolus stapfianus and Xerophyta viscosa. J Exp Bot **52**: 961–969

Willstaetter R, Stoll A (1911) Examinations on chloropyll, XI Chlorophyllase. Justus Liebigs Ann Chem **378**: 18–72

Winfield MO, Lu C, Wilson ID, Coghill JA, Edwards KJ (2010) Plant responses to cold: transcriptome analysis of wheat. Plant Biotechnol J **8**: 749–771

Woo HR, Chung KM, Park JH, Oh SA, Ahn T, Hong SH, Jang SK, Nam HG (2001) ORE9, an F-box protein that regulates leaf senescence in Arabidopsis. Plant Cell **13**: 1779–1790

Woo HR, Kim JH, Nam HG, Lim PO (2004) The delayed leaf senescence mutants of Arabidopsis, ore1, ore3, and ore9 are tolerant to oxidative stress. Plant Cell Physiol **45**: 923–932

Wu A, Allu AD, Garapati P, Siddiqui H, Dortay H, Zanor MI, Asensi-Fabado MA, Munne-Bosch S, Antonio C, Tohge T, et al (2012) JUNGBRUNNEN1, a reactive oxygen species-responsive NAC transcription factor, regulates longevity in Arabidopsis. Plant Cell **24**: 482–506

Wu K, Zhang L, Zhou C, Yu C-W, Chaikam V (2008) HDA6 is required for jasmonate response, senescence and flowering in Arabidopsis. J Exp Bot **59**: 225–234

Wüthrich KL, Bovet L, Hunziker PE, Donnison IS, Hörtensteiner S (2000) Molecular cloning, functional expression and characterisation of RCC reductase involved in chlorophyll catabolism. Plant J **21**: 189–198

X

Xu XM, Adams S, Chua N-H, Møller SG (2005) AtNAP1 represents an atypical SufB protein in Arabidopsis plastids. J Biol Chem **280**: 6648–6654

Yamada K, Shimada T, Nishimura M, Hara-Nishimura I (2005) A VPE family supporting various vacuolar functions in plants. Physiol Plant **123**: 369–375

Yamasato A, Nagata N, Tanaka R, Tanaka A (2005) The N-terminal domain of chlorophyllide a oxygenase confers protein instability in response to chlorophyll b accumulation in Arabidopsis. Plant Cell **17**: 1585–1597

Y

Yan H, Saika H, Maekawa M, Takamure I, Tsutsumi N, Kyozuka J, Nakazono M (2007) Rice tillering dwarf mutant dwarf3 has increased leaf longevity during darkness-induced senescence or hydrogen peroxide-induced cell death. Genes Genet Syst **82**: 361–366

Yancey PH, Clark ME, Hand SC, Bowlus RD, Somero GN (1982) Living with water stress: evolution of osmolyte systems. Science **217**: 1214–1222

Yao N, Greenberg JT (2006) Arabidopsis ACCELERATED CELL DEATH2 modulates programmed cell death. Plant Cell **18**: 397–411

Yen C-H, Yang C-H (1998) Evidence for programmed cell death during leaf senescence in plants. Plant Cell Physiol **39**: 922–927

Yin Y, Wang Z-Y, Mora-Garcia S, Li J, Yoshida S, Asami T, Chory J (2002) BES1 accumulates in the nucleus in response to brassinosteroids to regulate gene expression and promote stem elongation. Cell **109**: 181–191

Yoshimoto K, Jikumaru Y, Kamiya Y, Kusano M, Consonni C, Panstruga R, Ohsumi Y, Shirasu K (2009) Autophagy negatively regulates cell death by controlling NPR1-dependent salicylic acid signaling during senescence and the innate immune response in Arabidopsis. Plant Cell **21**: 2914–2927

Ytterberg AJ, Peltier JB, Van Wijk KJ (2006) Protein profiling of plastoglobules in chloroplasts and chromoplasts. A surprising site for differential accumulation of metabolic enzymes. Plant Physiol **140**: 984–997

Z

Zapata M, Garrido JL, Jeffrey SW (2006) Chlorophyll c pigments: current status. *In* B Grimm, RJ Porra, W Rüdiger, H Scheer, eds, Chlorophylls and Bacteriochlorophylls. Springer Netherlands, pp 39–53

Zavaleta-Mancera HA, Franklin KA, Ougham HJ, Thomas H, Scott IM (1999a) Regreening of senescent Nicotiana leaves I. Reappearance of NADPH-protochlorophyllide oxidoreductase and light-harvesting chlorophyll a/b-binding protein. J Exp Bot **50**: 1677–1682

Zavaleta-Mancera HA, Thomas BJ, Thomas H, Scott IM (1999b) Regreening of senescent Nicotiana leaves II. Redifferentiation of plastids. J Exp Bot **50**: 1683–1689

Zeiger E, Schwartz A (1982) Longevity of guard cell chloroplasts in falling leaves: implication for stomatal function and cellular aging. Science **218**: 680–682

Zelisko A, Garcia-Lorenzo M, Jackowski G, Jansson S, Funk C (2005) AtFtsH6 is involved in the degradation of the light-harvesting complex II during high-light acclimation and senescence. Proc Natl Acad Sci USA **102**: 13699–13704

Zeng Y, Pan Z, Ding Y, Zhu A, Cao H, Xu Q, Deng X (2011) A proteomic analysis of the chromoplasts isolated from sweet orange fruits [Citrus sinensis (L.) Osbeck]. J Exp Bot **62**: 5297–5309

Zhang K, Gan S (2012) An abscisic acid-AtNAP transcription factor-SAG113 protein phosphatase 2C regulatory chain for controlling dehydration in senescing Arabidopsis leaves. Plant Physiol **158**: 961–969

Zhao H-F, Qiu K, Ren G-D, Zhu Y, Kuai B-K (2010) A pleiotropic phenotype is associated with altered endogenous hormone balance in the developmentally stunted mutant (dsm1). J Plant Biol **53**: 79–87

Zhou C, Han L, Pislariu C, Nakashima J, Fu C, Jiang Q, Quan L, Blancaflor EB, Tang Y, Bouton JH, et al (2011) From model to crop: functional analysis of a STAY-GREEN gene in the model legume Medicago truncatula and effective use of the gene for Alfalfa improvement. Plant Physiol **157**: 1483–1496

Zhou CJ, Cai ZH, Guo Y, Gan S (2009) An Arabidopsis mitogen-activated protein kinase cascade, MKK9-MPK6, plays a role in leaf senescence. Plant Physiol **150**: 167–177

Zienkiewicz M, Ferenc A, Wasilewska W, Romanowska E (2012) High light stimulates Deg1-dependent cleavage of the minor LHCII antenna proteins CP26 and CP29 and the PsbS protein in Arabidopsis thaliana. Planta **235**: 279–288

Zimmermann P, Heinlein C, Orendi G, Zentgraf U (2006) Senescence-specific regulation of catalases in Arabidopsis thaliana (L.) Heynh. Plant Cell Environ **29**: 1049–1060

Zimmermann P, Hirsch-Hoffmann M, Hennig L, Gruissem W (2004) GENEVESTIGATOR. Arabidopsis microarray database and analysis toolbox. Plant Physiol **136**: 2621–2632

Zimmermann P, Zentgraf U (2005) The correlation between oxidative stress and leaf senescence during plant development. Cell Mol Biol Lett **10**: 515–534

Zuther E, Büchel K, Hundertmark M, Stitt M, Hincha DK, Heyer AG (2004) The role of raffinose in the cold acclimation response of Arabidopsis thaliana. FEBS Lett **576**: 169–173

ABBREVIATIONS

Arabidopsis	*Arabidopsis thaliana*
AAO3	ARABIDOPSIS ALDEHYDE OXIDASE 3
ABA	Abscisic acid
ABC	ATP BINDING CASSETTE
ACC	1-aminocyclopropane-1-carboxylic acid
acd	*accelerated cell death*
ACT	ACTIN
AHK3	ARABIDOPSIS HISTIDINE KINASE 3
ALA	5-aminolevulinic acid
AOS	ALLENE OXIDE SYNTHASE
AP	Aspartic protease
ARF2	AUXIN RESPONSE FACTOR2
ARR2	ARABIDOPSIS RESPONSE REGULATOR 2
ATAF	ARABIDOPSIS TRANSCRIPTION ACTIVATION FACTOR
ATG	Autophagy-related genes
ATR1	ARABIDOPSIS P450 REDUCTASE 1
BAK1	BRI1-ASSOCIATED RECEPTOR KINASE
BChl	Bacteriochlorophyll
BCRP1	BREAST CANCER RESISTANCE PROTEIN 1
BRI1	BRASSINOSTEROID INSENSITIVE 1
BR	Brassinosteroid
CAO	Chl *a* OXYGENASE
CAT	CATALASE
CBR	Chl *b* REDUCTASE
cDNA	Copy DNA
Chl	Chlorophyll
Chlide	Chlorophyllide
CLH	CHLOROPHYLLASE
CLSM	Confocal laser scanning microscopy
Clp	Caseinolytic protease
CND41	CHLOROPLAST NUCLEOID DNA-BINDING PROTEIN 41
CO	Carbon monoxide
coi1	*coronatine-insensitive 1*
Col-0	Columbia-0 ecotype
CP	Cysteine protease
CPR	CONSTITUTIVE EXPRESSION OF PATHOGENESIS-RELATED GENE
CS	Chl synthase
CUC2	CUP-SHAPED COTYLEDON 2
DAD1	DEFECTIVE IN ANTHER DEHISCENCE 1
DDI	Days of dark incubation
DGDG	Digalactosyldiacylglycerol

DIN	DARK INDUCIBLE
DP	Whole darkened plants
DTT	Dithiothreitol
DW	Dry weight
EDR1	ENHANCED DISEASE RESISTANCE 1
EPR	Electron paramagnetic resonance
ER	Endoplasmic reticulum
ERD1	EARLY RESPONSE TO DEHYDRATION 1
ESI-MS	Electrospray ionization-MS
ESR	EPITHIOSPECIFYING SENESCENCE REGULATOR
EtOH	Ethanol
FAPE	Fatty acid phytyl ester
FCC	Fluorescent Chl catabolite
FDCC	Fluorescent dioxobilin-type Chl catabolite
FDH	FORMATE DEHYDROGENASE
FLC	FLOWERING LOCUS C
FLU	FLUORESCENT IN BLUE LIGHT
FW	Fresh weight
G6P or Glc-6-P	Glucose-6-phosphate
GAs	Gibberellins
GFP	Green fluorescent protein
GluTR	GLUTAMYL-tRNA REDUCTASE
Gol	Galactinol
GUN	GENOME UNCOUPLED
HA	Hepatitis A
HCAR	7-HYDROXYMETHYL Chl *a* REDUCTASE
HDA6	HISTONE DEACETYLASE 6
HIN1	HAIRPIN-INDUCED 1
His	Histidine
HMChl *a*	Hydroxymethyl-Chl(ide) *a*
HR	Hypersensitive response
HsCAT	Human catalase
HSP	HEAT SHOCK PROTEIN
IDL	Individual darkened leaves
INVINH1	INHIBITOR OF CELL WALL INVERTASE
IPT	ISOPENTENYL TRANSFERASE
JA	Jasmonates
JUB1	JUNGBRUNNEN1
Ler	Lansdberg erecta ecotype
LEA	LATE EMBRYOGENESIS ABUNDANT PROTEIN
LHC	Light harvesting complex

MAPK	MITOGEN-ACTIVATED PROTEIN KINASE
MCS	Metal-chelating substance
MeIAA	Methyl-indole acetic acid
MeJA	Methyl-JA
Mel	Melibiose
MeOH	Methanol
MES	METYHL ESTERASE
MeSA	Methyl-SA
MFI	Mean fluorescence intensity
MgCh	MAGNESIUM CHELATASE
MGDG	Monogalactosyldiacylglycerol
MKK9	MAPK KINASE
MP	Metalloprotease
MPT	Mitochondrial membrane permeability transition
MRP	Metal-releasing protein or MULTIDRUG RESISTANCE–ASSOCIATED PROTEIN
MS	Mass spectrometry
NAC	Acronym of NAM, ATAF, CUC
NAM	NO APICAL MERISTEM
NATA	N-acetyltryptophanamide
NCC	Nonfluorescent Chl catabolite
NDC1	NAD(P)H dehydrogenase C1
NDCC	Nonfluorescent dioxobilin-type Chl catabolite
NO	Nitric oxide
NOL	NYC1-like
NYC1	NON-YELLOW COLORING1
OLD	ONSET OF LEAF DEATH
ORE	ORESARA
pad4	*phytoalexin deficient 4*
PAO	Pheide *a* OXYGENASE
PCD	Programmed cell death
PES	PHYTYL ESTER SYNTHASE
*p*FCC	*Primary* FCC
Pheide	Pheophorbide
Phein	Pheophytin
PMSF	Phenylmethanesulfonylfluoride
pNPαGal	Para-nitrophenyl-α-D-galactopyranoside
pNPβGal	Para-nitrophenyl-β-D-galactopyranoside
POR	PROTOCHLOROPHYLLIDE OXIDOREDUCTASE
PPIX	Protoporphyrin IX
PPD	Pheophorbidase
PPH	Phein Pheide HYDROLASE

PG	Pastoglobule
PP2C	Protein phosphatase 2C
PRAT	PLANT PREPROTEIN AND AMINO ACID TRANSPORTER
PSY1	PHYTOENE SYNTHASE 1
Raf	Raffinose
RafS	RAF SYNTHASE
RCB	Rubisco-containing body
RCC	Red Chl catabolite
RCCR	RCC REDUCTASE
RFF	RCC FORMING FACTOR
RFO	Raf family of oligosaccharides
RFP	Red fluorescent protein
ROS	Reactive oxygen species
RPK1	RECEPTOR PROTEIN KINASE 1
RWC	Relative water content
SA	Salicylic acid
SABP2	SA-BINDING PROTEIN 2
SAG	SENESCENCE ASSOCIATED GENE
SAUL1	SENESCENCE-ASSOCIATED E3 UBIQUITIN LIGASE 1
SAV	Senescence-associated vesicle
Sf9	*Spodoptera frugiperda* cell line 9
SGR	STAY-GREEN
SIP	SEED IMBIBITION PROTEIN
SnRK1	SUCROSE NONFERMENTING-1-RELATED PROTEIN KINASE-1
SOSG	Singlet oxygen sensor green
SP	Serine protease
Sta	Stachyose
SUF	Prokaryotic sulphur system
SUVH2	SU(VAR)3-9 HOMOLOG 2
TAG	Triacylglycerol
tAPX	THYLAKOID ASCORBATE PEROXIDASE
T-DNA	Transfer DNA
TEMP	2,2,6,6-tetramethylpiperidine
TEMPO	Nitroxy radical 2,2,6,6-tetramethylpiperidine-1-oxyl
THFS	10-FORMYL-THF SYNTHETASE
TOR	TARGET OF RAPAMYCIN
UCC	Urobilinogenoidic Chl catabolite
UGT	UDP-DEPENDENT GLYCOSYLTRANSFERASE
UPL5	E3 UBIQUITIN LIGASE PROTEIN 5
Ver	Verbascose
VPE	Vacuolar processing enzyme

VTE1	Tocopherol cyclase VITAMIN E 1
WS	Wassilewskija ecotype
WT	Wild-type
X.viscosa	*Xerophyta viscosa*
YCC	Yellow Chl catabolite

ACKNOWLEDGEMENTS

At first, I would like to thank Prof. Stefan Hörtensteiner for having given me the opportunity to join his group. Stefan, thanks a lot for your support, your help and your ideas, and also for the freedom you gave me during my PhD. All these aspects contribute a lot to the enjoyable and productive working environment of your group!

I would like to thank Prof. Enrico Martinoia for providing excellent working conditions in his chair and to join my thesis committee.

Thanks to Prof. Ivo Feussner (Göttingen, Germany) who agreed to act as an external examiner of my thesis.

Many thanks to former and present Stefan's group members, you all contribute(d) to the nice atmosphere of P1/17: Aditi, Kathrin, Lukas, Luzia, Maja, Nicole, Riccardo, Sandro, Sofia, Shinya, Silvia and Song. Special thanks to Silvia who helped me all lot while I was starting in Zürich. Big thanks to Kathrin: always so helpful and nice inside (and outside!) the lab. Thanks to Luzia for having taken over the "Blockkurs" while I was writing this thesis.

Thanks to former members of Prof. Felix Keller's group, Aurélie, Félix and Shaun, for their help and the nice time spent together, and also for our fruitful collaborations on Xerophyta and *At*DIN10 projects.

Thanks to the group of Prof. Berhard Kräutler (Innsbruck) with whom I closely collaborated during my PhD. Special thanks to Iris, Clemens and Thomas.

Thanks to all members of Enrico Martinoia's group for their help, advices and kindness. Thanks to Aurélien Bailly for his help with Indesign.

Merci à mes parents pour leur immense générosité. Merci d'avoir soutenu et financé mes études tout en me permettant d'effectuer nombreux loisirs.

Le dernier remerciement, mais de loin l'un des plus importants, revient pour toi Mégan, merci infiniment pour ton aide, ta présence et ton amour.

CURRICULUM VITAE

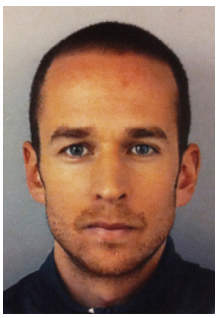

Bastien André CHRIST
06-09-1986
Gänsbrunnen SO

EDUCATION

2001-2004	Gymnasium – Biology and Chemistry – Porrentruy (JU)
2004-2007	**Bachelor of Sciences.** Biology – *Prix Jean Landry* – University of Neuchâtel
2007-2009	**Master of Sciences.** Plant Ecology and Physiology – *Summa cum laude* – University of Neuchâtel Master thesis under the supervison of Prof. Felix Kessler Title: *Regulation of protein import into chloroplasts: Toc159 A-domain and phosphorylation*
2009-2013	**PhD thesis**. Institute of Plant Biology – Universität Zürich Dissertation under the supervison of Prof. Stefan Hörtensteiner Title: *Chlorophyll Breakdown: Modifications of Colorless Chlorophyll Catabolites*

WORK AND RESEARCH EXPERIENCE

2004	Temporary job – Hôpital du Jura – Delémont (JU)
2006	Temporary job – British American Tobacco – Boncourt (JU)
2007	Internship (2 months) in Johnson & Johnson (Microbiology) – Le Locle (NE)
2008	Internship (4 months) in CABI Biosciences (Entomology) – Delémont (JU)
2003-2009	Temporary cleaning jobs – Delémont (JU)

PUBLICATIONS

Agne B, Andrès C, Montandon C, Christ B, Ertan A, Jung F, Infanger S, Bischof S, Baginsky S, Kessler F (2010) The Acidic A-Domain of Arabidopsis Toc159 Occurs as a Hyperphosphorylated Protein. Plant Physiol **153**: 1016–1030

Christ B, Schelbert S, Aubry S, Süssenbacher I, Müller T, Kräutler B, Hörtensteiner S (2012) MES16, a member of the methylesterase protein family, specifically demethylates fluorescent chlorophyll catabolites during chlorophyll breakdown in Arabidopsis. Plant Physiol **158**: 628–641

Pattanayak GK, Venkataramani S, Hortensteiner S, Kunz L, Christ B, Moulin M, Smith AG, Okamoto Y, Tamiaki H, Sugishima M, (2012) ACCELERATED CELL DEATH 2 suppresses mitochondrial oxidative bursts and modulates cell death in Arabidopsis. Plant J **69**: 589–600

Christ B[1], **Süssenbacher I**[1], **Moser S, Bichsel N, Egert A, Müller T, Kräutler B**[2], **Hörtensteiner S**[2] (2013) Arabidopsis thaliana cytochrome P450 CYP89A9 is involved in the formation of major chlorophyll catabolites during leaf senescence. Submitted to PNAS (2013-03-21)
[1,2] These authors contributed equally to this work